

**University of Alberta**

**Broadband Optoelectronic Switching and Signal Processing**

by

**Rohit Sharma**



A thesis submitted to the Faculty of Graduate Studies and Research in partial fulfillment of the requirements for the degree of **Doctor of Philosophy**.

**Department of Electrical Engineering**

**Edmonton, Alberta**

**Fall 1996**



National Library  
of Canada

Acquisitions and  
Bibliographic Services Branch

395 Wellington Street  
Ottawa, Ontario  
K1A 0N4

Bibliothèque nationale  
du Canada

Direction des acquisitions et  
des services bibliographiques

395, rue Wellington  
Ottawa (Ontario)  
K1A 0N4

*Your file* *Voire référence*

*Our file* *Notre référence*

**The author has granted an irrevocable non-exclusive licence allowing the National Library of Canada to reproduce, loan, distribute or sell copies of his/her thesis by any means and in any form or format, making this thesis available to interested persons.**

**L'auteur a accordé une licence irrévocable et non exclusive permettant à la Bibliothèque nationale du Canada de reproduire, prêter, distribuer ou vendre des copies de sa thèse de quelque manière et sous quelque forme que ce soit pour mettre des exemplaires de cette thèse à la disposition des personnes intéressées.**

**The author retains ownership of the copyright in his/her thesis. Neither the thesis nor substantial extracts from it may be printed or otherwise reproduced without his/her permission.**

**L'auteur conserve la propriété du droit d'auteur qui protège sa thèse. Ni la thèse ni des extraits substantiels de celle-ci ne doivent être imprimés ou autrement reproduits sans son autorisation.**

ISBN 0-612-18107-3

**Canada**

# University of Alberta

## Library Release Form

**Name of Author:** Rohit Sharma

**Title of Thesis:** Broadband Optoelectronic Switching and Signal Processing

**Degree:** Doctor of Philosophy

**Year this Degree Granted:** 1996

Permission is hereby granted to the University of Alberta Library to reproduce single copies of this thesis and to lend or sell such copies for private, scholarly, or scientific research purposes only.

The author reserves all other publication and other rights in association with the copyright in the thesis, and except as hereinbefore provided, neither the thesis nor any substantial portion thereof may be printed or otherwise reproduced in any material form whatever without the author's prior written permission.



**Rohit Sharma**

Banwari Lal Sharma  
Mustafabad, P.O. Subhanpur  
Dist. Kapurthala  
Panjab, INDIA


October 1, 1996


# University of Alberta


## Faculty of Graduate Studies and Research

The undersigned certify that they have read, and recommend to the Faculty of Graduate Studies and Research for acceptance, a thesis entitled **Broadband Switching and Signal Processing** submitted by **Rohit Sharma** in partial fulfillment of the requirements for the degree of **Doctor of Philosophy**.

  
\_\_\_\_\_  
R. I. MacDonald

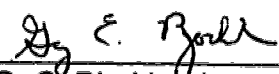
  
\_\_\_\_\_  
B. P. Keyworth

  
\_\_\_\_\_  
M. J. Brett

  
\_\_\_\_\_  
Z. J. Koles

  
\_\_\_\_\_  
J. N. McMullin

  
\_\_\_\_\_  
J. J. Harms

  
\_\_\_\_\_  
G. C. Bjorklund

25/9/96

i dedicate the thesis to my mother and father  
they gave me a world beyond what i could see

## Abstract

The ubiquitous use of photonic systems for transmission of unprecedented volumes of information through fibres requires development of devices to generate, detect, and route the optical signals. Optoelectronic switching techniques involve the use of optical to electronic conversions, inherent in photonic systems, to route the optical signals in the desired manner. Optical 'broadcast' and optoelectronic 'selection' methods are used to accomplish switching of broadband signals, resulting in a data format, rate, and modulation transparent, high quality path through the non-blocking matrix arrangement.

Optoelectronic switching of signal formats ranging from high quality analog video signals to broadband binary digital signals up to 2.5 Gbps is demonstrated with the design and construction of a 10x10 prototype. The optoelectronic switch fabric is shown to be fully transparent to data rates and formats. The use of spectrally efficient modulation formats for photonic interconnects is proposed and results are presented to confirm potential increase in data throughput without requiring an increase in bandwidth of the electronic components. Designs for photodetector arrays to enable routing of data rates exceeding 10 GHz bandwidth per channel are also described.

Applications for optoelectronic technology range from use in transparent switching fabrics for multi-wavelength networks to high speed broadband switches for network restoration. Use of optoelectronic switches for network restoration is proposed and results from a sample network study are presented.

Broadband signal processing using optoelectronic matrices and fibre delay lines is shown to achieve tunable filters with applications in equalization of multimode fibre dispersion.

Optoelectronic switching is shown to be a cost competitive and technology efficient way of achieving Gigabit data switching capabilities required for telecommunication and computer communication networks.

## Acknowledgement

I wish to thank the following for their contribution towards successful completion of this research work

- Ian MacDonald for supervising the work in a manner that created numerous opportunities for learning in diverse fields and for his confidence in me to explore the varied research areas. The degree program at TRLabs in the Optoelectronic Switching group has been a comprehensive education in the process of research in addition to the subjects covered in the research. Ian has been an ever encouraging supervisor and mentor.

- Barrie Keyworth for the positive examples set in the laboratory that embody the true spirit of creative research through his original ideas and their completion despite seemingly impossible odds. He has been a true 'educator' and supervisor without formal acknowledgement of his role in this work.

- Gary Bjorklund, Mike Brett, Z. Koles, Janelle Harms, and Jim McMullin for serving on the examination and supervisory committees and their helpful suggestions and corrections to the thesis draft.

- Dino Corazza for his help with the lab work throughout the project and for fabricating the fibre assemblies for the work.

- Jim Slevinsky and Mike MacGregor for introducing me to the possibilities of applications of this work in network restoration, and for patiently fielding my queries.

- Emannuelle Perrenoud for contributing to the signal processing



applications demonstrated with the optoelectronic switch.

- Sheldon Walklin for loan of equipment and data gathering software for multi-level modulation experiments.

- David Clegg, Jason Lamont, and Lorne Zmeko for assistance with construction of the switch.

- Ray DeCorby, Allan Hnatiw, and all other students in the HyPIC group for many creative discussions that helped me learn about a variety of research projects in progress at TRILabs.

- Jan Bartl and Philip Garel-Jones of JDS Fitel Inc. for providing the opportunity to be a part of Canadian technology and research showcase at the largest gathering of telecom companies and professionals at Telecom '95 in Geneva.

- Nona, Corinna, Faye, and Karen Adams for their always cheerful help and for tolerating my intrusions into their work.

I also acknowledge TRILabs for the Telecom Research Scholarship and the Telecom Research Award, University of Alberta for the G.R.A. Rice Scholarship in Communications and the Mary Louise Imrie Award that enabled me to undertake this work.

# Table of Contents

<b>1. Introduction .....</b>	<b>1</b>
1.1 Communications and Switching .....	1
1.2 Optoelectronic Switching .....	3
1.3 Signal Processing with Optoelectronic Elements .....	7
1.4 A Brief History of Optoelectronic Switching .....	8
1.4.1 Optoelectronic switching at University of Alberta .....	8
1.5 Organization of the Thesis .....	10
<b>2. Applications of Optoelectronic Switching .....</b>	<b>11</b>
2.1 Switching in Communication Networks .....	11
2.1.1 Continent wide networks .....	11
2.1.1a Network switching .....	11
2.1.1b Network restoration .....	16
2.1.2 Local area networks .....	17
2.1.2a Digital data networks .....	18
2.1.2b Cable TV networks .....	20
2.1.3 Short distance interconnects .....	21
2.2 Other Switching Techniques for Optical Signals .....	22
2.2.1 Optical switching .....	22
2.2.2 Other optoelectronic switching approaches .....	24
2.3 Signal Processing Applications .....	25
2.3.1 Optoelectronic matrix processor .....	25
2.3.2 Artificial neural networks .....	26
<b>3. Design and Construction of Prototype Switch .....</b>	<b>28</b>
3.1 Prototype System Overview .....	28

3.2 Optoelectronic Modules .....	30
3.3 Laser Transmitter Response .....	37
3.4 The Prototype Switch .....	41
3.5 Requirements for 10 GHz Channel Bandwidth .....	41
3.5.1 Bandwidth limitations in optoelectronic components .....	41
3.5.2 Power budget for 10 Gbps system .....	44
<b>4. Broadband Photodetector Arrays .....</b>	<b>49</b>
4.1 Metal-Semiconductor-Metal Photodetectors .....	49
4.2 MSM Photodetectors in Arrays .....	51
4.2.1 Conventional array designs .....	51
4.2.2 DC-bias circuit .....	55
4.3 Bandwidth Limitations in Conventional Designs .....	57
4.3.1 BNR 1x8 array .....	57
4.3.2 Position dependent frequency response .....	61
4.3.3 1x16 Arrays .....	64
4.4 Designs for Broadband Arrays .....	66
4.4.1 Simulation models for MSM photodetector arrays .....	66
4.5 Designs for TRILabs MSM mask .....	81
4.5.1 1x16 Array designs .....	81
4.5.2 1x8 Array designs .....	85
4.5.3 Mask design .....	87
4.6 Other Applications of Broadband Photodetector Arrays: Wavelength Tunable Receivers .....	88
<b>5. Format-Transparent Switching Results .....</b>	<b>91</b>
5.1 Characterizing Prototype Switch Performance .....	91
5.1.1 Channel bandwidth .....	92

5.1.2 Contrast between ON and OFF states of the switching elements ..	93
5.1.3 Crosstalk .....	96
5.2 Digital Signal Switching .....	98
5.3 Analog Signal Switching .....	100
5.3.1 Analog video signals .....	101
5.3.2 System impairments .....	102
5.3.2a Noise .....	102
5.3.2b Nonlinear distortion .....	105
5.3.2c Modulation index .....	109
5.3.2d CSO and CTB measurement for prototype switch .....	111
5.3.3 Format transparent switching .....	115
5.4 Spectrally Efficient Modulation for Photonic Interconnects .....	117
5.4.1 Spectrally efficient codes .....	118
5.4.2 Results .....	118
<b>6. Optoelectronic Signal Processing .....</b>	<b>123</b>
6.1 Optoelectronic Signal Processors .....	123
6.1.1 Discrete time processor .....	123
6.1.2 Matrix-vector processor .....	124
6.1.3 Generalized discrete time processor .....	125
6.2 Realization of Tunable Filters .....	127
6.2.1 FIR and IIR filters .....	127
6.2.1a Bias dependent frequency response of crosspoints .....	130
6.2.1b Results .....	132
6.2.2 Equalization of modal dispersion .....	135
<b>7. Broadband Optoelectronic Switches in Network Restoration .....</b>	<b>140</b>
7.1 Network Restoration .....	140
7.1.1 SONET network restoration .....	141
7.1.1a Self healing rings .....	142

7.2 Optoelectronic Switching for Network Restoration .....	144
7.2.1 SONET Cross-connect system .....	144
7.2.1a All optical cross-connects (OCX) .....	146
7.2.2 Broadband optoelectronic cross-connect (B-OECS) .....	147
7.2.3 Restoration methods .....	149
7.2.3a 'Bundled' restoration .....	149
7.2.3b Link restoration .....	153
7.3 A Case Study .....	154
7.4 WDM Networks .....	158
<b>8. Conclusions and Recommendations .....</b>	<b>163</b>
8.1 Project Summary .....	163
8.1.1 Prototype construction .....	163
8.1.2 Summary of results .....	165
8.1.3 Recommendations for future work .....	166
8.1.3a Laser transmitters .....	167
8.1.3b Optical signal distribution section .....	167
8.1.3c Optoelectronic receiver module .....	169
8.1.4 Hybrid integrated tunable receivers .....	169
8.2 Broadband Switching: Applications and Options .....	170
8.2.1 Applications for broadband switching .....	170
8.2.2 Optical switching and transparency issues .....	173
8.2.3 Conclusion .....	175
<b>Bibliography .....</b>	<b>176</b>
<b>Appendix A .....</b>	<b>194</b>
<b>Appendix B .....</b>	<b>201</b>
<b>Appendix C .....</b>	<b>203</b>
<b>Appendix D .....</b>	<b>205</b>

<b>Appendix E .....</b>	<b>207</b>
<b>Appendix F .....</b>	<b>211</b>
<b>Appendix G .....</b>	<b>222</b>
<b>Appendix H .....</b>	<b>224</b>

## List of Tables

Table 2.1	SONET data rates .....	13
Table 2.2	Comparison of switching technologies .....	24
Table 5.1	BER measurements .....	98
Table 5.2	NCTA recommended spectrum analyzer parameters .....	103
Table 5.3	Modulation index for measuring CSO, CTB .....	111
Table 7.1	Bellcore metropolitan network-I: traffic at each node .....	156
Table 7.2	Cross-connect switch sizes .....	157

# List of Figures

## Chapter 1

Figure 1.1	A signal switch .....	2
Figure 1.2	Optical-to-electronic signal conversion and its use in signal switching .....	4
Figure 1.3	A 2x2 optoelectronic switch using optoelectronic signal conversion based routing .....	5
Figure 1.4	Array of conversion elements (crosspoints) for optoelectronic switching .....	6
Figure 1.5	Optoelectronic equivalents of signal processing elements .....	7

## Chapter 2

Figure 2.1	A wide area network (WAN) .....	12
Figure 2.2	A typical network node with transit and local traffic .....	13
Figure 2.3	Broadband switch core for high throughput ATM switching applications .....	14
Figure 2.4	A crossbar switch matrix .....	15
Figure 2.5	Network restoration switching .....	17
Figure 2.6	Hybrid Fibre-Coaxial cable network .....	26
Figure 2.7	Optoelectronic matrix switch as a reconfigurable distributed optical interconnect .....	22
Figure 2.8	Optoelectronic signal processor structure .....	26

## Chapter 3

Figure 3.1	Prototype broadband optoelectronic switch system .....	28
------------	--	----



Figure 3.2	Broadband signal channel in the prototype switch .....	30
Figure 3.3	Optoelectronic module schematic .....	31
Figure 3.4	Silicon v-groove assembly for fibre placement in the optoelectronic module .....	32
Figure 3.5	Schematic view of optoelectronic module on circuit card .....	33
Figure 3.6	Substrate design for optoelectronic module .....	34
Figure 3.7	Substrate with surface mount components .....	34
Figure 3.8	Housing for the optoelectronic module .....	35
Figure 3.9	Schematic view of optoelectronic module with amplifiers .....	36
Figure 3.10	Photograph of the optoelectronic module with substrate .....	36
Figure 3.11	Photograph of an output port card with fibre input and electrical output .....	37
Figure 3.12	Simulation circuit for laser bias-tee .....	38
Figure 3.13 (a)	Simulated S11 for laser drive circuit .....	39
Figure 3.13 (b)	Measured S11 for the laser drive circuit .....	40
Figure 3.14	Equalizing circuit for laser drive .....	40
Figure 3.15 (a)	Frequency response of the unequalized laser drive circuit .....	41
Figure 3.15 (b)	Frequency response of the equalized laser drive circuit .....	42
Figure 3.16	Prototype optoelectronic switch .....	43
Figure 3.17	Equivalent circuit for the optoelectronic module .....	44

## Chapter 4

Figure 4.1	The Metal-Semiconductor-Metal (MSM) photodetector .....	50
Figure 4.2	Current-voltage characteristics of MSM photodetectors .....	51

Figure 4.3	MSM photodetector array as an optoelectronic signal selector	52
Figure 4.4	Effect of photodetector capacitance in arrays .....	53
Figure 4.5	BNR 1x8 array layout .....	54
Figure 4.6	CRC 1x16 array layout .....	55
Figure 4.7	DC-bias circuit for photodetectors .....	55
Figure 4.8	Test equipment arrangement for MSM array bandwidth tests	56
Figure 4.9	Frequency response of MSM photodetector no. 1 in the BNR 1x8 array .....	58
Figure 4.10	Frequency response of MSM photodetector no. 2 in the BNR 1x8 array .....	58
Figure 4.11	Frequency response of MSM photodetector no. 3 in the BNR 1x8 array .....	59
Figure 4.12	Frequency response of MSM photodetector no. 4 in the BNR 1x8 array .....	59
Figure 4.13	Frequency response of MSM photodetector no. 5 in the BNR 1x8 array .....	60
Figure 4.14	Frequency response of MSM photodetector no. 6 in the BNR 1x8 array .....	60
Figure 4.15	Frequency response of MSM photodetector no. 7 in the BNR 1x8 array .....	61
Figure 4.16	3 dB bandwidth of MSM photodetectors in the 1x8 array .....	62
Figure 4.17	Dependence of bandwidth of photodetector #7 in the BNR 1x8 array on number of MSMs in the array .....	64
Figure 4.18	Frequency response of MSM no. 7 (all other MSMs disconnected in 1x8 array) .....	65
Figure 4.19	Two port MSM model .....	67

Figure 4.20	Capacitance measurement for MSM photodetectors .....	68
Figure 4.21	Lumped element simulation circuit for MSM array .....	69
Figure 4.22	Modelled frequency response of MSM no. 1 with lumped element model .....	70
Figure 4.23	Interconnects as microstrip transmission lines .....	70
Figure 4.24	Combiner circuit for photodetector array .....	71
Figure 4.25	Wilkinson and 'fork' hybrid combiners .....	73
Figure 4.26	Single stage and two stage combiner hybrid circuits .....	74
Figure 4.27	Schematic of 1x4 combiner for photodetector array .....	76
Figure 4.28 (a)	Simulation circuit for MSM array .....	78
Figure 4.28 (b)	Detail of MSM branch .....	79
Figure 4.29	Frequency response comparison of MSM photodetectors in array design shown in Fig. 4.28 Vs conventional design .....	80
Figure 4.30 (a)	Layout for 1x16 array design, type A .....	81
Figure 4.30 (b)	Frequency response for 1x16 array, type A .....	84
Figure 4.31 (a)	Layout for 1x16 array, type B .....	82
Figure 4.31 (b)	Frequency response for 1x16 array, type B .....	84
Figure 4.32 (a)	Layout for 1x16 array, type C .....	83
Figure 4.32 (b)	Frequency response for 1x16 array, type C .....	85
Figure 4.33 (a)	Layout for 1x8 array, type A .....	86
Figure 4.33 (b)	Frequency response of photodetectors at the end, and in the middle of the 1x8 array, type A .....	87
Figure 4.34 (a)	Layout for 1x8 array, type B .....	88
Figure 4.34 (b)	Frequency response of all photodetectors in 1x8 array, type B	89

Figure 4.35	Wavelength tunable receiver using photodetector array .....	89
-------------	---	----

## Chapter 5

Figure 5.1	Channel bandwidth for prototype switch .....	92
Figure 5.2	ON/OFF Contrast and signal crosstalk .....	93
Figure 5.3	ON/OFF Contrast of optoelectronic switching elements .....	94
Figure 5.4	Channel spectrum scan showing ON/OFF contrast .....	95
Figure 5.5	Crosstalk measurement experiment .....	96
Figure 5.6	Crosstalk measurement at 1 GHz .....	97
Figure 5.7	Eye diagram for data rate = 622.08 Mbps (OC-12) .....	99
Figure 5.8	Eye diagram for data rate = 1.0 Gbps .....	99
Figure 5.9	Eye diagram for data rate = 1.50 Gbps .....	99
Figure 5.10	Eye diagram for data rate = 2.0 Gbps .....	100
Figure 5.11	Eye diagram for data rate = 2.488 Gbps (OC-48) .....	100
Figure 5.12	NTSC standard video channel spectrum .....	102
Figure 5.13	CNR for analog video signals .....	104
Figure 5.14	Intermodulation distortion products .....	106
Figure 5.15	Intermodulation products at Channel 43 .....	107
Figure 5.16	Experimental set up for measuring CSO and CTB .....	108
Figure 5.17	Composite CATV payload (Channel 2 to Channel 45) routed through the optoelectronic switch .....	108
Figure 5.18	Light-Current characteristics for calculating modulation index	109
Figure 5.19	CTB measurement at 55.25 MHz (Channel 2) .....	112
Figure 5.20	CSO measured in Channel 2 .....	112

Figure 5.21	CTB measurement at 337.25 MHz (Channel 43) .....	113
Figure 5.22	CSO measured in Channel 43 .....	114
Figure 5.23	Harmonic distortion in Lasers used in the prototype switch ..	115
Figure 5.24	Simultaneous analog signal and digital data switching .....	116
Figure 5.25	Multilevel input signal to the optoelectronic switch (Symbol Rate = 1.58 GHz) .....	119
Figure 5.26	Switched multilevel signal at output of optoelectronic switch (Symbol Rate = 1.58 GHz) .....	119
Figure 5.27	Switched multilevel signal at output of optoelectronic switch (Symbol Rate = 0.9 GHz) .....	120
Figure 5.28	Switched multilevel signal at output of optoelectronic switch (Symbol Rate = 1.1 GHz) .....	121
Figure 5.29	Switched multilevel signal at output of optoelectronic switch (Symbol Rate = 1.8 GHz) .....	121

## Chapter 6

Figure 6.1	Matrix-vector multiplication operation with optoelectronic crossbar switch .....	124
Figure 6.2	Generalized discrete time signal processor .....	126
Figure 6.3	FIR filter realization with optoelectronic matrix processor .....	128
Figure 6.4	IIR filter realization with optoelectronic matrix processor .....	129
Figure 6.5	Measured MSM crosspoint frequency response for different bias voltages .....	130
Figure 6.6	Adaptive calculation of filter coefficients .....	131
Figure 6.7	Modelled MSM crosspoint frequency response .....	131
Figure 6.8	Compensated frequency response .....	132

Figure 6.9	Measured and modelled tunable optoelectronic FIR filter frequency response .....	133
Figure 6.10	Possible IIR configuration with the optoelectronic switch.....	134
Figure 6.11	Schematic of the equalization simulation system .....	137
Figure 6.12	Signal eye diagrams for equalization .....	138
Figure 6.13	Equalizing filter response implementation .....	139

## Chapter 7

Figure 7.1	Digital cross-connect system (DCS) based mesh network restoration .....	142
Figure 7.2	Self-healing 'ring' restoration in SONET networks .....	143
Figure 7.3	1:N Protection ring arrangement with optoelectronic switch .	144
Figure 7.4	A SONET digital cross-connect system .....	146
Figure 7.5	Optical cross-connect (OCX) system .....	147
Figure 7.6	Broadband optoelectronic DCS .....	148
Figure 7.7	Optoelectronic switch in network restoration .....	151
Figure 7.8	Variable rate optoelectronic cross-connect switch .....	152
Figure 7.9	Optoelectronic cross-connects with protection for Laser transmitters .....	153
Figure 7.10	Bellcore metropolitan network-I .....	155
Figure 7.11	Optoelectronic switch as a wavelength routing switch .....	159
Figure 7.12	WDM based spare capacity in a network .....	160
Figure 7.13	Optoelectronic restoration switching at node A .....	161

## Chapter 8

Figure 8.1	Prototype optoelectronic switch at the Canada Pavilion, Telecom '95, Geneva .....	165
Figure 8.2	A fibre ribbon based optical signal distribution module .....	168

## List of Abbreviations

1 x N	Denotes a linear array with N elements
AC	Alternating Current
ADM	Add/Drop Multiplexers
ASK	Amplitude Shift Keying
ATM	Asynchronous Transfer Mode
B-OECS	Broadband Optoelectronic Cross-Connect
BER	Bit Error Ratio
BNR	Bell-Northern Research (now Nortel Inc.), Ottawa.
CATV	Cable Television
CNR	Carrier to Noise Ratio
CRC	Communications Research Centre, Ottawa.
CSO	Composite Second Order Distortion
CTB	Composite Triple Beat Distortion
D/A	Digital to Analog
dB	decibels
dBc	decibels referred to carrier power level
dBm	decibels referred to 1 milliwatt
DC	Direct Current
DCS	Digital Cross-Connect System
DEMUX	Demultiplexer
DQPSK	Differential Quadrature Phase Shift Keying



<b>FDDI</b>	<b>Fibre Distributed Data Interface</b>
<b>FIR</b>	<b>Finite Impulse Response</b>
<b>FM</b>	<b>Frequency Modulation</b>
<b>GHz</b>	<b>Giga-Hertz (<math>10^9</math>)</b>
<b>GaAs</b>	<b>Gallium Arsenide</b>
<b>Gbps</b>	<b>Gigabits per second</b>
<b>HDTV</b>	<b>High Definition Television</b>
<b>HFC</b>	<b>Hybrid Fibre-Coaxial</b>
<b>HIPPI</b>	<b>High Performance Parallel Interface</b>
<b>IIR</b>	<b>Infinite Impulse Response</b>
<b>InGaAs</b>	<b>Indium Gallium Arsenide</b>
<b>LAN</b>	<b>Local Area Networks</b>
<b>LMS</b>	<b>Least Mean Squares</b>
<b>MAN</b>	<b>Metropolitan Area Network</b>
<b>MHz</b>	<b>Mega-Hertz (<math>10^6</math>)</b>
<b>MMIC</b>	<b>Microwave Monolithic Integrated Circuit</b>
<b>MSE</b>	<b>Mean-Squared Error</b>
<b>MSM</b>	<b>Metal-Semiconductor-Metal</b>
<b>MUX</b>	<b>Multiplexer</b>
<b>Mbps</b>	<b>Megabits per second</b>
<b>N x N</b>	<b>Denotes a switch with N inputs and N outputs</b>
<b>NCTA</b>	<b>National Cable Television Association</b>
<b>NTSC</b>	<b>National Television Systems Committee</b>

OC-N	Optical Carrier level N, N = 3, 12, 48, 192, .....
	OC-3 = 155.52 Mbps
	OC-12 = 622.08 Mbps
	OC-48 = 2.48832 Gbps
	OC-192 = 9.95328 Gbps
RF	Radio Frequency
RIN	Relative Intensity Noise
RLS	Recursive Least Squares
SCI	Scalable Coherent Interface
SHR	Self Healing Ring
SNR	Signal to Noise Ratio
SOA	Semiconductor Optical Amplifier
SONET	Synchronous Optical Network
STS-N	Synchronous Transport Signal Level - N
TRLabs	Telecommunication Research Laboratories
TV	Television
VSB	Vestigial Side Band
WDM	Wavelength Division Multiplexing

# **1. Introduction**

## **1.1 Communications and Switching**

Human endeavours, ranging from the simplest of interaction amongst people to the most complex of intellectual pursuits, create an ever evolving need for communication. In the fundamental form of conveying information from one person to another through speech or signals, routing of the information is implicit in its transmission. But in the more complicated forms of communications, such as one to many, or from one to another at a distant location, perhaps related via intermediaries, controlled routing of information is necessary to ensure its successful transfer. Thus tele-communications necessitates switching of information in a controlled manner in order to realize the desired transfer of information from the source to its eventual destination.

In our brave new world, information gatherers and hunters, and their myriad communicating machines continuously fuel the need for transmission links with higher capacity in modern telecommunication networks. As soon as a new technological advance or innovation is introduced in the networks, it is utilized to near exhaustion. In the last century, since the invention of communication over conducting paths, the earth has been spanned by metallic conductors carrying signals in the form of electric current. And now, glass fibre cables are fast becoming ubiquitous for transport of many different kinds of information signals. The resulting telecommunication network is the largest infrastructure of any kind in the world and provides a medium to interconnect billions of people worldwide.

And as the flow of information increases in volume, so does the need for controlling and directing the flow such that there are no bottlenecks encountered between the origin and the end.

In electromagnetic methods of conveying information as flow of electrons, switching techniques, ranging from simple mechanical devices which break the path of current to complex crystal semiconductor structures, may be effectively used. The controlling signals which determine the routing paths are electronic as well and the particles (electrons) lend themselves well to be efficiently routed along one conducting path or another (Figure 1.1). But in photonic networks, which employ lightwave particles to carry great volumes of information, routing of signals is not as easily accomplished since the very properties that make photons ideal carriers of information, i.e; low mass and little interaction with the transmission medium, also make them harder to route as desired.

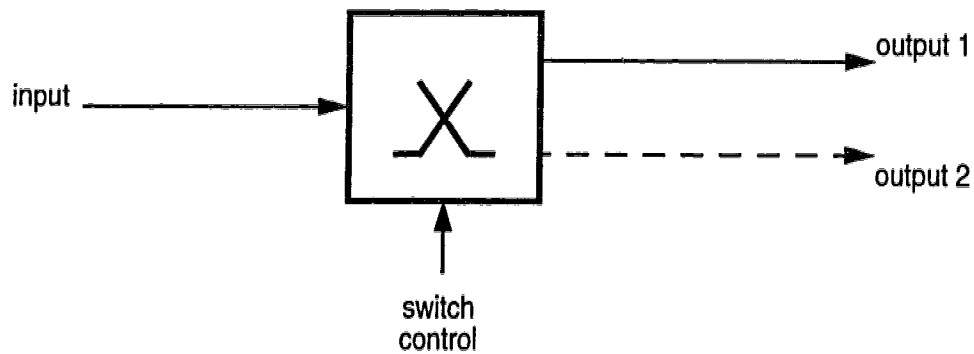


**Figure 1. 1 A signal switch: the input signal can be routed to either output path**

## 1.2 Optoelectronic Switching

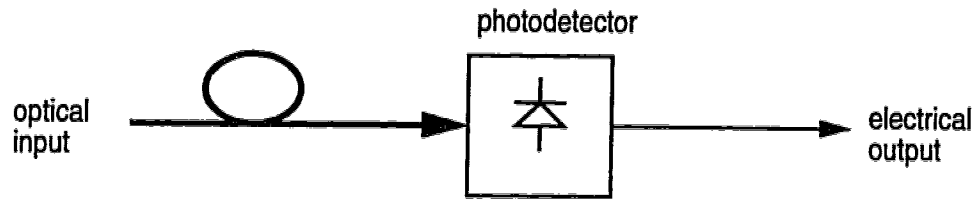
All photonic networks currently utilize optical-to-electronic conversions since the information originates and terminates in electronic interfaces and equipment. Also, since all of the control equipment is electronic, signals which determine the path for routing of signals are also electronic (all photonic or all optical control using optical computation is possible though neither practical nor prevalent in any systems in use today).

Optical-to-electronic conversion of signals (Figure 1.2(a)) is thus necessary in any photonic communication network. Optoelectronic switching techniques aim at utilizing this conversion to achieve the switching function as well (Figure 1.2(c)).

In Figure 1.2(c), it can be seen that any one of the inputs can be connected to any output path by controlling the conversion of the input optical signal. The element where the signal switches paths is called a "crosspoint". The crosspoint corresponding to the signal to be switched is turned 'ON' to detect the light while all others are left 'OFF' so that they are insensitive to the signal.

This topology in which each input optical signal is split and distributed to all output ports and then routed by controlling the signal conversion is the basis of optoelectronic switching [1, 2].

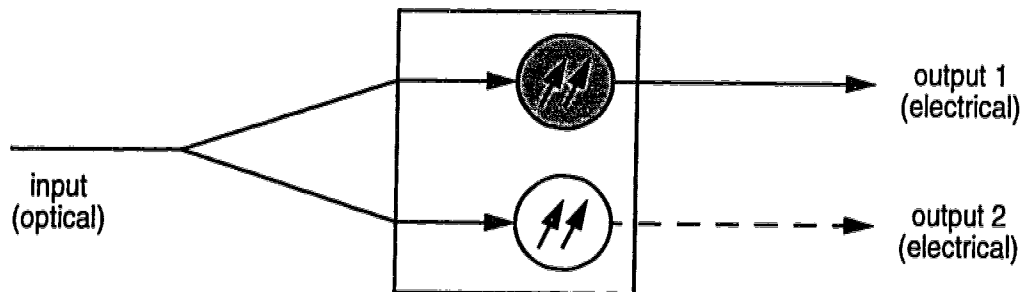
As shown in Figure 1.3, at each input port, the signal is required to be split or 'broadcast' to all the output ports. At the output port, the signal to be switched to that port is 'selected' out of all the (input) signals present at the crosspoints in that port by turning 'ON' the appropriate crosspoint (conversion) element. Thus this technique may also be termed 'broadcast and 'select'. It is pertinent to note



(a) Optical-to-electronic signal conversion



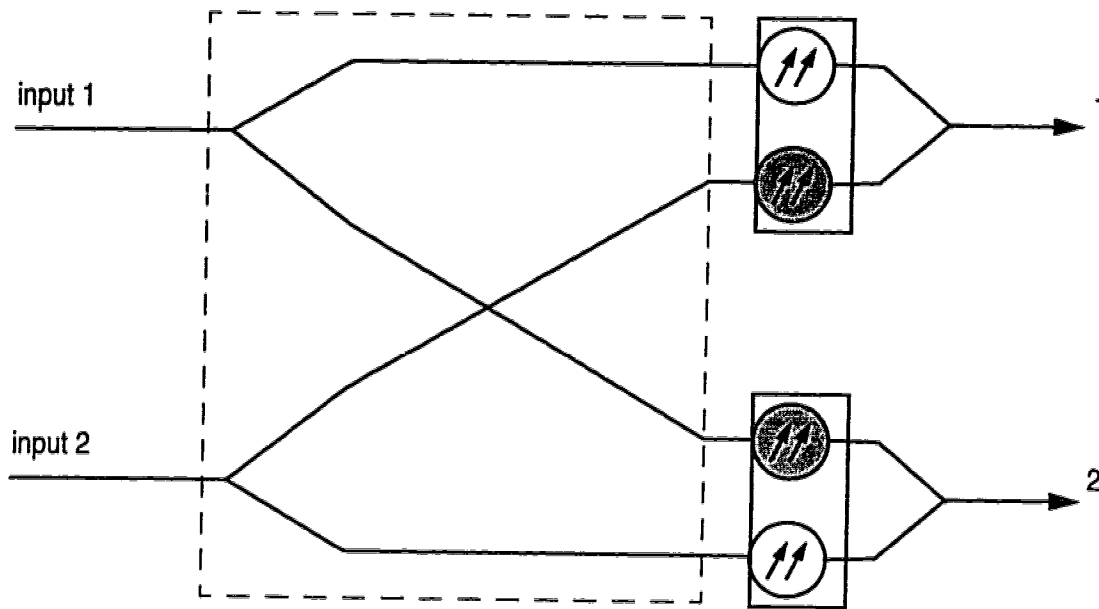
(b) Schematic representation of optical-to-electronic conversion



(c) Optical-to-electronic conversion used to achieve signal switching (corresponding to Fig. 1)

Figure 1.2 Optical-to-electronic signal conversion and its use in signal switching

here that in optoelectronic switching, 'broadcast' is implemented with optical signals (high noise immunity) guided in separate channels (low interference,



input 1 is routed to output port 2, and input 2 is routed to output port 1

**Figure 1.3 A 2x2 optoelectronic switch using optoelectronic conversion based routing**

crosstalk), while the 'selection' is done by choosing the right crosspoint (optoelectronic conversion). Thus, at the output port, since only one signal has been converted to electrical domain, crosstalk or interference of electrical signals is suppressed by eliminating the interfering signals altogether.

At the output port, since only one signal needs to be selected out of the 'N' signals present at that port by switching ON one of the 'N' photodetectors, the array may be designed to permit one output. Thus an array of crosspoints with a single output can be utilized to perform the selection of the desired signal (Figure 1.4). In signal processing applications however (see section 1.3 and 2.4), photocurrent from a number of optical signals incident on the photodetector array

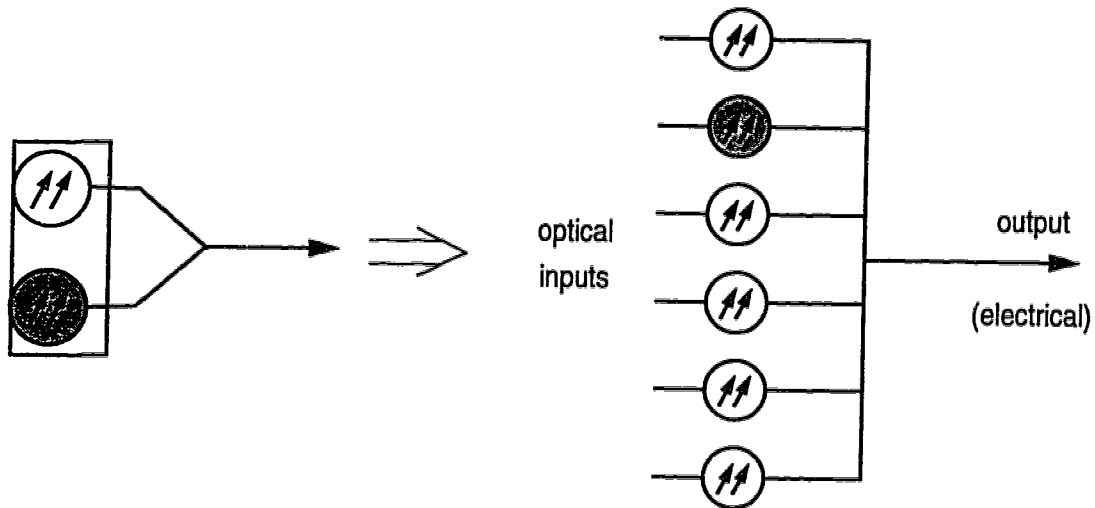


**Figure 1.4 Array of conversion elements (crosspoints) for optoelectronic switching**

may be combined (addition) with the use of such an array. Though almost any kind of photodetector may be used to perform the conversion from optical-to-electrical domain, Metal-Semiconductor-Metal (MSM) photodetectors are found to be especially suitable for the task. Chapter 4 provides a detailed look at the new and unique designs of MSM photodetector arrays prepared for optoelectronic switching applications.

As other components used in optoelectronic switch construction such as laser transmitters or electronic amplifiers are commercially available, development of broadband arrays of detectors capable of providing >10 GHz bandwidth, reported in Chapter 4, eliminates the only technological bottleneck for realizing switches capable of handling the highest data rates in use today - of the order of 10 Gbps and more.



### 1.3 Signal Processing with Optoelectronic Elements

The elements used in an optoelectronic switch: optical fibres, photodetectors for controlled detection of optical signals, and arrays of such devices for addition of photocurrents corresponding to the incident signals, may also be utilized to implement structures suitable for processing of broadband signals [2]. Optoelectronic elements, as shown in Figure 1.5, provide useful

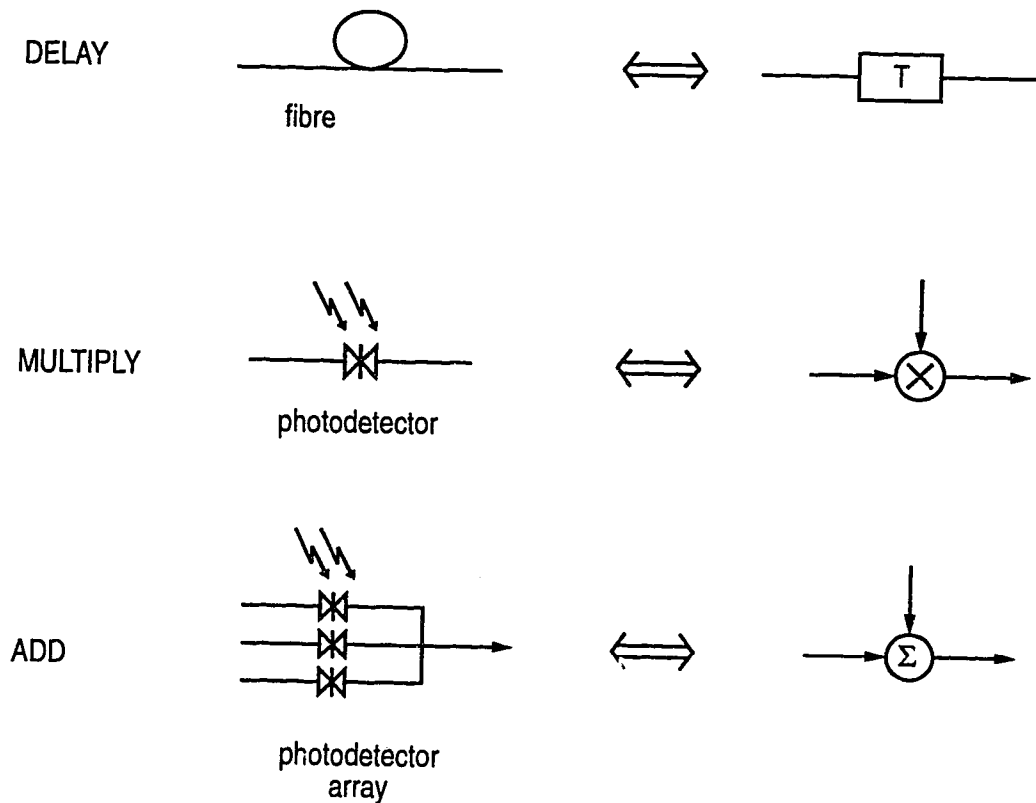


Figure 1.5 Optoelectronic equivalents of signal processing elements

means of processing the input signals via fibres used as delay lines, and

photodetectors used for weighting the input signals. The single output array structure serves to combine the various photocurrent contribution, thus realizing all the elements required in a discrete time signal processor. Optoelectronic processors have the potential for broadband operation, and Chapter 6 describes experiments which demonstrate implementations of reconfigurable filter structures with 1 GHz bandwidth.

## **1.4 A Brief History of Optoelectronic Switching**

The use of controlled optical-to-electronic signal conversions to achieve broadband switching was first demonstrated in 1978 in Canada [1] and has since been developed by other research groups around the world as well [3, 5, 6, 7, 8]. However, it is interesting to note that at the time of its inception, there were virtually no applications for this broadband switching mechanism since there were no information signals with more than a few hundred mega-Hertz bandwidth in use in any communication network. As a result the first few applications were in the area of analog video signals (6 MHz per channel bandwidth). Today, almost two decades later, information signal bandwidths are approaching the potential switching capacities demonstrated in the initial work. Chapter 2 introduces some applications of the broadband switching technology in communication networks as well as signal processing and Chapter 7 presents advanced network applications enabled by the technology.

### **1.4.1 Optoelectronic switching at University of Alberta**

Optoelectronic switching has been a major research area at TRLabs since

1987. Some preliminary work focused on investigating design and construction of matrices using photoconductor device crosspoints [3] in addition to exploring novel applications of the optoelectronic techniques [9] and optical fibre delay lines [10]. Research on novel means of distribution of optical signals ('broadcast' function) has also been initiated [11, 12, 13, 14].

In 1993, a project to fabricate a prototype 10x10 switch was undertaken [4]. This work laid strong foundations for the design and construction of such a prototype while demonstrating laboratory experiments with two channels of the switch. In October 1993, the author joined ongoing efforts to redesign and fabricate the optoelectronic modules, carry out the optics assembly, and to repackage the switch prototype. All redesign and construction work was finished in May 1995 and extensive tests have since been carried out with the prototype in the laboratory. In October, the completed prototype switch was exhibited at Telecom '95 - world's largest exposition of telecommunication equipment, in Geneva, Switzerland. This prototype has served as a testbed for exploring applications such as signal processing (Chapter 6) reported in this thesis in addition to the switching experiments. Following the successful demonstration of the optoelectronic switching technology through the prototype, several new research projects were initiated which aim to further extend the switching capacity achievable with this technique using low cost and compact packaging and integration techniques [15]. Since the current prototype is constructed with discrete optics and electronic components, it also serves as a useful benchmark for performance parameters such as signal crosstalk/interference (in optical or

electronic domain) which may be compromised in some integrated approaches.

## **1.5 Organization of the Thesis**

Techniques to accomplish broadband switching which are related to or compete with optoelectronic methods are described in Chapter 2. This chapter also describes the applications of optoelectronic switching in telecommunication networks in addition to processing of broadband signals. Design and fabrication details of the optoelectronic modules and the transmitter components is described in Chapter 3. Chapter 4 presents the new designs for achieving  $>10$  GHz bandwidths in arrays of MSM devices suitable for switching as well as signal processing applications. Results obtained with the prototype switch are described in Chapter 5. Signal processing results and applications realized with the use of the prototype in the processor configuration are presented in Chapter 6. Advanced network applications of broadband switches are investigated in Chapter 7. Chapter 8 concludes the thesis with a summary of the research project and recommendations for future work.

## **2. Applications of Optoelectronic Switching**

The impetus for an engineering research project must come from the applications that are enabled and facilitated through that research. Communication networks intended for transport of data, voice, or images, require routing elements at every node in the network, which is the fundamental application of a switching mechanism. The first part of this chapter (section 2.1, 2.2) considers this application, and the areas are pointed out where the unique properties of optoelectronic switching make it beneficial over other techniques. A brief overview of other competing technologies for broadband switching of optical signals is provided in section 2.3.

### **2.1 Switching in Communication Networks**

Communication networks can be divided into groups based on the distance covered by transmission links used in the network.

Continent-wide telecommunication networks, Wide Area Networks (WAN)

Local area networks (LAN), Metropolitan Area Networks (MAN)

Short distance interconnects

#### **2.1.1 Continent wide networks**

##### *2.1.1a Network switching:*

Continent wide networks typically consist of long distance links between cities and carry all types of information such as digitized voice signals, data, and analog or digital images. The synchronous optical network standard - SONET is

used to ensure compatibility between the equipment and services provided by different vendors and telephone companies which own or operate these networks. In a network spanning across long distances, the switching capability at each node is required for two purposes - to route the traffic passing through that node as well as select or multiplex the traffic which originates or terminates at that node. Figure 2.1 shows a schematic of a wide area network (WAN) in which each

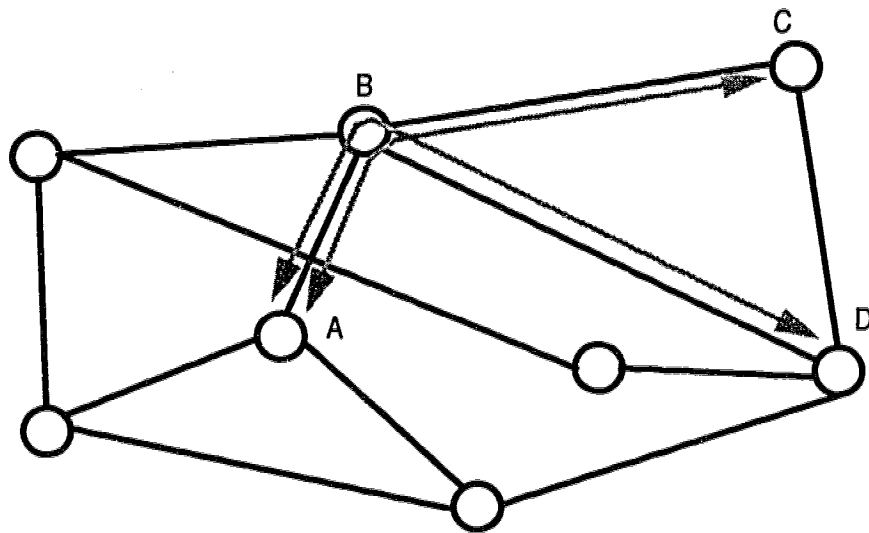


**Figure 2.1 A wide area network (WAN)**

node may represent a city and the whole network may span a continent. For the traffic traversing the network from node A to C or D through node B, switching equipment to route traffic as shown in Figure 2.2 would be required at the node B or any other similar transit node in the network.

Standard data transmission rates in SONET (fibre channels) are given below:

**Table 2.1 SONET data rates**

Optical Carrier (OC) Signal Level	Data Rate
OC-3	155.52 Mbps
OC-12	622.08 Mbps
OC-48	2.488 Gbps
OC-192	9.95 Gbps

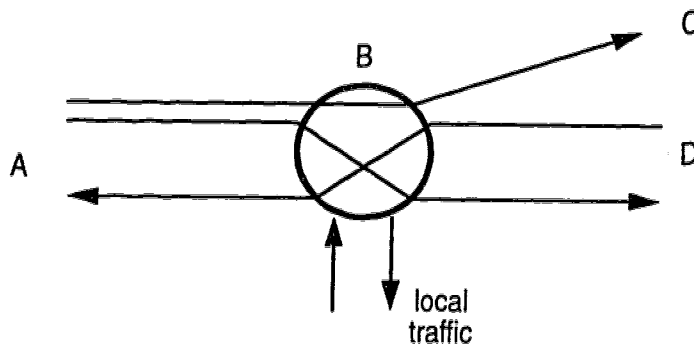


**Figure 2.2 A typical network node with transit and local traffic**

It is clear that broadband switches capable of handling up to 10 Gbps per channel are required in SONET network nodes to route transit traffic. The routing of traffic at the trunk rates is called "cross-connect".

Asynchronous Transfer Mode (ATM) techniques for switching and multiplexing of data have been chosen by CCITT to permit broadband access to networks which would also eventually require broadband switching nodes. Initially, the packet format data for ATM networks will be transported on SONET physical layers using the data rates given above. With the projected continuous rise in ATM broadband subscribers, switches capable of handling very large aggregate data throughputs (>100 Gbps) will be required [16, 17]. One switch

architecture suggested to implement such “Terabit” capacity nodes [16, 18] typically requires a broadband switch core to accomplish fast cross-connection of packet data streams at 2.5 to 10 Gbps (Figure 2.3). This application is considered

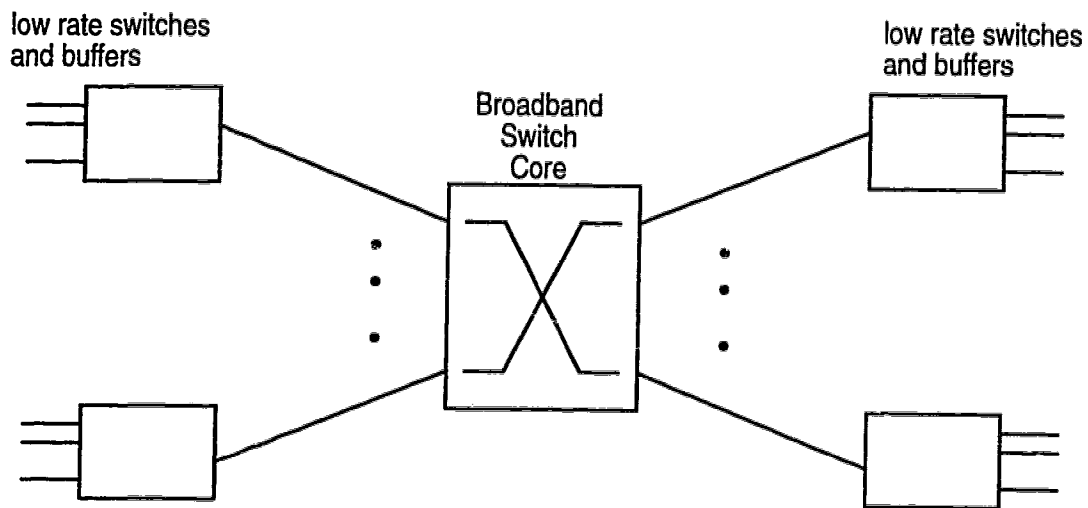
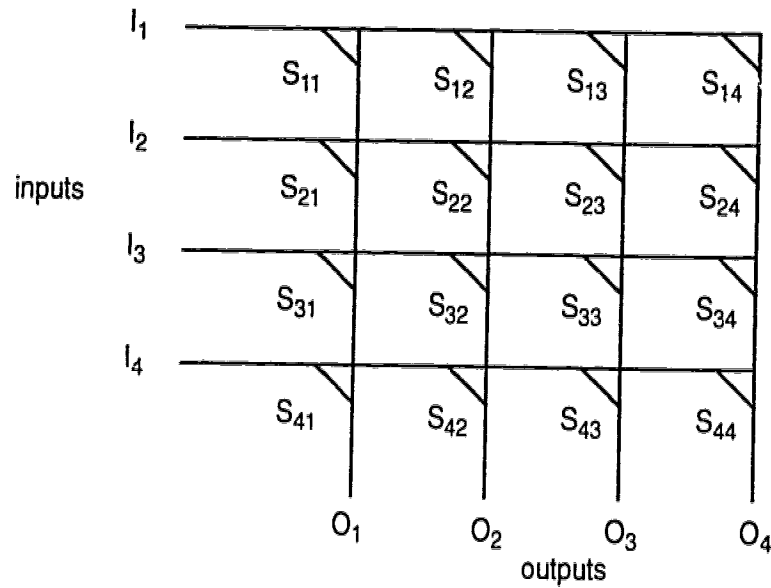



**Figure 2.3 Broadband switch core for high throughput ATM switching applications**

to be the most immediate one as evident in the reported research effort by major international telecommunication companies such as NTT and Nortel. The switch prototype described in this thesis is a suitable candidate for such applications. Nortel Inc., Canada, has recently reported the construction of a partial prototype similar to the optoelectronic switch concept [8, 16] but lacking some key advantages.

The switches required in such applications are also termed ‘crossbar’ switches for historical reasons. Such switches can be used to connect any input to any output in a non-blocking fashion. A general schematic of a crossbar switch is shown in Figure 2.4. Such a switch is called a “crosspoint” matrix.





 = crosspoint switch  $S_{ij}$

**Figure 2.4 A crossbar switch matrix**

The function of a network of crosspoint switch matrix can be described as a vector-matrix multiplication operation:

$$O_j = \sum_{i,j} W_{ij} I_i \quad (\text{Eqn 2.1})$$

Closing switch (or crosspoint)  $S_{ij}$  connects input  $I_i$  to output  $O_j$  with the weights  $W_{ij}$  being "0" for  $S_{ij}$  being open and "1" for  $S_{ij}$  closed. The two primary properties of a crossbar switch are that (i) only a single connection needs to be made to connect or disconnect an output from the input and (ii) the switch is non-blocking which implies that new connections between unused nodes can be made without changing or affecting the existing connections. Also, broadcast of any

input signal to all outputs is possible by setting all the appropriate  $S_{ij}$  switches to 'ON' in the row corresponding to the input signal to be broadcast. The application of such a switch to signal processing (section 2.4) follows as a direct result of the capability to execute the vector-matrix product (Equation 2.1) at a rate determined by the bandwidth of the signal path in the switch.

Results demonstrating the suitability of the optoelectronic prototype switch to various network routing applications are described in Chapter 5.

#### *2.1.1b Network restoration*

The switches used in a network can also be utilized to reconfigure the network in the event of a failure of a link. Dynamic restoration of all traffic being transported on the network with little or no loss of data is possible with the use of broadband cross-connect matrices capable of rerouting the affected data on to other links with spare capacity [19]. Figure 2.5 shows a schematic view of such a scenario where the link between nodes B and D is not operational and broadband switching capability would be required at node B to route the affected data (A to D) through other links (B to C), avoiding the failed link. This application is investigated in detail in Chapter 7. Powerful algorithms and protocols for implementing the restoration strategies have been suggested [20, 21] and the use of optoelectronic switching matrices is proposed in this work for the purpose of providing a physical medium in implementing advanced network restoration methods.

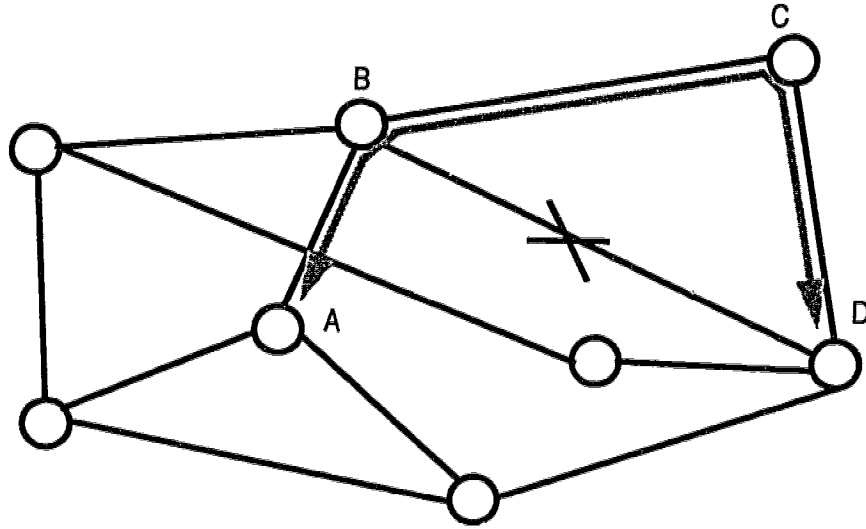


Figure 2.5 Network restoration switching

### 2.1.2 Local area networks

Networks for signal distribution and interconnection of equipment over areas within a typical city may be divided into two categories based on the type of signals carried over these communication networks.

- Digital Data Networks, and
- Cable TV Networks

“Digital data networks” refers to the medium and methods for interconnecting computers and computer networks while CATV networks primarily provide switched broadcast (downstream) services, and in some cases, such as Hybrid Fibre-Coaxial (HFC) networks, upstream communication paths for digital data.

### 2.1.2a Digital data networks

The rapid growth in the area of computers and computer networking is quickly outpacing existing technologies for transporting data over short distances between computers in a local area network such as an Ethernet. Technologies such as fast Ethernet and FDDI provide a maximum of 100 Mbps data rates for local area networks [22]. New and evolving techniques and standards to permit data transport at 1 Gbps and beyond are being developed. The most promising of these are listed below along with the channel bandwidth available with each technique:

GigaRing Channel [23]	6.4 Gbps
HIPPI [24]	800 Mbps
HIPPI-6400 [25, 26]	6.4 Gbps
Fibre Channel [28]	1 Gbps
SCI (Scalable Coherent Interface) [29]	8 Gbps
Myrinet [30]	1.28 Gbps
GigaNet [31]	622 Mbps (OC-12c)
ATM [32]	622 Mbps (OC-12c)

The most ambitious of these proposals is the HIPPI-6400 standard under preparation [26] which is the successor to the ANSI standard (X3T9.3) HIPPI (High Performance Parallel Interface) interface which provides 800 Mbps switched, non-blocking, point-to-point networking. HIPPI-6400, the next generation, extends the data rate to 6.4 Gbps [25]. To provide the required switched connections, switch fabrics capable of handling these data rates are

needed. Electronic solutions for switching are available up to a maximum data rate of 2.6 Gbps [33]. This rate is almost at the limit of electronic data switching capability. Also, since the transmission medium is optical fibre, switches capable of routing optical signals would be required for these fast data networks.

Other standards such as "Fibre Channel" or SCI (Scalable Coherent Interface) also plan for ultimately extending the data rates up to 4 Gbps though current proposals are much more modest (200-400 Mbps over copper).

High speed, high throughput data networks like the ones mentioned here will require cost efficient broadband switching technologies which are flexible enough to handle different data rates and formats as well as mixed transmission media (copper and multi mode or single mode fibre). Optoelectronic switching technology which can provide all the required capabilities, including either electrical or optical inputs, is especially suitable for such data network applications. Even though the data/packet formats and rates are likely to be different, optoelectronic switching provides a completely format-independent routing mechanism usable in all these networks. Chapter 5 presents results for different rate digital signals and analog signals transmitted simultaneously through the prototype switch which confirm the format transparency. This ability to handle different data rates and formats also imparts an invaluable capability to route legacy signals in the transition phase of the network while offering a convenient path for future upgrades without a change in the switching hardware.

Applications such as gateway switches to other networks which may have different formats and data rates, can also be envisioned for the bit rate and format

transparent optoelectronic switches.

### 2.1.2b Cable TV networks

CATV networks such as Hybrid Fibre-Coaxial (HFC) networks which carry mixed analog and digital CATV signals over trunk and distribution areas typically serviced by a cable TV provider (now also providing data services through cable modems) are another prime area of application for format transparent switching.

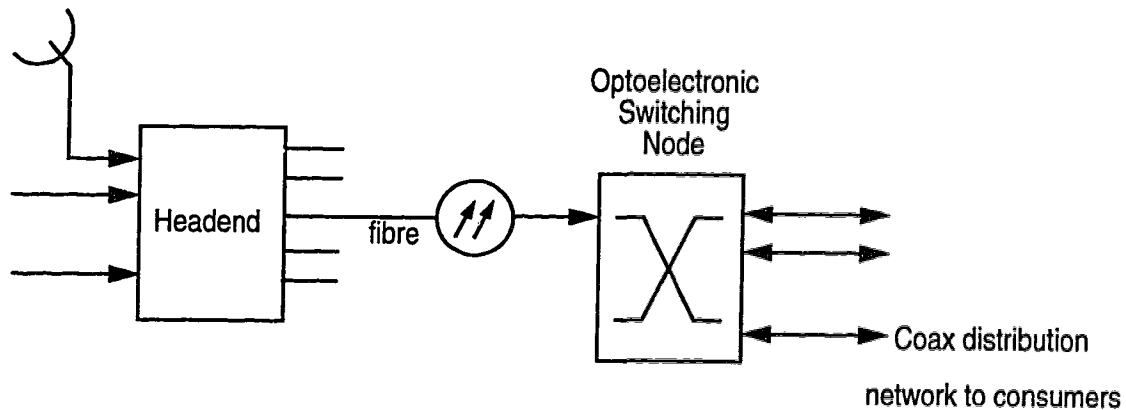


Figure 2.6 Hybrid Fibre-Coaxial cable network

HFC networks (Figure 2.6) are expected to carry both conventional analog TV signals, (NTSC or other standard video signals) as well as digitally encoded, high quality video signals (High Definition TV - HDTV signals), in addition to low rate digital data (tens of Mbps). Switches for these networks would require a 'broadcast' capability as well as format transparency (digital/analog signals). Optoelectronic switching fulfils these key requirements while providing ample bandwidth for switching of multiple video channels (the prototype's 1.25 GHz

analog bandwidth can accommodate more than 200 standard analog channels (NTSC, 6 MHz channel bandwidth).

### **2.1.3 Short distance interconnects**

Fast communication links are required between equipment which may need to be interconnected at distances as large as 1-2 km for rack-to-rack interconnects or as small as a few cm for board-to-board interconnects. The distinction between a LAN and an interconnect is admittedly unclear and some functions would overlap since the distances covered are similar. However, the distinguishing feature of interconnects is that they serve as fixed or dedicated links between two pieces of equipment which may form part of a larger system.

The technologies required for implementing photonic interconnects are similar in topology and requirements [34] to the optoelectronic prototype switch, which indeed performs all the functions required of an optical interconnect. In fact, the 10x10 optoelectronic matrix switch is also a fully reconfigurable optical interconnect since the optical distribution implemented in the switch with fibres may be stretched to 1-2 km distances to form a distributed switch. In most cases, the distances to be covered for rack-to-rack interconnects are < 100 meters. Again, the bit rate and format transparency properties, coupled with the low cost of the components (see section 3.4) required for implementation make optoelectronic matrices an attractive candidate for high bit rate reconfigurable optical interconnects [35].

Optical broadband signals can be switched with a number of other technologies, some of which are commercially available while most are under

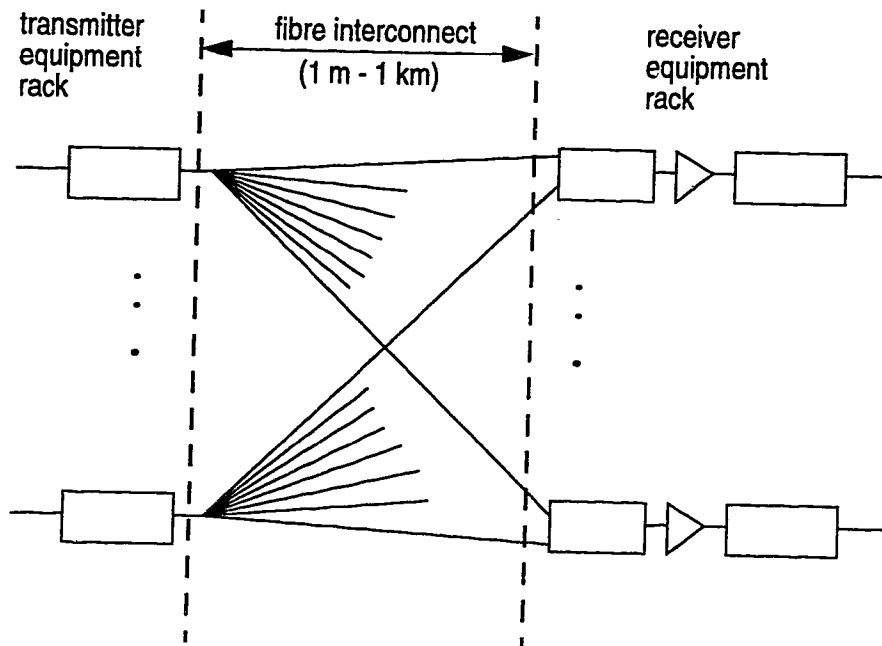


**Figure 2.7 Optoelectronic matrix switch as a reconfigurable distributed optical interconnect**

development. The next section provides a brief overview of these technologies and their salient features in comparison to optoelectronic approaches.

## **2.2 Other Switching Techniques for Optical Signals**

### **2.2.1 Optical switching**

Photonic switching technologies constitute a rapidly expanding research and product development area following on the heels of progress in fibre optic transmission systems. A variety of techniques have been developed to switch optical signals including the ones noted below, though none has found widespread acceptance and/or commercial use. Photonic switching techniques which aim at controlling flow of photons (usually referred to as all-optical



switching, see [36] for complete nomenclature) are constrained by fundamental physics in achieving practical dimensions or performance objectives [37, 38, 39]. The weak interaction between photons in a transparent transmission medium - which makes photons ideally suited for low loss, long distance information transmission, makes it equally difficult to achieve efficient ways of routing photons in controlled paths. Currently reported research and commercially available optical switching devices generally fall into one of the following categories:

Guided Wave Integrated Devices [40]

Semiconductor Optical Amplifier (SOA) Switches [41, 42]

Optomechanical Switches [43]

Thermo-Optic Polymer Switches [44]

Semiconductor Directional Switches [45]

Electro-Optic Polymer Switches [46]

Optical Beam Steering based Switches [47]

A comprehensive description of these approaches can be found in [48]. Although all of these technologies provide an optical through path, they suffer from other limitations (see Table 2.2 below). The primary reason for using all optical switches is complete signal transparency and the potential bandwidth, though their use for many applications in telecommunication networks is generally neither practical nor cost efficient [39, 49].

**Table 2.2 Comparison of switching technologies (after [50])**

Switch Type	Cost	Loss	Contrast	Speed
Opto-mechanical	Low	Low (<1 dB)	High (>80dB)	Slow (ms)
Lithium Niobate	Medium	Medium (<5dB)	Medium(~20dB)	Fast (ns)
SOA Switches	High	Low (<1dB)	High (>40dB)	Fast (ns)
Semiconductor Based	Medium	High (>6 dB)	Medium (~15dB)	Fast (ns)
Thermo-optic Polymer	Low	Low (<1 dB)	Medium (~20dB)	Slow (ms)
Electro-optic Polymer	Low	Medium (3-6dB)	Medium (~15dB)	Fast (ns)
Free-space Switches	Medium	Low (<3 dB)	Low (~10dB)	Slow ( $\mu$ s)
*Optoelectronic Switch	Low	Low (<1dB)	High (>60dB)	Fast (ns)

Within the limitations of a photonic network bounded by electronic interfaces which necessitate the use of optical-to-electronic conversions, optoelectronic technology introduces no new constraint [48], and provides complete signal transparency as proven by the results obtained (see Chapter 5) with the implementation of this technology with the prototype 10x10 switch.

### **2.2.2 Other optoelectronic switching approaches**

Some other variations of optoelectronic switching techniques have also been reported in literature, and follow a similar philosophy or derive from the technology utilized in this work. Notable among these are the approaches published by Nortel Inc. to fabricate a terabit switch prototype [8], and Hughes Research Labs in developing high isolation switch matrices for radar signals [5]. The next generation switching system under development at AT&T (now Lucent

Technologies) also uses a similar approach though implemented with different devices [51, 52]. All three of these methods utilize optical-to-electronic conversions in a controlled manner to implement switching of input optical signals.

## 2.3 Signal Processing Applications

The use of optoelectronic matrices for signal processing applications such as tunable filters and neural networks has been proposed in the past [53]. Since the hardware required for implementing a matrix processor and a broadband optoelectronic switch is substantially similar, the prototype is designed to accommodate both functions. In fact, the prototype switch may be considered a subset of the more general matrix processor as all the capabilities required for routing of broadband signals are available in an optoelectronic matrix processor.

### 2.3.1 Optoelectronic matrix processor

Optoelectronic elements to implement signal processing functions of delay, multiplication, and summation were introduced in Chapter 1 (section 1.3). By combining these elements as shown in Figure 2.8, the impulse response of a discrete time signal processor given below can be realized:

$$h(t) = \sum_{n=-\infty}^{\infty} a_n \delta(t - nT) \quad \text{Eqn. 2.2}$$

In the optoelectronic matrix, the input signal is launched on a fibre and an n-way splitter is used to distribute it to photodetectors which serve as multiplication elements ( $a_n$ ). [10] has demonstrated a transversal filter based on

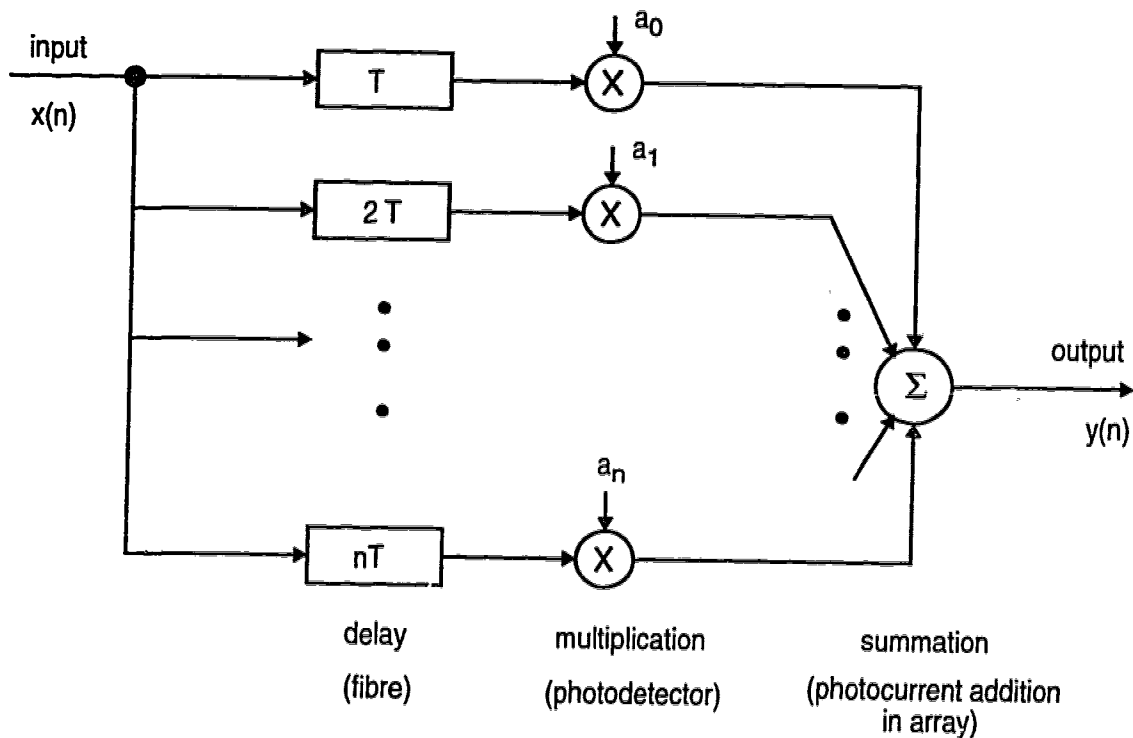


**Figure 2.8 Optoelectronic signal processor structure**

such a structure, and [4] describes partial implementation of a optoelectronic matrix processor.

This work extends the signal processing applications work and results are presented in Chapter 6 from the experiments conducted with the optoelectronic matrix processor to implement a variety of reconfigurable filter structures.

### 2.3.2 Artificial neural networks

The use of optical and optoelectronic information processing based on neural network models is becoming increasingly popular [54, 55, 56, 57, 58, 59, 60], due to the potential for massive parallelism. Most artificial neural network architectures seem to mimic the working of the human brain by using highly

interconnected processing elements to accomplish complex computations and processing tasks. One of the architectures in particular - Hopfield Neural Networks, which utilize interconnected simple analog processors to solve a variety of optimization problems [61, 62], is of interest for possible implementation using optoelectronic elements.

The architecture and elements of the optoelectronic matrix are uniquely suited to implementing the Hopfield neural networks at a processing rate which is much faster than the speeds currently achievable by conventional electronic means. Although simulations to gain an insight into the behaviour of Hopfield neural networks were carried out, this work is not reported here as hardware implementation of the network for a demonstration was not possible in the time allocated for this project.

### 3. Design and Construction of Prototype Switch

The prototype switch constructed to implement the optoelectronic switching technology is described in this chapter. Design details and characterization tests carried out on different modules in the prototype are presented in section 3.2 and 3.3. Requirements for extending the work to 10 GHz bandwidths per channel are discussed, and the key technology issue to be solved for achieving this target is introduced in section 3.4.

#### 3.1 Prototype System Overview

The prototype crossbar switch was designed to have ten broadband inputs and ten corresponding outputs as shown in Figure 3.1. For ease of

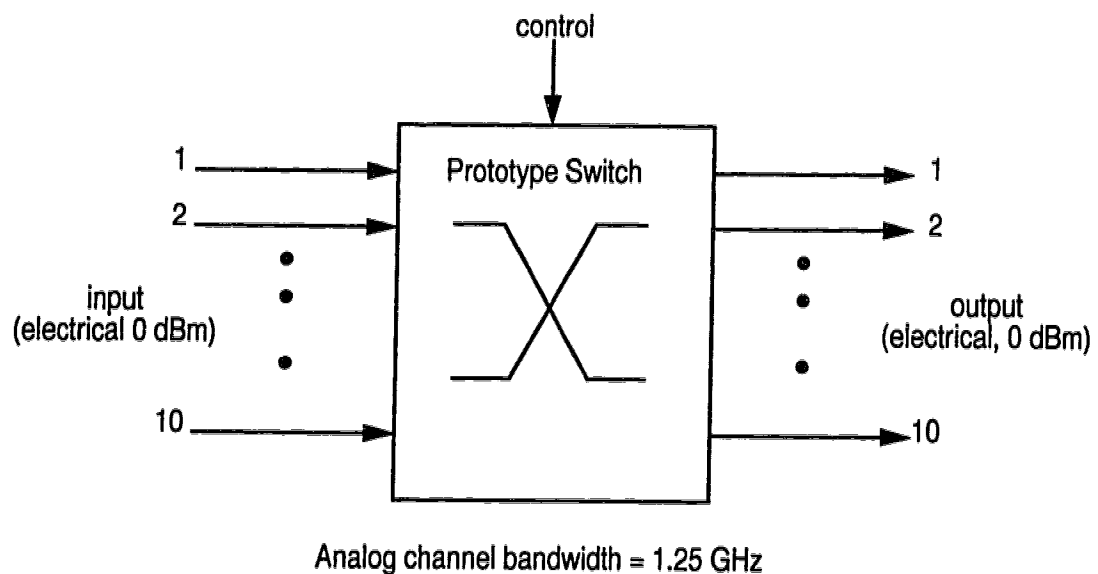


**Figure 3.1 Prototype broadband optoelectronic switch system**

characterization and testing of the switch, the inputs and outputs are electrical signals and the nominal power level at the input is chosen to be 0 dBm (50  $\Omega$  input

impedance) which is sufficient to drive the lasers in the input port section. The output signal power level is adjusted to 0 dBm, providing an insertion loss of 0 dB, and allowing a subsequent switching stage of a similar design to be used. Details of other components in each channel path in the switch are provided in the next section. The control information for the switch is supplied through a portable computer using a custom program described in [63].

Previous implementations of optoelectronic switching techniques [3, 4] have focused on solving some of the difficulties associated with developing reliable devices for use as crosspoints [3] or towards implementation of the switch as a reflex signal processor [4]. The design and construction of the current prototype was initiated with the project reported in [4]. The project reported in [4] was the point of departure for the design and construction of the current prototype. The project succeeded in demonstrating two channels as a laboratory experiment. Extensive redesign of the following subsystems was required to fabricate the prototype switch:

- Optoelectronic Module

- Wideband amplifiers for use with optoelectronic modules

- Laser Transmitters

Figure 3.2 shows a schematic diagram showing the above mentioned modules in each channel. The 10x10 prototype switch contains ten such channels (Figure 3.1). The input signal shown at the left in Figure 3.2 modulates the laser diode to produce an optical signal. This signal is split into ten signals through the 1x10 optical splitter and then the fibers are rearranged such that each output port

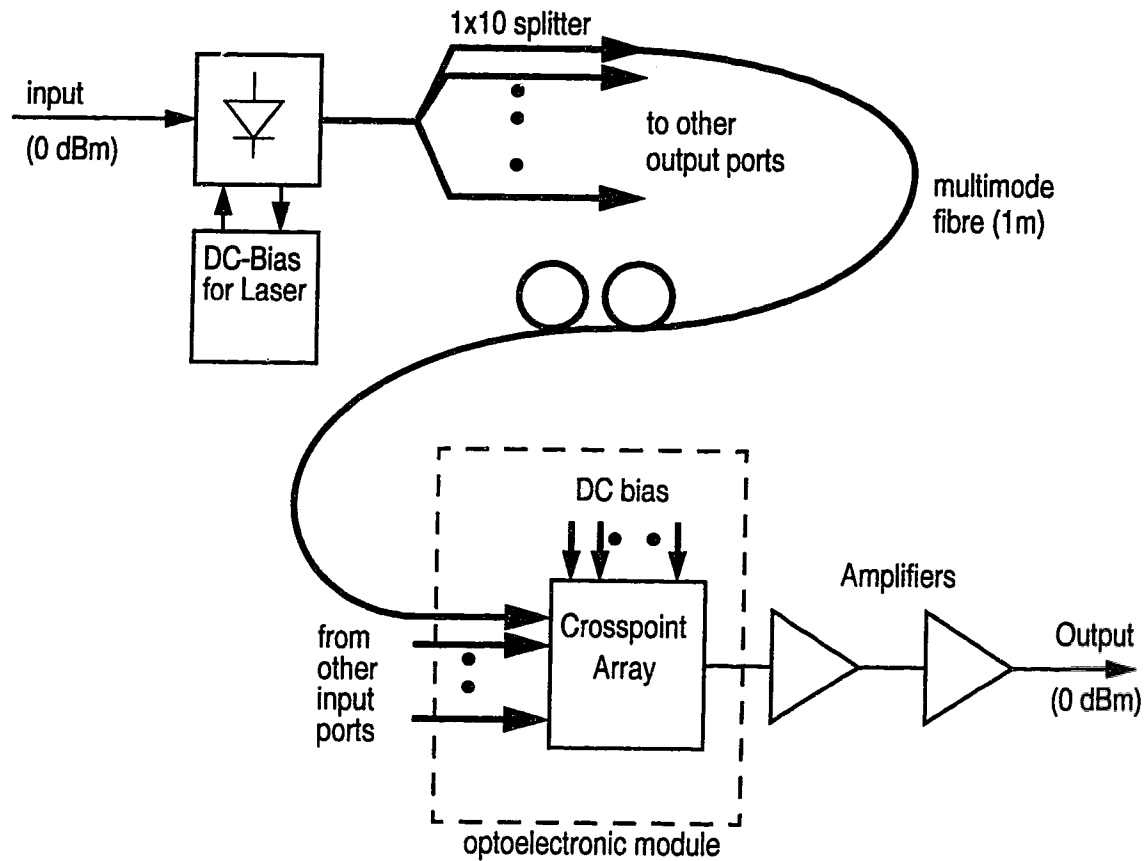


**Figure 3.2 Broadband signal channel in the prototype switch**

receives one optical signal each from every input port. The optoelectronic module is used to 'select' one out of the ten signals incident on the photodetector array by biasing ON the appropriate photodetector in the array, while leaving all others in the OFF state.

Power supply modules and other minor components used in the construction are not shown in this schematic.

### **3.2 Optoelectronic Modules**

The optoelectronic receiver module is designed to accept ten optical signal inputs (on optical fibres) which are incident on a photodetector array. The control



inputs for the ten photodetectors in the array are generated with D/A converters in the module. A single broadband (RF) signal output is coupled out of the detector array through an amplifier chain (56 dB) to the output port.

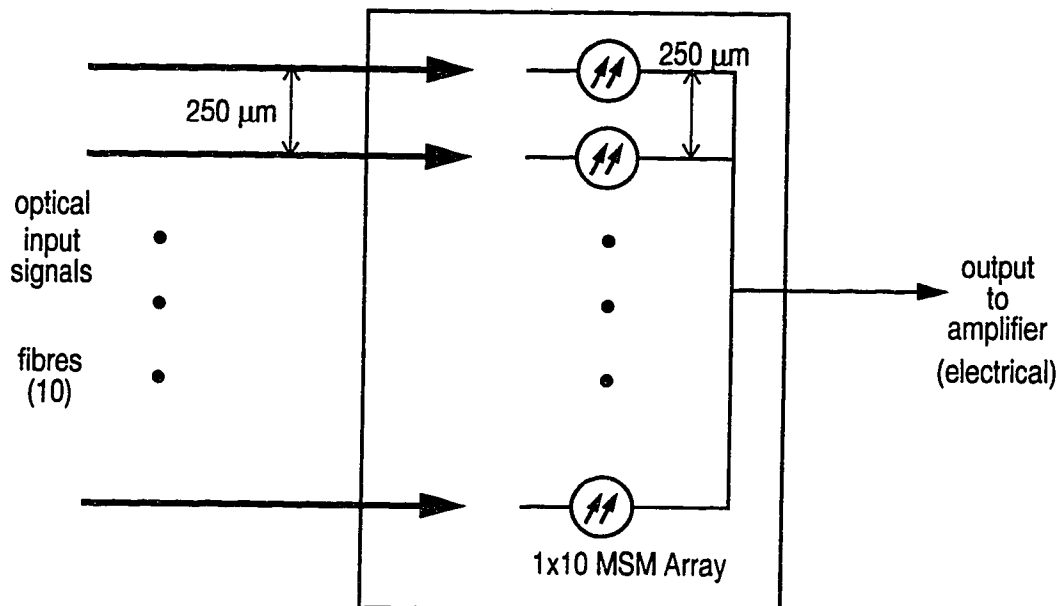


**Figure 3.3 Optoelectronic module schematic**

The photodetector array is coupled to the ten optical inputs (standard multi-mode fibre). Since the fibres in a standard ribbon arrangement are spaced at 250  $\mu\text{m}$  pitch, these arrays were designed to have the same photodetector centre-to-centre spacing. Cleaved fibre ends were placed in a Silicon micro-machined “v-groove” chip such that the fibres are at the same spacing as the photodetectors. Figure 3.4 shows the end view of the v-groove chip with fibres placed in the etched grooves. The Si v-groove holder is actively aligned to the photodetector array by monitoring the photocurrents from the MSM photodetectors at each end while the assembly is positioned for maximum photocurrent. The active alignment

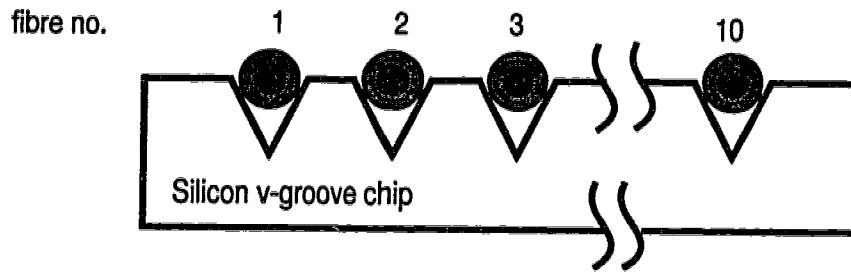


**Figure 3.4 Silicon v-groove assembly for fibre placement in the optoelectronic module**

was accomplished by illuminating the two end fibres in the v-groove holder and monitoring the photocurrent from each of the photodetectors while moving the v-groove assembly to get maximum current output. Individual contributions from the two photodetectors were monitored alternately by biasing them in turn.

DC bias voltage to each detector is supplied through a circuit which is designed to permit fast switching of the bias (see section 4.2 for more details). The bias circuit exhibits a 3 dB bandwidth of 210 MHz and thus can permit switching of the bias with approximately 5 ns response time, which is well matched to the switching time of the photodetectors [2]. In the current prototype, the switching speed for the bias is limited by the speed of the controller software [63].

With the constraints imposed by the optical assembly and the bias circuit, an optoelectronic module designed to sit upright on the circuit cards was conceived as shown in the schematic diagram in Figure 3.5.

The MSM photodetector array chip is required to be placed on a suitable

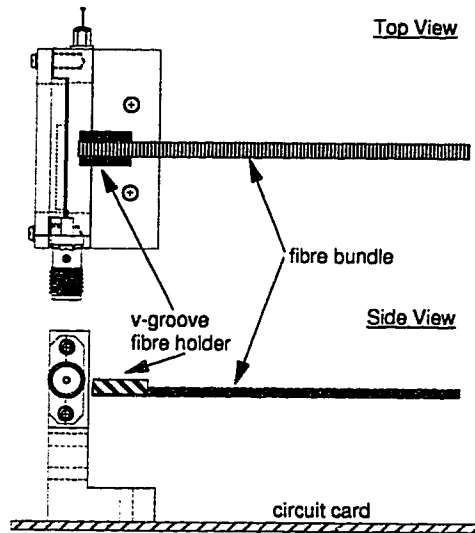


**Figure 3.5 Schematic view of optoelectronic module on circuit card (the fibre bundle terminates in the v-groove fibre holder shown in Fig. 3.4)**

substrate to interface with the dc bias circuits as well as to allow means of coupling the RF signal output to the amplifier chain. This substrate is required to have good microwave properties to permit fabrication of microstrip transmission line output. The substrate material is chosen to be TMM-3™ [64] which has a dielectric constant of 3.25 and also provides ceramic-like mechanical properties which are desirable since the photodetector chip is wire bonded on this substrate and good mechanical properties are necessary to achieve reliable wire bonds. The design for this substrate which provides ten decoupled dc bias lines and a micro-stripline for the output signal is shown in Figure 3.6 below.

A schematic of the substrate with the surface mount components in place is shown in Figure 3.7 below. In addition to the microcapacitors (82 pF) used for decoupling the AC signal from the DC bias line, two more stages of capacitors (1 nF and 10 nF) were added to provide immunity against noise from the DC bias

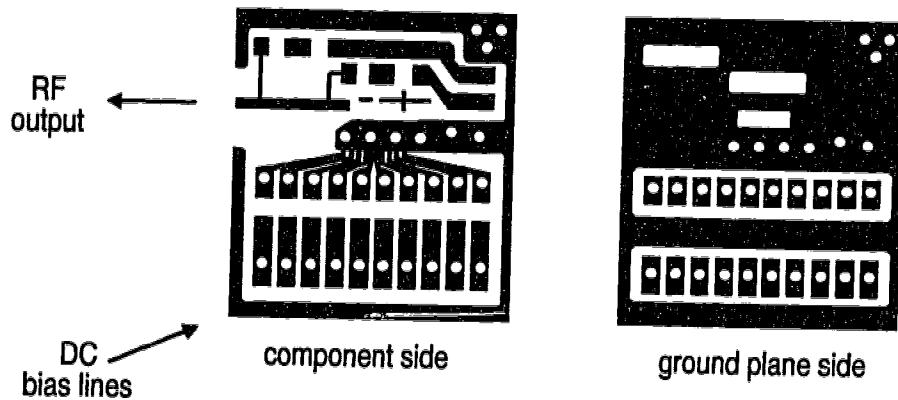


**Figure 3.6 Substrate design for optoelectronic module**

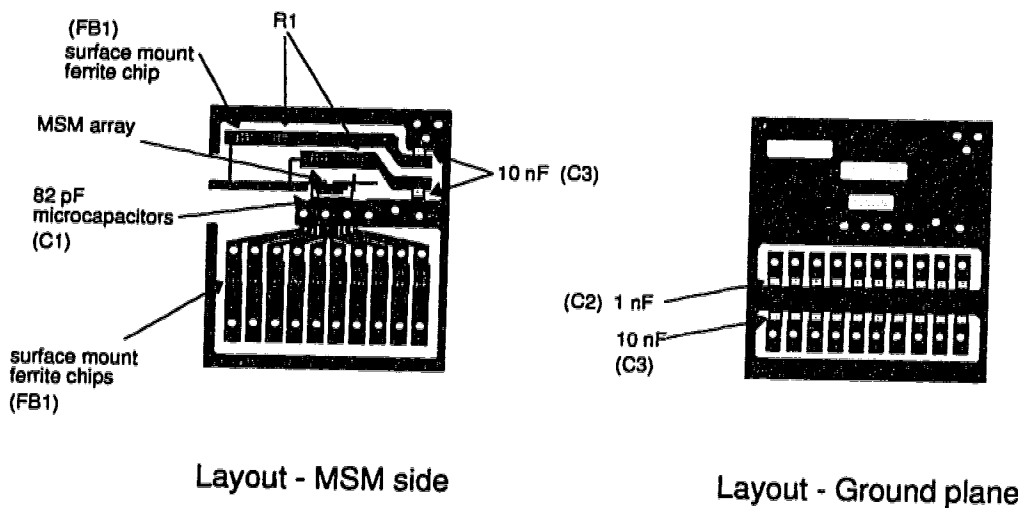


**Figure 3.7 Substrate with surface mount components**

lines. These capacitors are placed on the back of the substrate (ground plane side) as shown in Figure 3.7.

The mechanical assembly designed to hold the substrate shown above and to support the v-groove Si chip fibre holder is shown in Figure 3.8. The

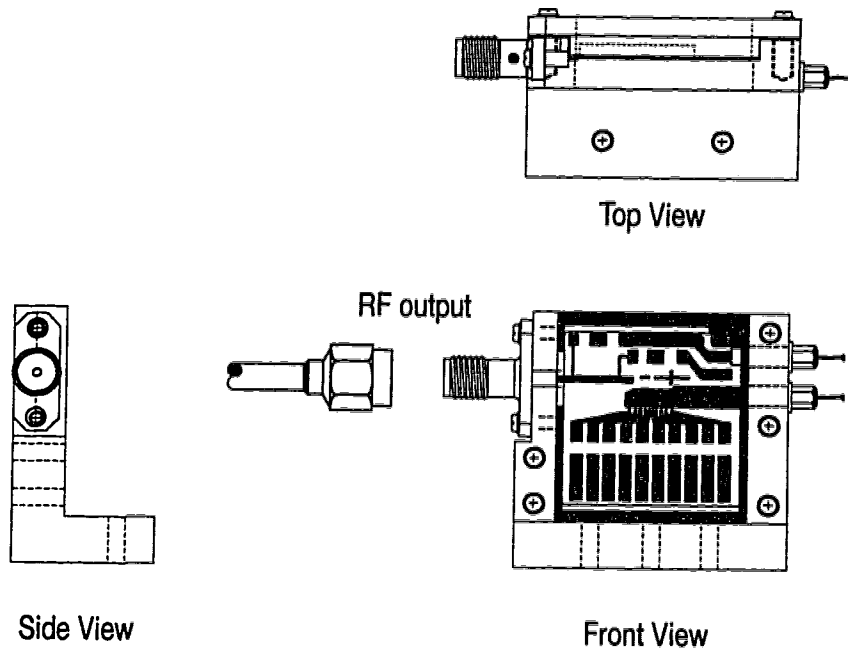


**Figure 3.8 Housing for the optoelectronic module: front, side and top views (substrate of Fig. 3.6 is shown mounted in the assembly)**

detailed drawings for the fabrication of this component are attached in Appendix A.

A schematic arrangement for the optoelectronic module along with the follow on amplifiers is shown in Figure 3.9, and a photograph of the module with the substrate is shown in Figure 3.10. Eleven such modules were built for the prototype switch, and more than five modules were built for testing

The amplifiers for providing a total of 56 dB signal gain over a bandwidth of 300 kHz-2.25 GHz were designed at TRILabs and constructed by the author using a packaged microwave monolithic integrated circuit (MMIC) based design. Details of the amplifier construction can be found in [63]. A photograph of a complete output port card with the optoelectronic module, fibre bundle input, and the amplifiers in place is shown in Figure 3.11.

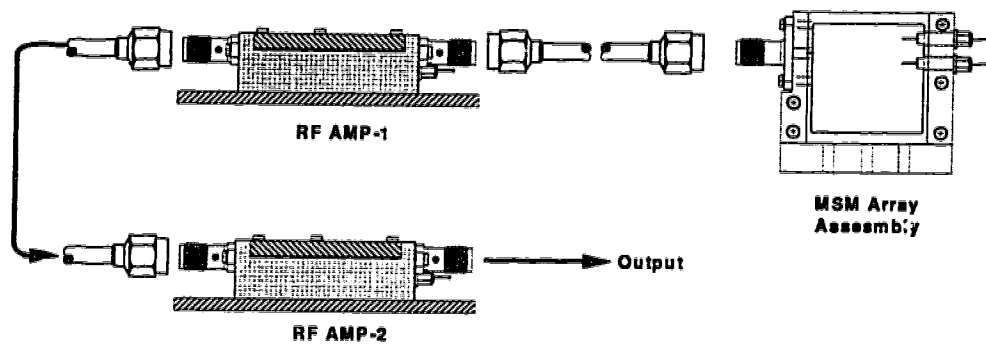


**Figure 3.9 Schematic view of optoelectronic module with amplifiers. RF-AMP 1 is the first stage amplifier, and RF-AMP 2 is the second stage. Together they provide 56 dB of gain over 2.25 GHz.**

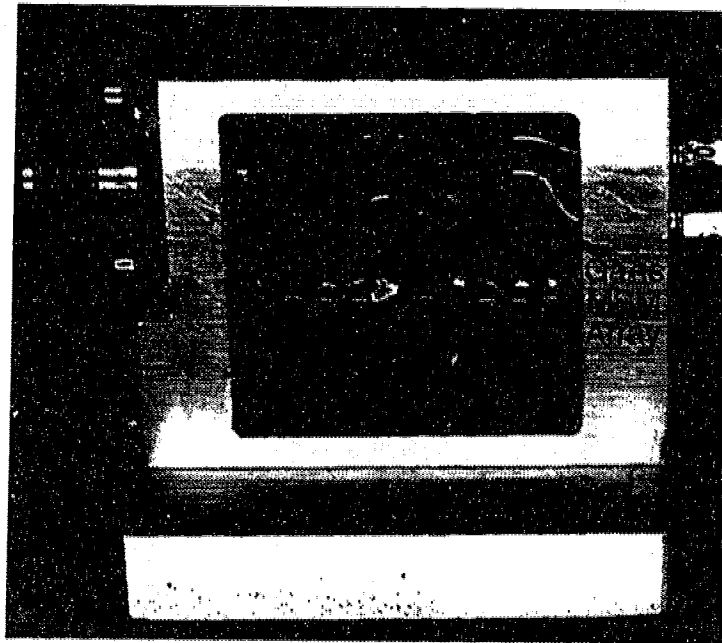


**Figure 3.10 Photograph of the optoelectronic module with substrate**

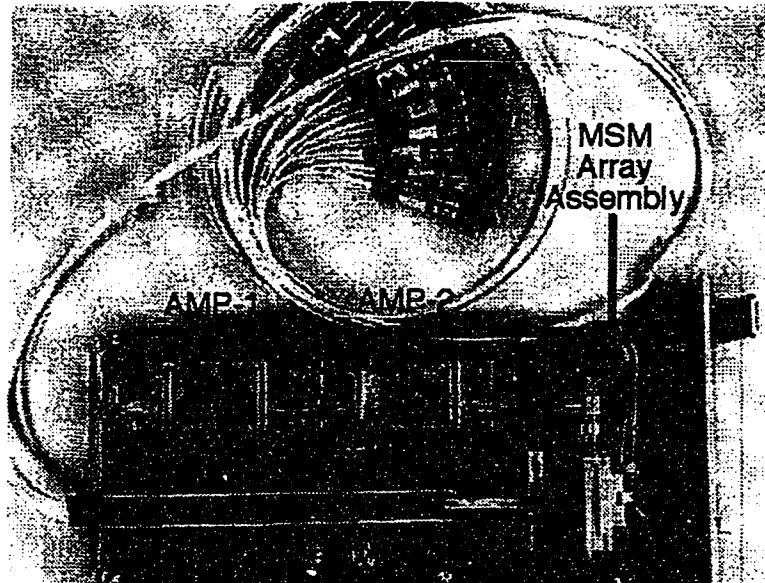


**Figure 3.11** Photograph of an output port card with fibre input and electrical output

### **3.3 Laser Transmitter Response**

The initial design for the laser transmitter bias tee (which combines the RF drive signal and the dc bias for the laser diode) exhibited a frequency response limited to  $< 500$  MHz due to the high inductance and other parasitic reactances in the laser package (Figure 3.15(a)).

The microwave portion of the circuit was modelled using the Hewlett Packard Microwave Design Software and Figure 3.12 shows the circuit used in the simulation. Simulated and measured S11 parameters for the circuit are shown in Figure 3.13(a) and 3.13(b) respectively. From the simulations, it was determined that a section of the layout in the bias-tee was causing extra inductance in the ground path (Appendix B). Since the substrate layouts could not be changed, different equalizing circuits were tried to extend the frequency

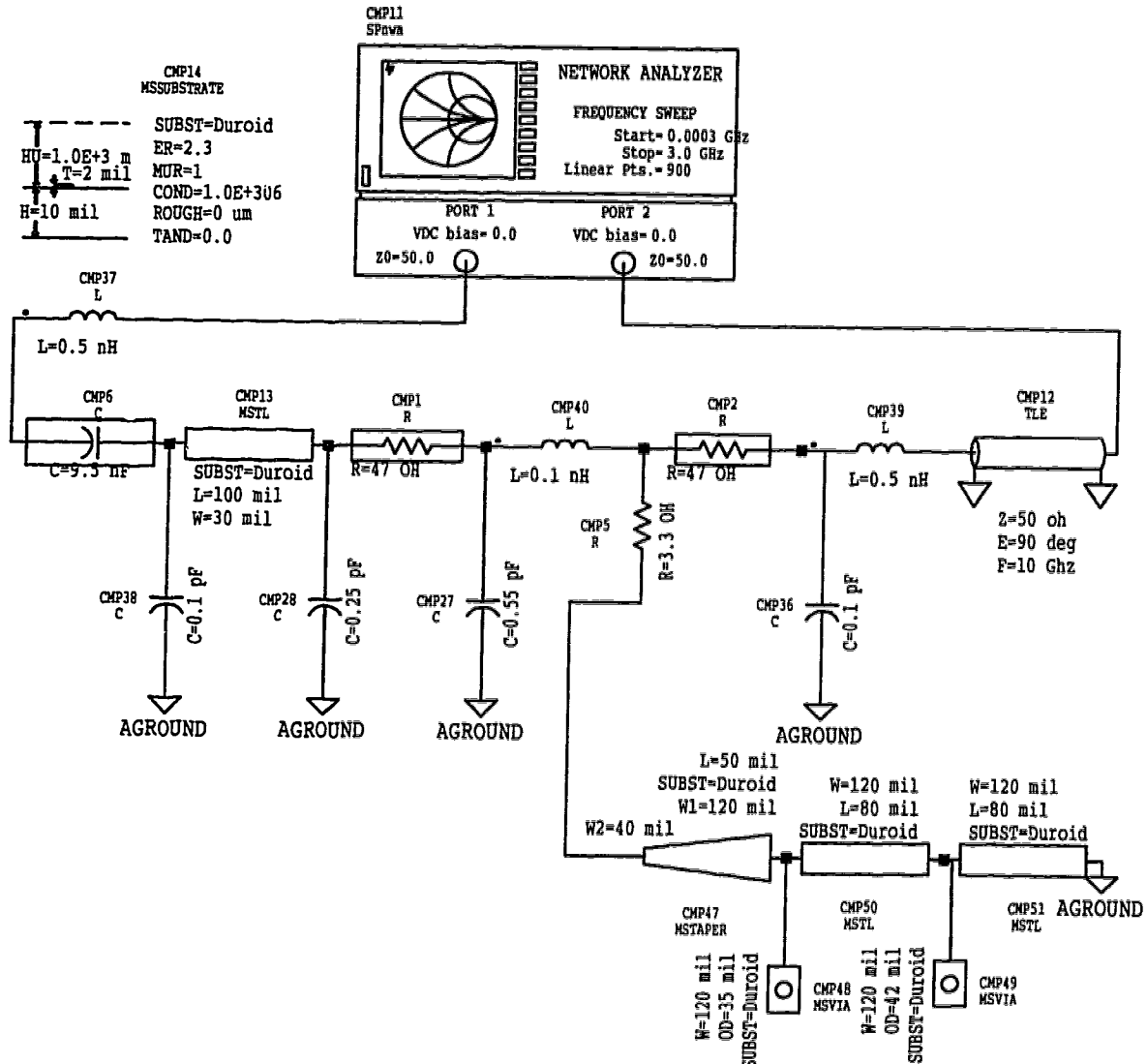
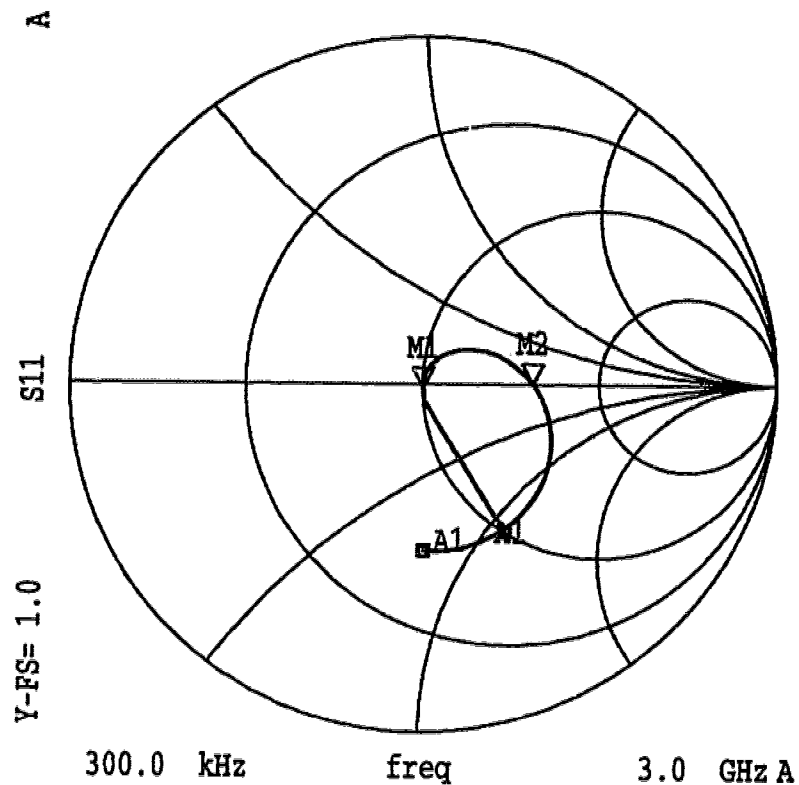


Figure 3.12 Simulation circuit for laser bias-tee

response, and the combination of 2.2 pF and 8 nH (Figure 3.14) was found to be the most suitable one.

The frequency response before equalization of the laser drive circuit exhibits a sharp roll off beginning around 100 MHz and the 3 dB bandwidth of the laser transmitter is less than 500 MHz as shown in Figure 3.15(a). With the use of the equalizing circuit, the 3 dB bandwidth is extended to 1.25 GHz as shown in





**Figure 3.13 (a) Simulated S11 for laser drive circuit**

Figure 3.15(b), even though manufacturer's data sheets for the laser diodes [65] suggest a maximum usable bandwidth of 500 MHz (the second trace in the figure is the response with the photodetector switched OFF). Note that the response shown in Figure 3.15(b) is obtained with the same photodetectors and amplifiers that are used in the switch, thus it represents the bandwidth of each channel in the prototype switch as well. The power level of the swept frequency modulation signal for the laser was kept at 0 dBm, and 5 mW optical power was measured at the fibre end before coupling to the photodetector.

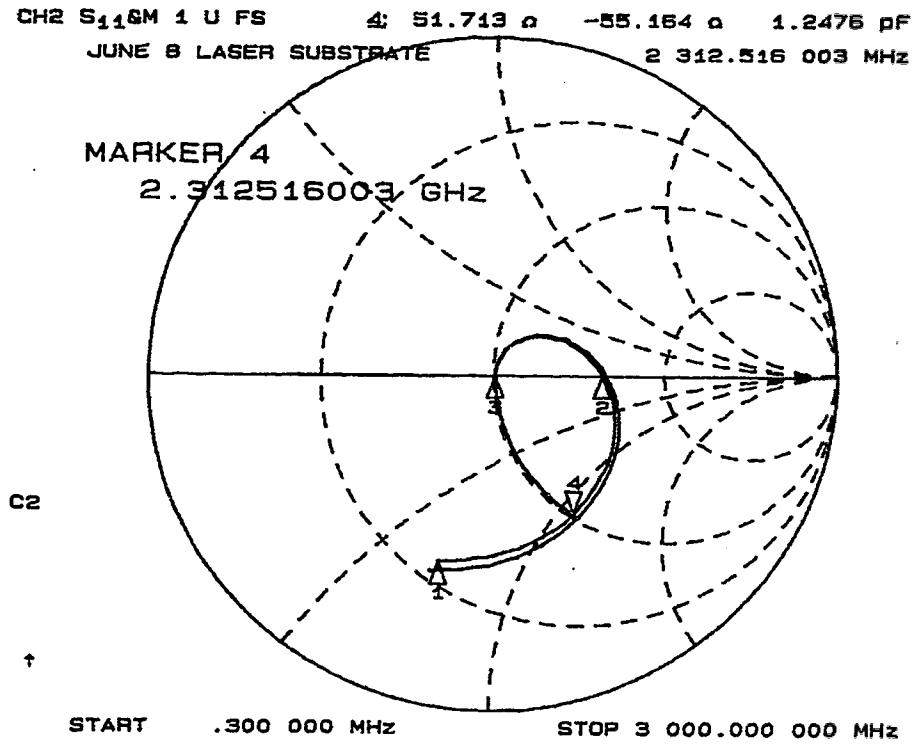


Figure 3.13 (b) Measured S<sub>11</sub> for the laser drive circuit

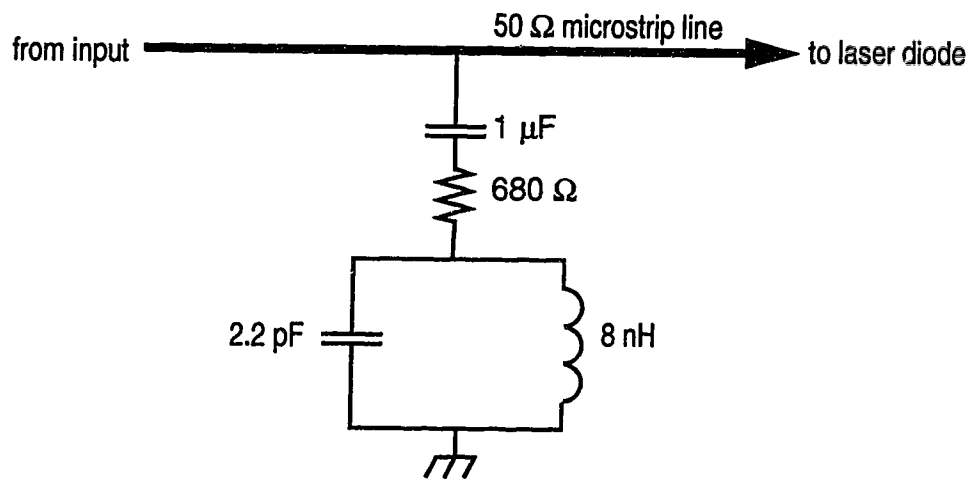


Figure 3.14 Equalizing circuit for laser drive

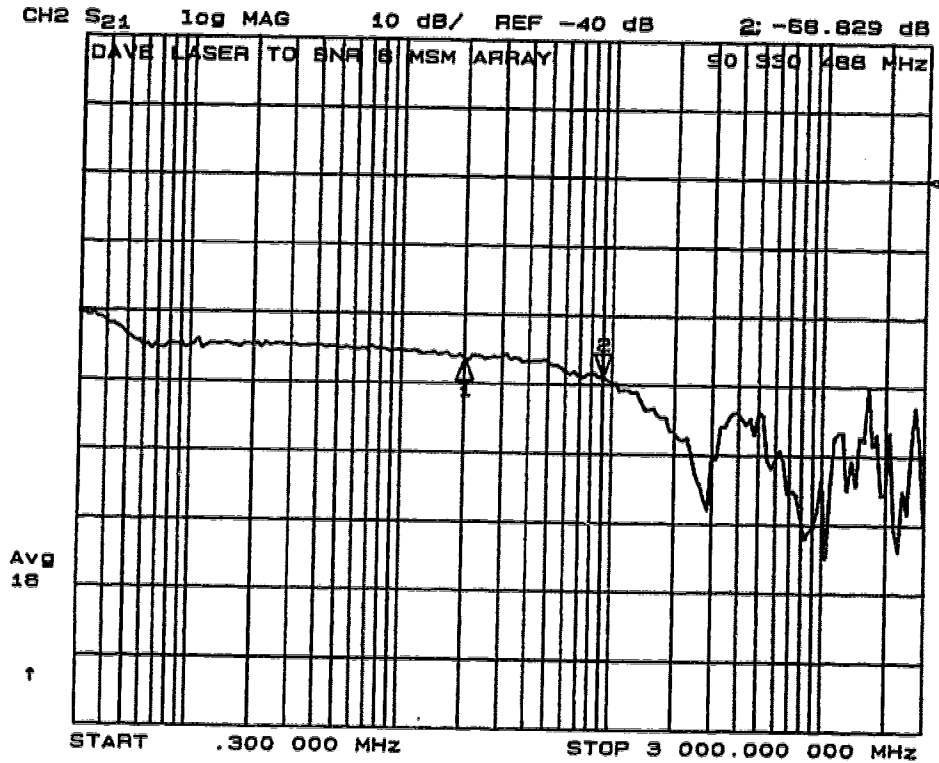


Figure 3.15 (a) Frequency response of the unequalized laser drive circuit

### 3.4 The Prototype Switch

The different sections of the optoelectronic switch - transmitters, optoelectronic modules with supporting circuitry, and power supplies were installed in industry standard racks. A photograph of the finished prototype is shown in Figure 3.16. Figure 3.16 (b) shows the prototype switch on display in the Canada Pavillion at Telecom '95, Geneva, Switzerland.

### 3.5 Requirements for 10 GHz Channel Bandwidth

#### 3.5.1 Bandwidth limitations in optoelectronic components

As explained in section 2.1, telecommunication networks and other

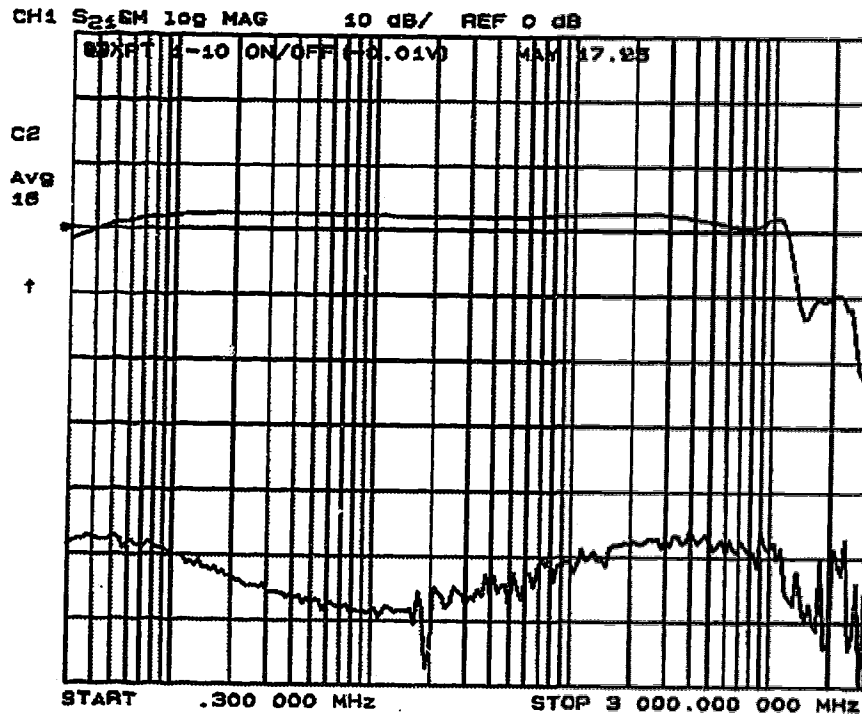
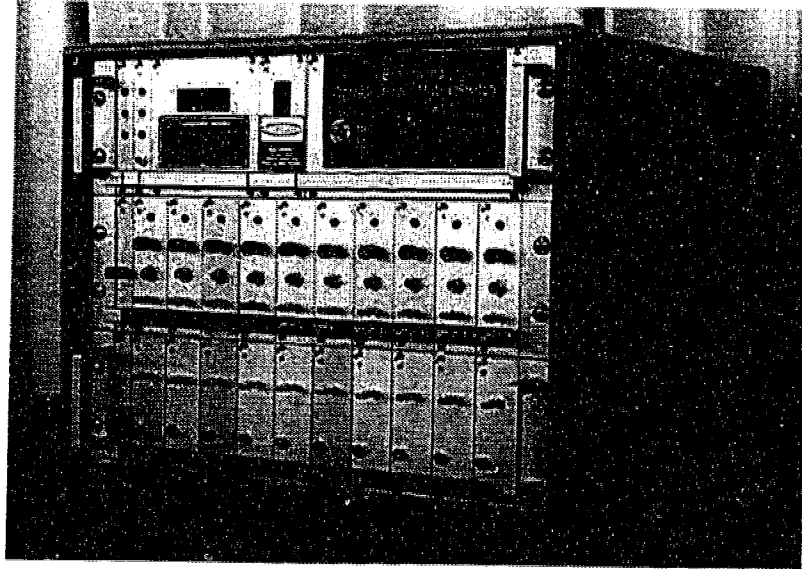


**Figure 3.15 (b) Frequency response of the equalized laser drive circuit**

applications of optoelectronic switching require bandwidths of the order of 10 Gbps. To realize these data capacities and to permit future applications with even greater data rates, future optoelectronic switches require bandwidths in excess of 10 GHz. The components which affect the frequency response of each channel (Figure 3.2) in an optoelectronic switch are:

- Laser transmitter bandwidth (for electrical inputs)
- Photodetector array bandwidth
- Amplifier bandwidth

To extend the frequency response to 10 GHz per channel, all three of these sub-systems would need sufficient bandwidth such that the cascade of all the components exhibits a bandwidth of 10 GHz. Laser transmitters with bandwidths



**(a) The prototype optoelectronic matrix switch**



**(b) The prototype on display at Telecom '95, Geneva.**

**Figure 3.16 Prototype optoelectronic switch**

in excess of 10 GHz are commercially available [66]. Broadband microwave amplifiers with dc-to-10 GHz bandwidths are also commercially available in packaged [67] or chip form [68]. However, photodetector arrays which can provide bandwidths greater than 10 GHz per photodetector are neither commercially

available nor reported in research literature.

If a uniform bandwidth of 10 GHz from each detector in the array can be achieved, it can be shown that the power budget/sensitivity requirements for a 10 Gbps channel data rate can be satisfied with available commercial components (lasers, amplifiers).

### 3.5.2 Power budget for 10 Gbps system

To calculate the power budget and required sensitivity of a 10 Gbps system, the following equivalent circuit for the optoelectronic (receiver) module is used:

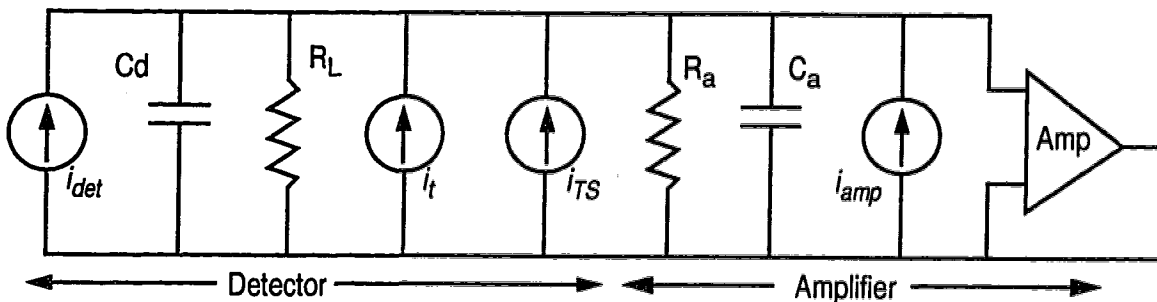


Figure 3.17 Equivalent circuit for the optoelectronic module

where:

$i_{det}$  = ideal current source representing the photodetector

$C_d$  = photodetector capacitance

$R_L$  = load resistor

$i_t$  = thermal noise equivalent current source (due to  $R_L$ )

$i_{TS}$  = shot noise equivalent current source

$R_a$  = amplifier input resistance

$C_a$  = amplifier input capacitance

$i_{amp}$  = amplifier noise contribution

The total shot noise contribution is given as:

$$\overline{i_{TS}^2} = 2eB(I_p + I_d) \quad \text{Eqn. 3.1}$$

where 'e' is the electron charge, and 'B' is the bandwidth of the system.  $I_p$  is the photogenerated current in the photodetector and  $I_d$  is the dark current (current generated in an unilluminated, biased photodetector).

Since the dark current ( $I_d$ ) in MSM photodetectors is usually quite small and has been measured to be below 1 nA for the photodetectors used in this project, its contribution to the shot noise is negligible.

The thermal noise due to load resistance  $R_L$  is given by:

$$\overline{i_t^2} = \frac{4kTB}{R_L} \quad \text{Eqn. 3.2}$$

where 'k' is Boltzmann's constant ( $1.381 \times 10^{-23}$  J/K), and 'T' is the temperature in degrees Kelvin.

Since the prototype switch uses low impedance amplifiers (50  $\Omega$  gain blocks), which present a  $R_L=50 \Omega$  to the detectors, the thermal noise contribution is expected to dominate the total noise.

The total noise associated with the amplifier ( $i_{amp}^2$ ) can be accounted for using the noise figure ( $F_n$ ) for the amplifier and referring the noise current to the

load resistor  $R_L$ . This allows the amplifier noise to be combined with the thermal noise from the load resistor ( $I_{TS}^2$ ) to give:

$$\overline{I_t^2} + \overline{I_{TS}^2} = \frac{4kTBF_n}{R_L} \quad \text{Eqn. 3.3}$$

If the photogenerated current due to incident optical power  $P_{opt}$  is  $I_p$ , the signal to noise ratio (SNR) can be written as:

$$SNR = \frac{I_p^2}{2eB(I_p + I_d) + \frac{4kTBF_n}{R_L}} \quad \text{Eqn. 3.4}$$

$I_p$  is related to the incident optical power,  $P_{opt}$ , by the *Responsivity* ( $\mathcal{R}$ ) of the photodetector as:

$$I_p = \mathcal{R} \cdot P_{opt} \quad \text{Eqn. 3.5}$$

Measured responsivities for MSM photodetectors range from 0.21 (850 nm) to 0.30 A/W (1330 nm). Using the following (conservative) values for the variables in the above equations, the required  $P_{opt}$  for a 10 Gbps system can be calculated.

$$SNR \text{ (for } 10^{-9} \text{ Bit Error Ratio [69])} = 22 \text{ dB}$$

$$R_L = 50 \ \Omega$$

$$B = 10 \text{ GHz}$$

$$T = 293 \text{ K}$$

$$F_n = 10 \text{ dB (commercial amplifiers are available with } <7 \text{ dB noise)}$$



figure)

$\mathcal{R} = 0.3 \text{ A/W}$  (assuming that the system operates at 1330 or 1550 nm)

Using equations 3.1 through 3.5, it can be seen that  $P_{opt} > 250 \text{ } \mu\text{Ws}$  will provide a SNR  $> 22 \text{ dB}$  for a system with the equivalent circuit shown in Figure 3.17. (Note that  $P_{opt}$  is the optical power coupled to the MSM photodetector, and coupling losses are extra).

Since, in a 'broadcast' and 'select' optoelectronic switch such as the prototype considered in this work, each input signal is split  $N$  ways (in an  $N \times N$  switch), the optical power at the input  $P_{in}$  is given by;

$$P_{in} = N \cdot P_{opt} + L_{excess} \quad \text{Eqn. 3.6}$$

where  $L_{excess}$  is the excess loss (in addition to the splitting loss) in the splitting mechanism.

Thus for an excess loss of  $\sim 3\text{-}5 \text{ dB}$ , and allowing coupling losses of  $3 \text{ dB}$  per photodetector, a  $10 \times 10$  switch matrix dimension, input optical power (launched on fibre)  $> 10 \text{ mW}$  would provide a Bit Error Ratio (BER) of less than  $10^{-9}$ . Laser diodes coupled to single mode fibres which are capable of direct modulation bandwidths of  $10 \text{ GHz}$  are commercially available [66]. Therefore if photodetectors with the requisite bandwidth ( $10 \text{ GHz}$ ) can be produced in arrays of at least  $1 \times 10$ , all other components required for a  $10$  channel,  $10 \text{ Gbps}$  per channel optoelectronic switch can be commercially obtained.

Chapter 4 describes results obtained from experimental analysis of existing

(conventional) array designs, and points out the limitations of these designs. Results with a new set of array designs are also presented which extend the bandwidth well past 10 GHz for each photodetector in arrays of 1x8 and 1x16.

## **4. Broadband Photodetector Arrays**

Broadband photodetectors arranged in linear arrays are key elements in implementing a variety of optoelectronic switching and signal processing technologies. This chapter presents results obtained with conventional array designs (the term 'conventional array designs' in this thesis refers to the designs fabricated as part of related research projects at University of Alberta and its affiliated research organizations, there are no commercial suppliers of broadband photodetector arrays). The frequency response of photodetectors in conventional arrays is in fact position dependent as described in section 4.2 and 4.3. A new approach towards design of broadband arrays for providing uniform bandwidth for each photodetector in the array is presented in section 4.4. These designs are expected to yield a minimum of 10 GHz bandwidth for each photodetector in 1x8 and 1x16 arrays.

### **4.1 Metal-Semiconductor-Metal Photodetectors**

The metal-semiconductor-metal (MSM) photodetector is a planar device consisting of interdigitated electrodes placed on a semiconductor absorbing layer. The photodetector consists of two Schottky barriers (forming diodes) connected back to back that form a structure essentially equivalent to two opposed diodes in series. When a bias is applied, one of the diodes is reverse biased while the other is forward biased.

Measured current-voltage characteristics depicted in Figure 4.2 are typical of MSM devices. Since the MSM photodiode is a bipolar device by virtue of its two

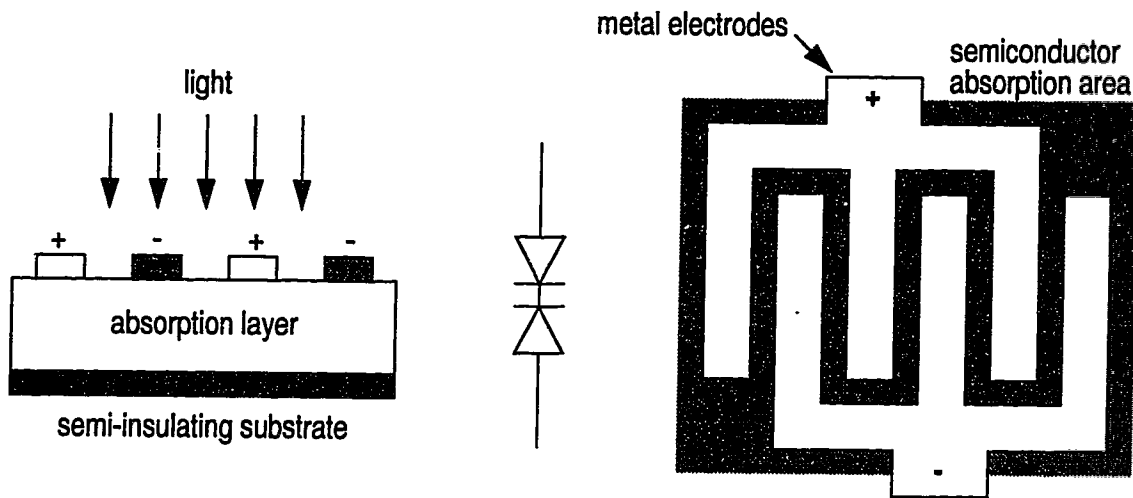


**Figure 4.1 The Metal-Semiconductor-Metal (MSM) photodetector**

opposed diodes, an almost symmetric (within the constraints of device fabrication methods) behaviour is observed for a bias of opposing polarity as well.

The planar metal-on-semiconductor fabrication process is potentially compatible with high speed electronic devices, thus making them attractive candidates for photonic systems which require integration of optical and electronic devices. MSM photodetectors have been shown to exhibit quite high bandwidths [70]. The fundamental physics and operation of these devices is well understood and reported in literature [71, 72, 73, 74] although there are a number of device fabrication issues which may adversely affect device performance [73, 75]. These issues need to be solved before these devices attain their full potential in optoelectronic device integration and applications. For optoelectronic switching and signal processing applications, arrays of these devices are required to provide the crosspoint elements (section 1.2, Figure 1.4), and as explained in the

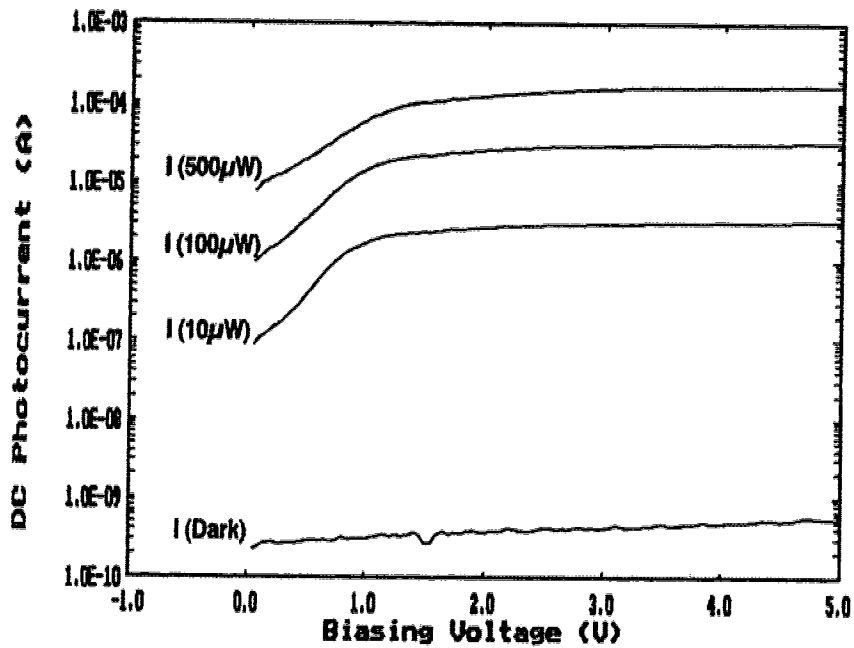


Figure 4.2 Current-voltage characteristics of MSM photodetectors

next section, even though single devices may be shown to exhibit tens of GHz bandwidth, devices arranged in arrays are limited by effects external to the devices.

## 4.2 MSM Photodetectors in Arrays

### 4.2.1 Conventional array designs

In the basic optoelectronic switching arrangement, the array functions as a selector of optical signals when only one of the detectors is switched 'ON' (biased) to detect the desired signal (detector number 2 in Figure 4.3) while all other signals are incident on detectors which are biased 'OFF' (insensitive to light) and thus make little or no contribution (crosstalk/interference) to the output signal. Results presented in Chapter 5 confirm that signals can be suppressed by more

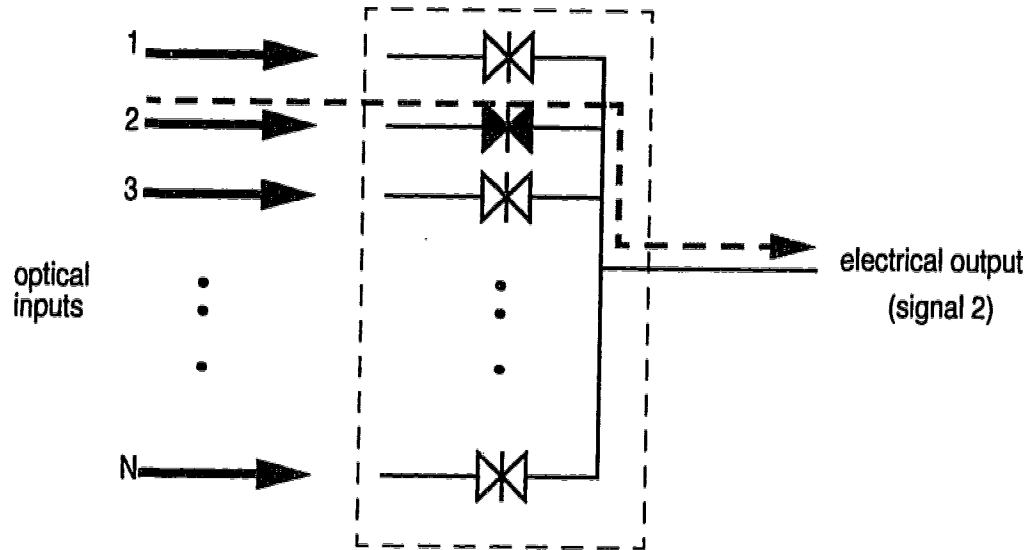


**Figure 4.3 MSM photodetector array as an optoelectronic signal selector**

than 60 dB when the bias on an active MSM is switched from ON to OFF. However, as far as the frequency response is concerned, each photodetector is affected by all the other photodetectors in the array. As each photodetector has a certain capacitance associated with it, the frequency response of the active photodetector is changed due to all the other capacitances connected to the common output line. In Figure 4.4, a 1x4 array schematic illustrates the case where photodetector 2 ( $I_2$ ) is active (ON) and the frequency response of the photocurrent collected at the output terminal would depend on  $C_{d1}$ ,  $C_{d3}$ ,  $C_{d4}$ , in addition to the capacitance  $C_{d2}$  of the active photodetector.

In optoelectronic switching applications, these effects would result in non-uniform bandwidths for different channels in a switch. Therefore, *arrays* of MSM

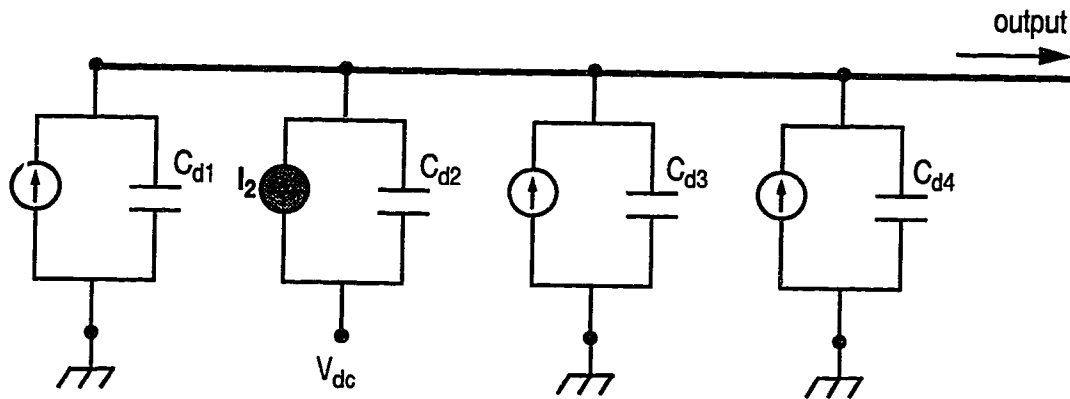


**Figure 4.4 Effect of photodetector capacitance in arrays**

photodetectors need to be characterized to determine the bandwidth available from each photodetector in the array. The substrate designed for the optoelectronic modules (section 3.2) was used along with the mechanical assembly to characterize the frequency response of the various MSM detectors in different positions in the array. A single fibre input used to provide the optical signal input for the frequency response measurements. Alignment was done by means of a three axis positioner which is manipulated manually to align the fibre end to the photodetector device under test.

To investigate the effect of the array layout on frequency response, arrays of two different sizes (1x8, and 1x16) were tested. These Gallium Arsenide (GaAs) arrays for use at 850 nm wavelength were fabricated at BNR-Nortel, Ottawa and Communications Research Centre (CRC), Ottawa. These are referred to as BNR 1x8, BNR 1x16, and CRC 1x16 MSM arrays respectively in

this work.

The MSM photodetectors in the BNR arrays (1x8 and 1x16) are  $100\mu\text{m}\times 100\mu\text{m}$  and can easily be coupled to standard multi-mode fibre. The photodetectors in all the arrays considered in this work are placed at a pitch of  $250\mu\text{m}$  as mentioned earlier. Figure 4.5 illustrates the layout of the BNR 1x8 MSM array. The arrays fabricated by CRC (Figure 4.6) contain 16 photodetectors,

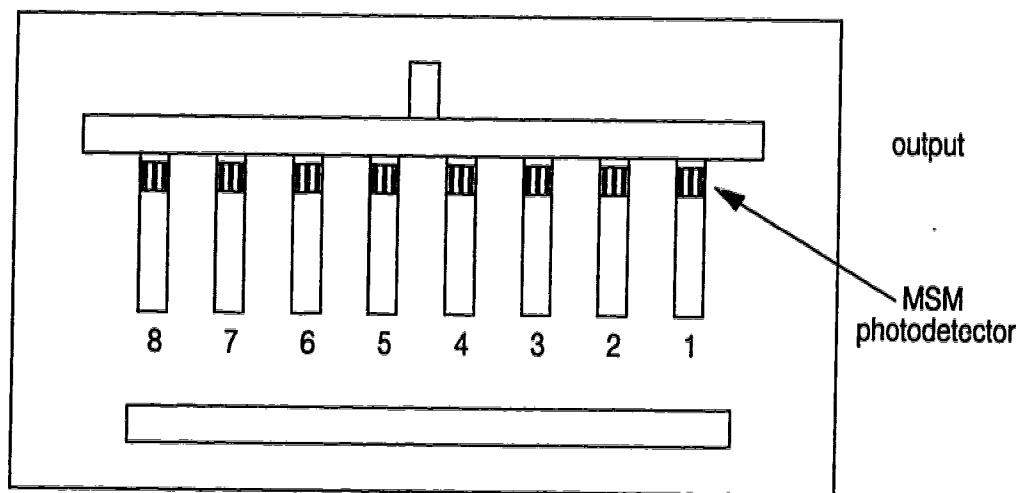


**Figure 4.5 BNR 1x8 array layout**

each of  $72\mu\text{m}\times 72\mu\text{m}$  size. Provision is made to collect the output signal from either end of the array or from the middle of the array. The metal strip near the bottom of the chip layout was originally intended to serve as a ground plane for a series of microcapacitors in the first stage of decoupling (similar to the  $82\text{ pF}$  capacitors in Figure 4.7). During this phase of testing, the appropriate microcapacitors were not available and the first set of decoupling capacitors was placed close to the edge of the array chip.



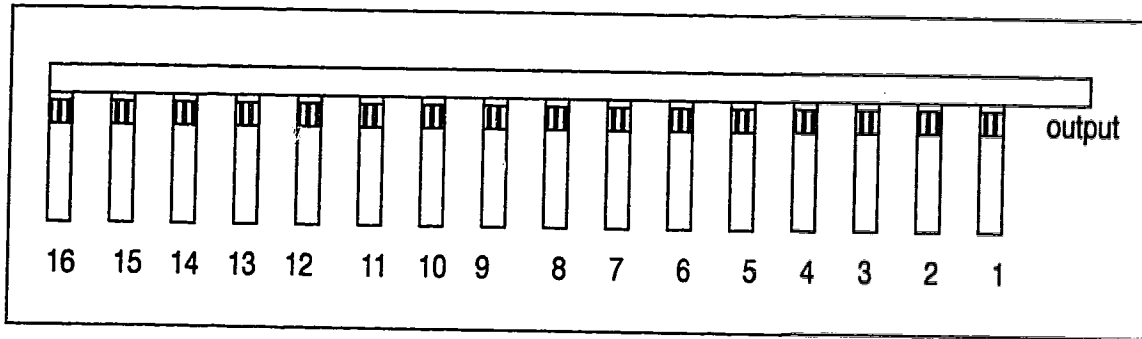


Figure 4.6 CRC 1x16 array layout

#### 4.2.2 DC-bias circuit

A two stage decoupling and isolation arrangement using thin film microcapacitors in the first stage and surface mount chip components in the second stage were used to supply a well isolated dc bias to each of the MSM photodetectors with a short decoupled path to the ground plane on the TMM-3™ [64] substrate (for ac signals) with minimum stray effects. The circuit schematic for the bias arrangement is shown in Figure 4.7. The substrate has ten such bias

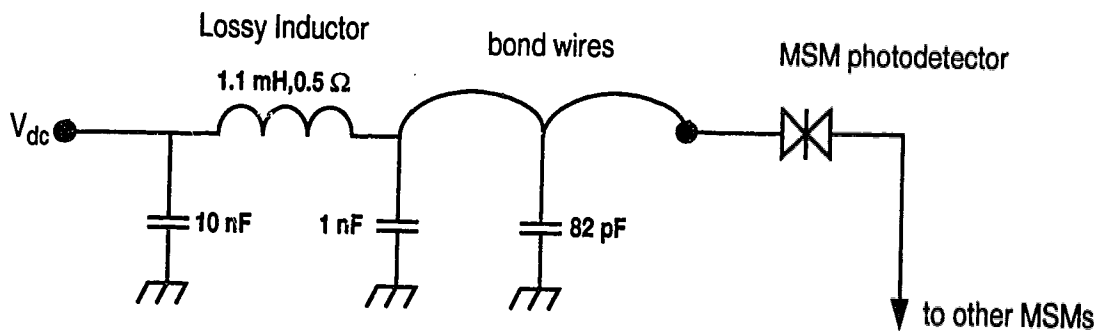
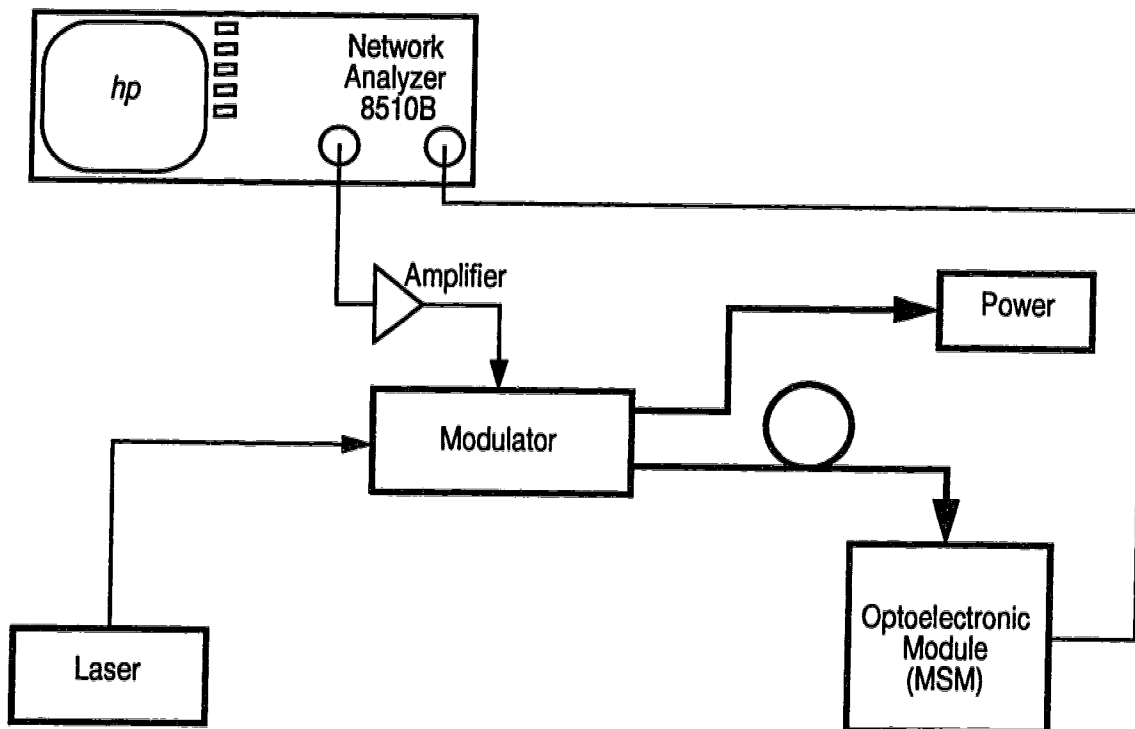


Figure 4.7 DC-bias circuit for photodetectors

lines for biasing ten different MSM photodetectors. The substrate with all the components mounted using surface mount technology is shown in Figure 3.7, and Figure 3.10 shows a photograph of the substrate assembled in the housing designed for the substrate.

Figure 4.8 shows the arrangement of equipment used to measure the bandwidth of the photodetectors in these arrays.



Laser: Seastar PM-550A-830, Sharp LT015MD0 diode

Modulator: UTP Mach-Zehnder modulator (Y-fed balanced bridge), dc-18 GHz

Power: Newport Power Meter

Amplifier: Miteq 0.1-18 GHz bandwidth, 18.0 dB gain

**Figure 4.8 Test equipment arrangement for MSM array bandwidth tests**

### **4.3 Bandwidth Limitations in Conventional Designs**

Frequency response results from three different MSM arrays are described in this section. These are referred to as BNR 1x8, BNR 1x16, and CRC 1x16 arrays according to the nomenclature and layouts described in section 4.2.1. The optical power incident on the photodetector is 0.480 +/- 0.005 mW and the photodetectors are biased at +5.0 volts unless otherwise indicated.

#### **4.3.1 BNR 1x8 array**

The response of the individual photodetectors in the array was measured by illuminating each device in turn with the fibre coupled optical signal, and biasing the photodetector at +5.0 volts, while grounding the bias lines of all other photodetectors in the array. The devices are numbered with the device closest to the output designated number 1 as shown in Figure 4.5. The frequency responses of the MSM detectors #1 through #7 are shown in Figures 4.9 through Figure 4.15. The shape and features of the frequency response show a distinct change with location in the array. A steady roll-off in the response, which begins around 100 MHz in the response can be noticed in all the photodetector responses. Spurious features such as the prominent peaks in response beyond 2 GHz are also observed in every case. The 3 dB bandwidth shows an increase from 970 MHz for photodetector #1 to 2.38 GHz for photodetector #7. The flatness of response in the < 2GHz region also increases with the position of the photodetector in the array.

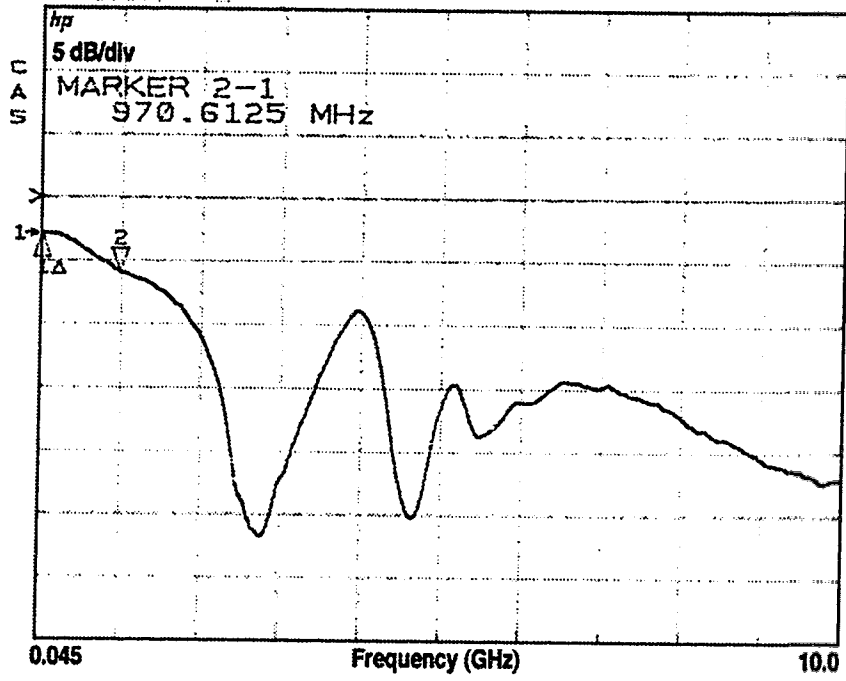


Figure 4.9 Frequency response of MSM photodetector no. 1 in the BNR 1x8 array

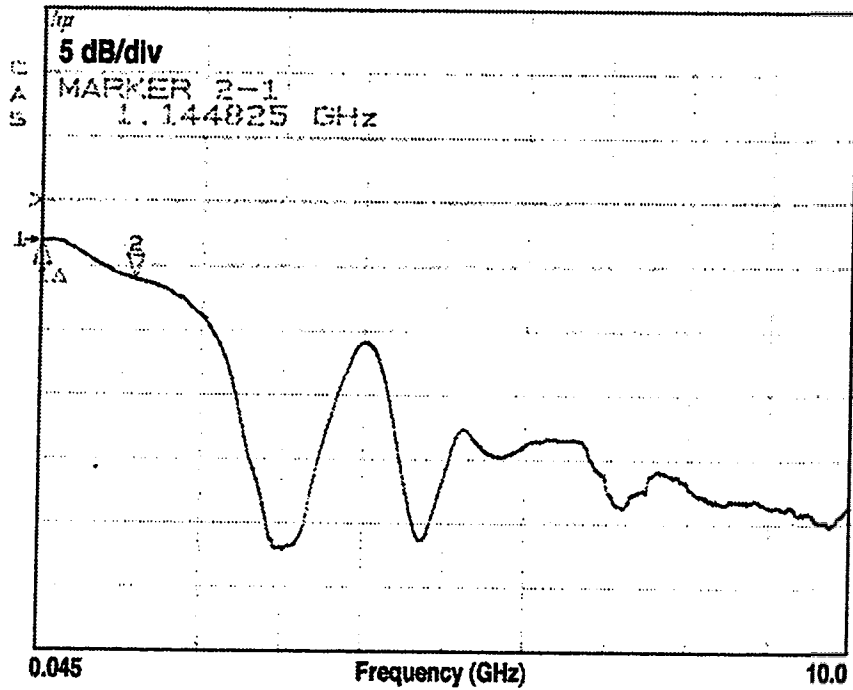


Figure 4.10 Frequency response of MSM photodetector no. 2 in the BNR 1x8 array

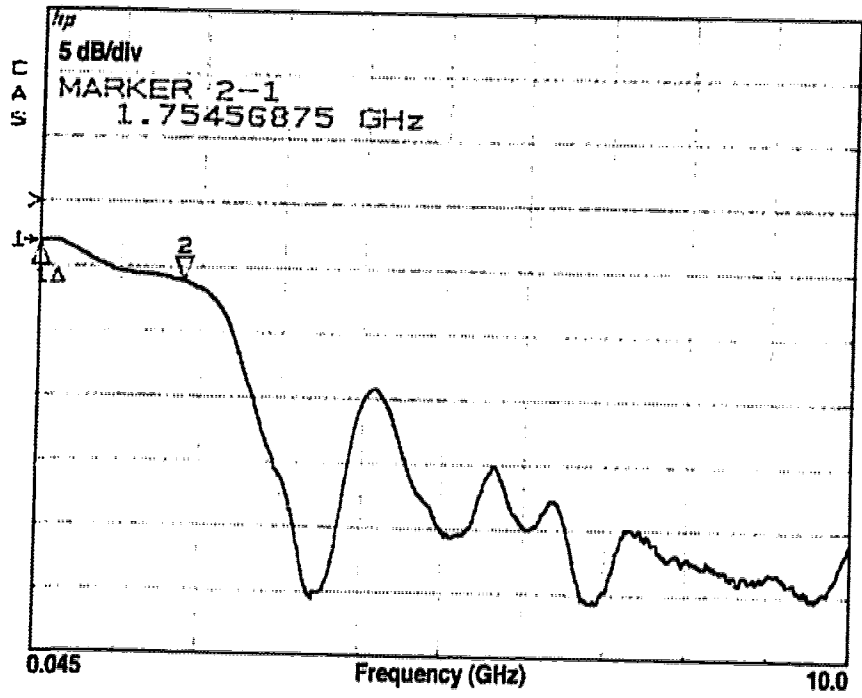


Figure 4.11 Frequency response of MSM photodetector no. 3 in the BNR 1x8 array

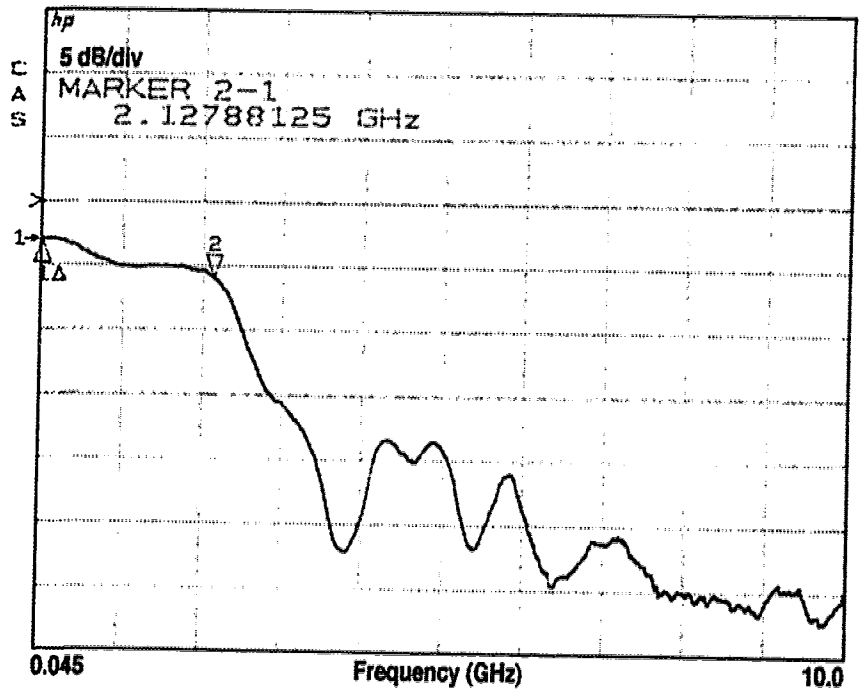


Figure 4.12 Frequency response of MSM photodetector no. 4 in the BNR 1x8 array

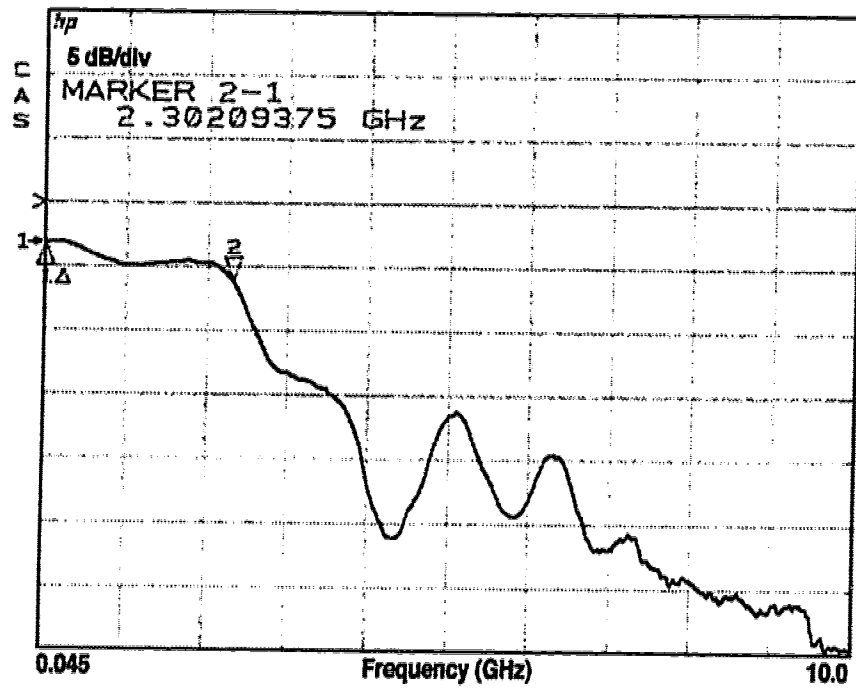


Figure 4.13 Frequency response of MSM photodetector no. 5 in the BNR 1x8 array

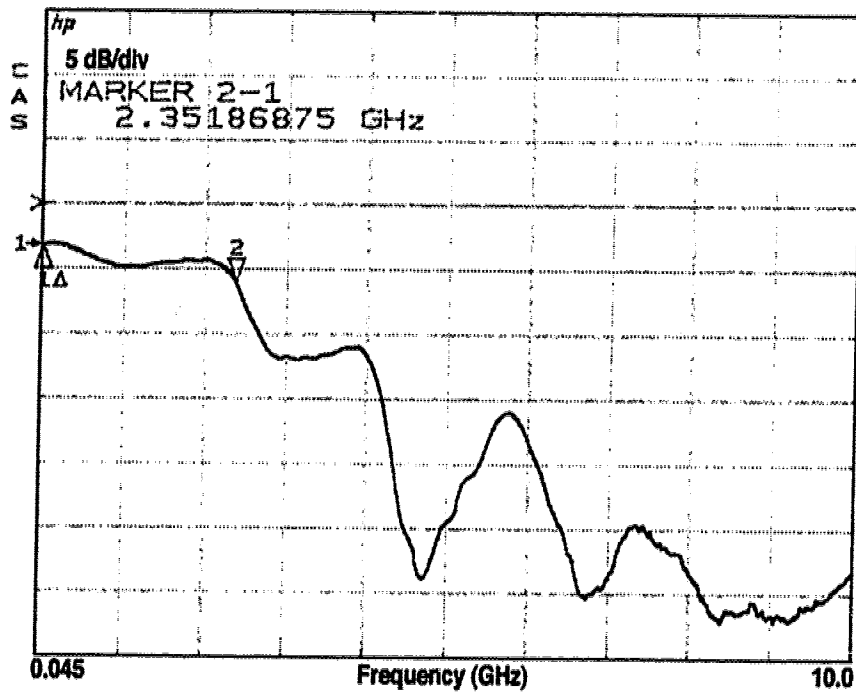


Figure 4.14 Frequency response of MSM photodetector no. 6 in the BNR 1x8 array

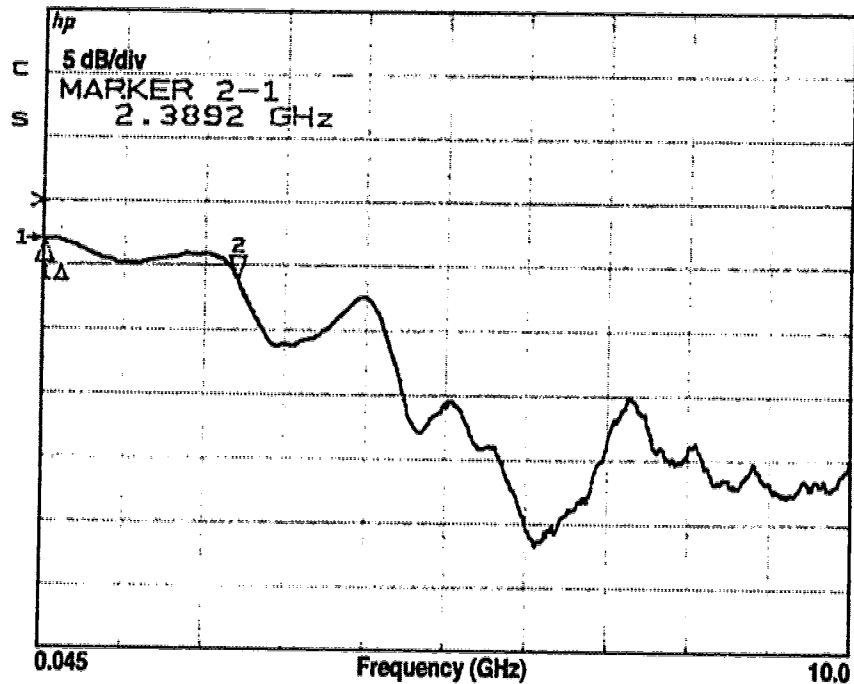
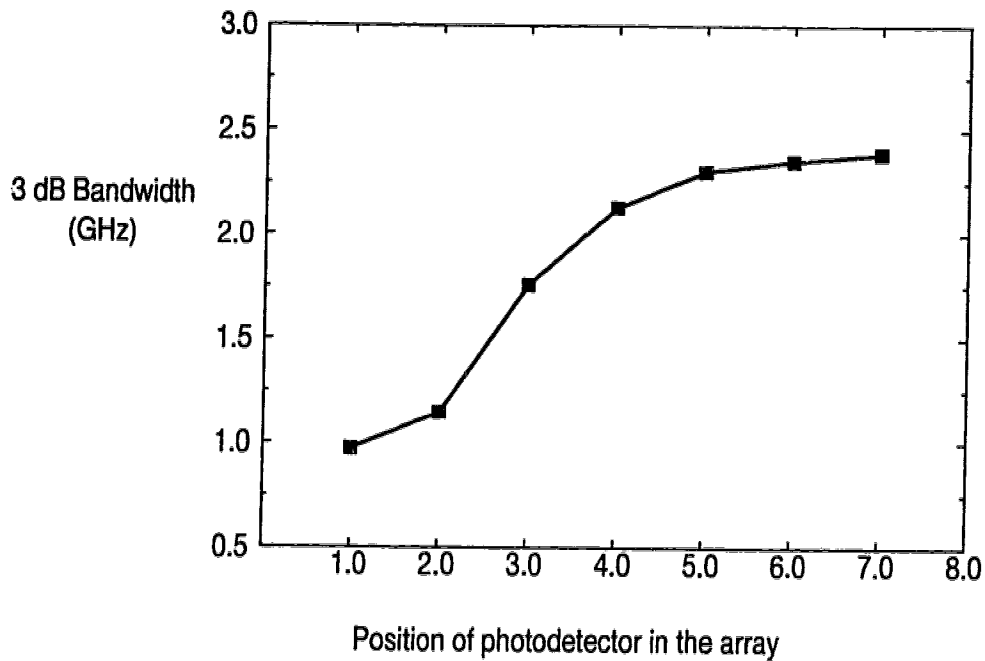


Figure 4.15 Frequency response of MSM photodetector no. 7 in the BNR 1x8 array

#### 4.3.2 Position dependent frequency response

The variation in the 3-dB bandwidth is summarized in Figure 4.16 which shows the 3 dB bandwidth versus the photodetector position in the array. The photodetector furthest away from the output terminal (photodetector #7) produces the maximum bandwidth while the photodetector closest to the output terminal (#1) exhibits the minimum bandwidth in the array. The bandwidths of other photodetectors show a monotonic increase as the position of the active photodetector moves further from the output terminal. The difference in the frequency response for each photodetector is primarily due to the different electrical paths to the output terminal from each photodetector. Also, the thin and long metallic trace which forms the common output signal bus (see Figure 4.5)



**Figure 4.16 3 dB bandwidth of MSM photodetectors in the 1x8 array**

contributes appreciable inductance to the photodetectors further away from the output terminal. The inductance of a metal trace can be calculated by the following empirical formula (after [76]):

$$L = \left( 0.002 \cdot \text{length} \cdot \left\{ \ln \left( \frac{2 \cdot \text{length}}{\text{width} + \text{thickness}} \right) + 0.5 \right\} \right) \mu H \quad \text{Eqn 4.1}$$

where:

L = inductance of the metal trace (in micro-Henry)

length = length of the conductor (in cm)

width = width of the conductor (in cm)

thickness = thickness of the conductor (in cm)



Using this formula, the inductance for the trace leading to photodetector #7, which is 2000  $\mu\text{m}$  away from the output terminal, is calculated to be 1.64 nH. While the photodetector closest to the output (#1) only sees an inductance of 0.1 nH to the output terminal. The difference in frequency response can be explained using the 'inductive peaking' phenomenon [77] in which increased gain is experienced due to a small (of the order of nano-Henries) inductance in series with the device under measurement. This technique is frequently used to extend the frequency response of wideband amplifiers [77]. Thus photodetector #7 experiences considerable inductive peaking as compared to photodetector #1, which helps in extending the frequency response further. In order for this technique to be beneficial towards extending the frequency response of all the photodetectors in the array, it must be ensured that the same inductance is experienced by all the devices; necessitating an electrically identical path from all devices to the common output terminal. This conclusion is used constructively to help with the design of new broadband photodetector arrays as explained in section 4.4.

To confirm the dependence of the response on the capacitances of inactive photodetectors in the array, the response of photodetector #7 was explored further by disconnecting the bond wires from all other MSM photodetectors in turn, leaving only MSM#7 connected to dc bias. Disconnecting a photodetector in the array essentially has the effect of eliminating its capacitance from being connected to the common output signal bus (Figure 4.4), and hence an improvement in the 3 dB frequency would be expected with each MSM

disconnected from the array. Figure 4.17 shows the change in bandwidth versus

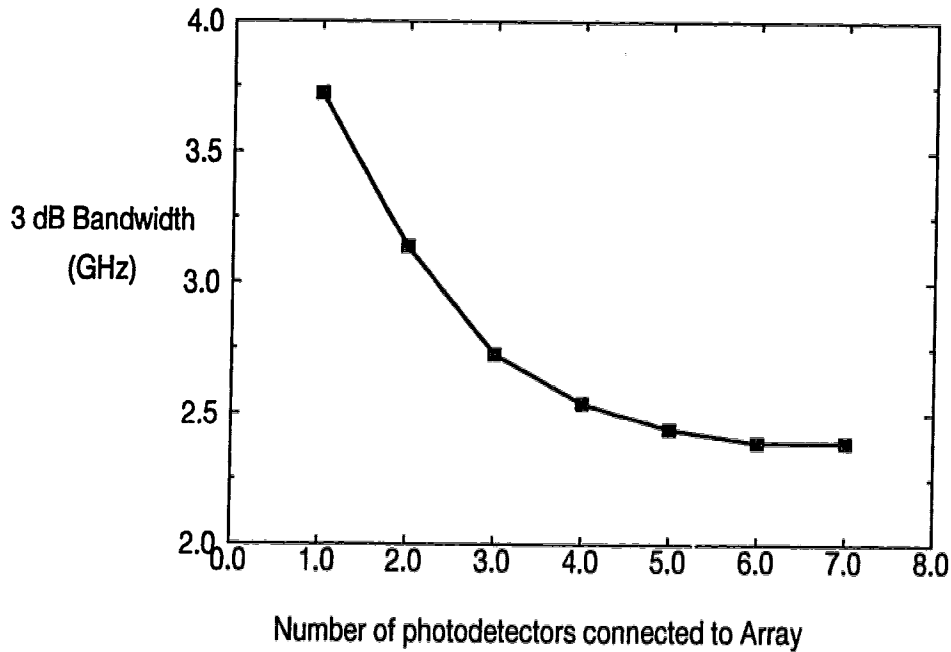


**Figure 4.17 Dependence of bandwidth of photodetector #7 in the BNR 1x8 array on number of MSMs in the array**

the number of MSM photodetectors disconnected from the array. Figure 4.18 shows the response of photodetector #7 while all other photodetectors are disconnected from the array. The inductive peaking due to the trace inductance is visible in the 2.5 - 4 GHz region.

### 4.3.3 1x16 Arrays

Similar results were obtained with 1x16 arrays fabricated by BNR and CRC. Since these arrays exhibited the same behaviour as the BNR 1x8 arrays, the results from the frequency response measurements on these arrays are not included here. A comprehensive report on the measurements on all the arrays

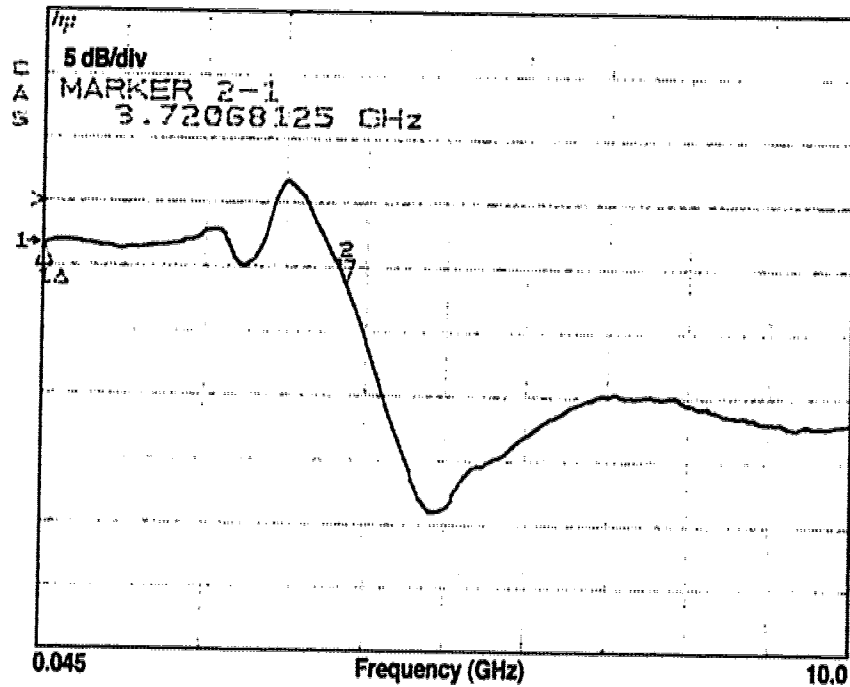


**Figure 4.18 Frequency response of MSM no. 7  
(all other MSMs disconnected in 1x8 array)**

can be found in [78].

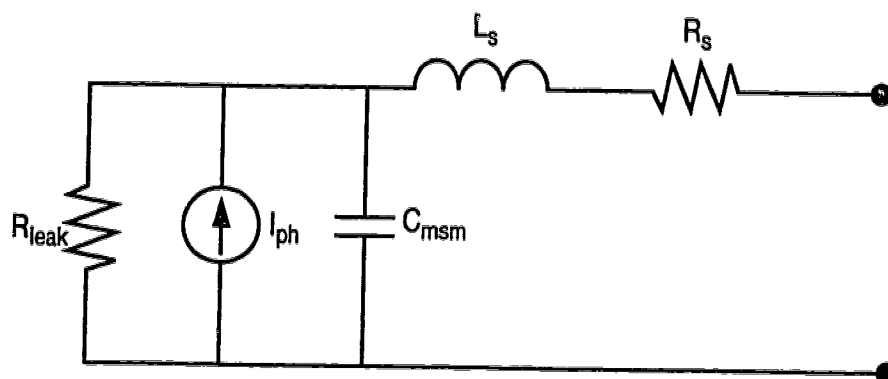
The position dependent response of MSM photodetectors in these array designs renders them unusable above a few GHz. Also, the non-uniformity of frequency response would result in non-uniform signal characteristics for different channels. Therefore new designs are required which permit 3 dB bandwidths up to 10 GHz while providing uniform frequency response for each photodetector in the array.

## 4.4 Designs for Broadband Arrays

After the observation of position dependent response in photodetector arrays, the effect of the layout pattern on the frequency response of the arrays was analyzed with the help of simulation models in the Microwave Design Software [79]. Using simple models defined for the MSM photodetector, the frequency response behaviour experimentally observed was confirmed and a family of optimized interconnect patterns was generated which eliminates the position dependence of the photodetector response while extending the frequency response past 10 GHz.

### 4.4.1 Simulation models for MSM photodetector arrays

A metal-semiconductor-metal photodetector can be represented by the equivalent circuit shown in Figure 4.19 as a combination of an ideal current source (generated photocurrent corresponding to the incident signal) with capacitance, inductance and resistance associated with the physical device. This simple model has been shown to be consistent with the measurements reported on similar photodetectors in literature [73, 80, 81, 82]. The series inductance due to the fingers is quite small ( $\sim 50$  pH) and generally negligible. The parallel resistance of 12 MOhms represents the surface leakage, and the series resistance due to the fingers and the metal interconnect is very low ( $\sim 1.5 - 2 \Omega$  for standard Ti/Pt/Au contact metallization on GaAs). The capacitance due to the interdigitated finger structure for a  $100\mu\text{m} \times 100 \mu\text{m}$  MSM photodetector is theoretically calculated to be  $\sim 75$  fF [73, 75, 80, 81] even though measurements by researchers have shown consistently higher capacitance of 0.15 - 0.30 pF



$I_{ph}$  = photocurrent generated in the photodetector corresponding to incident optical signal

$C_{msm}$  = capacitance of the photodetector (0.1 - 0.25 pF when biased)

$R_s$  = series resistance of fingers (1.5 - 2.0  $\Omega$ )

$L_s$  = series inductance of fingers (~50 pH)

$R_{leak}$  = resistance to account for surface leakage current (10-12 M $\Omega$ )

**Figure 4.19 Two port MSM model  
(the values indicated are typical values for a 100 $\mu\text{m}$ x100 $\mu\text{m}$  MSM device)**

(Figure 4.20). For the purposes of modelling the effects of photodetectors in an array, conservative estimates with high values of MSM capacitance (0.2 to 0.5 pF) were used in evaluating the frequency response. Figure 4.20 shows capacitance measurements carried out at CRC for 100 $\mu\text{m}$ x100 $\mu\text{m}$  MSM photodetectors at different voltages and incident optical power of 0.5 mW. It can be seen that for photodetectors with 2  $\mu\text{m}$  finger spacing (topmost trace in Figure 4.20), capacitance in the illuminated state can be as high as 0.3 pF for low bias conditions. Since photogenerated carriers in the photodetector absorption region

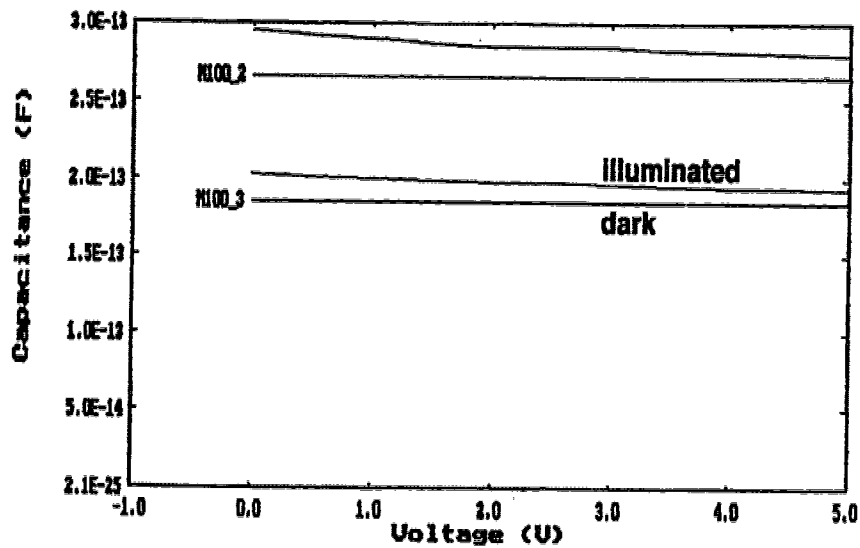


**Figure 4.20 Capacitance measurement for MSM photodetectors**

result in formation of space charge regions which screen the applied field, capacitance of the device increases as the charge on each electrode increases while the potential difference is decreased [75, 80, 83, 84].

This simple device model can be combined with other elements present in the array to form a lumped element representation of the MSM array. Figure 4.21 shows the lumped element model used for an initial investigation of the position dependent frequency response observed experimentally for the array shown in Figure 4.5.

In this simulation circuit model, the metal interconnect is modelled as lumped inductances calculated with the help of "ribbon over substrate" module in HP-MDS software package [79]. This submodule provides a value of inductance (1.61 nH for a trace 2000  $\mu\text{m}$  long, 100  $\mu\text{m}$  wide, 10  $\mu\text{m}$  thick) which agrees well with the calculation done with Equation 4.1. The frequency response obtained

## BNR 1x8 Array (with 7 detectors connected)

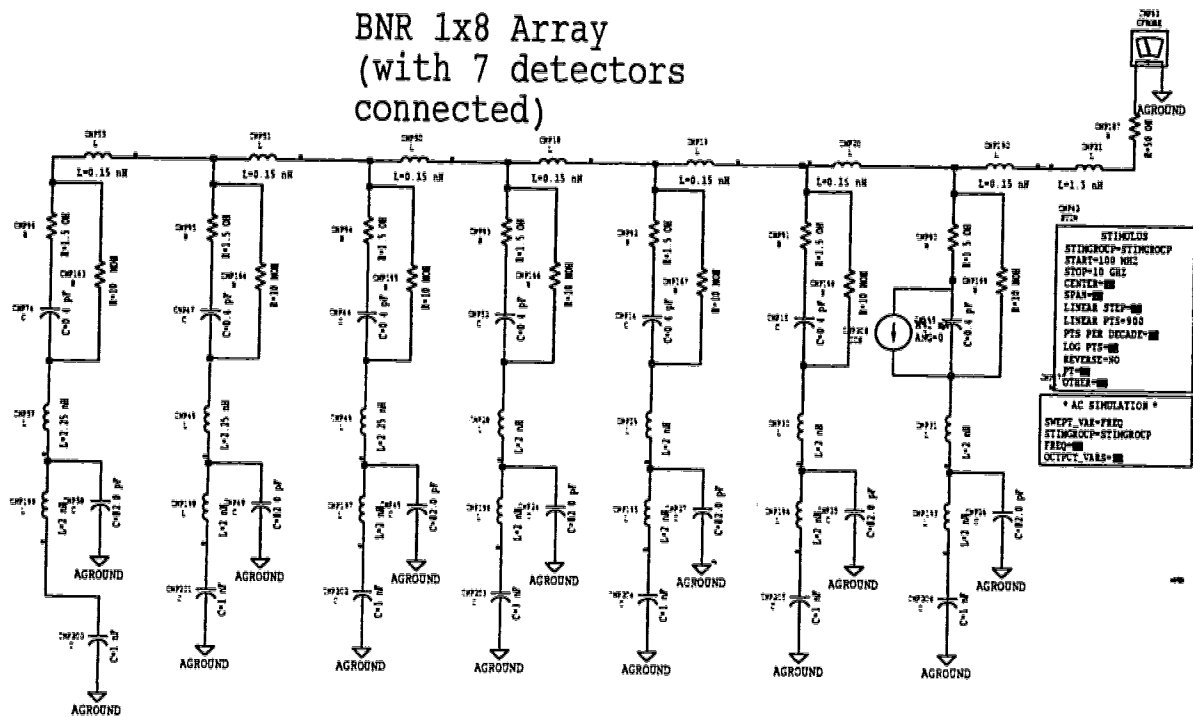


**Figure 4.21 Lumped element simulation circuit for MSM array**

with this model is shown in Figure 4.22. The simulated frequency response shown here for photodetector #1 in the array confirms the measured frequency response and also exhibits spurious features in the 3-10 GHz region which are consistent with measurements (Figure 4.9).

Even though a lumped element simulation model such as the one in Figure 4.21 is helpful towards gaining an understanding for the frequency response behaviour of photodetector arrays, a more comprehensive distributed element microwave circuit model is required to characterize the array performance at higher frequencies (>1 GHz).

Since the layout geometry of the metal interconnect pattern in MSM arrays

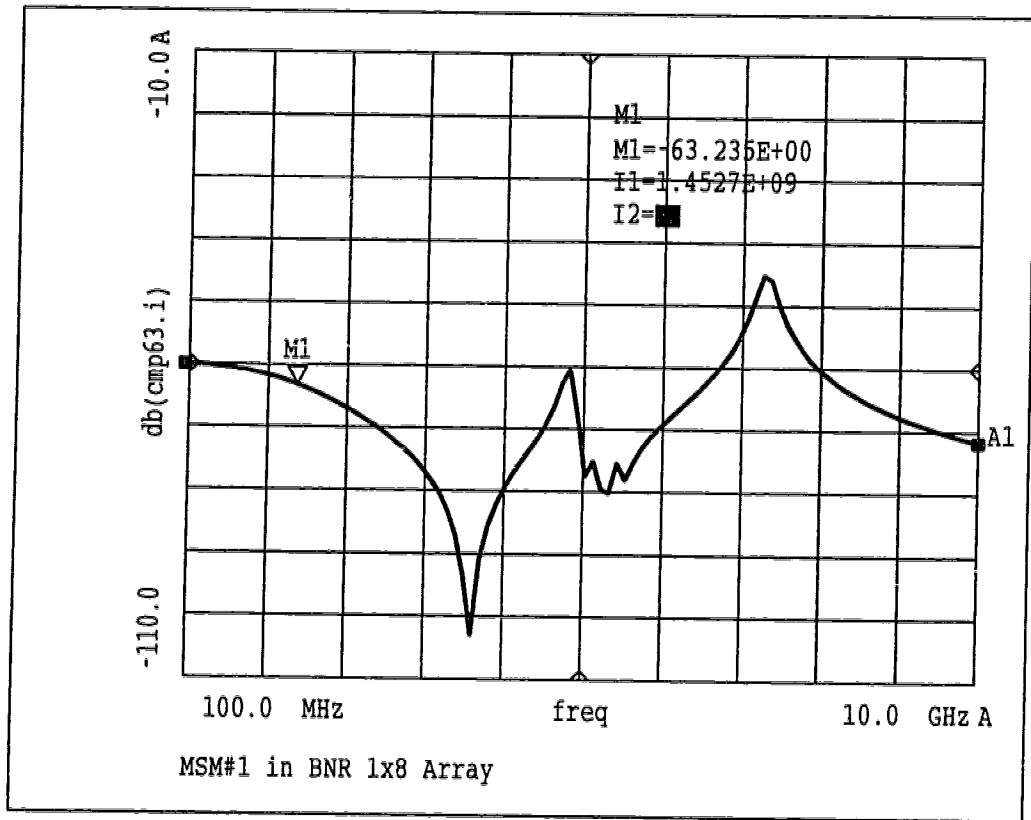


Figure 4.22 Modelled frequency response of MSM no. 1 with lumped element model

(Figure 4.5, 4.6) lends itself to use as microwave transmission line elements, it

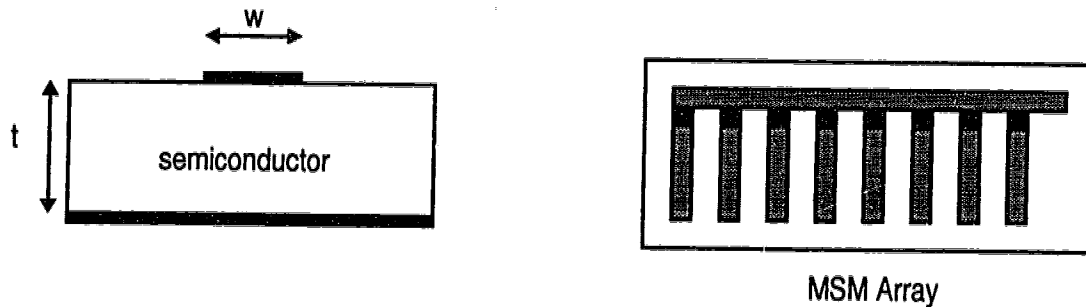


Figure 4.23 Interconnects as microstrip transmission lines

was decided to place a ground plane on the other side of the semiconductor chip



(the other side of the wafer can be metallized to fabricate the ground plane, the wafer can be thinned to specified thicknesses by lapping to 400-750  $\mu\text{m}$  before metallization). The interconnect elements can then be simulated as transmission line structures and their design can be optimized such that maximum and uniform bandwidth across the array is obtained.

With the use of distributed element models, the problem of designing an interconnect pattern to combine possible photocurrent contributions from each photodetector can be schematically shown in Figure 4.24 where a microwave combiner circuit is required between the devices and the common output terminal (which connects to 50  $\Omega$  transmission line). The target bandwidth to be achieved

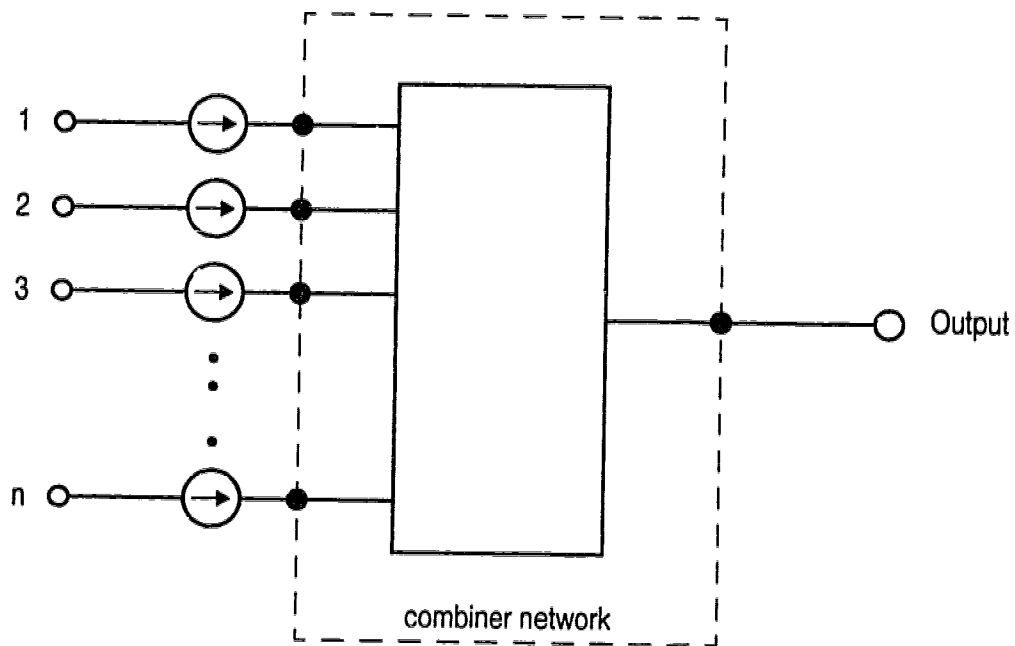


**Figure 4.24 Combiner circuit for photodetector array**

from the array designs was selected to be at least 10 GHz so that the arrays may

be utilized in switching of data channels at 10 Gbps and above.

The microwave combiner circuit must have broadband characteristics such that the frequency response of photodetectors is not adversely affected. Also, the combiner circuit should provide a uniform frequency response for each photodetector in the array.

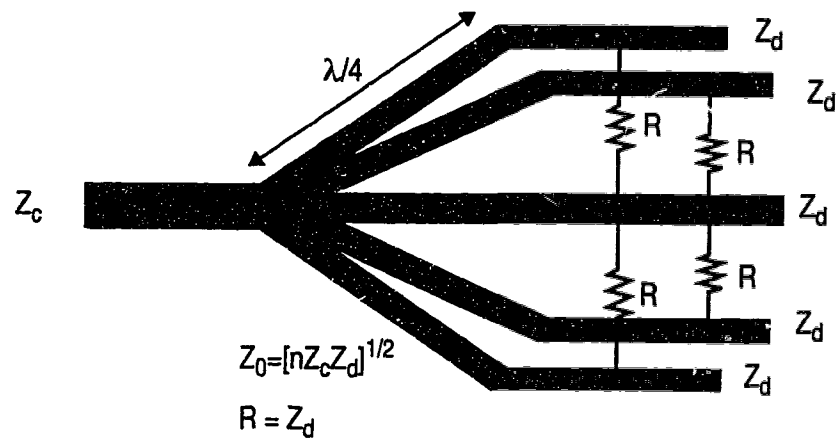
An analogous problem is encountered in high power microwave circuits where power combiner circuits are used to arrange multiple devices (amplifiers or oscillators) in parallel and consequently the power handling capability of the circuit can be increased.

Desirable properties of such a combiner circuit include:

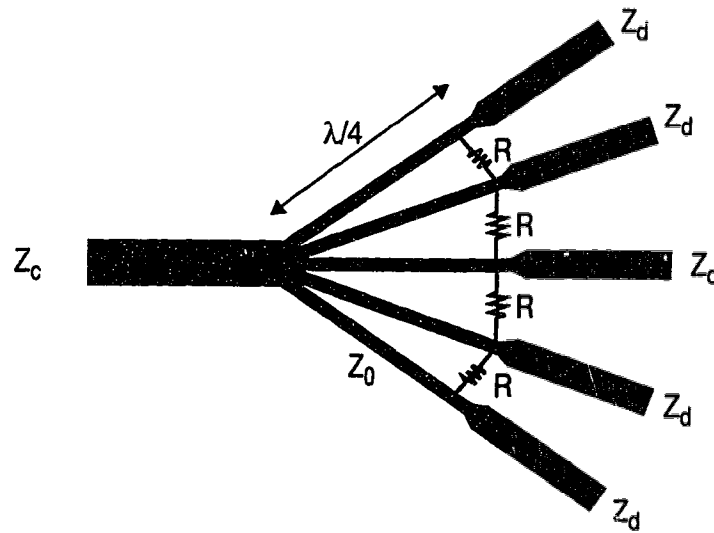
- input ports should be well matched to the source impedance
- isolation between different input ports should be high
- the frequency transfer function from input to output port should be broadband
- amplitude and phase response of the different signal paths should be similar

These requirements are satisfied with structures such as the Wilkinson  $n$ -way hybrid combiner [85], and the “fork” hybrid combiner [86]. These structures are shown in Figure 4.25. These combiner structures are called ‘hybrids’ because they require the use of additional elements - resistors, as well as transmission line elements.

The  $n$ -way Wilkinson hybrid provides a broadband match for the inputs to



Wilkinson hybrid combiner



'fork' hybrid combiner

**Figure 4.25 Wilkinson and 'fork' hybrid combiners**

be combined [87] though the structure is not planar for  $n > 2$  since resistors are required between each of the  $n$  input branches and the centre branch, including the two at the extreme ends (Figure 4.25).

Fork hybrids permit planar structures to be realized for any number of ports, but the match and isolation is not as good as the Wilkinson combiner and the bandwidth is  $< 20\%$  around the centre frequency used for design [88]. Both kinds of hybrid structures may be improved by using two (or more) stages of isolation resistors [88] as shown in Figure 4.26.

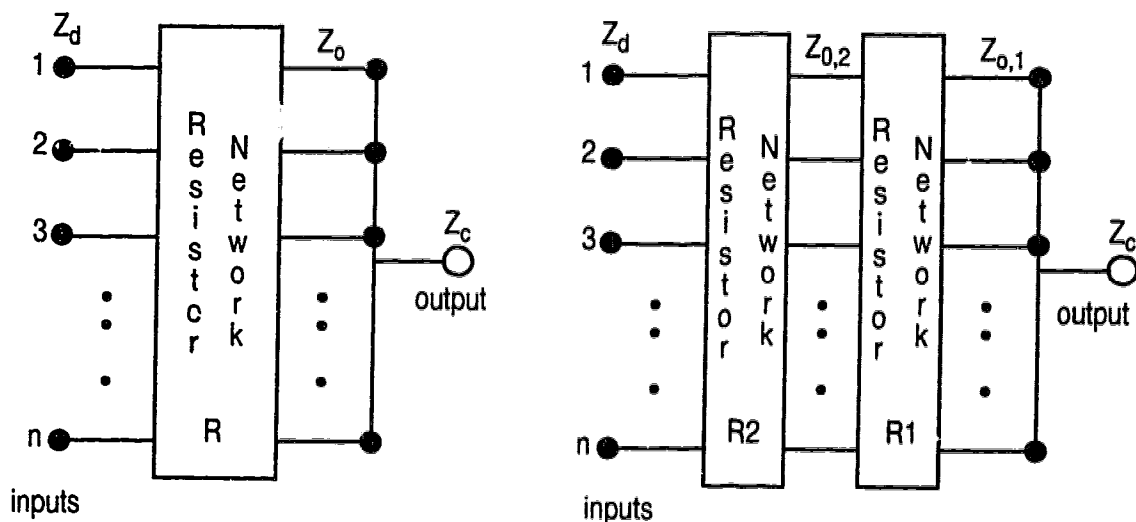


Figure 4.26 Single stage and two stage combiner hybrid circuits

Design of  $n$ -way combiner circuits for MSM photodetector arrays, however, has important additional constraints which make the Wilkinson or Fork hybrids unsuitable. The primary constraint is that the sources to be combined are essentially (photo) current sources (ideal current sources are open circuits) which make the use of  $\lambda/4$  sections impractical and the expressions for calculating the impedance of the combiner stage transmission lines ( $Z_0$ ,  $Z_{0,1}$ ,  $Z_{0,2}$  in Figure 4.26)

are no longer valid [88].

Also, the use of isolation resistor stages in combiners introduces complex additional processes (thin film resistors) to the fabrication of photodetector arrays (in GaAs or InGaAs systems). In addition to these limitations, the planar hybrid structure (fork) also has a limited bandwidth. Despite these factors which negate the use of these circuits for photodetector arrays, a number of combiner arrangements inspired by these hybrid structures were explored. The HP-MDS software package [79], which provides an extensive library of distributed and lumped passive microwave component models for RF simulations, was used to investigate the frequency response behaviour of various combiner designs. The MSM photodetector device model shown in Figure 4.27 was used in all of these simulations.

A four port schematic representative of the simulation circuits is shown in Figure 4.27. The minimum array size for the simulations was kept at 1x10 to yield designs which are usable in optoelectronic switching applications, although most of the designs were for 1x16 arrays to permit 16x16 switches.

The impedance between the MSM photodetector and the output port ( $50\Omega$ ) is split into three sections  $Z_1$ ,  $Z_2$ , and  $Z_o$  as shown in Figure 4.27. These are varied and jointly optimized to yield a target bandwidth of dc to more than 10GHz for each photodetector in the array in addition to ensuring that all the photodetectors exhibit a uniform frequency response.

The three different impedance sections ( $Z_1$ ,  $Z_2$ ,  $Z_o$ ) consist of multiple transmission line components including tapered transmission line sections and

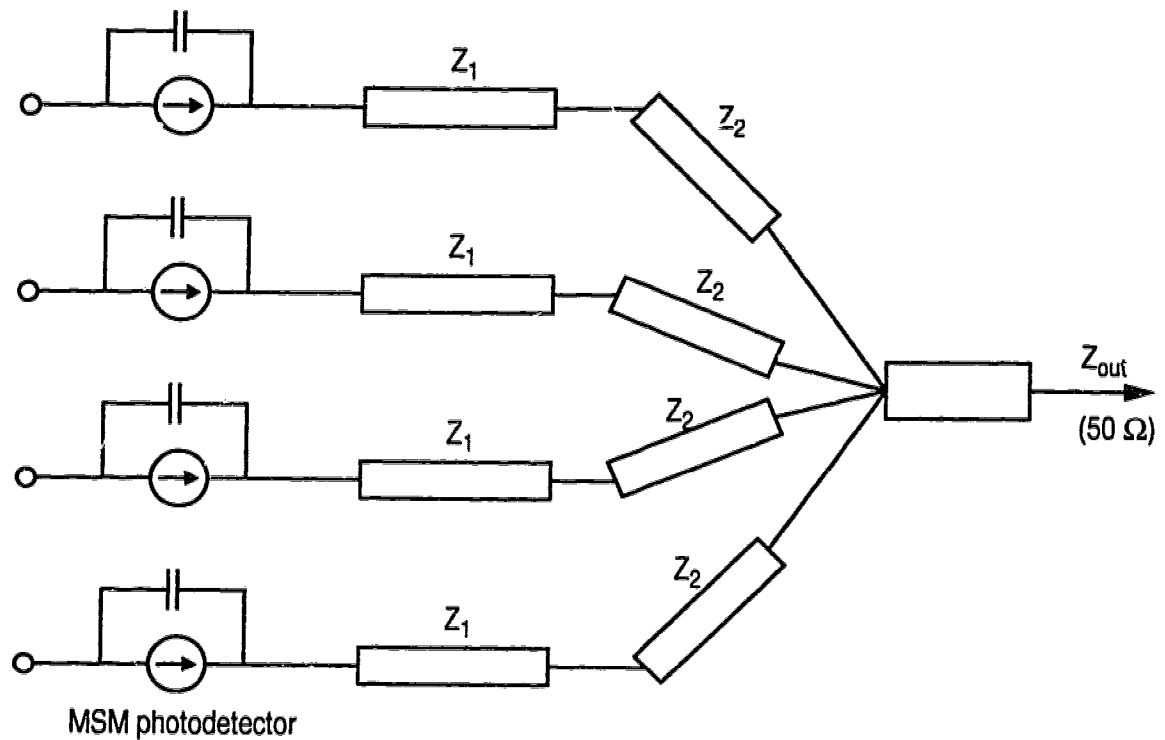


**Figure 4.27 Schematic of 1x4 combiner for photodetector array**

transmission line sections of different characteristic impedances. The effect of each impedance section on the frequency response was observed and then varied to achieve the bandwidth targets for the photodetector array. Extensive simulations executed on an alpha 3000 workstation were used to empirically optimize the designs for maximum bandwidth as well as uniformity of bandwidth.

The MSM array designs using these combiners were carried out for two categories of applications:

- optoelectronic switching, and
- optoelectronic signal processing

Array designs intended for switching applications are optimized for the case where the array functions as a 'selector' of incident signals and only one out of  $N$  photodetectors in the array is biased 'ON' at any given time. This fact has implications for the capacitance used in the photodetector models. Capacitance of a photodetector in the 'ON' state ( $C_{\text{msmON}}$ ) in the model is taken to be 0.1 to 0.25 pF, while the capacitance of a photodetector which is switched 'OFF' ( $C_{\text{msmOFF}}$ ) is slightly higher - 0.25 to 0.5 pF. These values used in the simulations are conservative. Somewhat lower values have generally been reported in the literature [81, 84] on experimental measurements of MSM devices. However, the designs are such that the bandwidth would be higher than reported here if the capacitance values of the devices were to be lower.

For signal processing applications, all photodetectors in the array may be 'ON' ( $C_{\text{msmON}} < 0.25$  pF) and therefore the designs were optimized accordingly.

Figure 4.28 shows the simulation circuit diagram for a 1x16 array intended for optoelectronic switching applications. 16 identical segments which include the MSM device models and the symmetric branches are visible in the circuit diagram, and an expanded view of two such segments is shown in Figure 4.28(b). DC-bias circuitry and decoupling capacitors (similar to the circuit in Figure 4.7) are included in the simulation. The effect of bond wires which would connect the array to the substrate is also included by incorporating appropriate inductances at the output and at each MSM photodetector. Figure 4.29 shows the frequency response of a MSM photodetector in the 1x16 array of Figure 4.28, and the frequency response of a photodetector in a conventional array is also included for

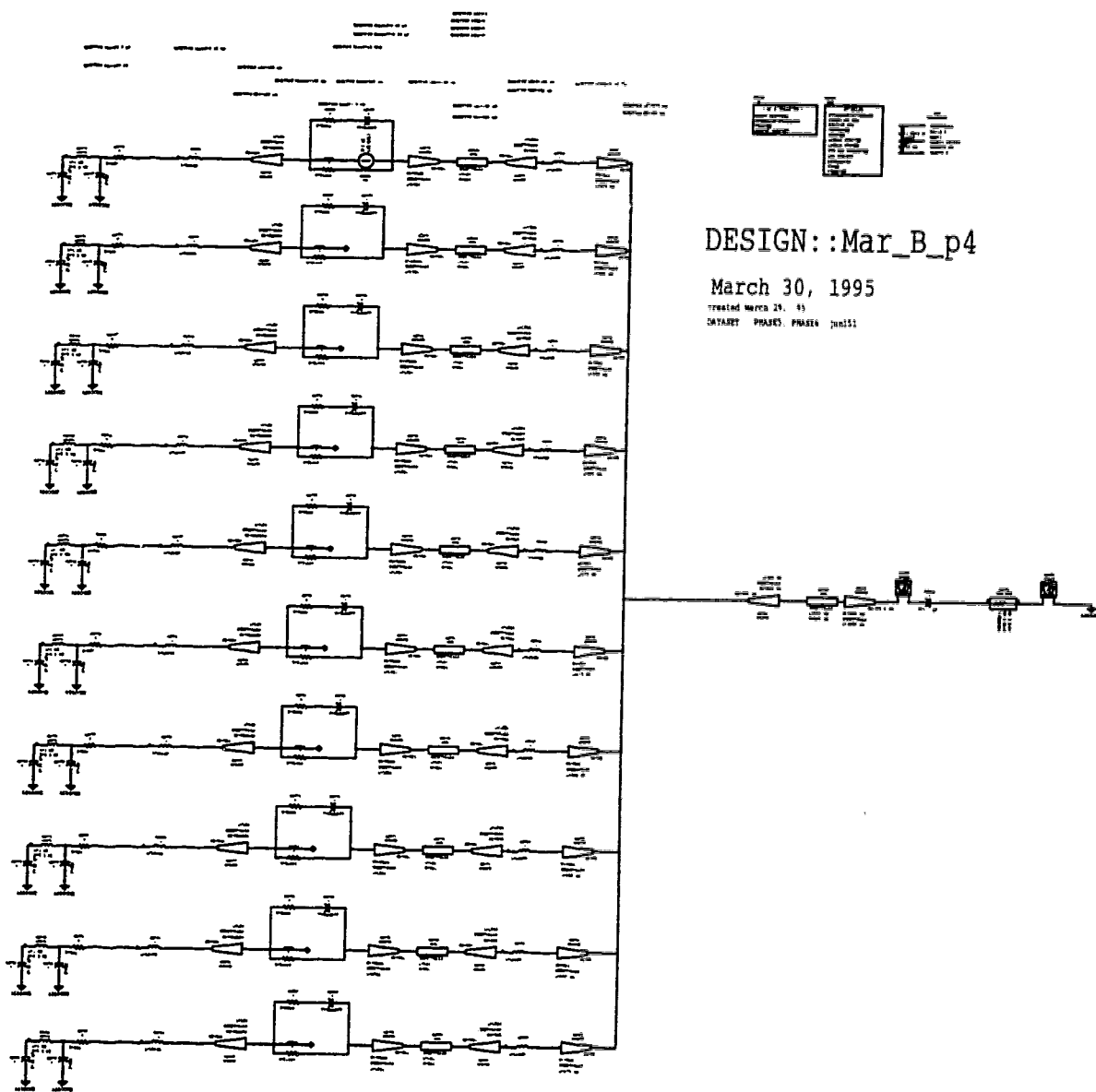


**Figure 4.28 (a) Simulation circuit for MSM array**

comparison. The frequency response of the photodetector exhibits better than  $\pm 1$  dB flatness over the entire pass band which extends past 18 GHz.



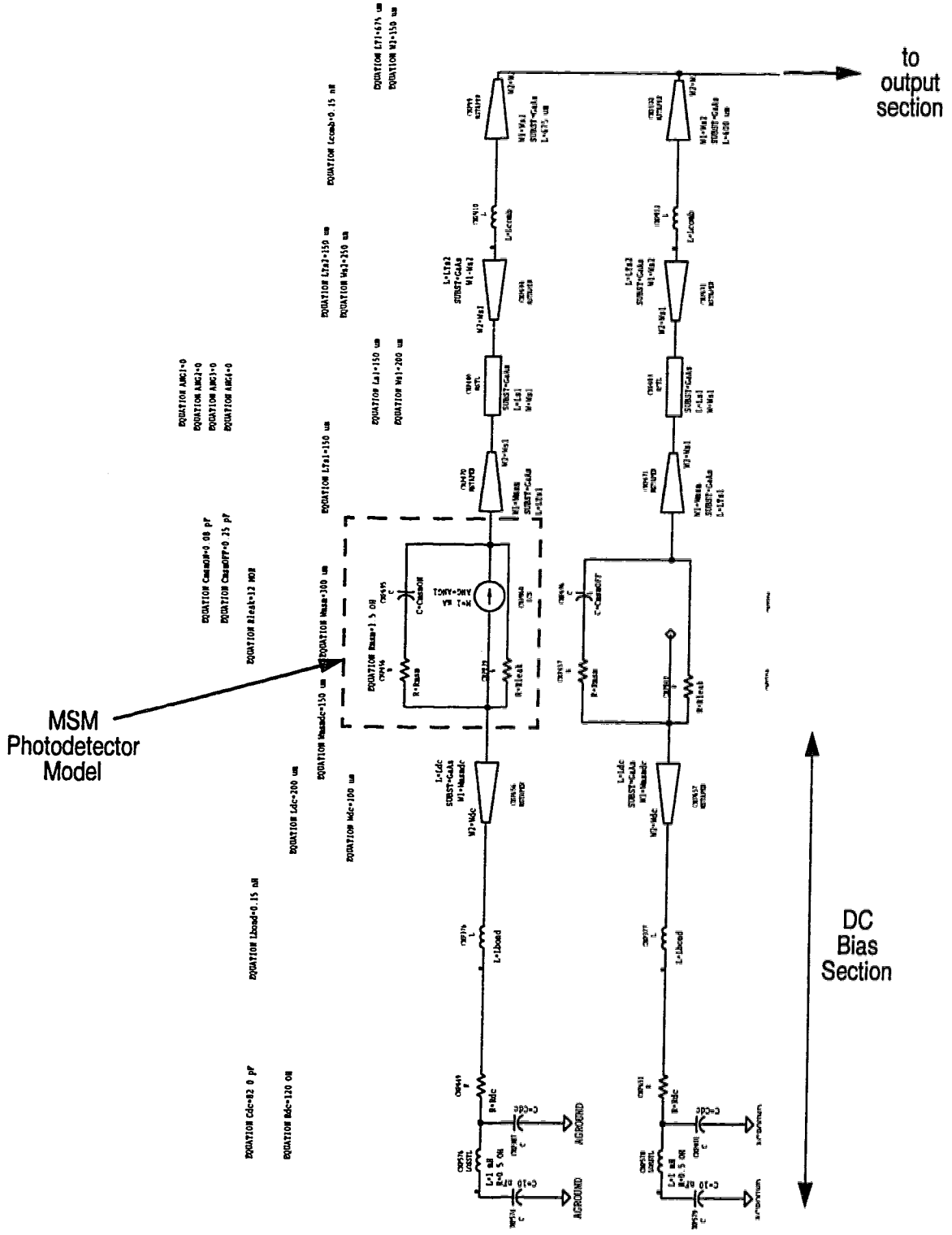


Figure 4.28 (b) Detail of MSM branch

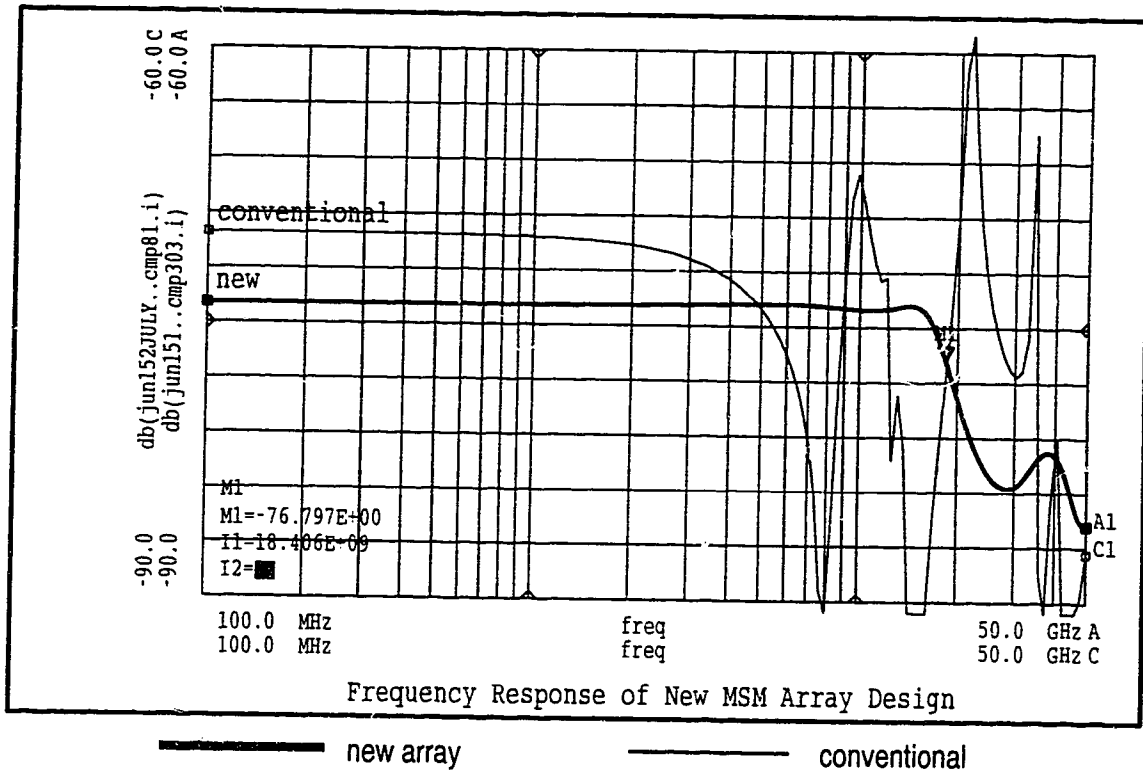


Figure 4.29 Frequency response comparison of MSM photodetectors in array design shown in Fig. 4.28 Vs conventional design

## 4.5 Designs for TR Labs MSM Mask

Following the circuit depicted in Figure 4.28, a number of array designs were selected for various switching applications at TR Labs. The layouts for these designs and the simulated frequency responses obtained are given in the following sections.

### 4.5.1 1x16 Array designs

The MSM photodetector arrays for use as signal selecting crosspoints in 16x16 broadband switches are shown in Figure 4.30(a), 4.31(a), and 4.32(a).

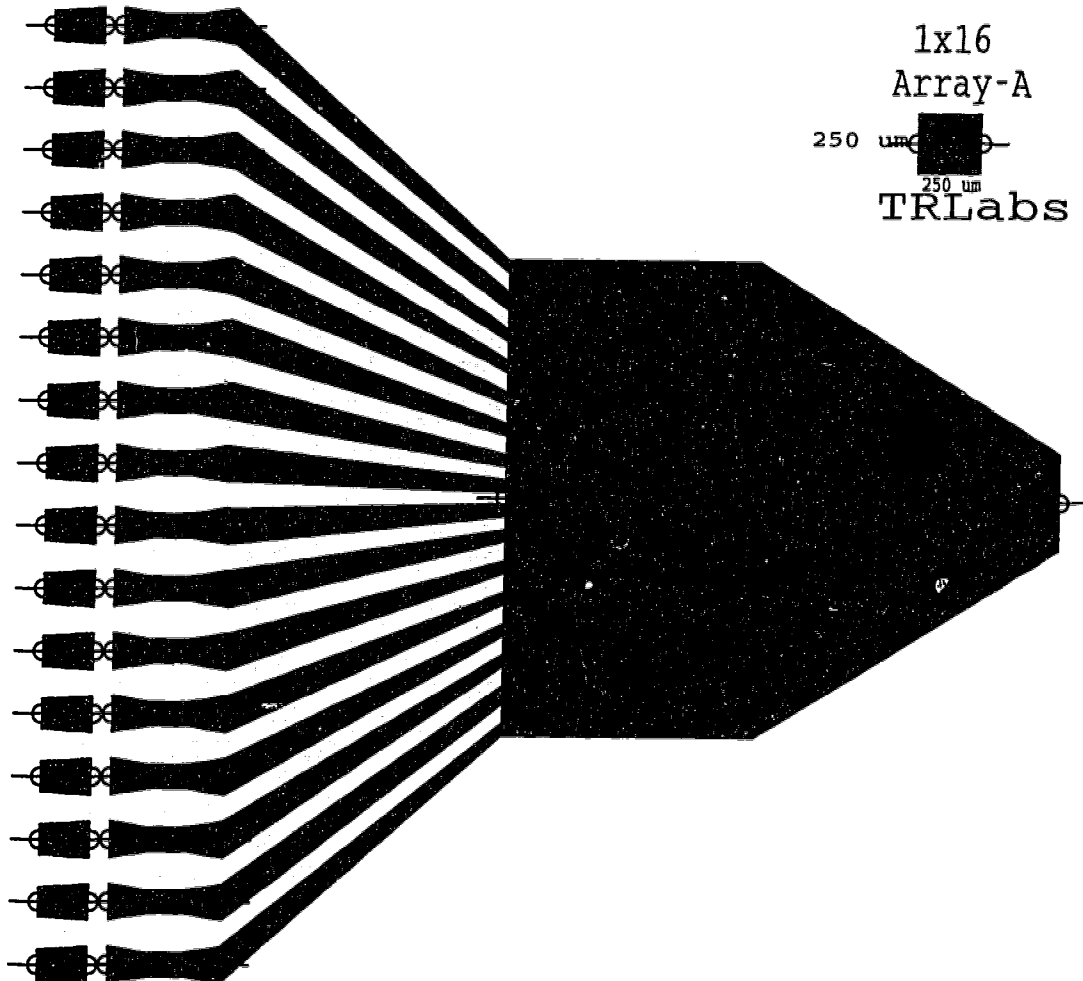
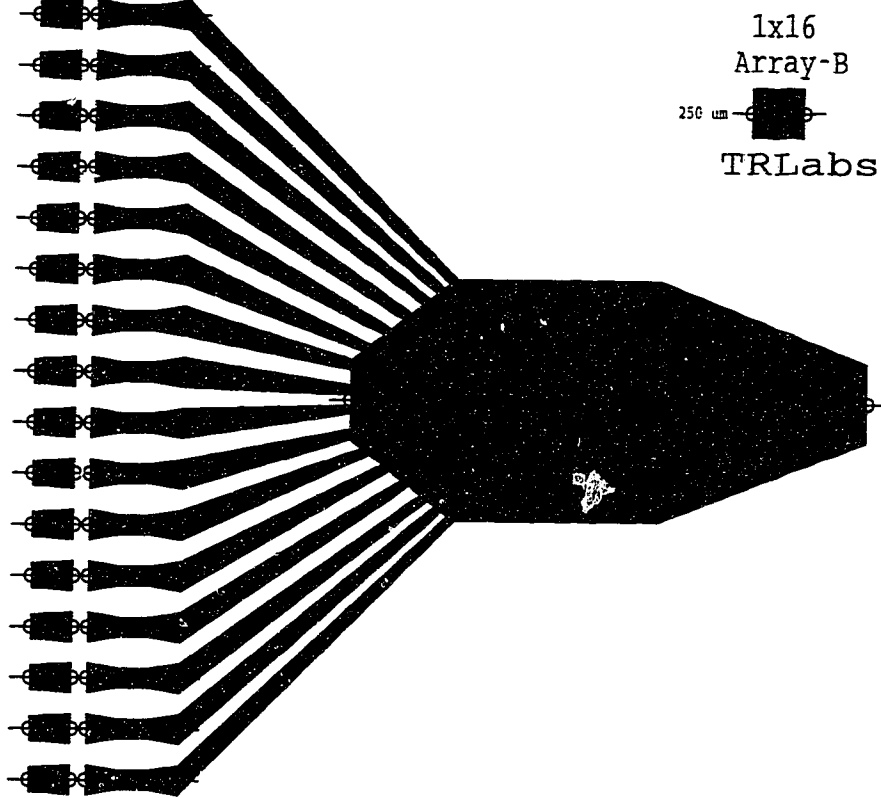


Figure 4.30(a) Layout for 1x16 array design, type A



**Figure 4.31 (a) Layout for 1x16 array, type B**

The frequency response of the array designs is shown in Figures 4.30(b), 4.31(b), and 4.32(b) respectively. The photodetectors are arranged at 250 μm pitch to match the fibre spacing in fibre-ribbons which constitutes the easiest method to distribute optical signals to the devices.

The array design shown in Figure 4.32(a) is intended for use in integrated versions of optoelectronic switch [50]. The constraints imposed by the use of polymer laser written waveguides for signal distribution [15, 89] require the output terminal to be situated close to one end of the array rather than the middle as in Figure 4.30(a) or 4.31(a). Also, the total width of the chip ( $W$  in figure 4.32(a)), is constrained to be as small as possible and therefore the optimized form of the

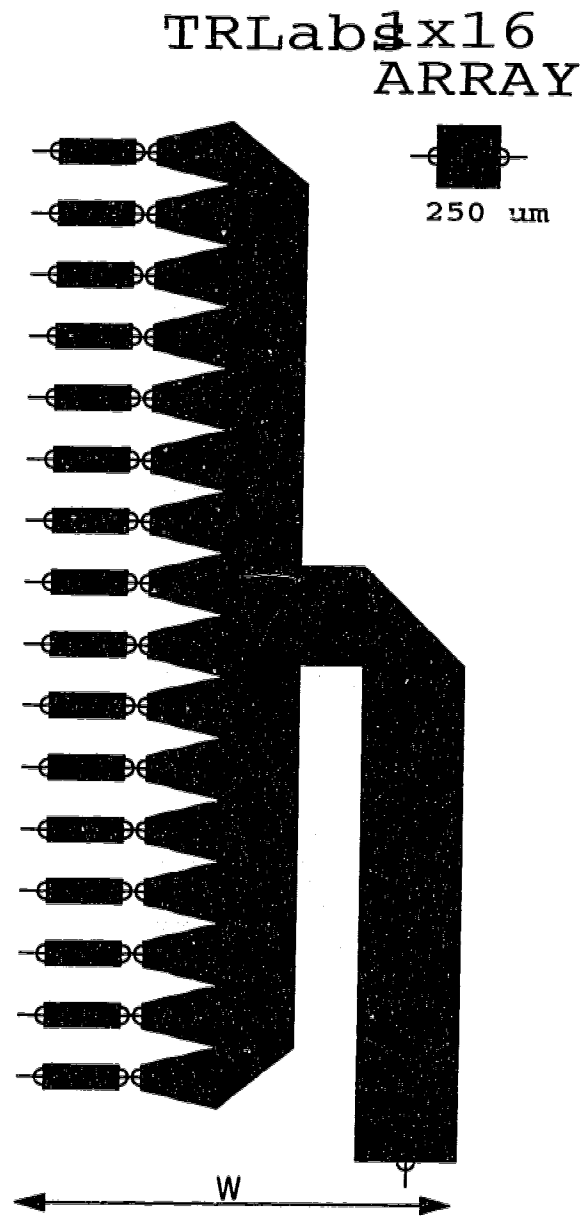


Figure 4.32 (a) Layout for 1x16 array, type C

output section used in other designs cannot be utilized for this application. As a result, the frequency response for this design exhibits a lower 3 dB roll off point (8 GHz in Figure 4.32(b)) as compared to >10 GHz for other designs. However, binary data up to 10 Gbps may be transmitted through an 8 GHz channel

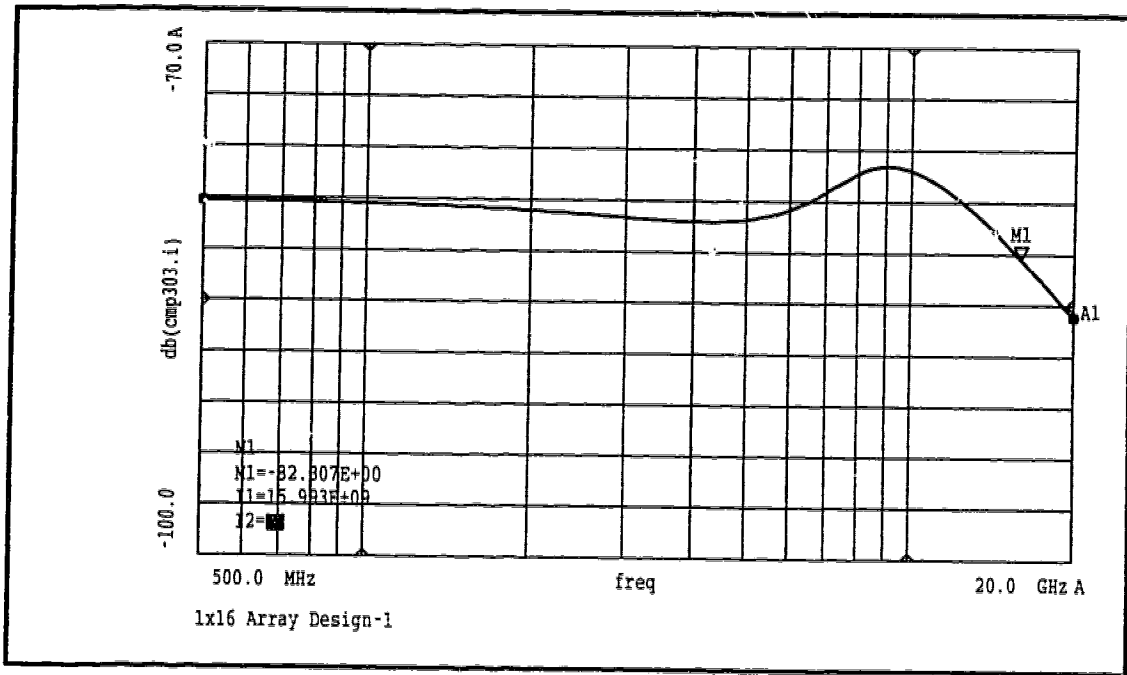


Figure 4.30 (b) Frequency response for 1x16 array, type A

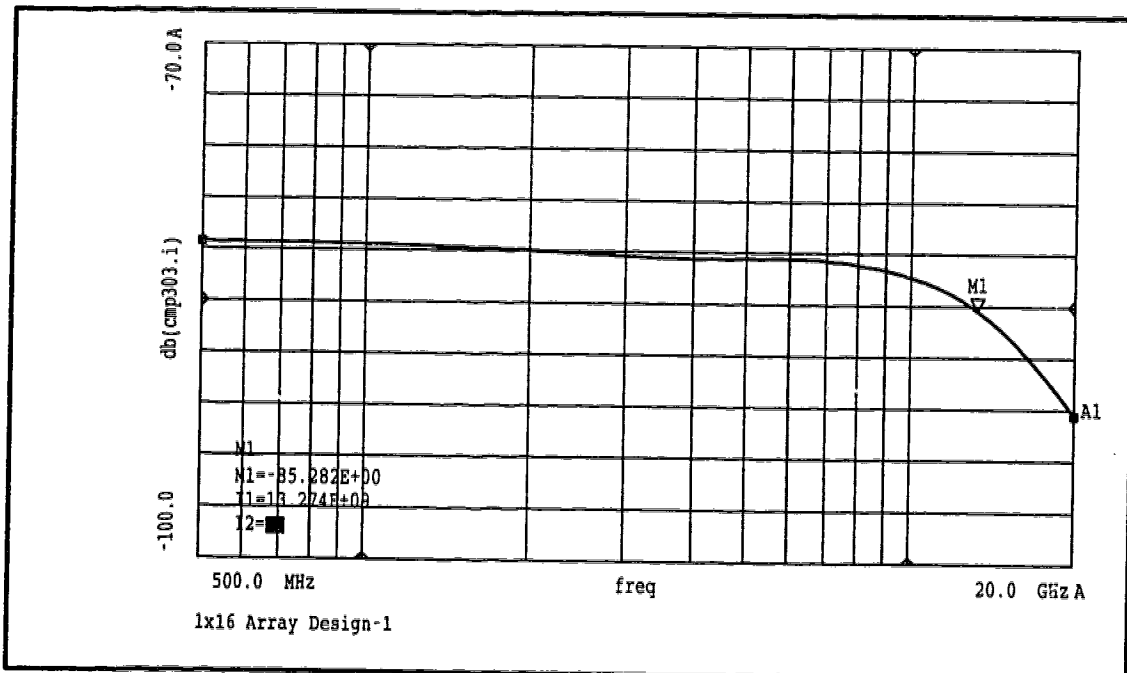
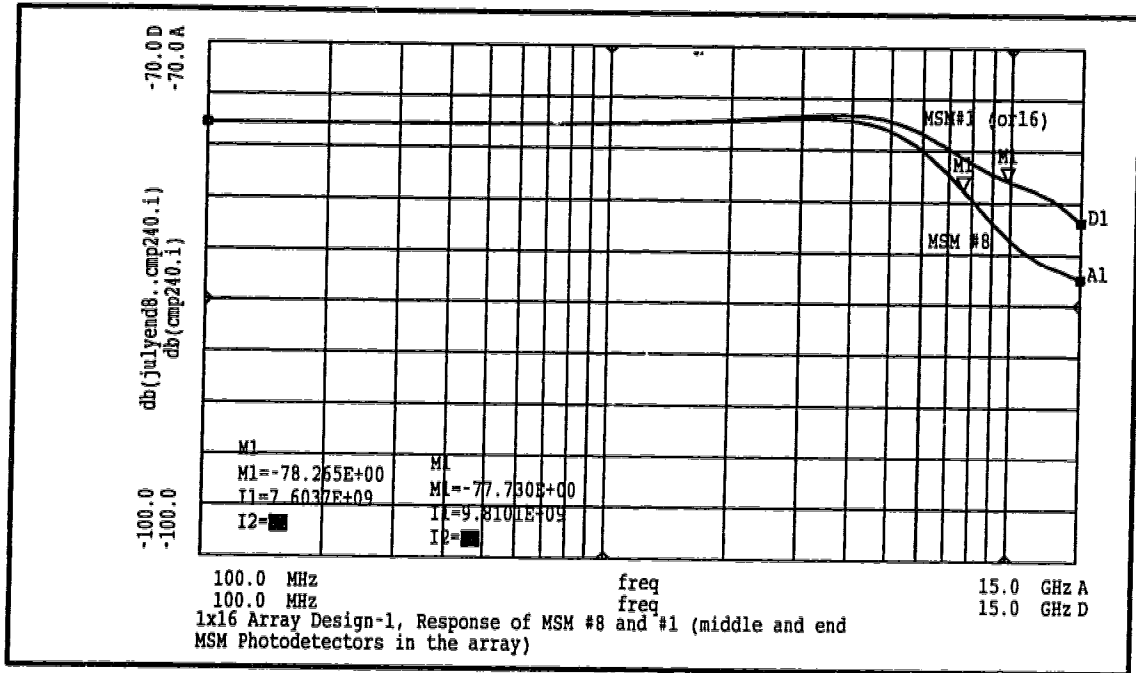


Figure 4.31 (b) Frequency response for 1x16 array, type B



**Figure 4.32 (b) Frequency response for 1x16 array, type C**

bandwidth at acceptable bit error ratio ( $<10^{-9}$ ), and these arrays may be used for switches with aggregate capacity exceeding 150 Gbps.

### 4.5.2 1x8 Array designs

Broadband photodetector arrays for use with free space distribution methods for optical signals are shown in Figure 4.33 and 4.34. Free space optical signal distribution entails the use of beam steering methods with diffractive optic elements [90] or micro-optic components [47, 91]. The designs shown in this section can be used with guided wave distribution techniques as well [15]. The 1x8 array shown in Figure 4.33(a) follows from the 1x16 array design of Figure 4.32(a).

The photodetectors in these arrays are spaced at  $500 \mu\text{m}$  each to match

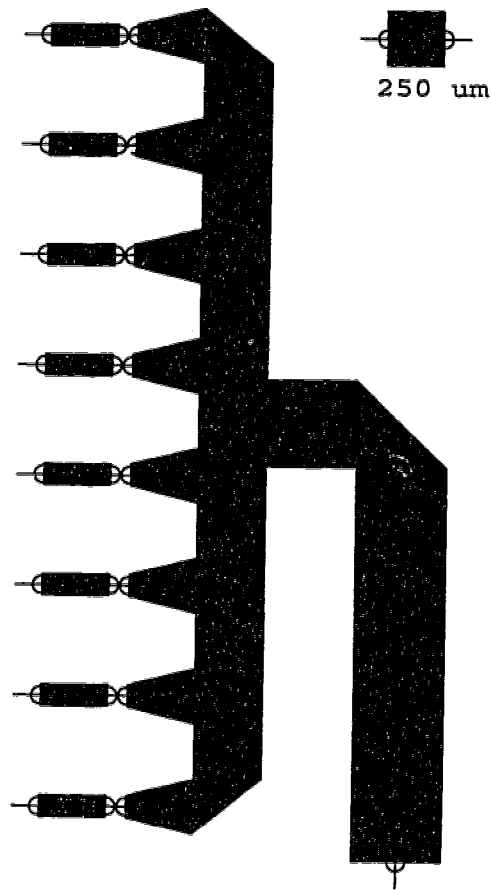


**Figure 4.33 (a) Layout for 1x8 array, type A**

the separation best suited for achieving low crosstalk with free space optical signal distribution [92]. (Note that the 1x16 arrays with 250  $\mu\text{m}$  device spacing can also be used as 1x8 arrays with 500  $\mu\text{m}$  pitch by using alternate photodetectors. There are negligible spurious effects introduced by the impedance of the unused detectors.) The array design shown in Figure 4.34(a) is based on simply ensuring equal length, identical paths from each photodetector to the output terminal, and is different from the other designs since it is a combination of two-port combiner





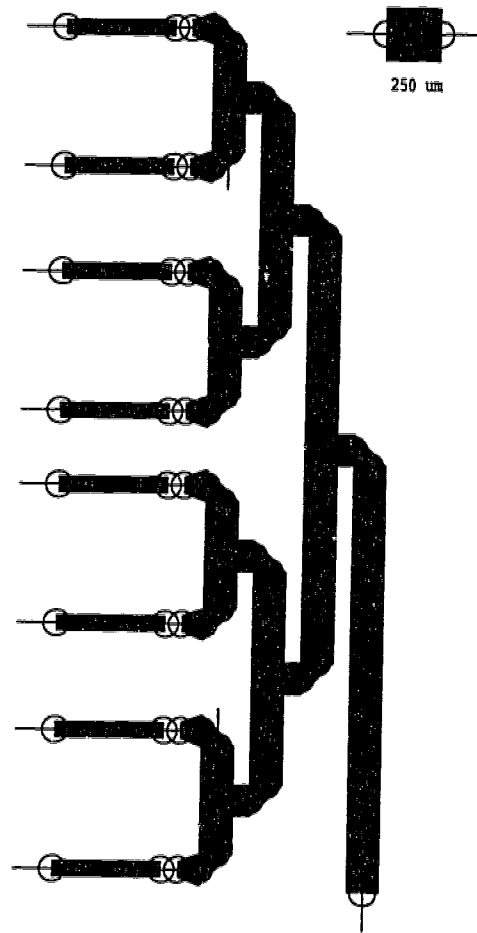


Figure 4.34 (a) Layout for 1x8 array, type B

#### 4.6 Other Applications of Broadband Photodetector Arrays: Wavelength Tunable Receivers

In addition to the optoelectronic switching applications, arrays of photodetectors may also be employed in tunable receivers for wavelength division multiplexing (WDM) systems. As shown in Figure 4.35, multiple wavelengths

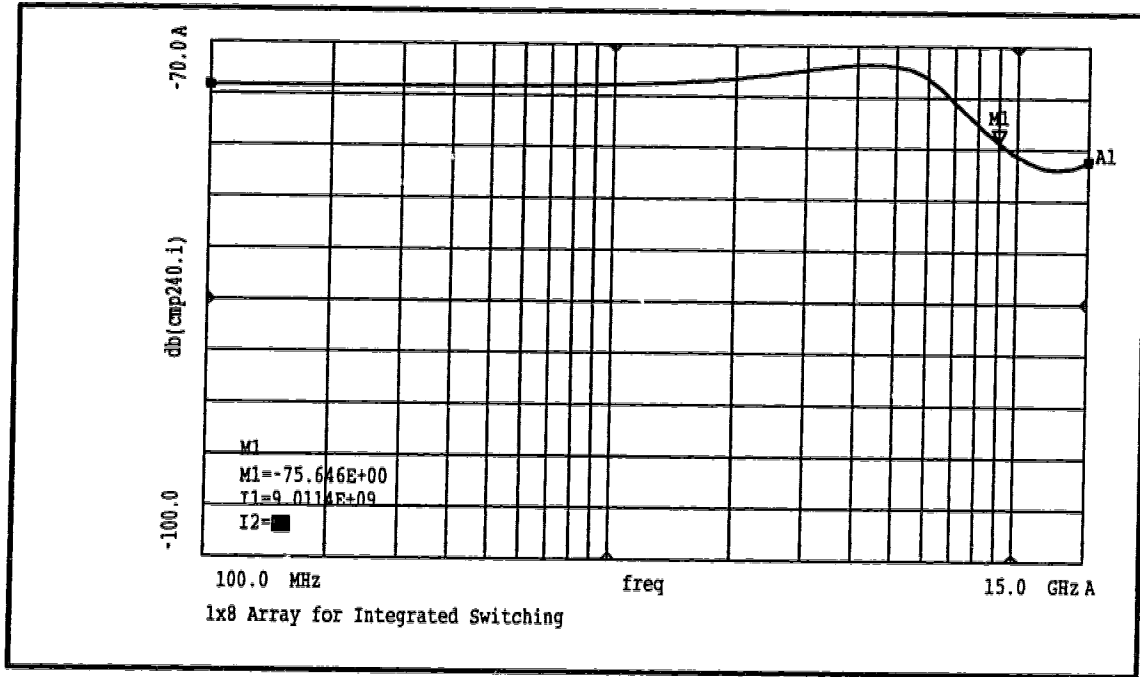


Figure 4.34 (b) Frequency response of all photodetectors in 1x8 array, type B

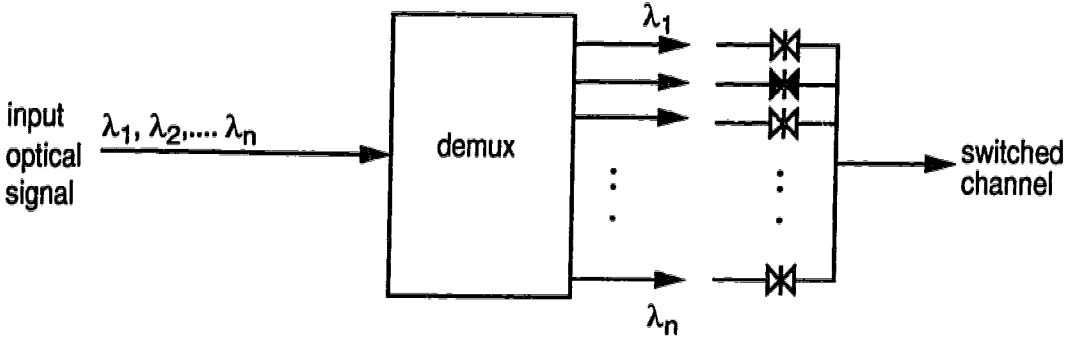


Figure 4.35 Wavelength tunable receiver using photodetector array

contained in the incoming optical signal are separated using an optical demultiplexer (such as a grating), and an array of photodetectors is used to select '1 of N' signals by switching 'ON' the appropriate photodetector. MSM photodetectors are suitable for this application due to the ease of integration, good sensitivity, and low switching voltages [84]. Tunable receivers for low bit rate (700 Mbps) signals based on a similar concept will be commercially available by end of 1996 [93, 94] and the use of broadband MSM arrays reported here can potentially extend the data rate per channel in such receivers to more than 10 Gbps.

## **5. Format-Transparent Switching Results**

Parameters used to characterize the performance of a switching element for various signal formats in a communications network are introduced in this chapter and results for the optoelectronic prototype switch are presented. Data format and bit rate transparency properties of optoelectronic switching are demonstrated with results presented for a variety of data rates. Performance of the optoelectronic prototype switch for switching of analog CATV signals is also characterized.

The use of spectrally efficient modulation formats for photonic interconnects is proposed in section 5.4. Comprehensive experimental results are presented in support of the proposed technique to demonstrate an increase in the throughput of a photonic interconnect by using multilevel modulation.

### **5.1 Characterizing Prototype Switch Performance**

The primary characteristics that determine the performance of a switching mechanism and help evaluate its suitability for applications in broadband communication networks are:

Channel bandwidth

Contrast between ON and OFF states of the switch elements

Crosstalk levels

Signal quality for switched signals

### 5.1.1 Channel bandwidth

The elements which determine the bandwidth in an optoelectronic switch, as in any other photonic communication link, are the components at source and termination of the link. These electronic-to-optical (laser) and optical-to-electronic (photodetector) conversion elements limit the usable bandwidth of optoelectronic switches. In the prototype switch, the channel bandwidth is determined by the transmitter bandwidth (section 3.3). Figure 5.1 shows a plot of the channel

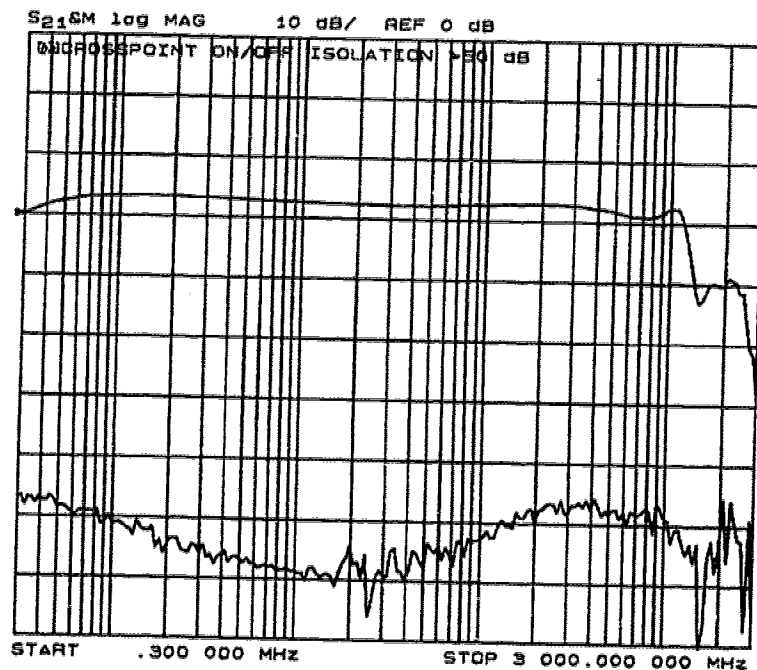


Figure 5.1 Channel bandwidth for prototype switch

bandwidth. 3 dB bandwidth of 1.25 GHz is measured for each of the ten transmitter channels in the prototype. The channel bandwidth can be extended by using laser transmitters and photodetector arrays with higher bandwidth. Array designs presented in Chapter 4 can potentially allow channel bandwidths in

excess of 10 GHz with appropriate lasers.

### 5.1.2 Contrast between ON and OFF states of the switching elements

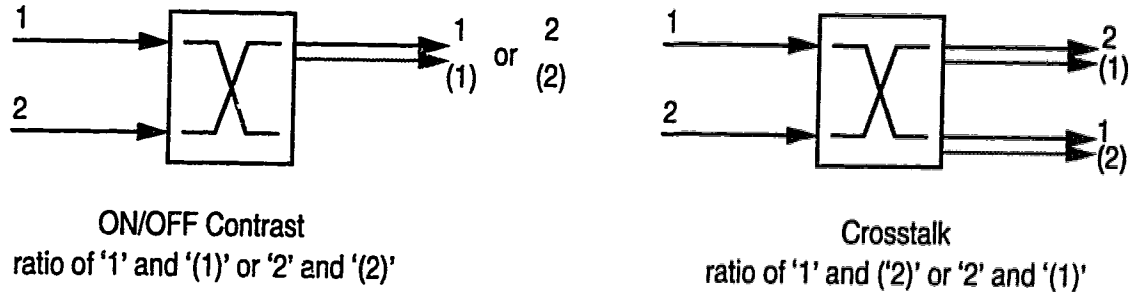
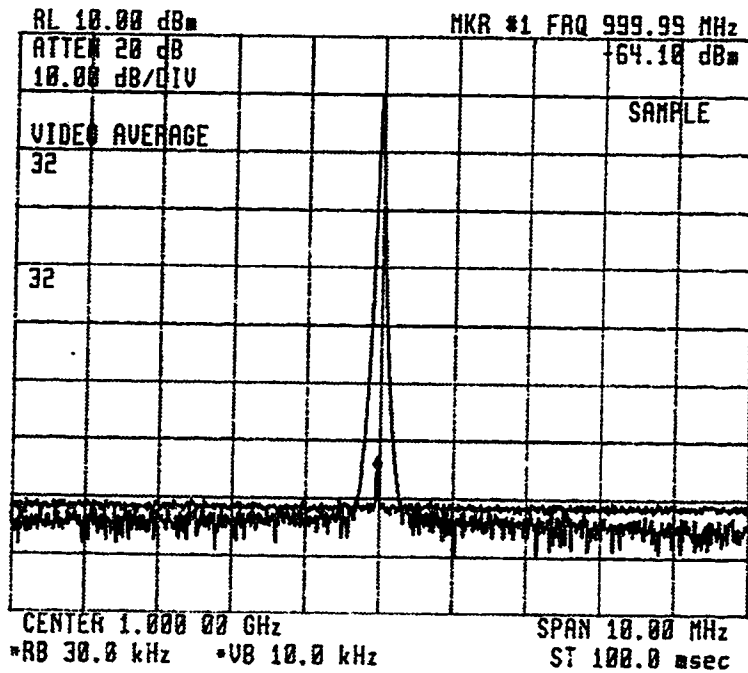


Figure 5.2 ON/OFF Contrast and signal crosstalk

The ON/OFF contrast ratio in a switching element depends on the extent to which the switching element can suppress the signal incident on that element, when the element is rendered inactive. In optoelectronic switching, this contrast is the ratio of the signal from the MSM photodetector in the ON (biased) and OFF (unbiased) states. Since the MSM photodetector consists of two back to back diodes, very little photocurrent is generated when the device is in the unbiased state. Figure 5.3 shows the ON/OFF signal contrast measured for a port in the prototype switch. More than 60 dB of signal contrast is achieved for a signal modulated at 1 GHz. The excellent contrast obtained with optoelectronic techniques is illustrated further in Figure 5.4 with a high resolution scan (resolution bandwidth = 30 kHz) of the channel passband. The channel scan in Figure 5.4(a) shows a 500 MHz tone (-4.81 dBm) in the ON state at the output port of the switch. Interference signals from various radio sources (FM broadcast



**Figure 5.3 ON/OFF Contrast of optoelectronic switching elements**

radio: 80-110 MHz, Alberta private licensed radio networks: 100-200 MHz, Northern Alberta analog radio network: 400 - 430 MHz, Cellular radio: 800-930 MHz) picked up in the high gain (56 dB) receiver circuitry can be seen in the scan. Figure 5.4(b) shows the output port switched to 'OFF' state and the signal tone at 500 MHz is suppressed to -67.76 dBm, below the narrowband interference signals. Another indication of the ON/OFF contrast is available from the channel bandwidth plot of Figure 5.1 where the difference between upper trace (ON) and lower trace (OFF) indicates the isolation between ON and OFF states across the entire channel passband.



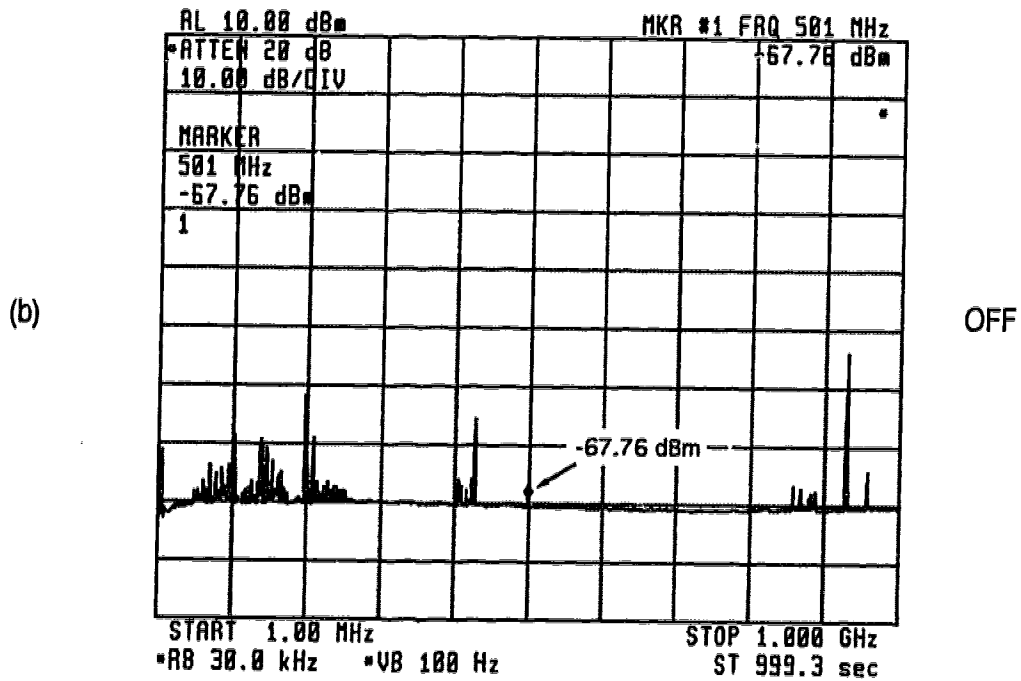
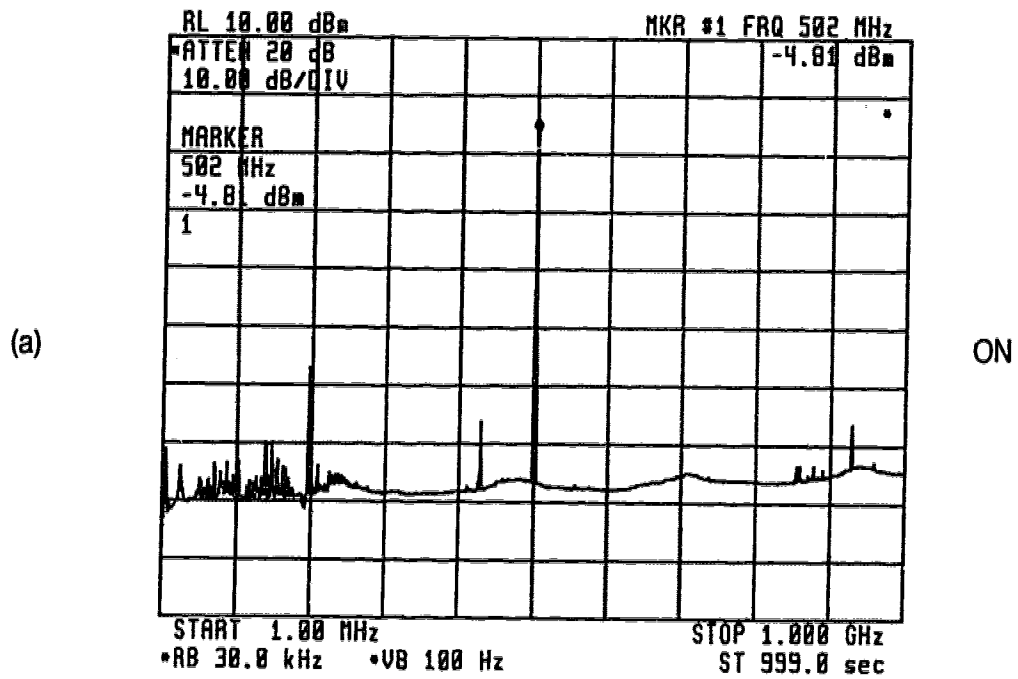


Figure 5.4 Channel spectrum scan showing ON/OFF contrast

### 5.1.3 Crosstalk

Interference caused by signals present in a channel due to cross coupling from other channels in the switch is termed 'crosstalk'. Optoelectronic techniques provide high immunity from crosstalk since signals are never present on a common substrate in either the electronic or photonic domain. The primary cause of crosstalk is the residual signal contribution by the inactive photodetectors in the array due to very small amounts of bias that may be present as a result of non-zero ground potential in the array biasing circuit. Since the photodetectors in the array are individually biased, two adjacent photodetectors can be biased ON (worst case crosstalk) to measure the strength of the interfering signal. By switching OFF one of the photodetectors, and measuring the difference in resultant signal levels, crosstalk can be directly measured (Figure 5.5). Figure 5.6

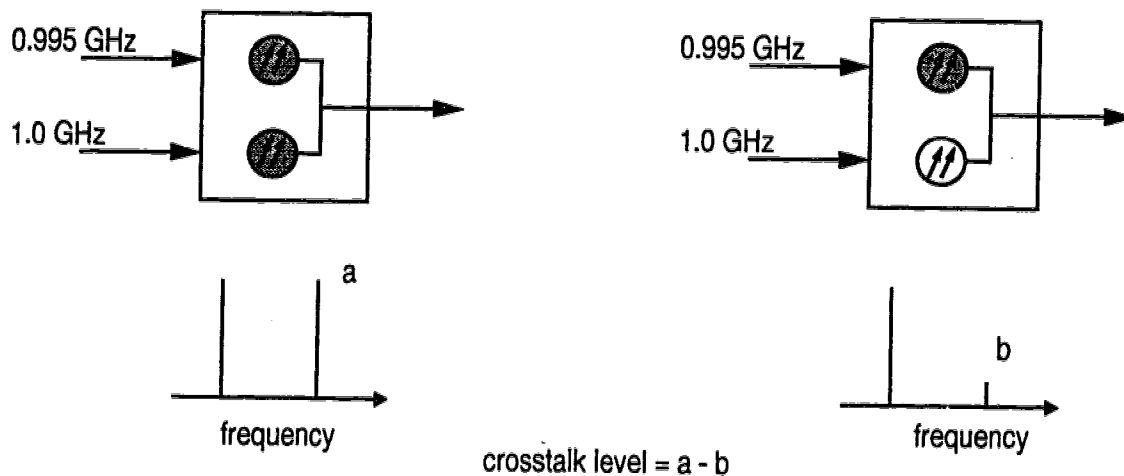
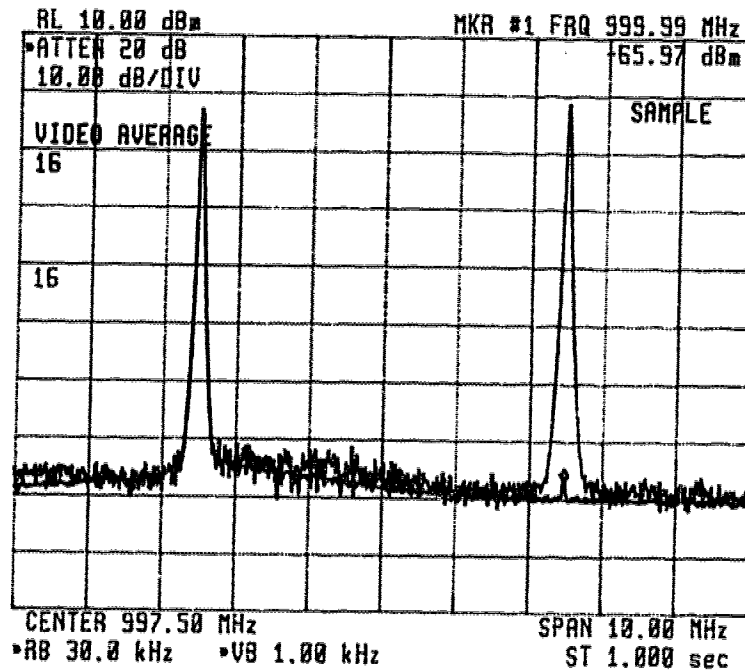


Figure 5.5 Crosstalk measurement experiment

shows superimposed traces corresponding to the two cases shown in Figure 5.5. The crosstalk suppression level in the prototype switch is measured at more than



**Figure 5.6 Crosstalk measurement at 1 GHz**

60 dB. Note that this experiment provides a measure of the total crosstalk contribution. This consists of the 'OFF' state photocurrents from all photodetectors except one that is switched 'ON', as well as the optical crosscoupling between the two adjacent inputs. A qualitative indication of the signal crosstalk immunity of the optoelectronic switch prototype is also available in the experiment described in section 5.3.3 where an analog TV signal and a broadband data signal (622 Mbps to 2.488 Gbps) are routed simultaneously through the prototype switch.

In addition to these factors which help evaluate the performance of the switch, signal quality measurements are also important in order to fully characterize the switch fabric. Results for digital and analog signals switched through the prototype are presented in the following sections.

## 5.2 Digital Signal Switching

The broadband binary digital signal constitutes the most commonly used format of data used for information transfer in communication networks today. The quality of a transmission channel for binary signals is characterized in terms of bit error rate (BER) for a given data rate through the channel. Eye diagrams are also useful in indicating the quality of the channel. BER measurements at different data rates for binary signals routed through the switch are given in Table 5.1.

**Table 5.1 BER measurements**

Data Rate	Data Sequence Length	Bit Error Rate (BER)
622.08 Mbps (OC-12)	$2^{23}-1$	error free (30 minutes)
1.0 Gbps	$2^{23}-1$	error free (30 minutes)
1.5 Gbps	$2^{23}-1$	error free (30 minutes)
2.0 Gbps	$2^7-1$	$3 \times 10^{-10}$
2.48832 Gbps (OC-48)	$2^7-1$	$2 \times 10^{-9}$

Eye diagrams for various data rates are shown in Figures 5.7 to Figure 5.11. Since the switch has no digital circuitry, the data rate at any input can be continuously changed without any changes required in the switch hardware or software. The prototype switch is capable of routing any data rate up to a maximum of OC-48 (2.48832 Gbps) per channel, which is currently the highest data rate in commercial use anywhere in the world. The current aggregate capacity of the 10x10 prototype switch is thus 25 Gbps. Section 5.4 proposes the use of multilevel signalling in switch fabrics to extend the capacity to 3.6 Gbps per channel or an aggregate of 36 Gbps. With the arrays designed for > 10 GHz

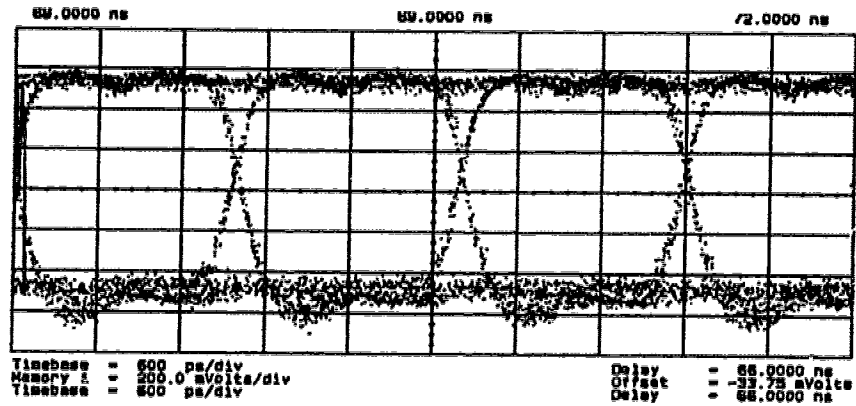


Figure 5.7 Eye diagram for data rate = 622.08 Mbps (OC-12)

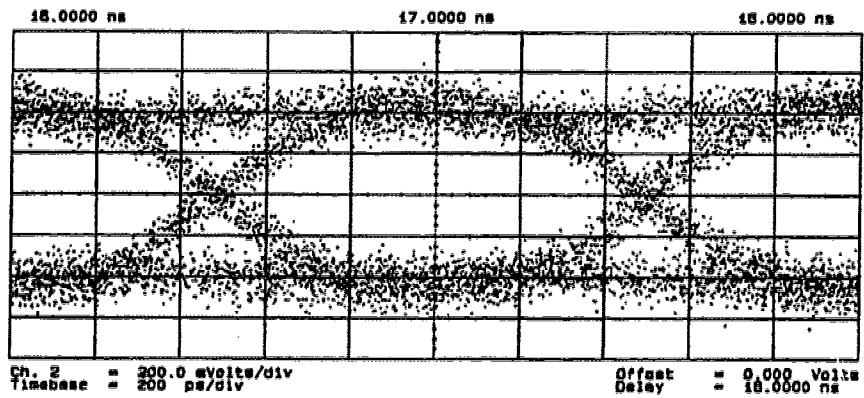


Figure 5.8 Eye diagram for data rate = 1.0 Gbps

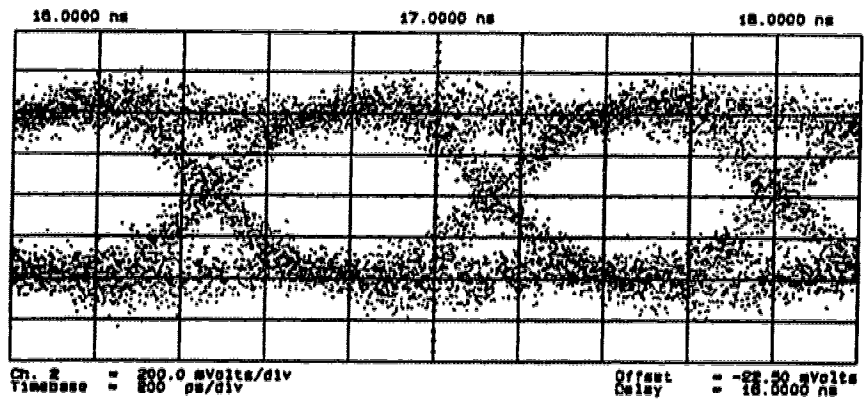


Figure 5.9 Eye diagram for data rate = 1.50 Gbps

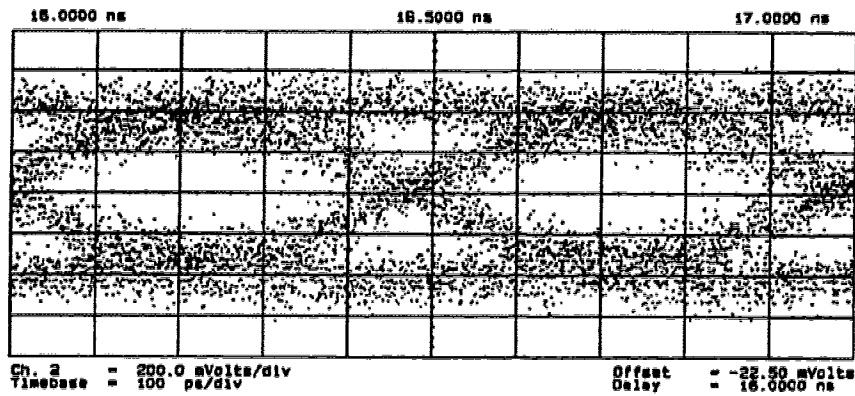


Figure 5.10 Eye diagram for data rate = 2.0 Gbps

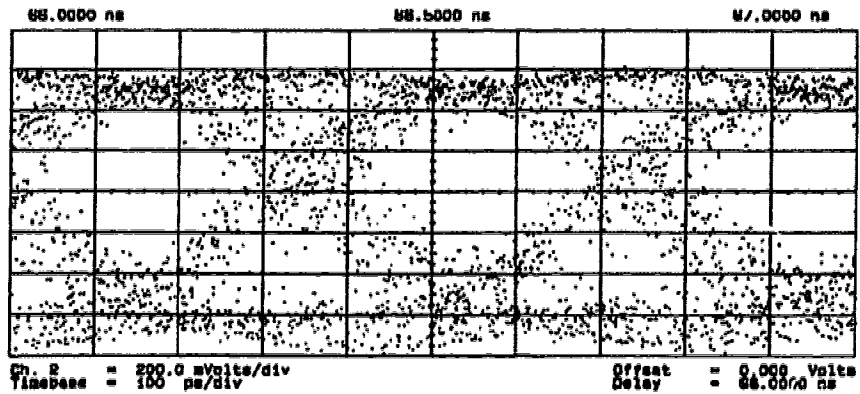


Figure 5.11 Eye diagram for data rate = 2.488 Gbps (OC-48)

channel bandwidth, data rates of 10 Gbps (OC-192) and above which may be in commercial use in the near future, can be routed through an optoelectronic switch.

### 5.3 Analog Signal Switching

Broadband cable TV (CATV) networks are one of the fastest growing areas in telecommunications. Even as new standards for digital transmission of high quality video signals are being established, it is clear that analog video signals

would continue to be carried on these networks as well. The application of optoelectronic switch for routing analog video signals is evaluated in this section.

### **5.3.1 Analog video signals**

The signal path through the prototype optoelectronic switch provides a high quality channel capable of routing analog video signals in addition to the digital signals described in section 5.2. Signal quality measurements with video carrier signals generated in the laboratory were carried out with the prototype switch. A bank of single frequency video carrier signals generated by a special purpose signal generator is used to represent the CATV multichannel video payload. Performance testing of analog systems can be carried out with this 'matrix generator' which can generate a comb of video carrier frequencies with variable power level for each frequency.

It is useful to review the video signal format characteristics so that the impairments caused in the transmission or routing of these signals may be characterized. The NTSC (National Television Systems Committee) standard video signal spectrum is shown in Figure 5.12. The video carrier signal is located 1.25 MHz above the low frequency cut off for the channel, and is the dominant frequency component in the signal.

Performance of the optoelectronic prototype switch is characterized for a composite 42 channel standard CATV payload (see Appendix D for CATV channel designations) with video carrier frequencies ranging from 55.25 MHz (channel 2) to 349.25 MHz (channel 45).

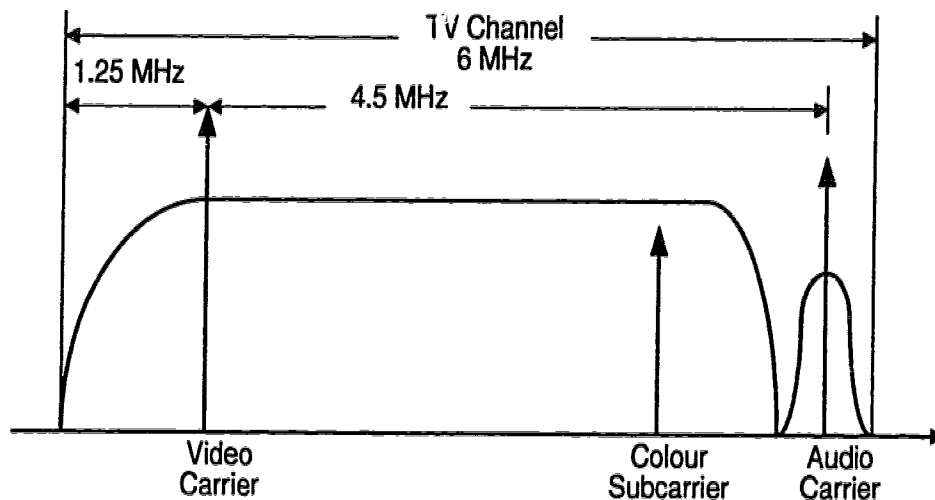


**Figure 5.12 NTSC standard video channel spectrum**

### **5.3.2 System impairments**

Transmission of analog video signals in a lightwave system (such as the optoelectronic switch which consists of a laser transmitter and a receiver in each path) is affected by the noise present in the system as well as the distortion effects due to nonlinearities in the system.

#### *5.3.2a Noise*

The three dominant types of noise in the system are receiver thermal noise, shot noise, and relative intensity noise (RIN). For the optoelectronic switch, the receiver thermal noise is measured to be 116 dB/Hz (see Figure 5.13 and CNR calculation), RIN noise or laser excess noise, for the laser diodes used in the switch is 125-130 dB/Hz [3, 65]. Another potential source of noise (optical) in the switch is the multimode splitter in which modal noise (speckle noise) effects could



limit the average power to variance ratio to ~30 dB for devices under severe mechanical stress [95], though no such effects are observed with the prototype switch. Modal dispersion limitation in the case of optoelectronic switch is negligible due to the short fibre length (1 m) used for signal distribution in the switch (bandwidth.distance product: 500 MHz-km).

Based on the contributions of various sources of noise in the switch, the dynamic range of each channel is expected to be dominated by the receiver thermal noise.

The noise performance of an analog system is measured in terms of Carrier power to noise power ratio termed Carrier-to-Noise ratio (CNR). The National Cable TV Association (NCTA) recommends the following settings in Table 5.2 for the spectrum analyzer to measure CNR and other distortion products.

**Table 5.2 NCTA recommended spectrum analyzer parameters**

<b>Parameter</b>	<b>Recommended Value</b>
Resolution Bandwidth	30 kHz
Video Bandwidth	100 Hz
Frequency Span	10 MHz
Sweep Time	6 seconds

NCTA also recommends a procedure to be followed for measuring CNR and distortion products for analog video systems. All measurements reported here follow the procedure given in [96].

To measure CNR, carrier power is measured by tuning the marker to the

carrier frequency and recording the power level while the instrument is set to the parameters given above in Table 5.2. Noise power is measured at the carrier frequency when the carrier signal is turned off at the source. Figure 5.13 shows

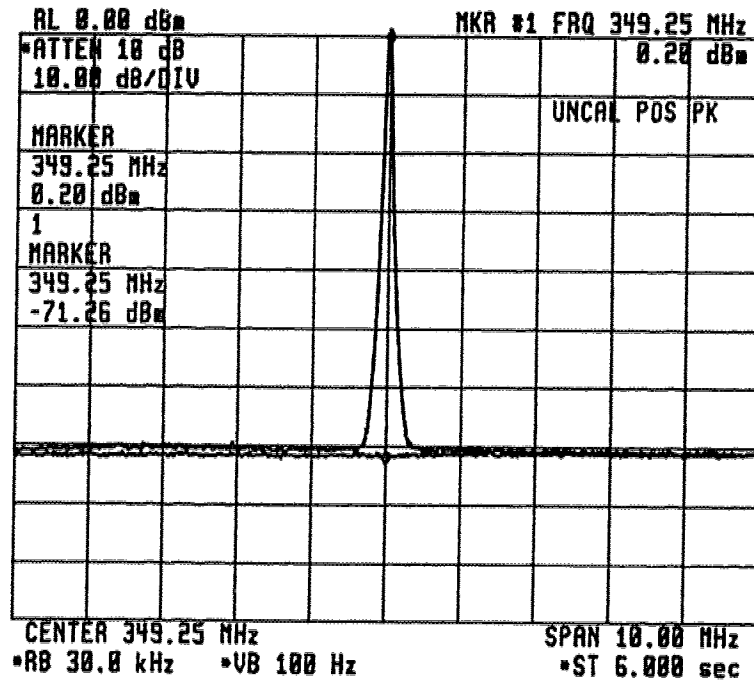


Figure 5.13 CNR for analog video signals

the two traces corresponding to carrier power (0.20 dBm, the input signal level to the switch is set at 0 dBm or a modulation depth of 21.2%, see calculation in section 5.3.3 for calculation of modulation index) and noise power (-71.26 dBm) measured at 349.25 MHz (video carrier frequency, Channel 45).

The CNR is calculated as:

$$\begin{aligned}
 \text{CNR} &= 0.20 - (-71.26) \text{ dB} = 71.46 \text{ dB (in 30 kHz} \\
 &\text{measurement bandwidth)} \\
 &= 116.2 \text{ dB/Hz} \\
 &= 49.96 \text{ dB in 4.25 MHz video bandwidth}
 \end{aligned}$$

NCTA recommends a minimum CNR of 44 dB for coaxial tv networks [96].

### 5.3.2b Nonlinear distortion

There are three kinds of nonlinear distortion effects in an analog video system:

Cross modulation

Harmonic distortion

Intermodulation distortion

Cross modulation is a form of distortion where modulation from a channel is superimposed on other channels in the system as a result of nonlinear gain mechanisms in the system [97].

Harmonic distortion, as the name implies, results from harmonic frequencies of different carriers present within the channel passband of interest.

Cross modulation and harmonic distortion effects in a lightwave analog CATV system are usually small compared to the intermodulation distortion products [97].

Intermodulation distortion is the result of an interaction between two or more subcarrier frequencies that may result in products present in the band of interest.

As shown in Figure 5.14, intermodulation products resulting from two carrier frequencies  $f_1$  and  $f_2$  give rise to the following signals:

second order distortion product at:  $|f_1 \pm f_2|$

third order distortion product at:  $|2f_1 \pm f_2|$  &  $|2f_2 \pm f_1|$

Third order distortion can also be present as a result of three different

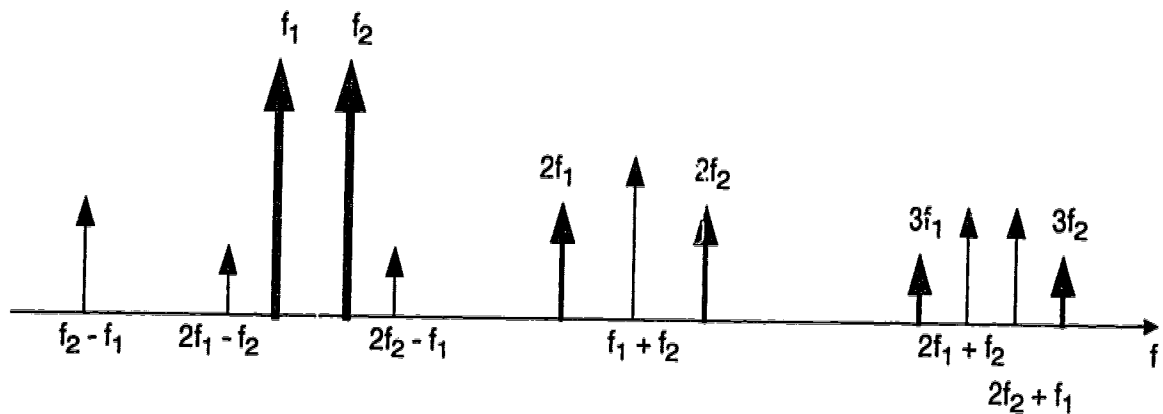


**Figure 5.14 Intermodulation distortion products for two carrier frequencies**

carrier frequencies  $f_1, f_2, f_3$  which will give rise to “triple beats” at  $|f_1 \pm f_2 \pm f_3|$ . Other higher products are usually insignificant compared to second and third order products.

In multichannel systems such as a CATV system, several nonlinear distortion products will fall at the same frequency, causing “beat stacking”. For these systems, nonlinear distortion is characterized in terms of Composite Second Order (CSO) distortion, and Composite Triple Beat (CTB) products which are the strongest second and third order beat stacks within the 6 MHz channel bandwidth.

With the standard CATV channel allocation (Appendix D), it can be seen that CSO products will fall 1.25 MHz above or below the video carrier frequencies (since  $f_1, f_2, \dots$  are 1.25 MHz above a frequency that is an integer multiple of 6 MHz). CSO is measured (in dBc) as the power present at a frequency  $\pm 1.25$  MHz from the video carrier frequency of channel under test, relative to the power of the

video carrier signal.

The third order beat stack products are located at the video carrier frequencies themselves and thus CTB is measured at the video carrier frequency in the channel of interest as the difference between the carrier power at that frequency, and the signal power present at that frequency when the carrier signal is switched off at the source.

CSO and CTB measurements are also done with the NCTA specified instrument settings [96] as listed in Table 5.2. Figure 5.15 shows a view of the intermodulation beat products for Channel 43 (video carrier at 337.25 MHz) while all 44 video carriers are active (-10 dBm per channel).

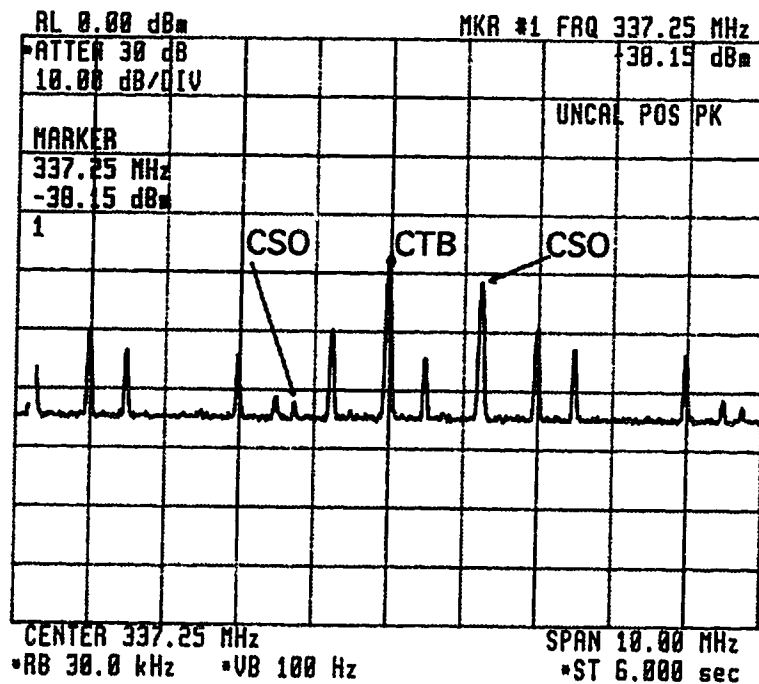
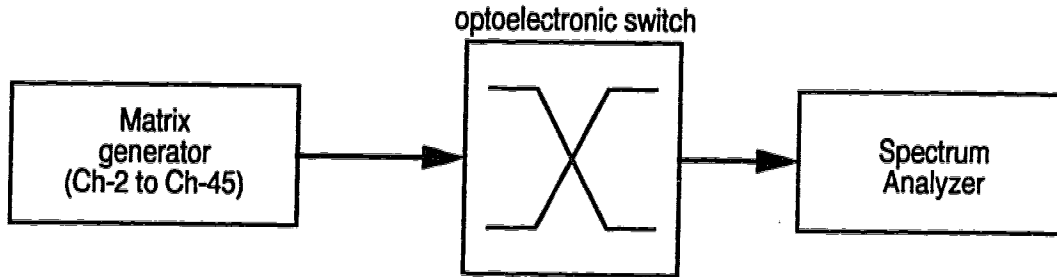


Figure 5.15 Intermodulation products at Channel 43

CTB product is visible at 337.25 MHz, CSO products are present at  $\pm 1.25$  MHz from the centre frequency

The experimental set up for measurement of CNR, CSO, and CTB in a 42 channel bank routed through the prototype switch is shown in Figure 5.16 while



**Figure 5.16 Experimental set up for measuring CSO and CTB**

5.17 shows the entire channel CATV channel bank switched through a single switch port. CSO and CTB results are reported for different modulation depths

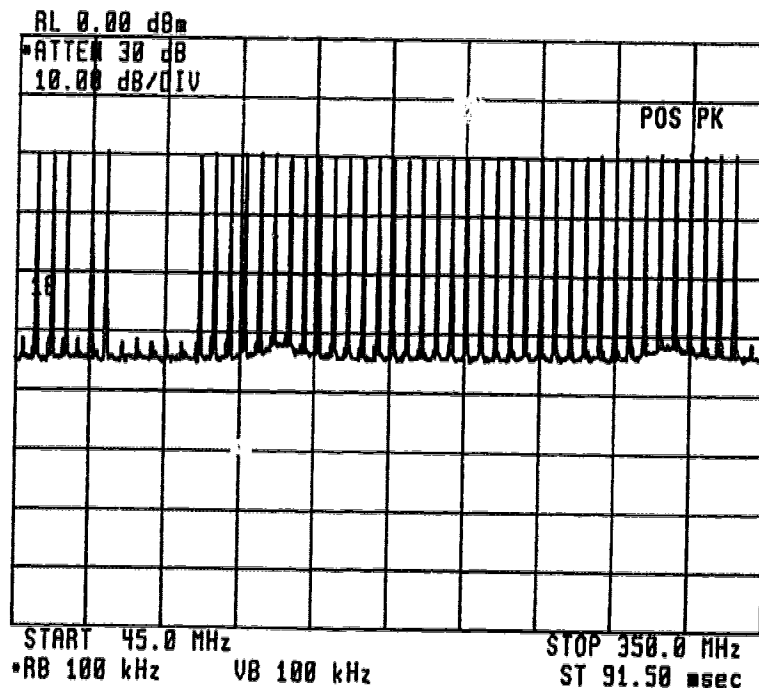


**Figure 5.17 Composite CATV payload (Channel 2 to Channel 45) routed through the optoelectronic switch**

represented by 'modulation index' defined in the next section.

### 5.3.2c Modulation index

Modulation index is used to indicate the depth of the modulation imposed on the laser output signal by the drive signal current. Figure 5.18 shows a characteristic Light-Current (L-I curve) relationship for a semiconductor laser diode, and indicates the various parameters used to define modulation index. The

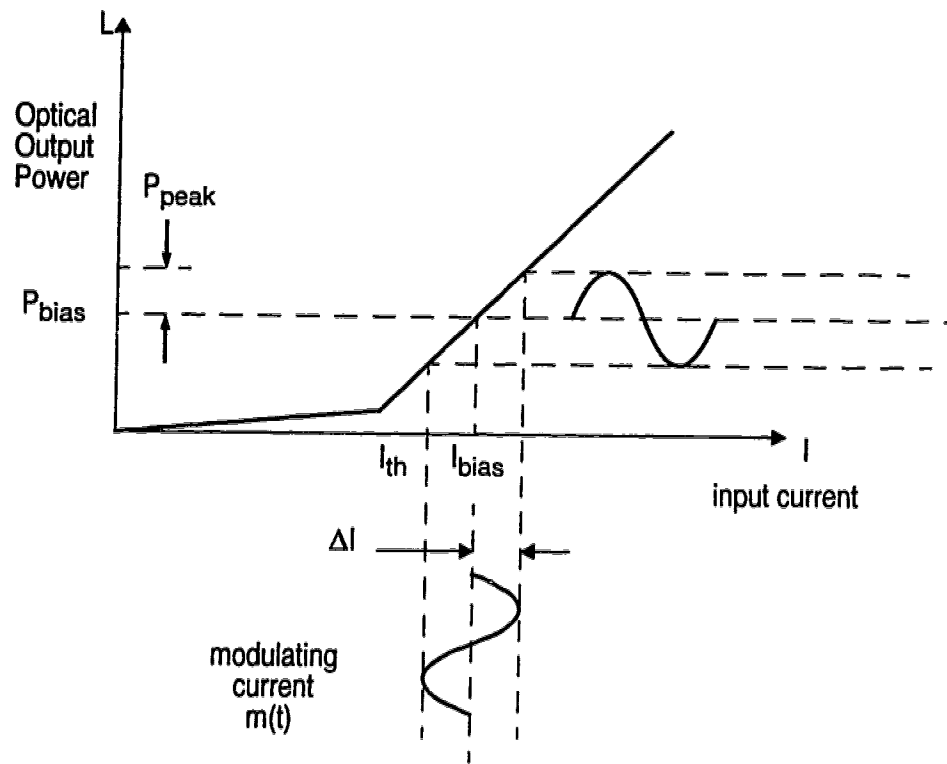


Figure 5.18 Light-Current characteristics for calculating modulation index

input current to the laser consists of a fixed portion (DC bias current) and the RF modulation signal. The optical output waveform may be written as:

$$P_o(t) = P_{bias} \cdot (1 + m(t)) \quad \text{Eqn. 5.1}$$

where  $P_{\text{bias}}$  is the average optical power at the bias current  $I_{\text{bias}}$ , and  $m(t)$  is the input signal. For a single channel:

$$m(t) = m \cdot \cos(2\pi f_c t) \quad \text{Eqn. 5.2}$$

where  $f_c$  is the carrier frequency and 'm' is the peak modulation index given by:

$$m = \frac{P_{\text{peak}}}{P_{\text{bias}}} = \frac{\Delta I}{I_{\text{bias}} - I_{\text{th}}} \quad \text{Eqn. 5.3}$$

(assuming optical power corresponding to  $I_{\text{th}}$  to be negligible as compared to  $P_{\text{bias}}$  or  $P_{\text{peak}}$ )

For the lasers used in the prototype switch:

$I_{\text{th}} = 44 \text{ mA}$ , and  $I_{\text{bias}} = 65 \text{ mA}$ .

The optical power output at 65 mA is 5 mW coupled into the fibres [65].

For input RF signal power = 0 dBm (into 50  $\Omega$ )

$\Delta I = I_{\text{peak}} - I_{\text{bias}} = 4.47 \text{ mA}$

Thus,  $m = 0.212$  or 21.2 %

For multichannel systems, the effective modulation index (since there are multiple carrier signals, each with a modulation index 'm' of its own) for N carriers is defined as [98]:

$$m_{\text{eff}} = \sqrt{\frac{Nm^2}{2}} \quad \text{Eqn. 5.4}$$

For  $N=44$ , and  $I_{\text{th}}$  and  $I_{\text{bias}}$  values given above, Table 5.3 provides the modulation indices corresponding to different power levels per channel used to



measure CSO and CTB.

**Table 5.3 Modulation index for measuring CSO, CTB**

RF Power per channel (dBm)	Modulation Index 'm' per channel	Total effective modulation index 'm <sub>eff</sub> '
-20.0	0.021	0.10
-15.0	0.038	0.18
-10.0	0.067	0.32
-5.0	0.12	0.57

*5.3.2d CSO and CTB measurement for prototype switch*

Using the NCTA standard procedures and instrument settings given in Table 5.2 and the modulation indices shown above, CSO and CTB products were measured at two channels (Channel 2 and Channel 43) situated at either end of the composite channel spectrum.

Figure 5.19 shows the CTB distortion products measured with respect to the carrier power at 55.25 MHz for different modulation depths. The video carrier frequency 55.25 MHz corresponds to Channel 2 in the standard CATV designation. The composite second order beat products (CSO) measured at 54.0 MHz and 56.5 MHz in channel 2 are shown in Figure 5.20. It can be seen that the CSO and CTB degrade with increased modulation drive levels since the RF signal current now produces more distortion as a result of the nonlinear L-I characteristics of a semiconductor laser.

Similar measurements for distortion products were carried out at Channel 43 (337.25 MHz) in order to fully characterize the CTB and CSO effects across the composite CATV payload. Results for CTB measured at 337.25 MHz, and

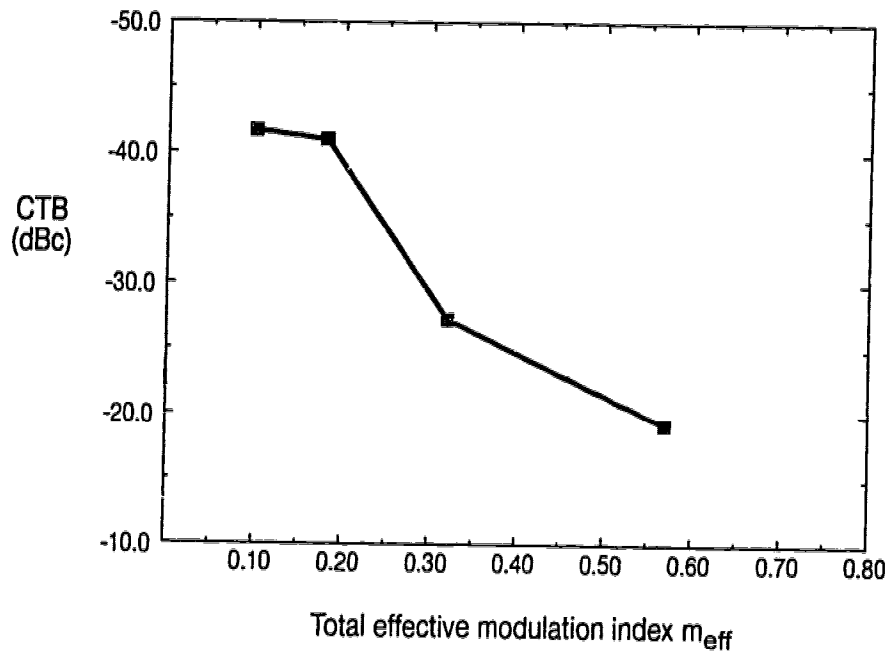


Figure 5.19 CTB measurement at 55.25 MHz (Channel 2)

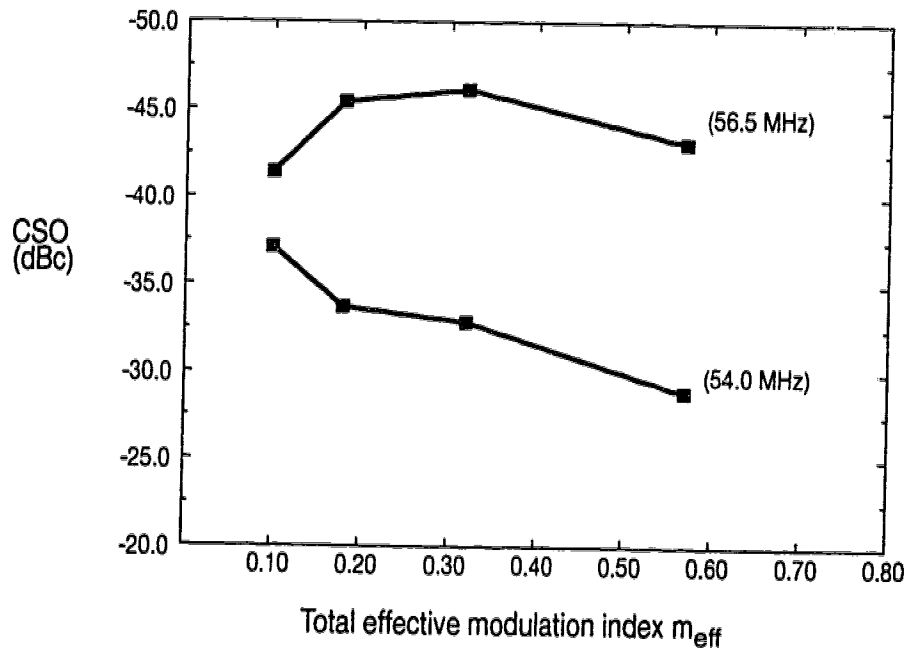
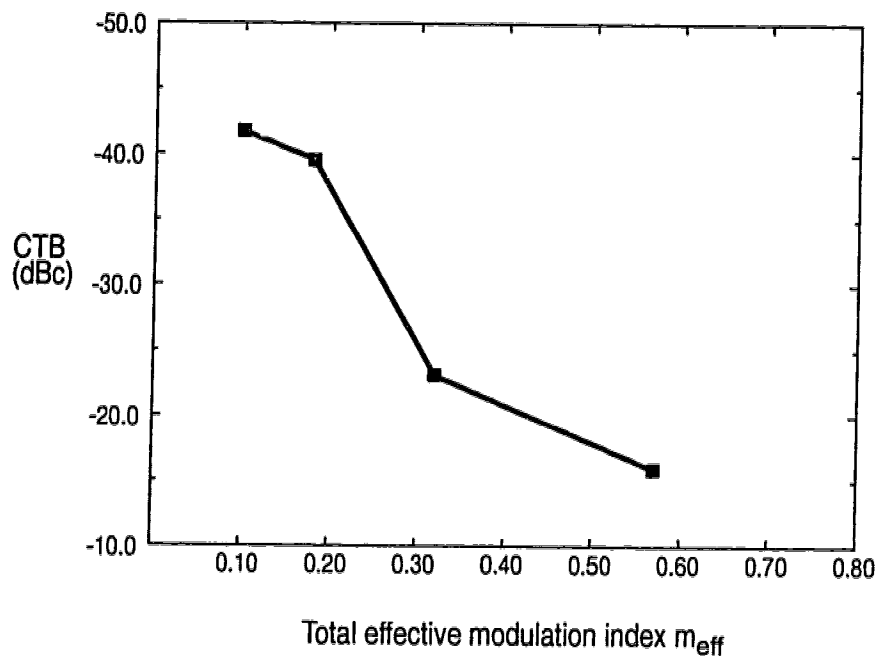


Figure 5.20 CSO measured in Channel 2

CSO measured at 336.0 MHz & 338.5 MHz are shown in Figure 5.21 and Figure 5.22 respectively.



**Figure 5.21 CTB measurement at 337.25 MHz (Channel 43)**

NCTA specifies CSO and CTB to be better than -52 dBc [96]. With the current lasers which have rather nonlinear L-I characteristics, these requirements are not satisfied. However, linear lasers intended for CATV applications which exhibit > 65 dBc second order harmonic distortion suppression are commercially available, and can be utilized at the input ports in the prototype if composite analog video signals are to be switched with the required distortion specifications.

An indication of the nonlinearity of the lasers currently used in the prototype switch can be obtained with a simple single tone modulation input to the laser. As shown in Figure 5.23, the lasers are highly non-linear with second harmonic at -35.75 dBc and third order harmonic at -25 dBc for 0 dBm signal

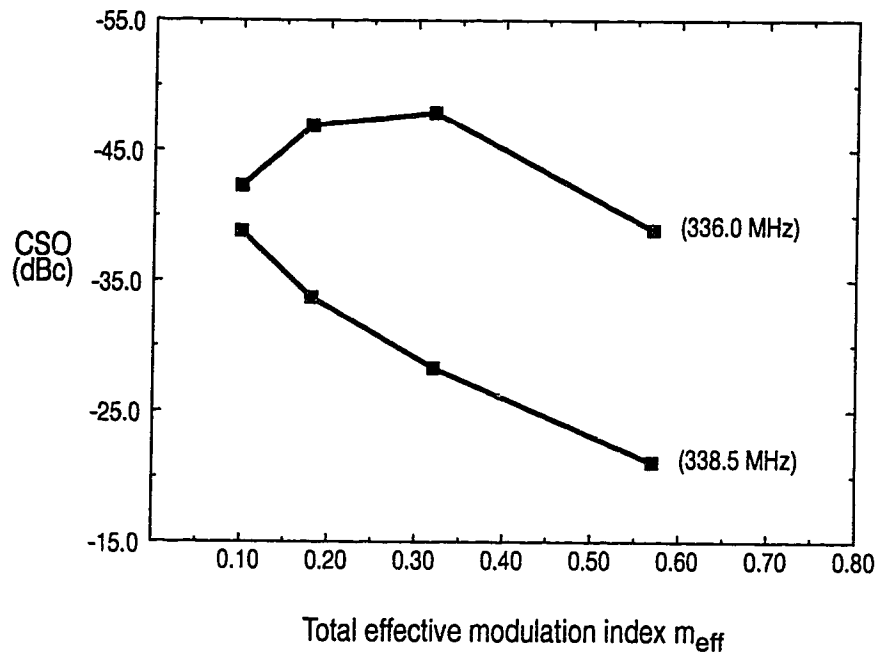


**Figure 5.22 CSO measured in Channel 43**

modulation (modulation index 0.212). However, this is not a true test of the linearity since the signal generator (HP 8642A) used for measuring the linearity of the laser (Figure 5.23) was found to exhibit signal harmonics in its output. The output of the signal generator measured with the spectrum analyzer (HP 70000) showed that the fundamental signal (0 dBm) is accompanied by a second harmonic tone at -57.7 dBc, and third harmonic tone at -67 dBc. The matrix generator used for measuring CSO and CTB was found to be free of any measurable signal harmonics.

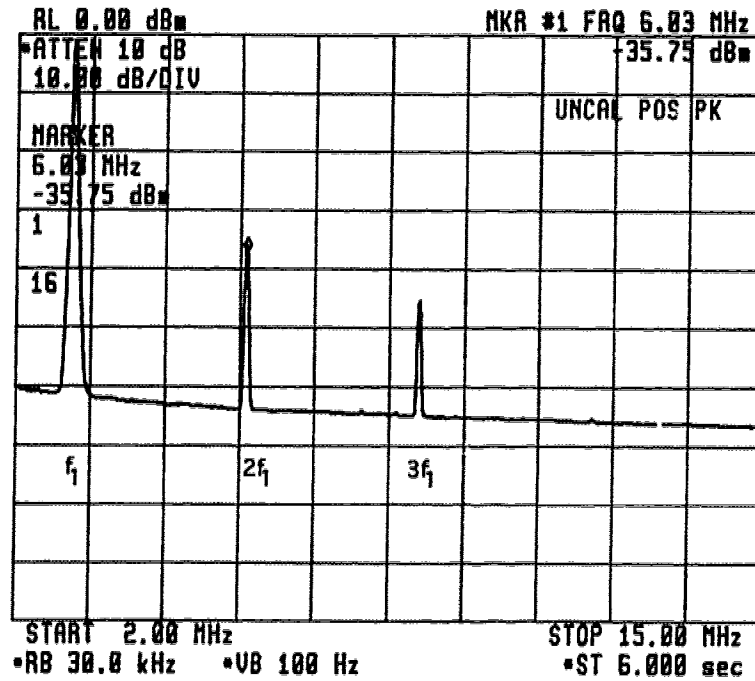
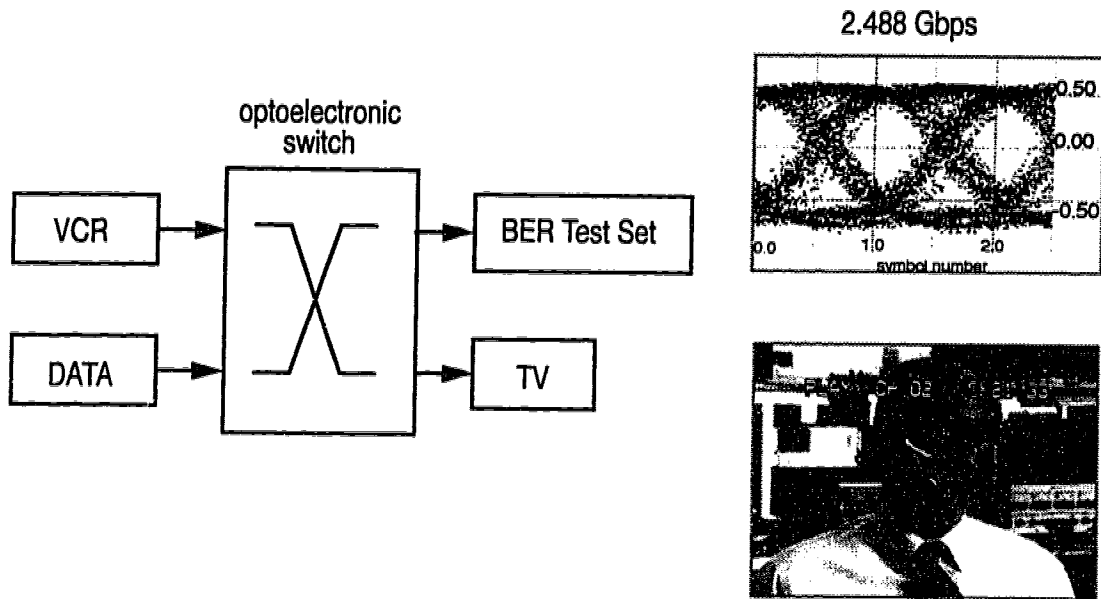


Figure 5.23 Harmonic distortion in Lasers used in the prototype switch

### 5.3.3 Format transparent switching

Simultaneous routing of digital and analog signals is achievable through the prototype optoelectronic switch. Figure 5.24 shows the experimental set up which uses a single standard NTSC video signal from a video cassette recorder in addition to a broadband digital data source to serve as signal inputs to the prototype. The signal outputs are shown in the inset photograph and eye diagram. The photograph corresponding to the video signal is a video-print of the analog signal at the output of the switch as displayed on a television monitor.

The format independent switching capability demonstrated with this experiment has important bearing on the nature of applications that may be enabled through such switches. Multimedia networks requiring routing



**Figure 5.24 Simultaneous analog signal and digital data switching**

mechanism for many kinds of signals including high quality analog signals are obvious applications for format independent switches. Perhaps a bigger impact can be envisioned in other areas such as high speed switches required for computer LANs where a single technology can support a variety of formats and data rates. Thus no hardware modification is required for the switching mechanism as networks undergo changes at the higher level protocols or change to different data rates and formats. Use of a single technology to produce switches suitable for various data rates or indeed, various networks, also has implications for simplified and low cost production of broadband switches.

Some other signal formats that can be routed through the prototype include  $\pi/4$  DQPSK (used in digital cellular radio systems in North America), and N-VSB (N-level, vestigial side band signal which is a 8 or 16 level signal proposed for digital broadcast of high definition TV signals in North America [99]).

## **5.4 Spectrally Efficient Modulation for Photonic Interconnects**

The wide dynamic range characteristic of photonic interconnects or switch fabrics can be utilized to increase the data throughput in photonic switches by using spectrally efficient modulation schemes and without requiring increased bandwidth of electronic components in the laser transmitter or receivers in the switching system.

Bandwidth efficient multilevel signalling schemes have been suggested [100, 101] and demonstrated [102, 103] to overcome dispersion limitations in fibre based direct detection transmission systems. However, use of bandwidth efficient multilevel codes has not been prevalent in long haul fibre optic transmission systems due to the increased dynamic range required although there is some benefit available due to the reduced transmission bandwidth and consequently reduced dispersion penalties [102].

In short distance photonic interconnects, such as the ones used in the prototype switch for signal distribution, where neither dispersion nor available power is a limitation (even multimode fibres provide 500 MHz-km or 50 GHz over 10 m), spectrally efficient baseband modulation techniques such as M-level amplitude shift keying (ASK) can effectively utilize the available dynamic range in a photonic interconnect based switch to increase data throughput.

This work presents the first demonstration of the application of spectrally efficient codes to increase the throughput of a broadband switch based on photonic interconnects. This increase is achieved without the added cost of requiring high bit rate electronic components for optical transmitters and

receivers.

Since relatively inexpensive lasers (780 nm, multimode fibre pigtail, TO-can packaged lasers) with external bias-tees are used, in the prototype switch, the bandwidth is restricted to 1.25 GHz on each of the transmitters (section 3.3). However, a wide dynamic range is available across the entire bandwidth. The typical input-port-to-output-port channel in the switch matrix dynamic range of 116 dB/Hz (Section 5.3.2) corresponds to 24 dB over the 1.25 GHz bandwidth of each channel.

#### *5.4.1 Spectrally efficient codes*

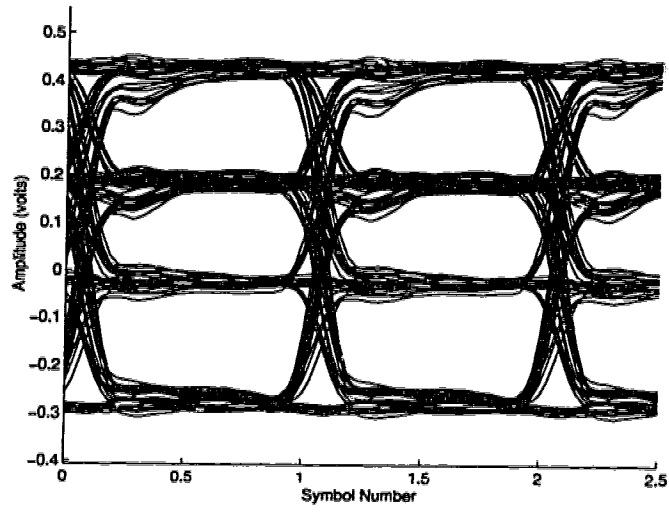
Multilevel signalling formats such as duobinary and M-ary modulation, offer an increase in the spectral efficiency of the baseband signal over the binary scheme by using the dynamic range of the signal [104]. Multilevel signalling with M levels would increase the data throughput at the same signalling rate by a factor of  $\log_2 M$  [104]. Since relatively short distances are involved, the limiting factor for use of highly efficient baseband modulation schemes is the required dynamic range and not the dispersion effects as it would in a long haul fibre optic transmission system. For equally spaced levels, the eye opening is reduced by a factor of 3 over the binary case and for a given symbol error rate, the power penalty is  $10 \log \left( \frac{(M-1)}{\sqrt{\log(\text{base } 2)(M)}} \right)$  (3.2 dB for 4 levels) [101].

#### *5.4.2 Results*

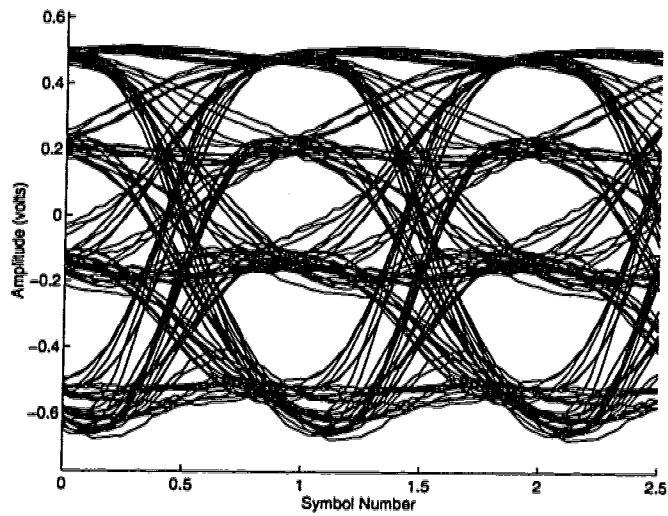
The eye diagram for binary data transmission at various rates were shown in Figures 5.7 through Figure 5.11.

Figure 5.25 shows the input multilevel electrical signal (1.58 Giga-symbols/





**Figure 5.25 Multilevel input signal to the optoelectronic switch**  
**Symbol Rate = 1.58 GHz**



**Figure 5.26 Switched multilevel signal at output of optoelectronic switch**  
**Symbol Rate = 1.58 GHz**

sec), and Figure 5.26 shows the corresponding multilevel signal after the input signal is switched to an output port in the switch. The tributary signals for this eye diagram are at 1.58 Gbps each, which results in a symbol rate of 1.58 Giga-symbols/second (2 bits per 4 level symbol), thus extending the data throughput of the switch to > 3 Gbps per port. Figures 5.27, 5.28, and 5.29 show four level eye

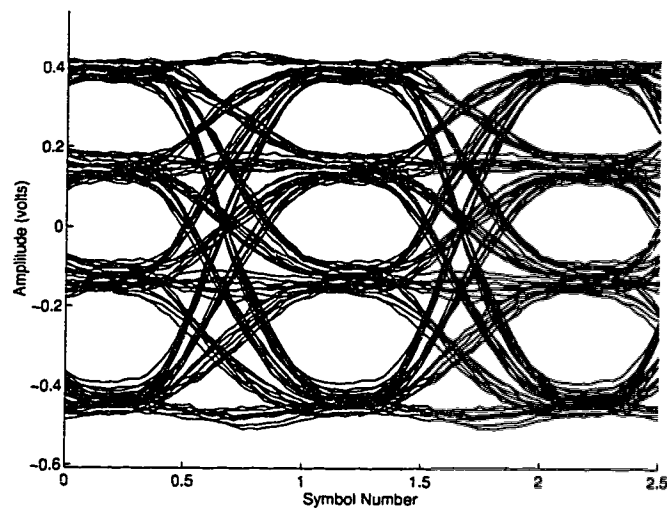


**Figure 5.27 Switched multilevel signal at output of optoelectronic switch  
Symbol Rate = 0.9 GHz**

diagrams for data signals at symbol rates of 0.9 GHz, 1.1 GHz, and 1.8 GHz respectively. All eye diagrams show time-averaged traces captured with a high bandwidth digitizing oscilloscope.

The eye closure at 1.8 GHz symbol rate appears to result from the bandwidth limitation of the laser diode (Figure 5.29) and the distortion present in the input four-level signal (Figure 5.25). For other symbol rates up to 1.5 GHz, the four level signal retains open eyes after switching with some eye closure visible. It

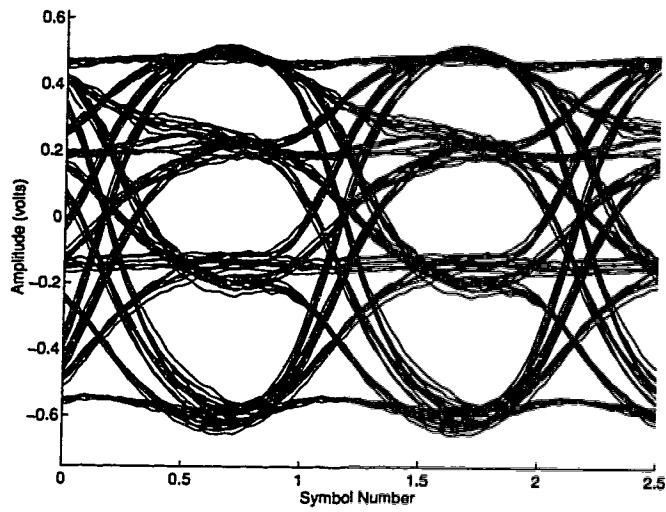


**Figure 5.28 Switched multilevel signal at output of optoelectronic switch**  
**Symbol Rate = 1.1 GHz**

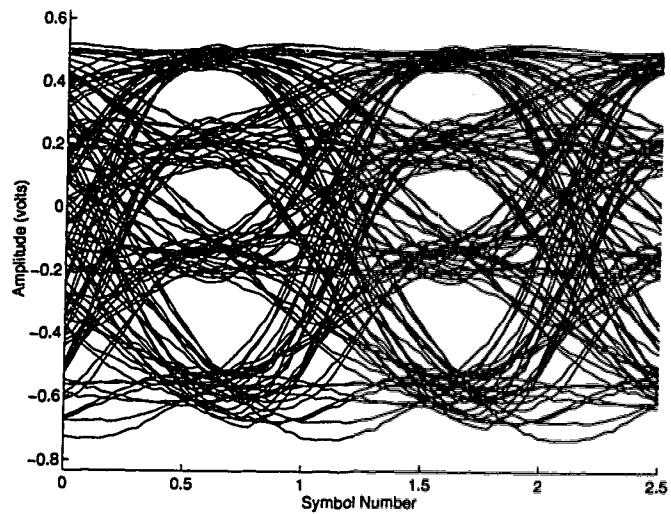


**Figure 5.29 Switched multilevel signal at output of optoelectronic switch**  
**Symbol Rate = 1.8 GHz**

is anticipated that with suitable broadband lasers and receivers, better results can be achieved at higher bit rates. For a 10 GHz channel bandwidth, a data throughput of 20 Gbps per port should be possible with the use of four level signalling in the optoelectronic switch.

## **6. Optoelectronic Signal Processing**

Broadband signal processing can be accomplished using optoelectronic structures with the elements present in the prototype switch reported in this work. Fibre delay lines and switched metal-semiconductor-metal (MSM) photodetectors used to realize filter coefficients, can implement fully tunable finite impulse response (FIR) and infinite impulse response (IIR) structures. This chapter presents results for FIR and IIR signal processing structures synthesized with the optoelectronic switch. The application of such filter structures to equalization of modal dispersion in multimode fibres is described, and an eightfold improvement in bandwidth-distance product is shown possible in experimental results obtained with the implementation.

### **6.1 Optoelectronic Signal Processors**

#### **6.1.1 Discrete time processor**

Controlled detection of intensity modulated optical signals with appropriate delays can provide a delay-and-weight function for an input signal while photocurrent addition provides the summing function required for canonical discrete time signal processors. Implementation of a 16-tap finite impulse response (transversal) filter using this optoelectronic technique has been reported in [105, 106, 107]. [4] extends the concept by demonstrating elementary discrete time processors realized with hardware available in the optoelectronic switch matrix. Optoelectronic discrete time processors were introduced in section 2.4.1. Basic elements to demonstrate a discrete time signal processor were

incorporated in the optoelectronic switch to permit demonstration of signal processing features. These consist of continuously tunable bipolar photodetector bias and a set of delay lines. The bias to each of the 100 photodetector crosspoints is set via an analog to digital converter which allows either negative or positive bias to be applied with fine resolution (2mV steps, -5.000 to 4.998 v), allowing essentially continuous, bipolar control over the crosspoint sensitivities.

### 6.1.2 Matrix-vector processor

A two dimensional matrix of controlled photodetectors with optical signal distributed to them row-wise, and photocurrent summation column-wise provides the inner product operation among a vector of broadband signals and the matrix of weights set by the photodetector array (Figure 6.1). A similar structure can be

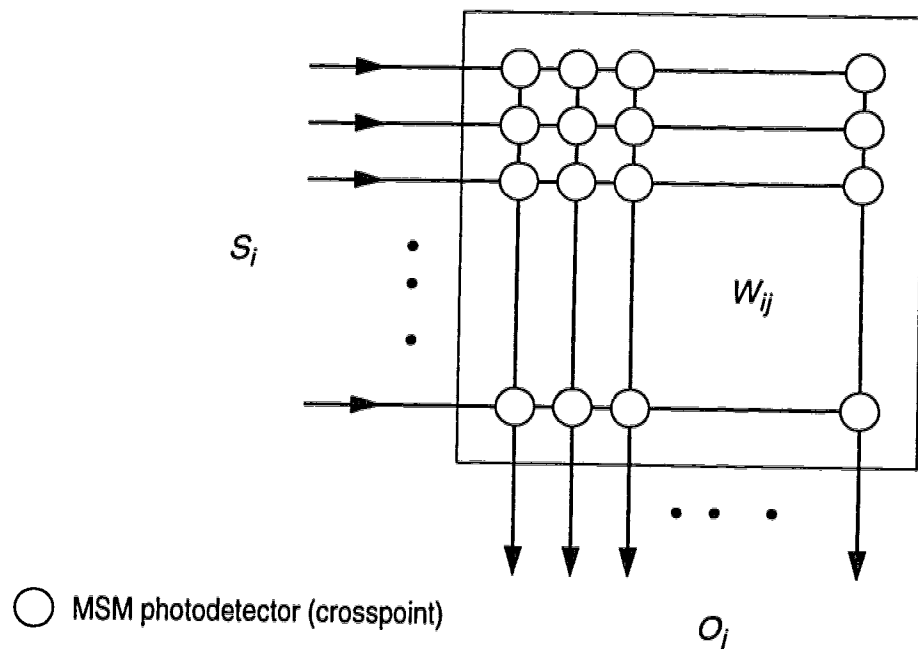


Figure 6.1 Matrix-vector multiplication operation with optoelectronic crossbar switch

used as a basic device for a broadband neural processor [108] and an optoelectronic neural device has since been implemented at low bandwidth [109].

The input signals (electronic) are converted to optical domain to be distributed over fibres in the matrix. Each incoming signal is split and distributed to ten photodetectors (each row), and the output of each column is summed to provide the weighted contribution  $W_{ij}S_i$ , where  $S_i$  is the vector of input signals. The output vector  $O_j$  thus provides the vector-matrix product:

$$O_j = \sum_{i=1}^{10} W_{ij} \cdot S_i \quad i = 1,2,\dots,10 \quad \text{Eqn. 6.1}$$

where  $W_{ij}$  is the coefficient in  $i$ th row and  $j$ th column of the matrix of crosspoints.

### 6.1.3 Generalized discrete time processor

The combination of a broadband matrix-vector multiplier with a set of fibre delay lines, and reflex (feedback) connections [53] constitutes a general discrete time signal processor [4] capable of implementing a wide variety of broadband filters through electronic control of the photodetector bias voltages (Figure 6.2).

The input signals for the signal processing application traverse the same path as in the switch application. The crosspoints in the processor matrix implement an optoelectronic form of weight setting [108, 110] by means of setting the bias on the photodetector. A Metal-Semiconductor-Metal detector is used to provide the bias dependent, bipolar response to weight the intensity modulated input signal. The photocurrent generated by the photodetector is dependent on the incident optical power and the applied bias (see Figure 4.2). Since the MSM

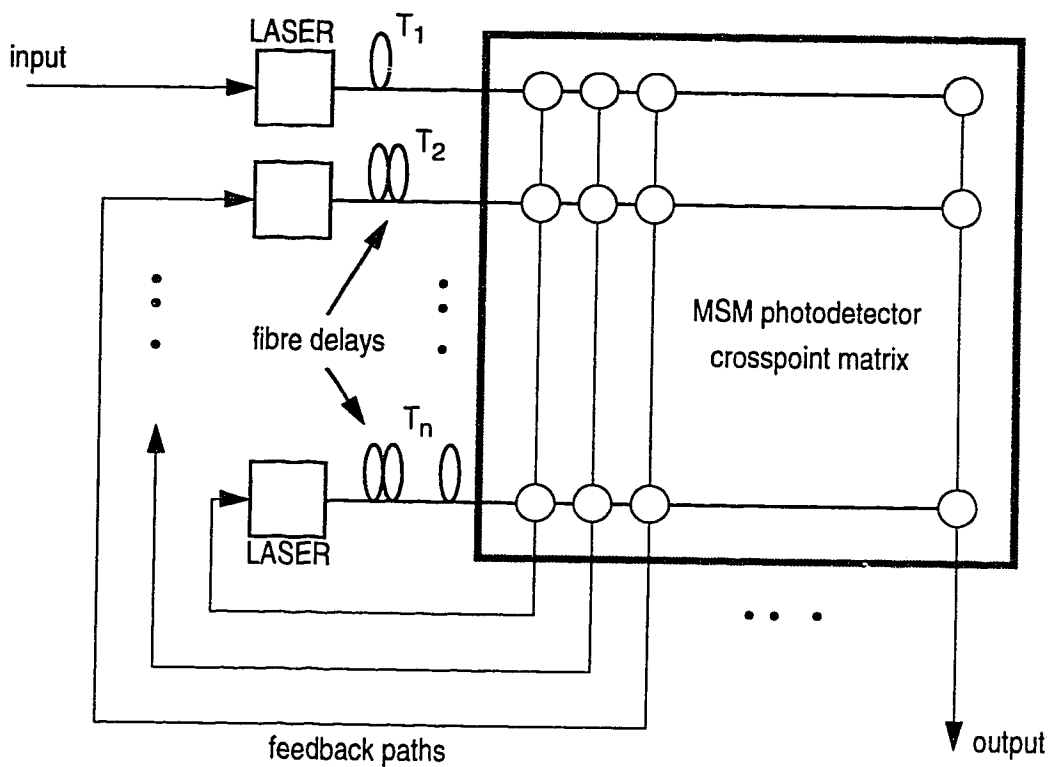


Figure 6.2 Generalized discrete time signal processor

photodetector provides bipolar, symmetric response with respect to the bias voltage polarity, the photodetector can be used to provide tap weights in the digital filter application. The bandwidth of the processor is limited by the transmitter to ~ 1.25 GHz [7] , though the MSM photodetector is capable of producing transit time limited response in the tens of GHz range [70]. The bias is tunable over the range of -5.000 V to +4.998 V with a precision of 2 mV and provides variable bipolar tap weights.

Semi-rigid coaxial cable is used to circulate the output electrical signals



back to the input ports where they are converted to optical signals (Figure 6.2). Delays in increments of 1 ns each (tap intervals) are introduced between the laser and the following signal splitter using multimode fibres. The fibres provide an optical delay medium with high bandwidth, low loss, low dispersion (~500 MHz-km), high linearity (>80 dB fundamental dynamic range for a 10 GHz signal in a 200 m fibre length [111]), in addition to a propagation delay of ~5 μs/km. 1 ns incremental delays result in a sampling frequency of 1 GHz. The free tuning range of a transversal filter made with this device is thus 500 MHz, and up to 20 taps can be implemented using three signal passes through the switch matrix in the FIR configuration (Figure 6.3).

## 6.2 Realization of Tunable Filters

### 6.2.1 FIR and IIR filters

The matrix arrangement shown in Figure 6.2 can be configured to realize a 20 tap FIR filter structure by setting crosspoints in the pattern shown in Figure 6.3.

The output signal is:

$$y(n) = \sum_{k=0}^{19} a_k \cdot x(n-k) \quad \text{Eqn. 6.2}$$

where  $a_k$  are the filter coefficients and  $x(n-k)$  represents the input signal delayed by  $k$  tap intervals.

The structure shown in Figure 6.3 is equivalent to a transversal FIR filter (see Figure 2.8). The 10x10 switching matrix can implement a programmable (the tap weights are computer controlled) FIR filter with up to 20 taps.

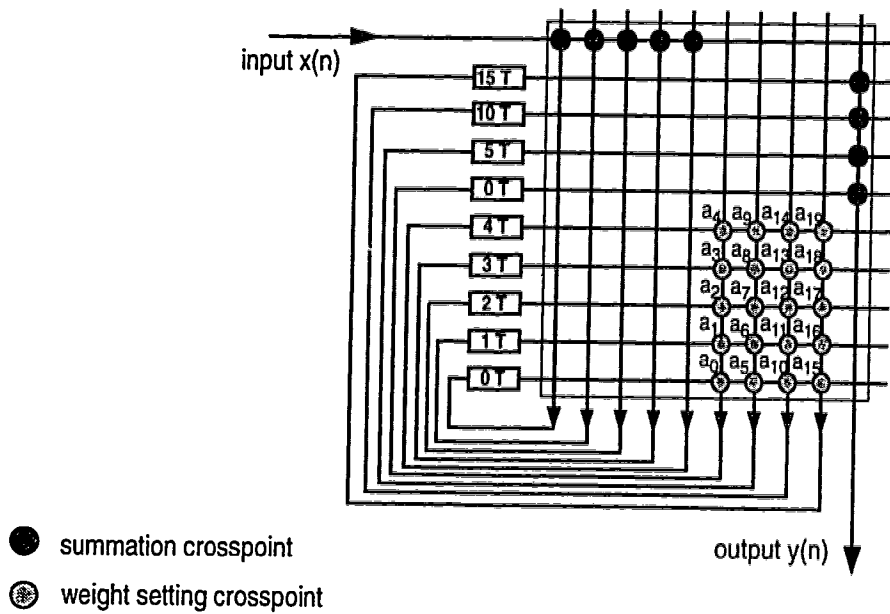


Figure 6.3 FIR filter realization with optoelectronic matrix processor

Direct Form I as well as Direct Form II IIR filters [112] can also be realized with the matrix using the pattern of crosspoints turned OFF or ON as shown in Figure 6.4.

For the Direct Form I configuration, the output is:

$$H(z) = \frac{\sum_{k=0}^{N_a} a_k z^{-k}}{1 + \sum_{k=1}^{N_b} b_k z^{-k}} \quad \text{Eqn. 6.3}$$

with  $a_k = -\frac{A_k}{B_0}$        $b_k = \frac{B_k}{B_0}$        $N_a = 7, N_b = 7$

In the second configuration (Direct Form II), the transfer function  $H(z)$  is

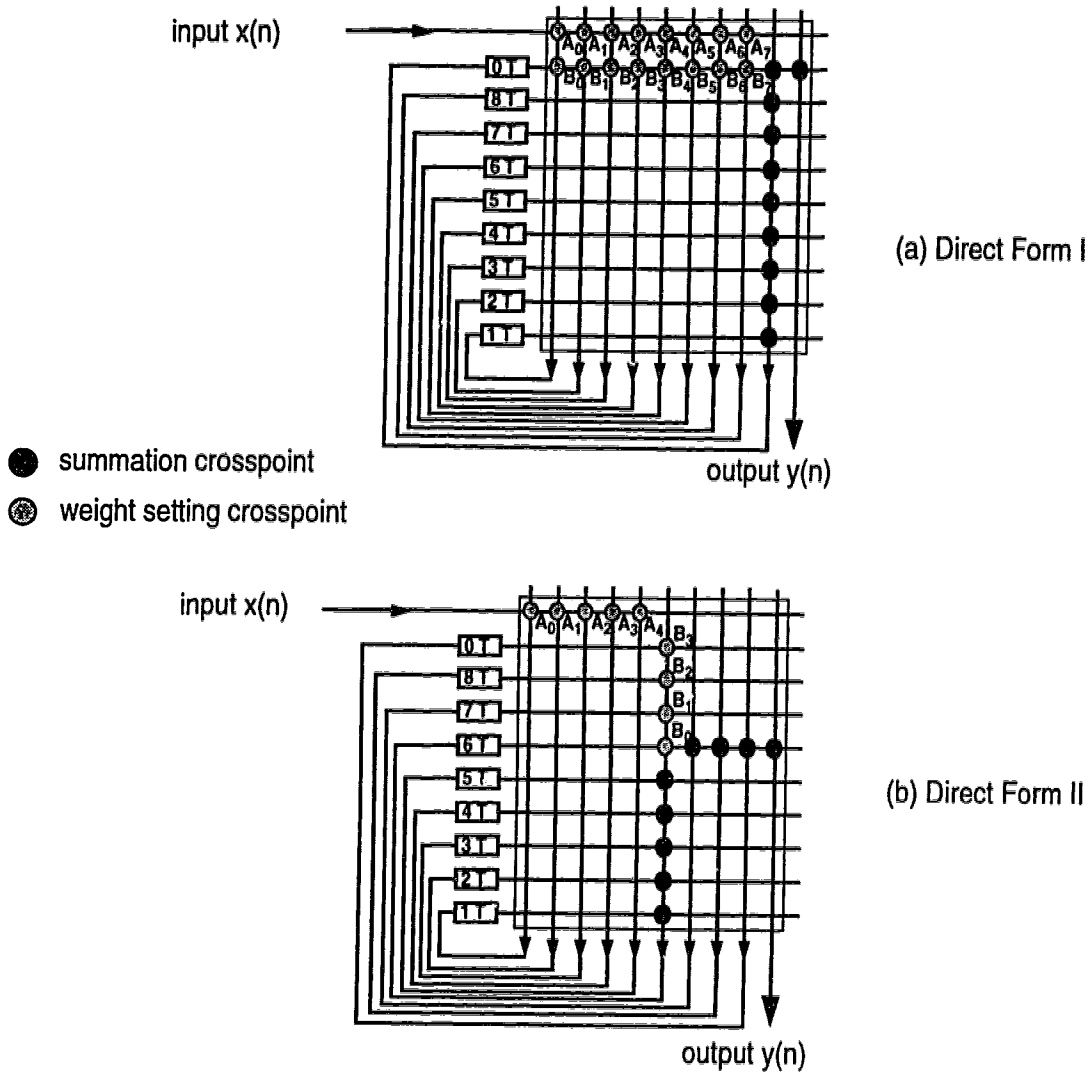


Figure 6.4 IIR filter realization with optoelectronic matrix processor

realized with the following coefficients:

$$a_k = -\frac{A_k}{1-B_0} \quad b_k = \frac{B_k}{1-B_0} \quad N_a = 4, N_b = 3$$

The Direct Form I realization results in a higher order filter with a matrix of given dimension as compared to the Direct Form II realization.

### 6.2.1a Bias dependent frequency response of crosspoints

The frequency response of a typical crosspoint in the switch matrix is shown in Figure 6.5 for several bias voltages ranging from -0.004 V (lowermost

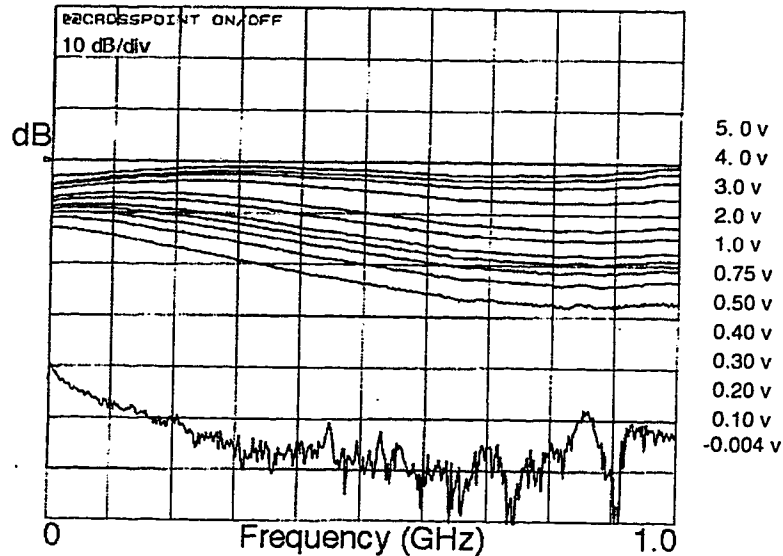
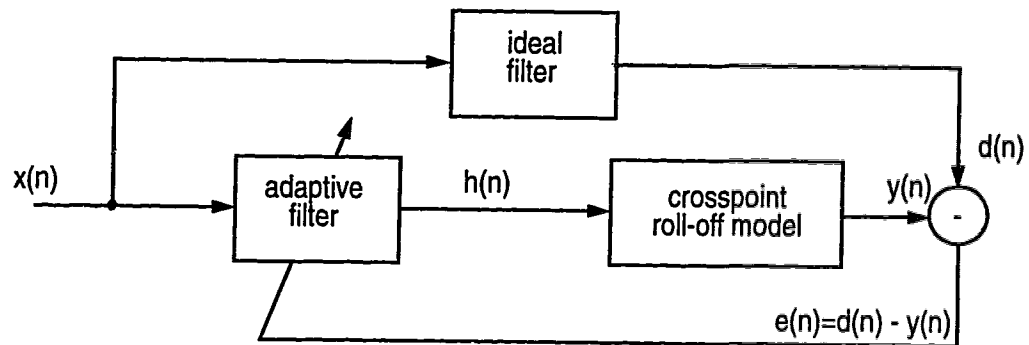


Figure 6.5 Measured MSM crosspoint frequency response for different bias voltages

trace) to 4.998 V. It is evident that reducing the bias causes the crosspoint response to roll off more quickly at high frequency. This bias dependence of the response is a characteristic of MSM photodetectors and is caused by the lack of sufficient electric field to sweep out photogenerated charge carriers at low bias voltages. In order to realize the given frequency response with the crosspoints in the matrix signal processor, compensation for this roll off is necessary. This compensation may be provided through automatic adjustment of the tap weights by an adaptation algorithm that can optimally calculate the compensated tap weights for the given response by accounting for the crosspoint roll off as shown

schematically in Figure 6.6. The Recursive Least Squares - RLS algorithm [113,



**Figure 6.6 Adaptive calculation of filter coefficients**

114, 115] was used in this case. The roll off was modeled using a simple piecewise linear approach as shown in Figure 6.7.

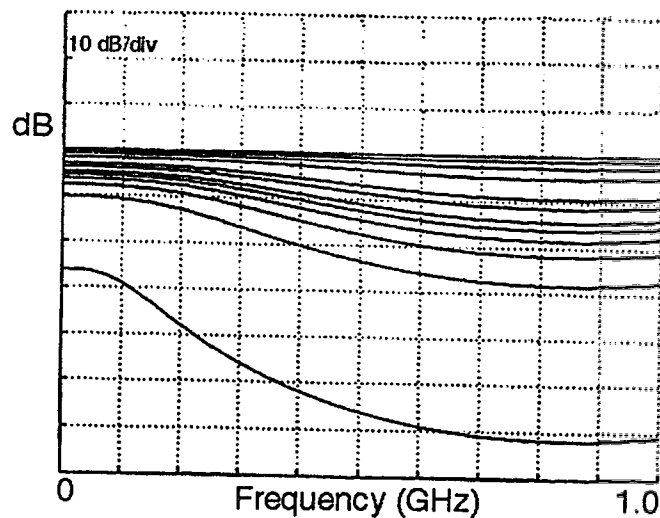


**Figure 6.7 Modelled MSM crosspoint frequency response**

A simulated example of the response obtained with an adaptive bias compensated design is shown in Figure 6.8. The uncompensated response

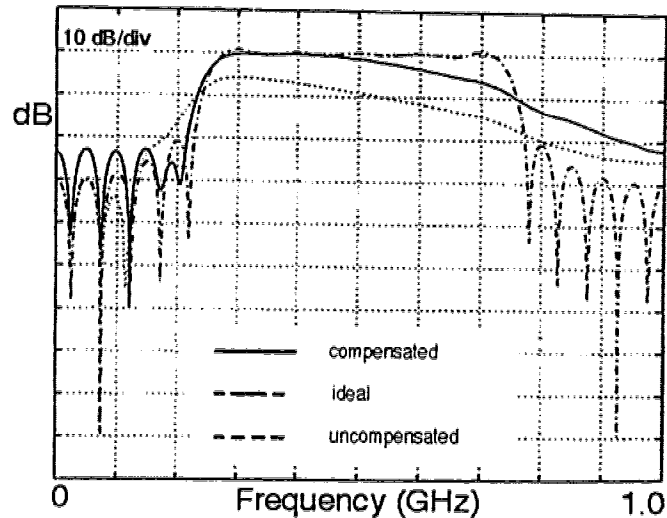


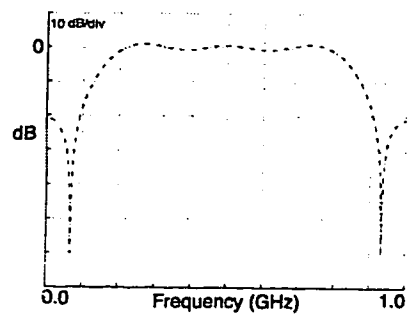
**Figure 6.8 Compensated frequency response**

(dotted line) falls off rapidly after ~300 MHz. The simulated filter response with bias-compensation (solid line) closely follows the ideal response (dashed line) till 500 MHz (Nyquist frequency since sampling rate is 1 GHz).

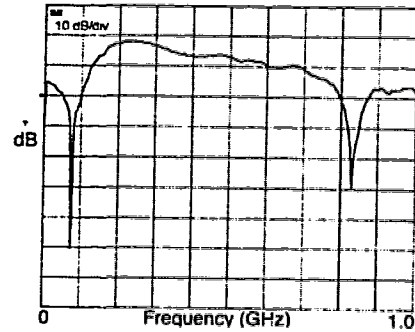
### *6.2.1b Results*

A 9 tap configuration was used to implement bias-compensated, tunable optoelectronic FIR filters. The simulated results with ideal coefficients (no error, no frequency dependence) and the experimentally obtained results with the matrix processor realization of the programmable digital FIR filter are shown in Figure 6.9 (a) and (b). A comprehensive summary of filter responses realized with the matrix processor can be found in [116].

The experimental results show that a tunable filter response can be

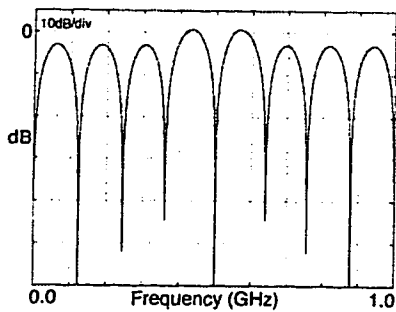


modelled filter response

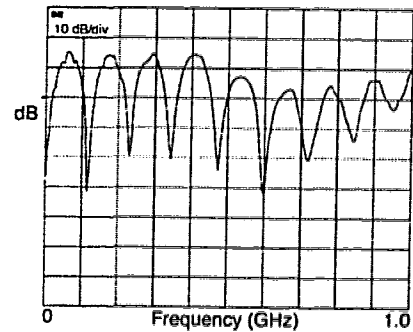


measured filter response

(a)



modelled filter response



measured filter response

(b)

**Figure 6.9 Measured and modelled tunable FIR filter frequency response**

achieved with the matrix processor up to 500 MHz. Compensation was optimized for the 0-500 MHz region. Computer control of the coefficients allows rapid reconfiguration of the filter response as no hardware components need to be changed to implement a different frequency response.

IIR filter structures provide sharper cutoff in the shape of the response than an FIR filter of the same order [112], therefore they can be advantageous in that they require fewer elements to achieve high rejection. However, the IIR configuration is potentially unstable, and the range of element coefficients that

can be used may be reduced.

The IIR implementation using the matrix-processor is more complex than the FIR structures. The main limitation is that the '0 delay' feedback necessary in IIR configurations (Figure 6.4) cannot be achieved in reality. As a consequence, the unit delay can be no less than the minimum propagation delay through the processor. Accounting for the optical fibre delay lines (1 ns to 10 ns inclusive) and the electronic components at different ports, this loop delay was calculated to be ~16 ns. A simple single resonant loop was implemented to measure this delay from the frequency separation of the resonances (see Appendix E). A possible IIR configuration is given in Figure 6.10. The delays shown on left side of the diagram

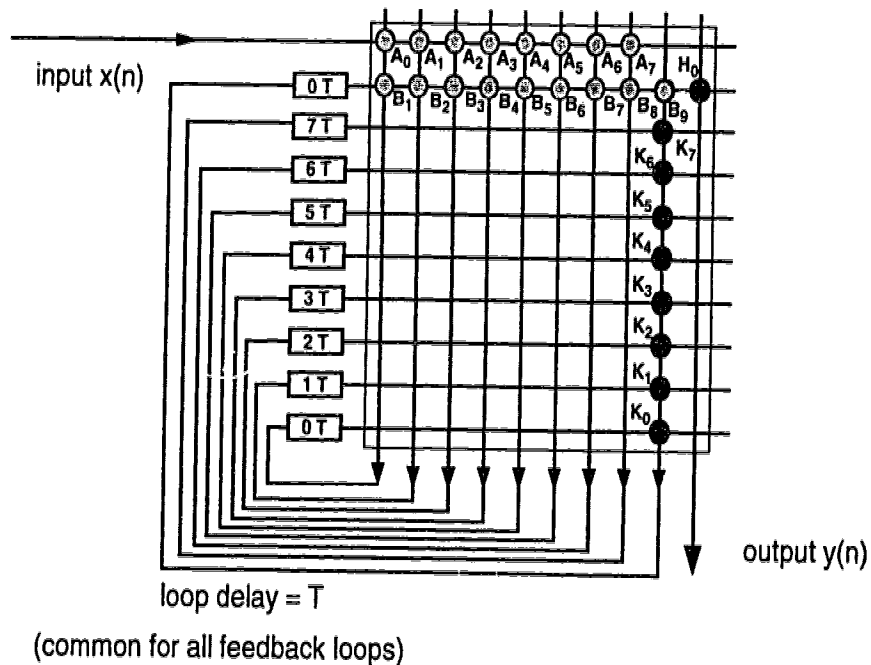


**Figure 6.10 Possible IIR configuration with the optoelectronic switch**

represent the total delay for each path which is given by the loop delay (16 ns)



plus the fibre delay lines in that path. The output would be given by the following expression:

$$y(t) = \begin{matrix} H_0K_0A_0x(t-2T) + H_0K_1A_1x(t-3T) + & + H_0K_7A_7x(t-9T) + \\ B_1y(t-T) + K_0B_2y(t-2T) + & + K_7B_9y(t-9T) \end{matrix} \quad \text{Eqn. 6.4}$$

where the frequency response is given by:

$$H(z) = \frac{\sum_{k=0}^{N_a} a_k z^{-k}}{1 + \sum_{k=1}^{N_b} b_k z^{-k}} H_0 z^{-2} \quad \text{Eqn. 6.5}$$

with:

$$a_k = K_k A_k, \quad b_k = -K_{k-2} B_k \quad \text{except, } b_1 = -B_1 \quad (N_a = 7, N_b = 9)$$

This configuration (Figure 6.10) could be used to implement an IIR filter with 8 coefficients in the numerator and 10 in the denominator. With a value of 16 ns for the loop delay, the filter would work at a sampling rate of 62.5 MHz.

### 6.2.2 Equalization of modal dispersion

Signals transmitted through multimode optical fibres propagate via different modes through the length of the fibre. As each mode of propagation has a different group velocity, the signals in different modes will have different propagation delays. Consequently received signals will be dispersed in time. The effect of dispersion is to limit the information capacity since high rate data pulses are 'smeared' into adjacent data pulses by dispersion [69, 117, 118]. To combat the resultant intersymbol interference, a tunable filter can be used at the receiver to compensate for the channel distortion. Such filters are called 'equalizers' and are preferably tunable so that the same filter structure can be employed for

different channel characteristics. In the case of fibre channels, this situation would arise when different lengths of fibres are used for various links. When such a tunable filter is used along with an adaptation algorithm to help adjust the filter coefficients in a continuous manner, the filter structure is called an *adaptive equalizer*. Adaptive filters are useful where the channel distortion effects are not known beforehand, and also where the channel frequency response may vary with time [119].

For high data rates ( $>1$  Gbps), such tunable filters are complex to implement since they must be tuned over the bandwidth of the information signal ( $\sim$ GHz or more). Tunable optoelectronic broadband filters, such as the ones described in the earlier sections, may be used as adaptive equalizers to help combat modal dispersion.

Equalization of multimode fibre dispersion by using MSM photodetector based filter structures has been previously suggested to improve the bandwidth distance product [120]. The required frequency response of the filter depends on the amount of dispersion to be compensated which in turn depends on the length of the fibre link. The optimum frequency response to compensate for such dispersion is an exact complex inverse of the channel impulse response [113, 119]. Figure 6.11 shows a schematic of the simulations system used to calculate the adaptive filter coefficients for various cases.

In the system shown in Figure 6.11, the input signal (delayed to match the propagation delay through the channel and filter) is used to calculate the error signal which is the difference between the undistorted signal and the distorted

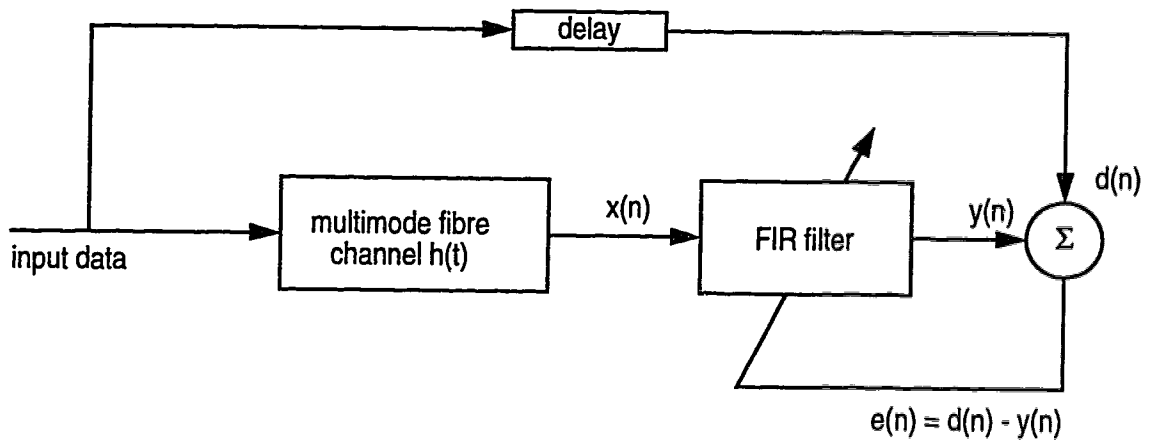


**Figure 6.11 Schematic of the equalization simulation system**

signal. The error signal  $e(n)$  is used at each calculation step to recursively compute the filter coefficients using the RLS algorithm [113, 114, 115]. The impulse response  $h(t)$  of the fibre channel used in the simulations is given in Appendix E.

The matrix processor (FIR configuration) working with an adaptation algorithm can implement such a structure for high data rates (1 Gbps and above) to extend the bandwidth-distance product. The Recursive Least Squares (RLS) algorithm is used to calculate the optimal filter that will compensate for the channel distortion. The RLS algorithm is chosen since it converges to a lower mean-squared error (MSE), and requires fewer iterations for the filter as compared to other algorithms (such as the Least Mean Squares - LMS algorithm) [113]. In theory, the effect of intersymbol interference can be made arbitrarily small by increasing the number of adjustable tap weights in the adaptive filter, so the response of this filter closely matches the inverse of the channel response [113].

Equalization performance for 19 tap and 9 tap adaptive FIR filters was calculated for fibre lengths ranging from 1 km to 8 km at a data rate of 1 Gbps.

Figure 6.12 (a) shows the simulated eye diagram of the distorted signal

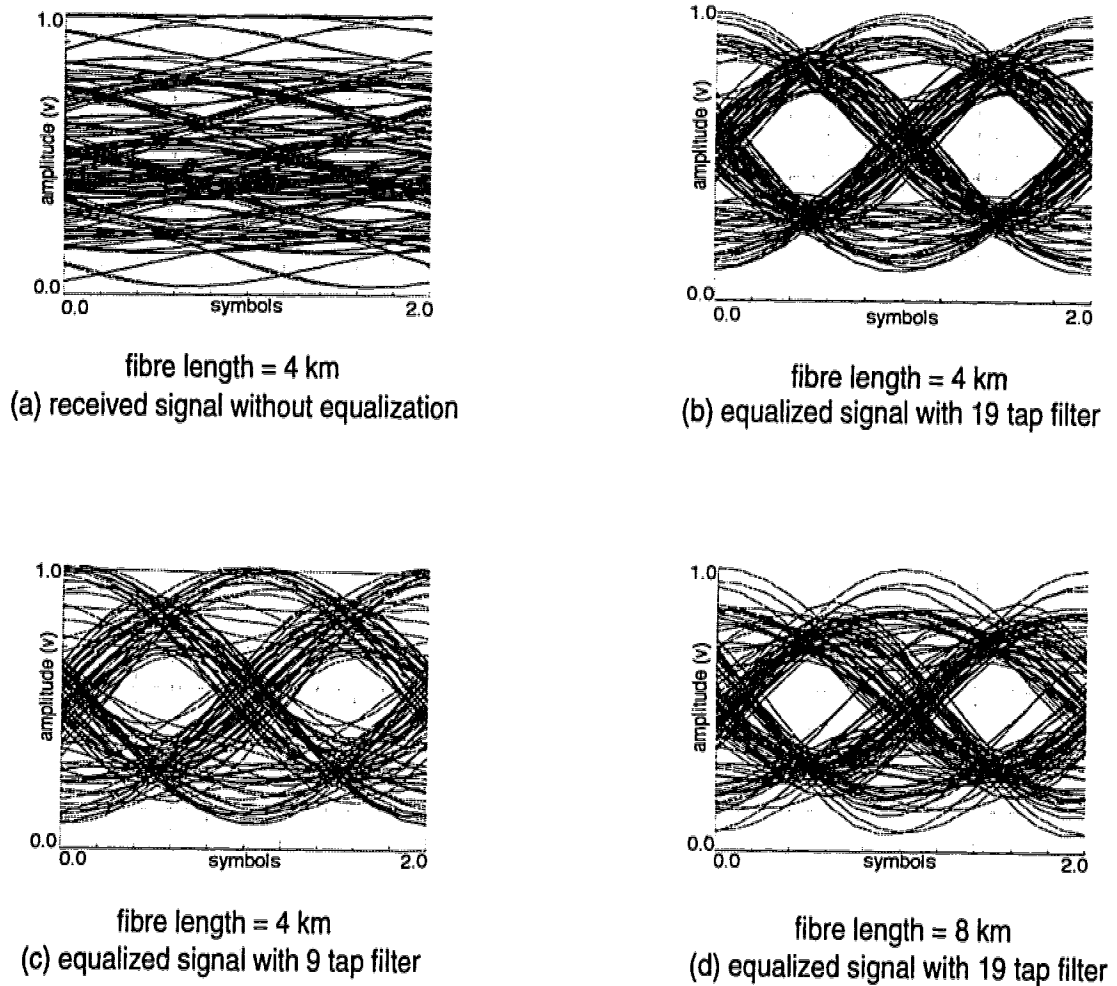


**Figure 6.12 Signal eye diagrams for equalization**

received after transmission through 4 km of multimode fibre. The eye is completely closed due to the dispersion in the channel. The equalized response obtained with 19 tap and 9 tap filters operating on the distorted signal is shown in

Figure 6.12 (b) and (c) respectively. Figure 6.12 (d) shows a 19 tap filter with an 8 km fibre channel length.

Experimental confirmation of the filter response required to equalize for 4 km of dispersive multimode fibre is shown in Figure 6.13 which shows the response of the ideal equalizing filter as well as calculated and measured 9 tap FIR filter responses for comparison.

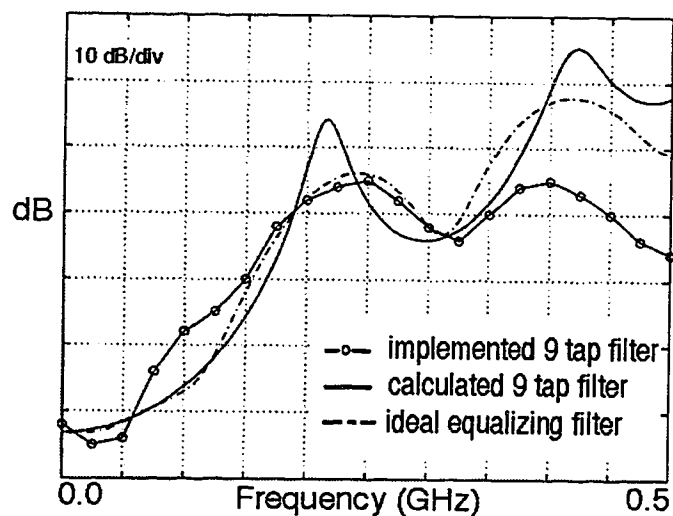


Figure 6.13 Equalizing filter response implementation

Optoelectronic techniques for implementing tunable filters show promise, although bias dependent behaviour of the MSM photodetector crosspoints potentially limits the use of the technique to frequencies below the 3 dB bandwidth of the photodetector. Improvements in device design are required to permit greater bandwidths at low bias voltages so that optoelectronic signal processors may be implemented which use the full bandwidth of MSM photodetectors.

## **7. Broadband Optoelectronic Switches in Network Restoration**

Broadband switching mechanisms are integral to the methods used for restoring services in telecommunication networks when a failure of equipment or a fibre channel occurs. The use of the optoelectronic switches to perform restoration switching is proposed in this chapter. Restoration techniques which can utilize optoelectronic switches to ensure dynamic reconfiguration of the network facilities are described. A case study using a sample network is presented to help compare optoelectronic restoration methods with restoration based on optical switching. Optical networks employing wavelength division multiplexing (WDM) to increase the capacity form another area of application for broadband optoelectronic switches for restoration as well as routing. The last section in this chapter presents proposals outlining the use of optoelectronic switching in WDM networks.

### **7.1 Network Restoration**

High capacity fibre optic telecommunication technologies provide multi-gigabit links on each fibre in each cable between transmission and receiving equipment at the nodes in a network. However, this capability to transmit many low rate constituent channels multiplexed to a higher rate on each link also makes the network highly vulnerable to major failures as the potential loss of a single link affects a large number of channels. For example, a single OC-48 data rate (2.488 Gbps) link contains 32,256 telephone voice channels. Since a number of

important services can be disrupted due to failure at a single point in the network, dynamic methods are necessary to help restore services as soon as possible. In addition to loss of revenue from the dropped calls, the traffic loads in the rest of the network may also be affected. The access nodes adjacent to the failure point can experience heavy loads as a large number of disconnected subscribers attempt to reconnect to the network in a short period of time immediately following the failure [121].

### **7.1.1 SONET network restoration**

With the introduction of SONET standard rates and formats for broadband optical transmission, dynamic restoration methods can be implemented [19, 122, 123] which utilize spare capacity in the transmission links controlled by the switching equipment in the nodes. The required switching equipment to accomplish such switching at the network nodes is known as a Digital Cross-Connect system (DCS). A DCS in a SONET network is capable of routing incoming data traffic according to information embedded in the signal overhead which contains routing information in addition to OAM&P (operations, administration, maintenance, & provisioning) information. The control information for routing purposes may also be contained in separate data channels which interlink the control equipment at various nodes in a network. A DCS based restoration scenario is shown in Figure 7.1. In case of a link failure, the affected traffic is re-routed through node 'D' if sufficient capacity is available on links A-D and D-B. The node equipment at all the nodes involved in restoration activity *cross-connects* the affected traffic on to various transmission links.

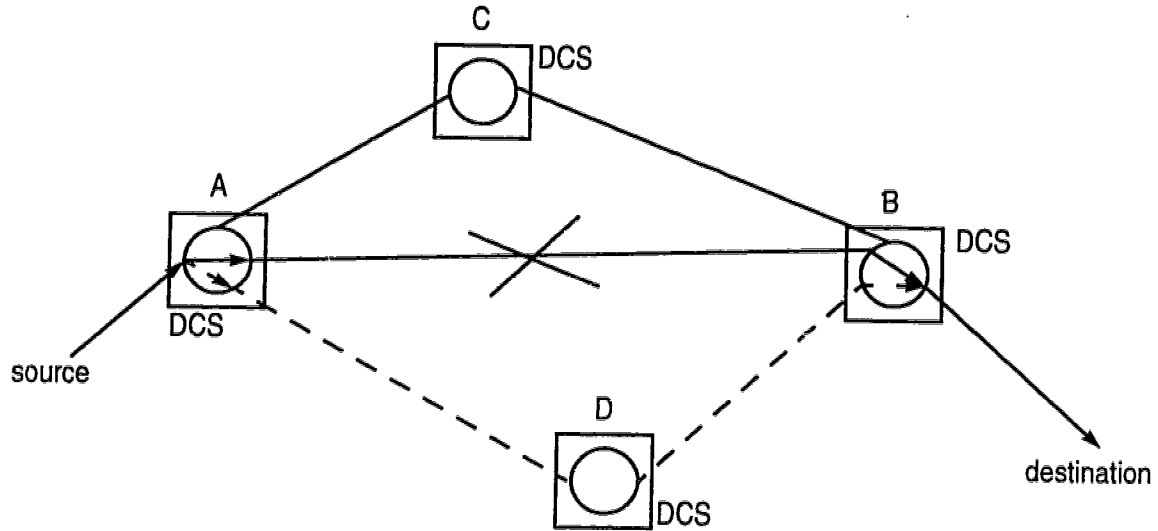


**Figure 7.1 Digital cross-connect system (DCS) based network restoration**

#### *7.1.1a Self healing rings*

Service restoration in a SONET network can also be performed using self-healing ring (SHR) techniques [124, 125]. A ring network utilizes a group of nodes within the network to form closed loops in which each node is connected to the adjacent nodes through a full duplex link (Figure 7.2). In fibre networks, this implies the use of a spare fibre (protection fibre) for each working fibre span as shown in Figure 7.2. In the event of a fibre span failure, the node equipment (ADM - add/drop multiplexers) routes affected traffic onto protection fibres. ADMs consist of optical transceiver interfaces to fibres in addition to the electrical multiplexing equipment required to add or drop the required traffic at the node (signals originating from the local node are 'added' to signal stream, and signals terminating at that node are 'dropped' from signal streams crossing the node). Since a protection fibre path ('P' in Figure 7.2) is available for each working fibre



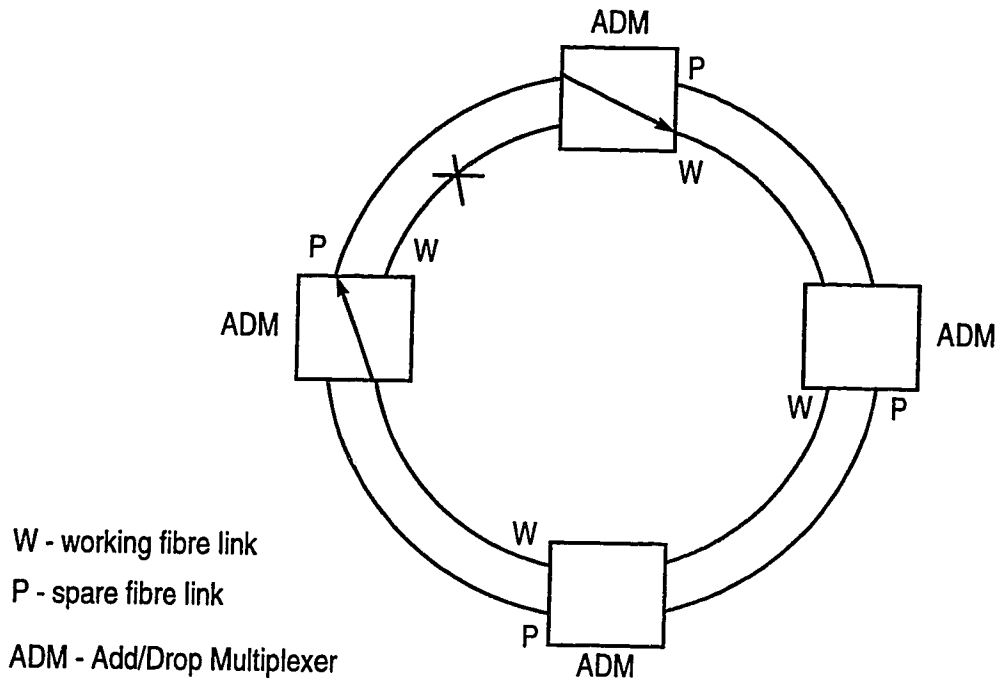


**Figure 7.2 Self-healing 'ring' restoration in SONET networks**

link ('W'), optical switches of 1x2 and 2x2 sizes are required to perform the required switching in event of a fibre failure [126]. The 1x2 switches can help direct the traffic from the failed 'W' fibre link on to the protection fibre link 'P' at any node.

As a number of technologies are available (section 2.2) for providing broadband switches of 1x2, 2x2 dimensions, optoelectronic switches are not considered suitable for self-healing rings employing 1:1 fibre protection (one protection path exists for each working path). However, for 1:N fibre protection strategies where only one protection fibre path is available for N working fibre paths, broadband optoelectronic switches can be used to perform the required

routing of signals using a NxN switch matrix as shown in Figure 7.3.

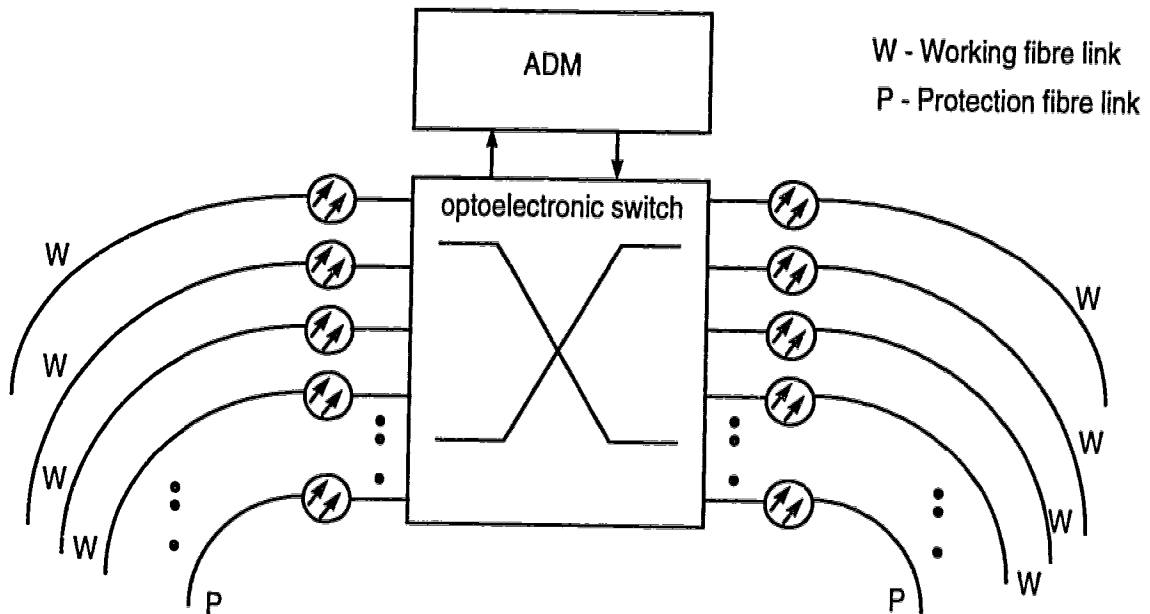


**Figure 7.3 1:N Protection ring arrangement with optoelectronic switch, 1 protection fibre link is available for N working fibre links**

For DCS based networks (known as Mesh networks), required switch sizes are large (up to 16x16 or more). Optical switches of this size are difficult to make with the required speed, loss, and cost. The use of optoelectronic switches is proposed here to help implement efficient restoration techniques.

## **7.2 Optoelectronic Switching for Network Restoration**

### **7.2.1 SONET cross-connect system**

A digital cross-connect system used in SONET networks terminates digital signals and cross-connects the constituent time division multiplexed channels according to the 'routing map' stored in the controller. Functions performed by a

DCS may include: signal add-drop (signals originating from the local node are 'added' to signal stream, and signals terminating at that node are 'dropped' from the signal streams crossing the node), signal cross-connect, and multiplexing, demultiplexing [127]. Broadband DCS (B-DCS) in SONET provides cross connections at the basic 51.84 Mbps data rate which is designated as Synchronous Transport Signal Level-1 or STS-1. The B-DCS therefore includes all (de) multiplexing functions required to interface with STS-N rate signals (current networks employ up to STS-48 data rates). The OC-48 (optical carrier level-48) signal carries the equivalent of 48 STS-1 signals as a single STS-48 signal. In general, OC-N signal levels refer to the corresponding STS-N level of data traffic being transported, though standard OC-N levels are defined at OC-3, 12, 48, and 192 only. According to Bellcore standards, the cross-connect needs to be non-blocking (see section 2.1.1), and must switch in less than 50 msec [127, 128].

The primary function of the DCS is to provide two way cross-connection of various STS-n rate signals. Since the switching matrices employed in the equipment are electronic, existing B-DCSs cross-connect at a single fixed data rate. Figure 7.4 shows a schematic view of the SONET DCS after [127]. The incoming signals (shown on left side of the figure) are at the SONET standard data rates OC-N. After an optical-to-electronic conversion, these signals are split into the constituent signal levels by the demultiplexers (DMUX). The cross-connect matrix is used to perform the required routing of signals (at a fixed rate STS-N) and then the signals are multiplexed (MUX) together to form the higher bit

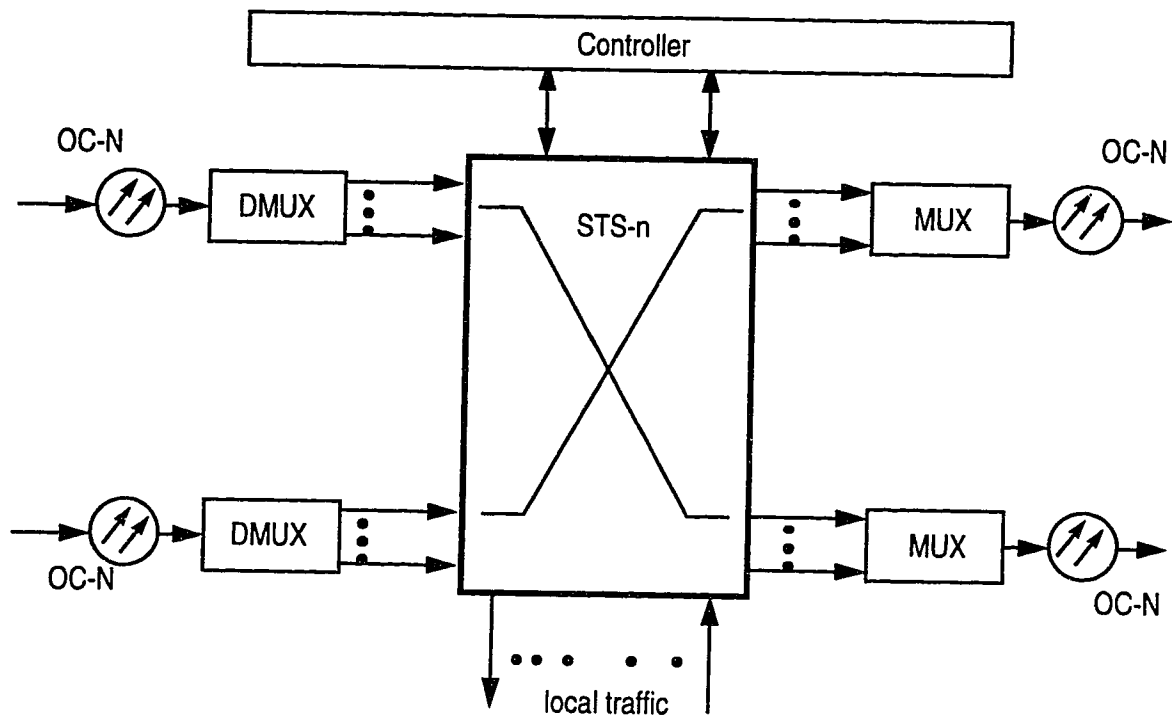


Figure 7.4 A SONET Digital Cross-connect System

rate OC-N signals which are transmitted as optical signals.

### 7.2.1a All optical cross-connects (OCX)

Switches with optical input and output signals may also be used to perform cross-connection of high bit rate optical data streams. Such switches can then be used in conjunction with conventional DCS equipment which provide the (de)multiplexing and add-drop capabilities. Additional equipment in the form of optical amplifiers and 1x2 switches is required in such cases since optical data streams are routed without signal re-generation [126]. Figure 7.5 shows an

example of an optical cross-connect (OCX) switch used with a DCS.

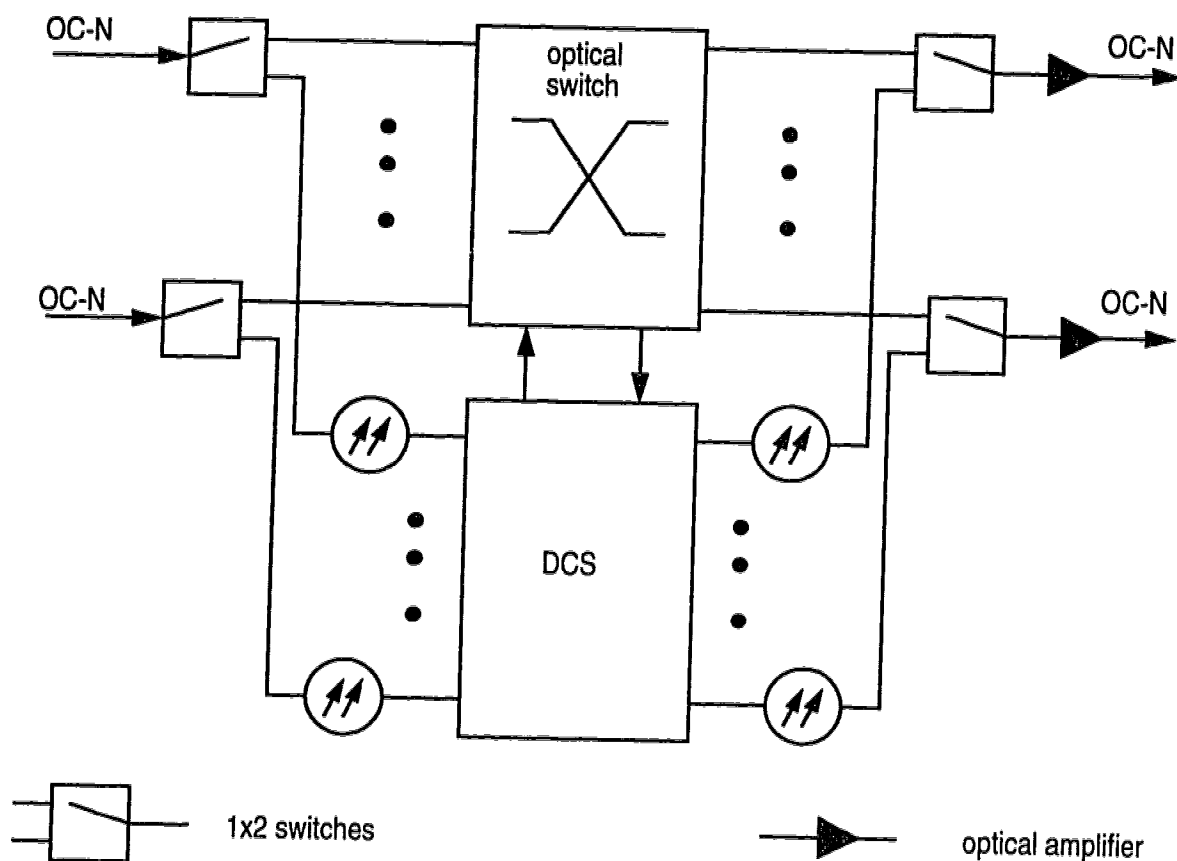


Figure 7.5 Optical cross-connect (OCX) system

### 7.2.2 Broadband optoelectronic cross-connect (B-OECS)

The optoelectronic switch matrix provides a capability to cross-connect analog signals and digital signals at any rate up to the maximum supported by the switch (2.488 Gbps in the prototype). The variable bandwidth and format insensitive features of the broadband switch can enhance the capabilities of a DCS and make it possible to implement a cross-connect system for various data

rates and formats with the same hardware. Figure 7.6 shows the proposed broadband optoelectronic cross-connect system which is capable of handling analog signals in addition to any data rate between STS-1 and STS-48 at any given time at any port. Since any data rate (SONET standard STS-x or otherwise)

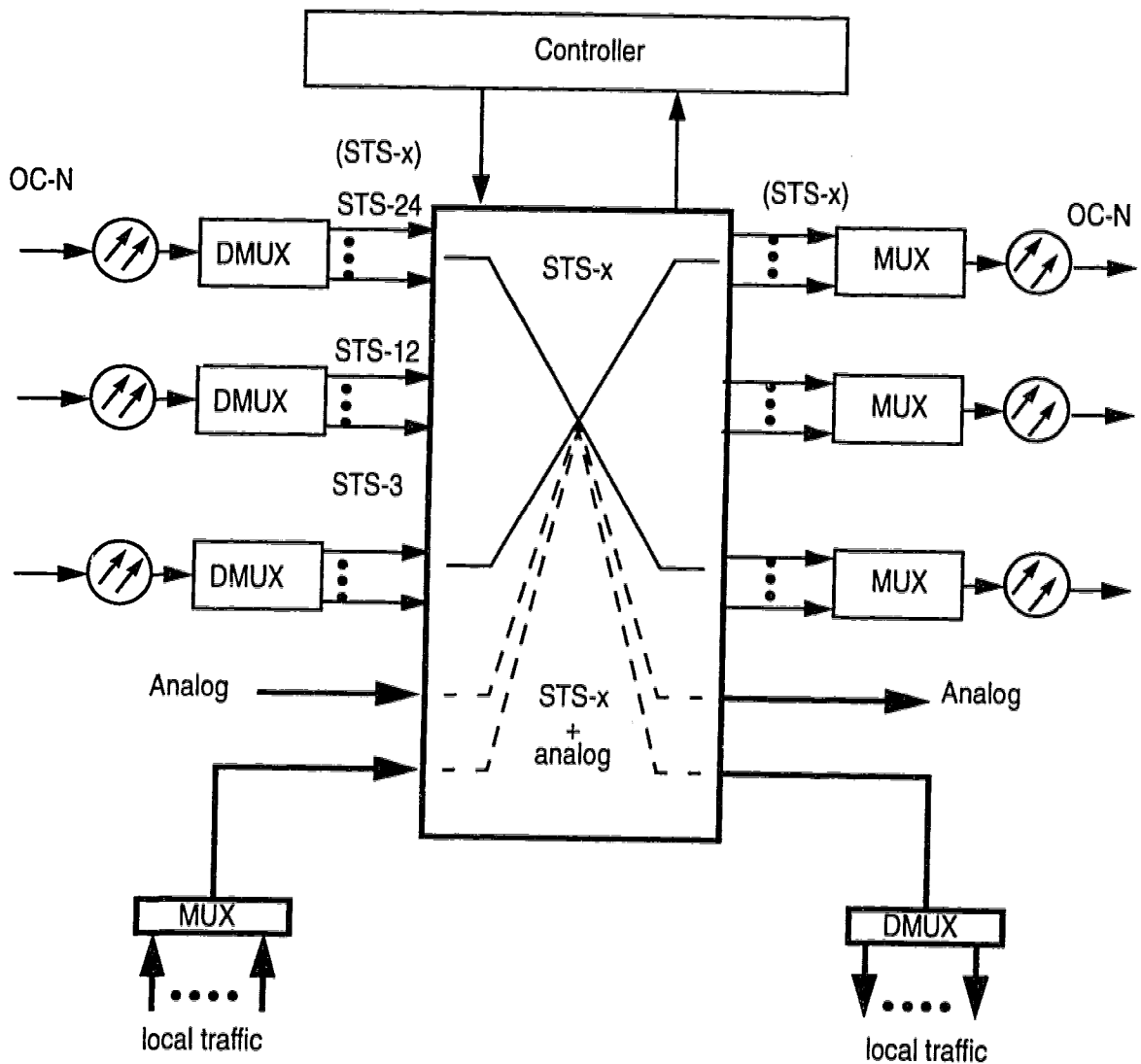


Figure 7.6 Broadband Optoelectronic DCS

can be used, a natural transition is possible to any other transmission standard including the new packet based ATM transport and routing architecture. The B-OECS fulfils all the requirements for ATM cross-connect switches, where the key requirement is the need to handle various bandwidths and rates in a uniform manner using the same hardware [129, 130]. The B-OECS would allow a fully functional true ATM cross-connect carrying native ATM format signals, and at the same time permit the use of any other signal format if so desired. For evolution from SONET to ATM based transport networks, the B-OECS can continue to support legacy and analog signals because the cross-connect is transparent to the formats. The capability to transfer arbitrary rates and formats may also suggest a use in gateway applications to international networks.

In addition to these properties, the B-OECS can switch at extremely fast rates limited only by the controller speed (Appendix G). The crosspoints are capable of switching in less than 10 ns [2]. Since electronic components are available for >100 MHz speeds, the Bellcore objective of 50 msec switching time [128] for the matrix can be easily accomplished in the switch fabric.

### **7.2.3 Restoration methods**

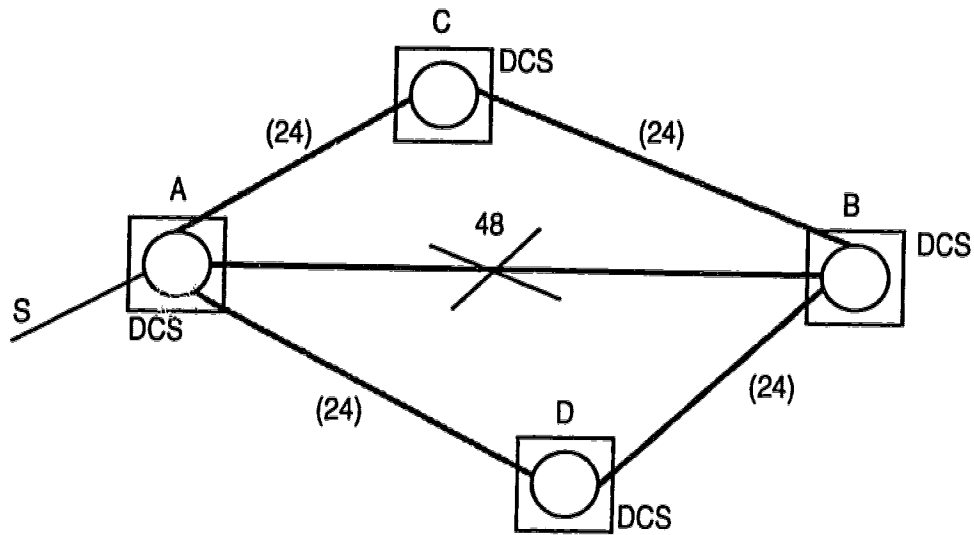
#### *7.2.3a 'Bundled' restoration*

DCS based mesh networks can be designed to be fully restorable in the case of a fibre link failure by introducing redundancy in the transmission link capacity and node switching equipment. Spare capacity is provided in form of spare fibres in the transmission links ('dark' fibre) or through providing higher capacity transceivers than needed, e.g, a STS-48 capacity may be installed

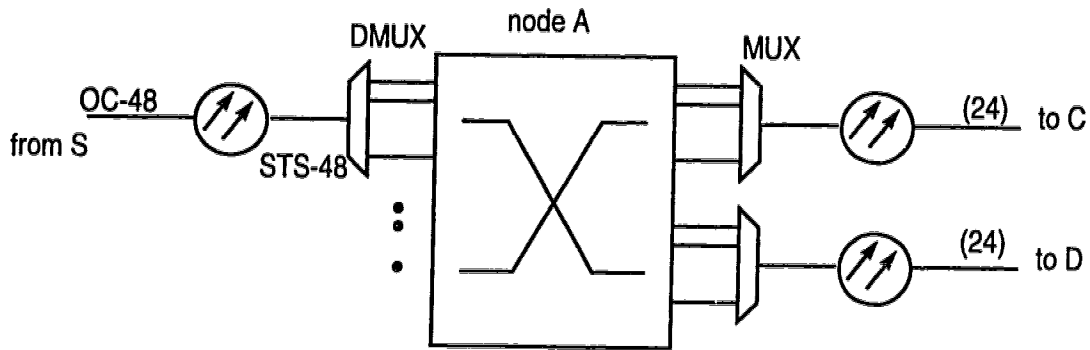
where only STS-24 units of traffic are present. A part of that capacity - STS-24 units, is available as spare capacity. Corresponding extra ports and (de) multiplexing equipment is required in the cross-connect systems as well (see Figure 7.4) to help implement a survivable network. In B-DCS based networks, the switch matrix cross-connects STS-1 rate (51.84 Mbps) signals [127, 131]. Thus, the redundancy required is also provided at the STS-1 signal rate which is the lowest standard transport signal rate in the SONET standard. Consequently, a larger number of ports are required in the (de) mux equipment as well as the switch matrix. For example, 48 STS-1 ports are required to provide a single OC-48 rate redundant path.

With broadband optoelectronic switch based cross-connect systems, data rates ranging from STS-1 to STS-48 are available at each port. Thus redundant ports required for restoration purposes can be provided at any rate. Therefore the optoelectronic switch matrix can be used with a variety of (de) mux equipment that may be required and this equipment may be changed or upgraded without requiring any changes in the switch matrix. In the case of restoration with optoelectronic cross-connects, the broadband payloads can be interconnected at any rate (STS-x) instead of STS-1 rate. Figure 7.7 illustrates the use of a bit rate independent optoelectronic switch in the network restoration application. In the case shown here, STS-48 units of traffic (2.488 Gbps) are lost on span A-B due to a failure, and the lost traffic is routed via nodes C and D where STS-24 units of spare capacity each are assumed to be available (indicated as '(24)' in the diagram). A schematic view of the broadband switching capability required at





(a) Link failure A-B (48 units of traffic) is restored via A-C and A-D



(b) Broadband switching required at node A

**Figure 7.7 Optoelectronic switch in network restoration**

node A is shown in Figure 7.7 (b). The incoming traffic from node S (OC-48 or STS-48) is demultiplexed only down to STS-24 rate and switched on to the outgoing links AC and AD which have the required spare capacity.

In addition to the ability to switch broadband fractions of the lost traffic (STS-24 in this case), efficient algorithms are required to compute the paths

available to achieve service restoration. Design of such algorithms is an advanced research field [19, 20, 21, 132, 133, 134]. The focus of this work is on the hardware or physical layer switches required for efficient implementation of such algorithms.

Extending the previous example by considering capabilities offered by the optoelectronic switch, STS- $x$  ( $1 \leq x \leq 48$ ) rate data channels can be considered to be bundled together for the purposes of restoration (Figure 7.8). The capability to

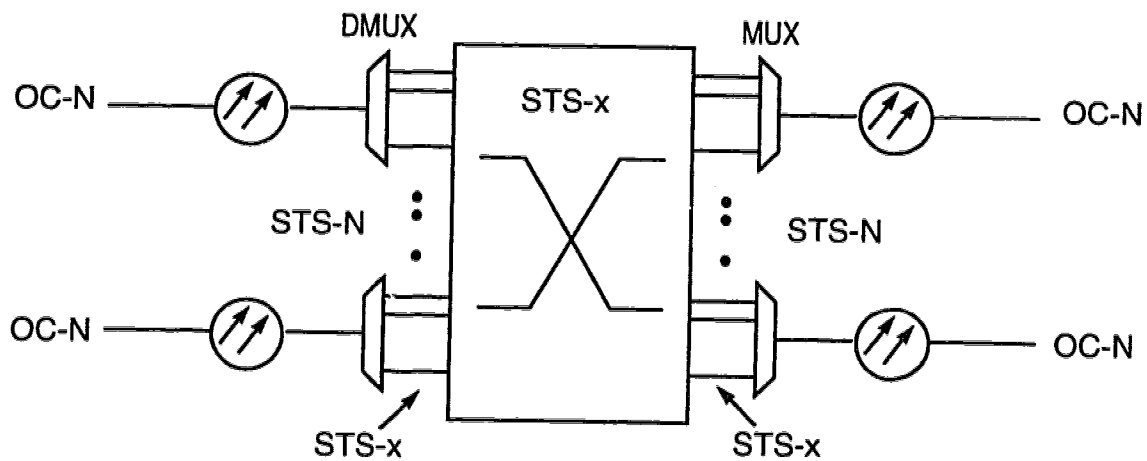


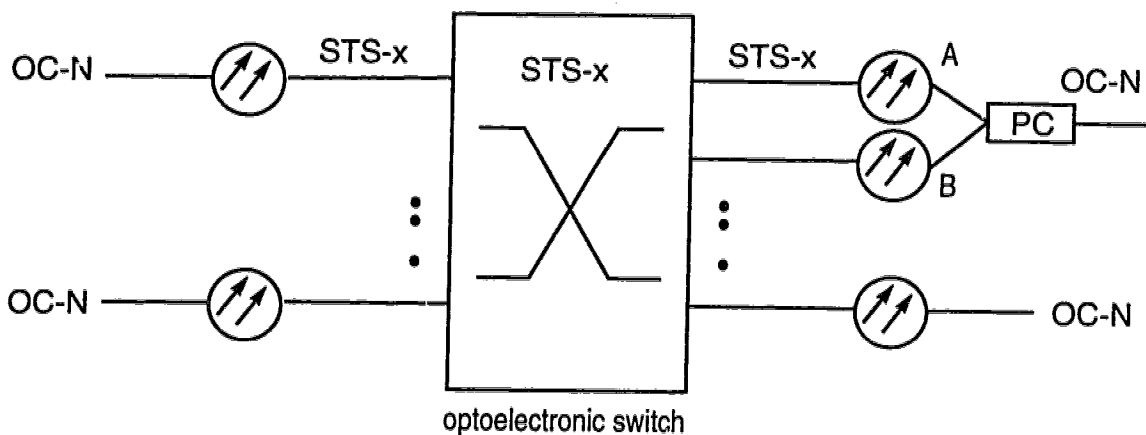
**Figure 7.8 Variable rate optoelectronic cross-connect switch**

switch bundled channels STS- $x$ , where 'x' may be different at different nodes in a network, provides a physical layer equivalent of a particular class of network restoration algorithms [131, 135, 136]. These algorithms provide efficient means of allocating and managing bundled spare capacity over other methods which may consider STS-1 rate traffic and cross-connect equipment [135]. Optoelectronic switch based cross-connect systems provide ideal platforms for

implementing bundled demand restoration algorithms. This particular application makes full use of the format and bit rate transparency in combination with electrical inputs and outputs available in the optoelectronic switches. No other switching technique provides this form of transparency for broadband signals. The highest bandwidth in commercially available electronic analog crosspoint switches which can provide such transparency is 300 MHz [137].

### 7.2.3b Link restoration

The broadband capabilities of the optoelectronic switch can also be used to cross-connect full rate (OC-N) data transport streams to provide network restoration facilities when spare fibre paths are available. In this case, the data channel affected by a link failure can be routed to another fibre path at the output as shown in Figure 7.9. This technique also provides extra protection for the laser



PC - passive optical combiner

**Figure 7.9 Optoelectronic cross-connects with protection for Laser transmitters**

transmitters at the output as shown in Figure 7.9. The broadband electronic data

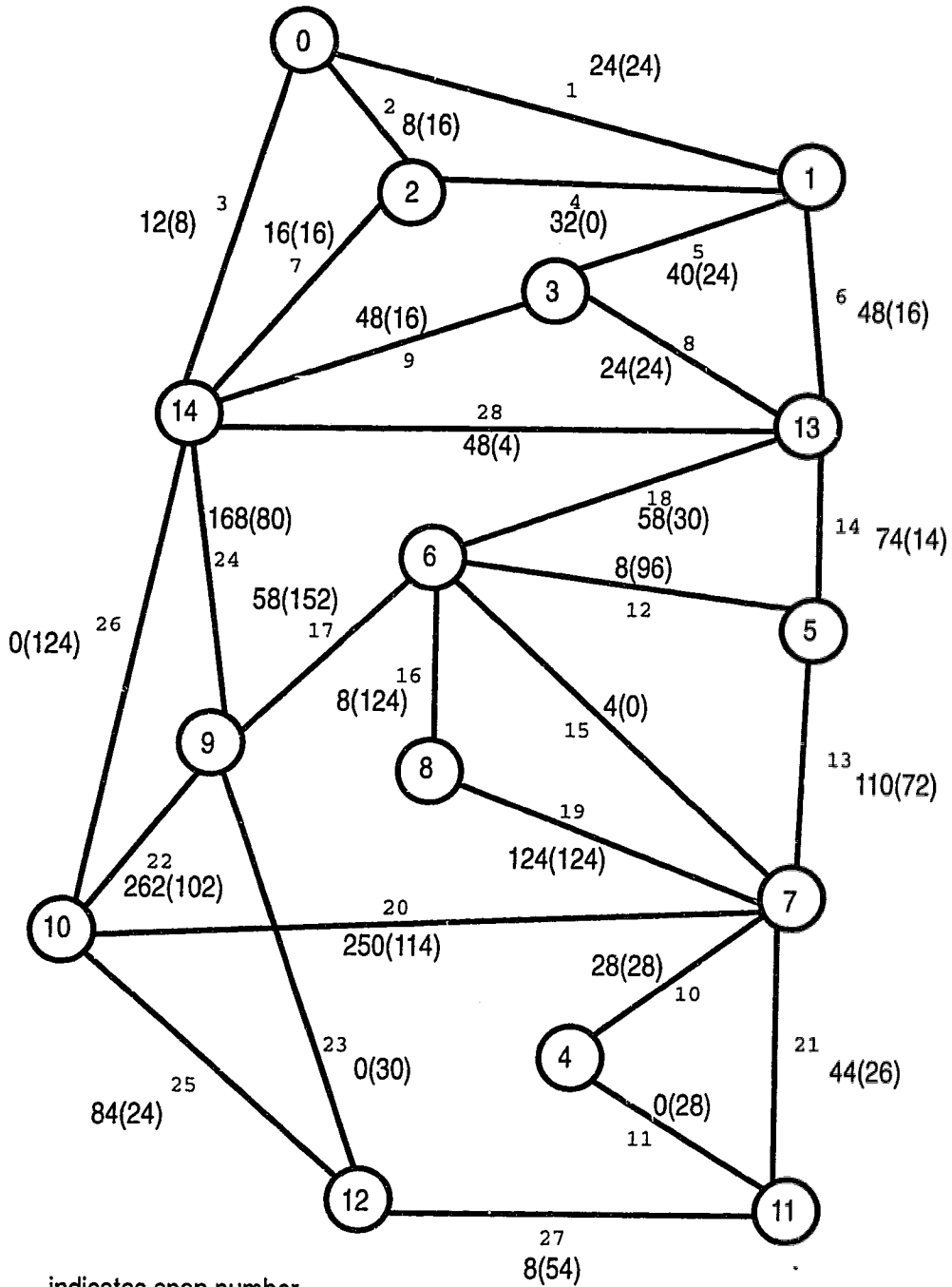
streams can be routed to either transmitter (A or B) in the event of a transmitter failure. Note that if optical switches are to be used in a similar role, protection against laser transmitters is not possible.

In the next section, a sample metropolitan network [138] is used to demonstrate that the optoelectronic switching based cross-connect approach will require switches of comparable sizes to the optical switches required for restoration. In general, it is easier to make optoelectronic switches of large sizes than optical switch matrices of the same size.

### **7.3 A Case Study**

The model network, called *Bellcore Metropolitan Network-1* has been frequently used to evaluate the benefits of restoration strategies [19, 20, 21, 126, 131, 133] since initial disclosure by Bellcore [138]. A schematic of the network, along with the transmission capacities on every link, is shown in Figure 7.10. The source and terminating nodes for each constituent traffic demand (called point-to-point demand map) for the network is given in Appendix F. From the working capacities (in STS-1 units) indicated on the map of the network and the point-to-point demand map, traffic demand to be cross-connected at each node can be calculated along with the traffic originating or terminating at that node which does not need to be cross-connected. The details of the traffic for each node are also given in Appendix F.

Table 7.1 presents the break up of the total demand at each node in the network in terms of originating/terminating traffic and cross-connected traffic.



$n$  indicates span number

X(Y) represents X (STS-1) working capacity with Y (STS-1) spare capacity on each span

$\textcircled{N}$  indicates the node number

Figure 7.10 Bellcore metropolitan network-I

**Table 7.1 Bellcore metropolitan network-I: traffic at each node.**

<b>Node</b>	<b>Demand (STS-1) originating/ terminating at Node</b>	<b>Demand (STS-1) Cross-Connected at Node</b>	<b>Total Capacity (Working) at Node</b>
0	44	None	44
1	88	56	144
2	56	None	56
3	72	40	112
4	28	None	28
5	108	84	192
6	108	28	136
7	52	508	560
8	132	None	132
9	108	380	488
10	380	216	596
11	52	None	52
12	92	None	92
13	92	160	252
14	236	56	292

After the demands have been separated into cross-connected demands and originating/terminating demands as shown in Table 7.1, requirements for the number of cross-connected streams at any node can be calculated. The number of data streams to be cross-connected corresponds to the number of ports required in the cross-connect switch at that node as long as the data stream carries less than STS-48 units of traffic (maximum capacity per port for the optoelectronic switch). For data streams with more than STS-48 units, the number of ports is calculated by splitting the data stream into sections of STS-48 each. Following these calculations (see Appendix F), the cross-connect size required at

each node is given in Table 7.2. Note that optical crosspoint switches operate at the data rate presented to the switch and may be smaller than the optoelectronic switch required if that data rate exceeds 2.488 Gbps.

**Table 7.2 Cross-connect switch sizes**

<b>NODE</b>	<b>Total Demand (to be cross- connected) STS-1 units</b>	<b>Cross-Connect Size (assuming 2.488 Gbps max)</b>	<b>Optical switch cross-connect size</b>
0	None	None	None
1	56	6 x 6	6 x 6
2	None	None	None
3	40	2 x 2	2 x 2
4	None	None	None
5	84	2 x 2	2 x 2
6	28	2 x 2	2 x 2
7	508	20 x 20	18 x 18
8	None	None	None
9	380	10 x 10	4 x 4
10	216	8 x 8	6 x 6
11	None	None	None
12	None	None	None
13	160	12 x 12	12 x 12
14	56	6 x 6	6 x 6

It is seen that the matrix sizes required with optoelectronic cross-connect are identical to the switch sizes required for optical switch based cross-connect systems for 6 out of the 9 nodes which require cross-connect elements. For two other nodes (node number 7 and 10), the size required is only 2 ports more than the optical equivalent, and only for one node in the network does the size required

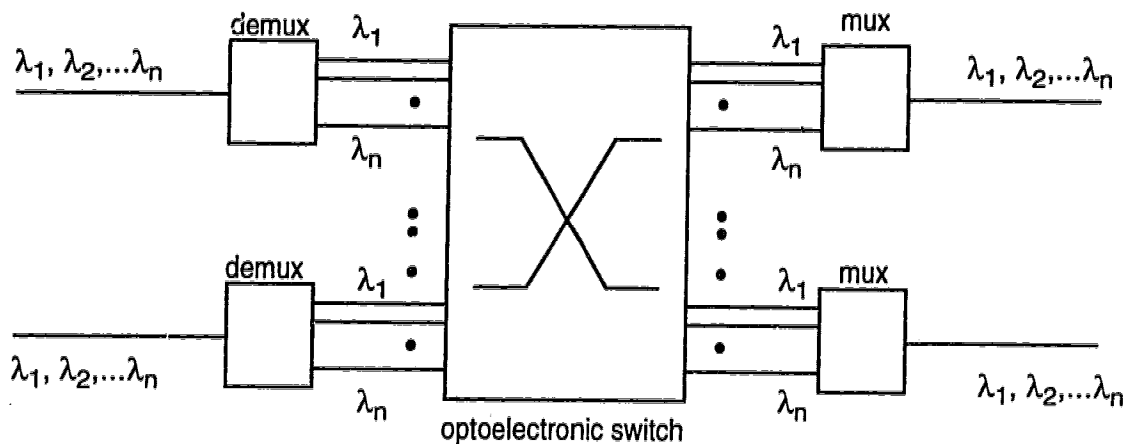
show a large difference (node number 9). The only optical switching technology capable of providing the required switch dimensions is opto-mechanical switching, but the switching times are too slow to be useful in dynamic reconfiguration (of the order of 500 ms [43]). Semiconductor optical amplifier based switches also provide similar switch sizes, though the cost is prohibitively high at these dimensions [41, 42]. The use of optoelectronic switches could, however provide a viable solution. It should be noted that optoelectronic switch capabilities in future may extend to higher bit rates than OC-48 (2.488 Gbps).

## **7.4 WDM Networks**

Wavelength division multiplexing techniques are used to transmit a number of optical wavelengths on the same fibre, each with its own broadband data payload to increase the capacity of the optical fibre networks. WDM networks currently being used in research test beds carry up to 10 Gbps or more on each wavelength [139]. The bit rate and format transparency of the optoelectronic switch can be used to perform a number of useful switching functions required in a WDM network (see Appendix H).

Optoelectronic switches in conjunction with commercially available optical wavelength multiplexers and demultiplexers [140] may be used to perform wavelength switching as shown in Figure 7.11. A data channel at any incoming wavelength can be converted to another wavelength by first separating the wavelengths with the help of an optical demultiplexer, and then switching the information carried to any outgoing port with the help of the optoelectronic switch.





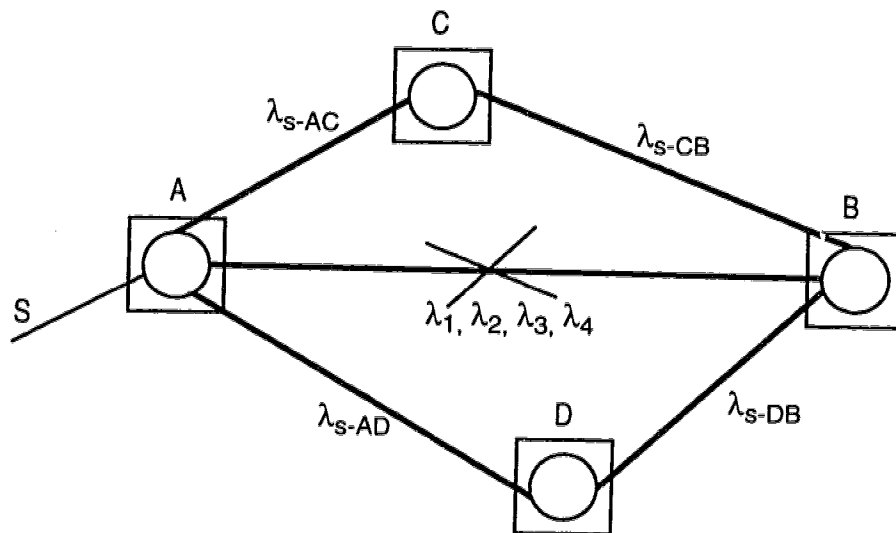
(de) mux are optical wavelength (de) multiplexers

**Figure 7.11 Optoelectronic switch as a wavelength routing switch  
(optical-to-electronic conversion elements are not shown)**

Laser transmitters placed at the output of the switch can then provide the required optical signal at the desired wavelength, and optical multiplexers can be used to couple the different wavelengths at the outputs into a single optical fibre. Similar techniques of optoelectronic wavelength conversion in WDM networks have been shown to result in a higher capacity network as compared to one with optical switches performing cross-connection of wavelengths [37, 39]. These techniques require the use of broadband electronic switches to switch the data after wavelength separation and conversion to electronic form [141]. It should be noted that such techniques require an additional broadband electronic switching stage with sufficient bandwidth to handle the data streams. In optoelectronic switching, where the routing is achieved through the optical-to-electronic conversion

process, no such additional electronic switching stage is required. The bandwidth is only limited by the conversion process, and not the switching stage.

The WDM routing capability may be effectively used in network restoration methods based on WDM techniques where the spare capacity on the links is provided in the form of discrete wavelengths on the same fibre. Figure 7.12 shows



$\lambda_{s-XY}$  - denotes spare capacity wavelengths between nodes X and Y

**Figure 7.12 WDM based spare capacity in a network**

a schematic view of a WDM network where spare transmission capacity in the form of wavelengths denoted as  $\lambda_s$  can help restore traffic in the event of a link failure. In the example shown here, the traffic lost between nodes A and B ( $\lambda_1 - \lambda_n$ ) is re-routed through links A-C and A-D over spare wavelengths  $\lambda_s$ .

To perform dynamic reconfiguration of wavelengths in a WDM network, wavelength conversion and routing functions would be required at node A to transfer the traffic affected by the link failure on to wavelengths reserved for

restoration on other links. A detailed schematic view of the optoelectronic switch in such a role corresponding to the link failure shown in Figure 7.12 is shown in Figure 7.13.

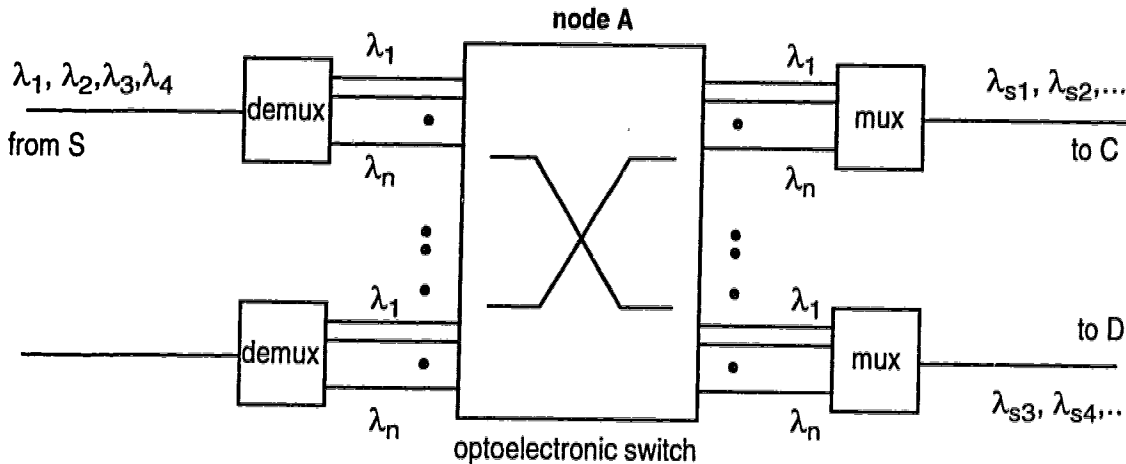


Figure 7.13 Optoelectronic restoration switching at node A

The affected traffic on wavelengths  $\lambda_1, \lambda_2, \lambda_3,$  and  $\lambda_4$  between nodes A and B in the scenario shown in Figure 7.12 is routed through the optoelectronic switch to the laser transmitters at the respective output ports. Wavelengths  $\lambda_{s1}$  &  $\lambda_{s2}$  on link A-C now carry the data previously carried on  $\lambda_1$  &  $\lambda_2$  on A-B, and  $\lambda_{s3}, \lambda_{s4}$  on link A-D carry the data previously on  $\lambda_3, \lambda_4$  on A-B. Similar routing using spare wavelengths  $\lambda_{s-CB}$  and  $\lambda_{s-DB}$  can be carried out on links C-B and D-B respectively as illustrated in Figure 7.12.

The optoelectronic switch in this case is used in a similar manner to DCS based restoration except that the (de) multiplexing mechanisms are optical.

These (de) multiplexers (separate) combine the wavelengths. Since the optoelectronic switch is transparent to the data carried, any format or bit rate may be transported and cross-connected through the optoelectronic switch in the WDM network.

The optoelectronic switching techniques thus provide a single technology solution to a variety of network architecture ranging from DCS based SONET networks to WDM networks.

## **8. Conclusions and Recommendations**

In conclusion, a summary of the project is presented which focuses on salient features of the prototype switch, and a brief description of results obtained for digital and analog signals follows. Conclusions are drawn from the issues encountered in the course of the project.

The broadband, format-transparent signal routing capabilities demonstrated with the prototype switch provides impetus for developing a next generation of optoelectronic switches employing fabrication techniques more suitable to manufacturing. Optoelectronic switching is compared to other optical switching techniques for these applications. Benefits and unique features demonstrated with the prototype switch are pointed out to identify new directions in optoelectronic switch development driven by these niche applications.

### **8.1 Project Summary**

A brief description of the design and construction of the prototype is presented here as an overview of the project and to help formulate recommendations for future work. A brief summary of results demonstrated with the prototype is also included to permit evaluation of some key applications for optoelectronic switching.

#### **8.1.1 Prototype construction**

A 10x10 prototype crosspoint matrix switch was constructed to implement optoelectronic 'broadcast and select' techniques for routing and processing of broadband signals. This prototype switch used low cost laser diodes

(manufactured for compact disc players) which served as transmitters for broadcast of input signal to all output ports in the switch. The microwave bias-tee circuit in the laser transmitters was redesigned to achieve 1.25 GHz bandwidth for each signal path in the switch. Signal distribution in the prototype is accomplished with multimode fibres terminated in a silicon v-groove fibre holder which contains ten fibres with cleaved facets. Each group of ten fibres provides optical signals which are incident on a MSM photodetector array. The MSM array chip is placed on a suitable substrate (TMM-3™) that is designed to support surface-mounted component based de-coupling and bias circuitry. A 50  $\Omega$  (characteristic impedance) microstrip transmission line is provided on the substrate to carry the output signal from the MSM array to the output port through the amplifier chain. A precision machined housing for the substrate was designed and fabricated that provides support for the v-groove fibre assembly as well. The optoelectronic receiver modules were also used for extensive tests on conventional designs of MSM arrays to characterize the frequency response of photodetectors. Position dependent frequency response, limited to a few GHz, of the conventional arrays was discovered as a result of these tests. New designs were produced to help overcome these limitations.

The completed prototype was put through extensive tests and results from these tests were reported in Chapter 5 and 6. In September 1995, a leading manufacturer of optical components and switches signed an agreement to evaluate commercial potential for the optoelectronic switching technology. The prototype switch underwent further tests at the manufacturer's premises under the

author's supervision and advanced network applications of optoelectronic switches were explored as part of the agreement. The prototype switch was then successfully demonstrated at Telecom '95 in Geneva, Switzerland, from October

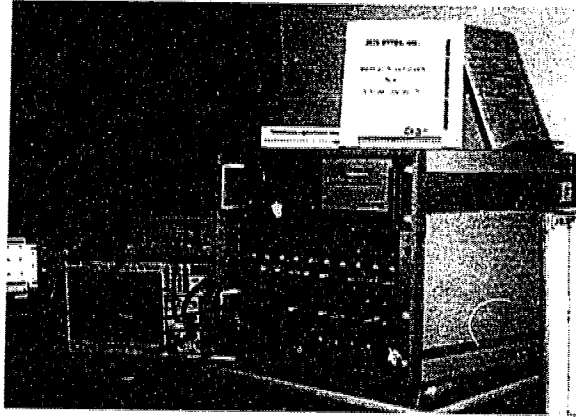


**Figure 8.1 Prototype optoelectronic switch at the Canada Pavilion, Telecom '95, Geneva.**

3 to 11, 1995 (Figure 8.1). Telecom '95 was the largest exposition of telecommunication industry to date and helped gain invaluable exposure for the technology and its potential applications.

### **8.1.2 Summary of results**

Broadband signals of various formats were used to characterize the performance, and demonstrate the capabilities of the prototype optoelectronic switch. It was shown that the prototype is capable of routing signals with an ON/OFF ratio of more than 60 dB. The crosstalk experienced by signal traversing the optoelectronic switch was shown to be less than 60 dB. Binary digital signals

ranging from 622 Mbps to 2.5 Gbps were successfully transmitted through the switch. The prototype was also used to perform routing of analog video signals. Performance of the switch for routing a composite payload consisting of 42 CATV video carrier frequencies was characterized.

Complete format transparent switching capability was demonstrated with simultaneous routing of a 2.5 Gbps data signal and a standard NTSC video channel through the prototype switch.

Spectrally efficient modulation for photonic interconnects was proposed and demonstrated with the help of four level signals. Data throughput for each port in the prototype may be improved up to 3.6 Gbps with the use of four-level data at a symbol rate of 1.8 GHz.

Broadband signal processing capabilities of the optoelectronic crosspoint matrix were also demonstrated through realization of reconfigurable filters with a free tuning range of 500 MHz. Such tunable filters can be applied to equalize modal dispersion encountered in multimode fibre systems.

### **8.1.3 Recommendations for future work**

The lessons learnt in the process of designing and fabrication of the first 10x10 prototype switch may be applied to further development of the switching technology for higher data rates. An optoelectronic switch system can be considered to consist of three sub-systems:

- Laser transmitters
- Optical signal distribution section
- Optoelectronic receiver module



### *8.1.3a Laser transmitters*

The function of a laser transmitter module is to accept a broadband electrical signal and deliver the corresponding optical signal to the signal distribution section. In the current prototype, laser diodes manufactured for compact-disc player applications sufficed for obtaining 1.25 GHz bandwidth. However, package parasitics must be carefully avoided or eliminated to achieve bandwidths of the order of 10 GHz and above. Directly driven lasers with a bias-tee placed close to the laser chip (commercially available or custom engineered) are required to obtain sufficient bandwidth without being limited by package parasitics elements.

### *8.1.3b Optical signal distribution section*

The signal distribution section consists of 1xN optical splitters to divide the signal from each input port for distribution to the N output ports. The outputs from each splitter then need to be 'shuffled' such that each output port receives one signal from every input port. In the prototype switch, this signal shuffle is accomplished through separate fibres (100 fibres with connectors in the 10x10 switch). This approach, though simple to envisage, is cost and labour intensive in its execution as  $N^2$  connectors and fibres are required for a NxN switch. For the next generation of optoelectronic switches, a number of alternatives are being explored in the high speed switching research group at TR Labs and University of Alberta which utilize hybrid integrated polymer waveguides [15], and free space optical beam distribution methods [90, 92, 92].

In addition to these promising initiatives, a simple fibre-ribbon based

approach shown in Figure 8.2 may also be considered. Fibre-ribbon pigtailed 1xN splitters can be used to provide a single ribbon output which contains the N fibres carrying signals from each input port. To accomplish the fibre shuffle, the ribbon

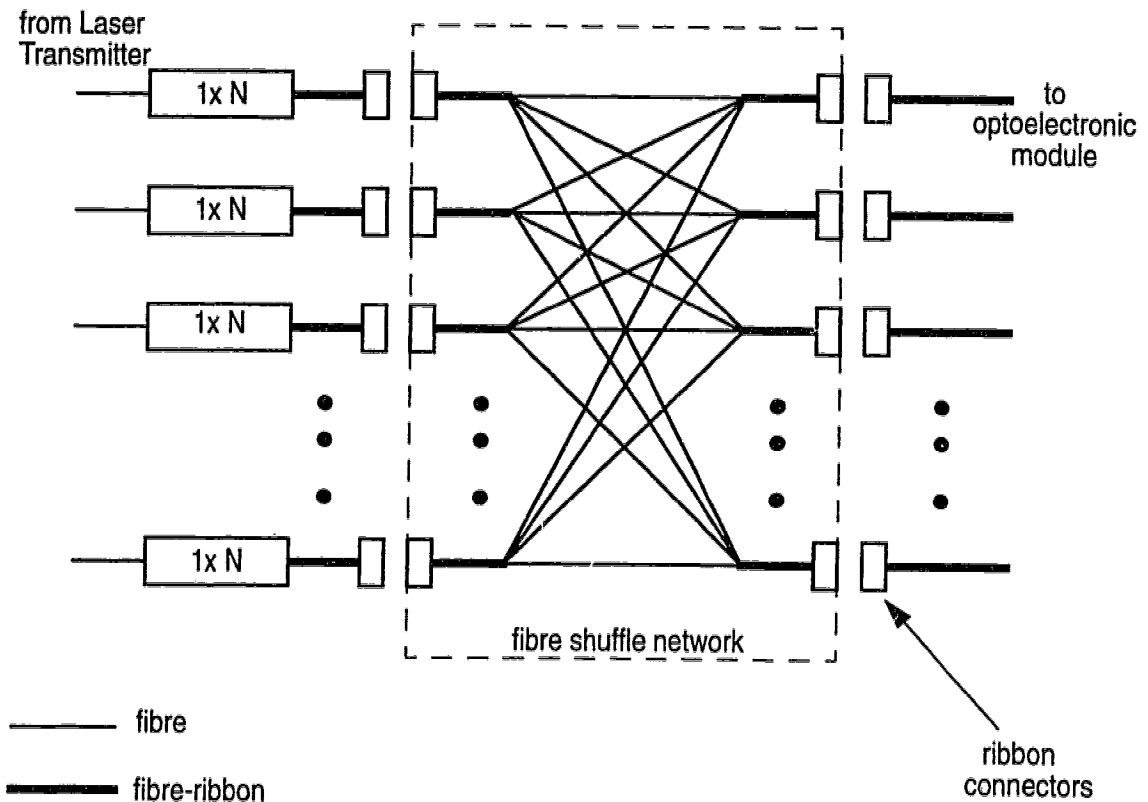


Figure 8.2 A fibre-ribbon based optical signal distribution module

can be separated into individual fibres. One fibre from each input ribbon is taken and the group of fibres is 'reformed' into a ribbon with the help of a ribbon-forming tool. Such tools are available commercially as accessories for ribbon splicing machines [142]. Placing fibres into ribbons is advantageous since a single connector can be used with each ribbon, which reduces the number of connectors

required and makes the management of the resultant  $2N$  fibre-ribbons (compared to  $N^2$  individual fibres) in optoelectronic switches much easier. Standard fibre-ribbons are fabricated with fibres placed at  $250\ \mu\text{m}$  pitch, which makes the alignment to photodetector arrays easier as well.

Thus a complete  $N \times N$ , connectorized fibre-shuffle module can be fabricated which may be used to with any laser transmitter or optoelectronic receiver modules.

#### *8.1.3c Optoelectronic receiver module*

The optoelectronic module designed for the prototype switch successfully combines the required DC bias circuits and RF output sections for the MSM photodetector array, while providing a simple optical assembly and ease of alignment. Other methods of coupling light to the MSM photodetectors that use polymer waveguides with out of plane taps are under investigation [91]. These approaches can potentially provide a planar package for the optoelectronic module. Use of a transimpedance amplifier in the first stage immediately following the photodetectors will provide better noise performance (higher sensitivity, dynamic range) than the  $50\ \Omega$  input impedance amplifiers used in the prototype switch and may be incorporated into future designs.

#### **8.1.4 Hybrid integrated tunable receivers**

Broadband MSM photodetector arrays used in conjunction with optical means of separating the wavelengths in a WDM system can provide convenient means of selecting the wavelength to be received (see section 4.6, Figure 4.35).

Mature research projects are in progress at University of Alberta and TRLabs regarding WDM components [143]. Hybrid integration of these components with MSM arrays on a common suitable substrate may be explored to provide low cost tunable receivers operating at more than 2.5 Gbps per channel with 8 or more channels. Each optoelectronic receiver module of the current prototype switch in fact implements the signal selection function. A discrete component based, high capacity (2.5 Gbps per port) tunable receiver can be demonstrated with an appropriate fibre pigtailed wavelength demultiplexer such as the one reported in [143], used with the module.

## **8.2 Broadband Switching: Applications and Options**

Engineering research projects need to be closely coupled to their applications while advancing the capabilities of the technology under development to enable and facilitate still newer applications. Optoelectronic switching has been shown to be suitable for fulfilling the requirements for routing mechanisms needed in diverse applications. The areas where optoelectronic switching may find applications range from short distance photonic interconnects to telecommunication network cross-connect systems. A summary of the suitability of optoelectronic switching to these applications follows along with some comments on other technologies available for switching of photonic broadband signals.

### **8.2.1 Applications for broadband switching**

Conventional applications of broadband switches have been in the area of

long distance *telecommunication* networks since the data signals in a majority of other networks were generally at lower rates. However, as explained in Chapter 2, recent proliferation of high performance computers has created a demand for very high rate interconnections among these computers. This area is comparatively new and is growing faster than the traditional telecommunication network areas. Data rates in such networks have increased from ~2 Mbps (Ethernet) to >1 Gbps (HIPPI) over the last 5-7 years. This development mirrors a similar growth in telecommunications networks, albeit in a much shorter time period.

Computer networks also provide an inherently richer field of applications than telecommunication networks in that several different and disparate standards can coexist (see section 2.1.2), whereas telecommunication equipment networks and equipment need to follow a common standard so that equipment from various vendors can be connected together over the same network (i.e, SONET, ATM networks). Since local area computer networks can always be linked through the telecommunication network, there is no need for a single standard which governs interconnections between clusters of computers. Indeed, the only governing factors for development of new standards and protocols are market demand and acceptability by users, thus freeing the developers from the restricted regime of regulated research encountered in telecommunications.

This observation has important consequences when the size and the captive research process of telecommunication equipment manufacturers are considered. Virtually all of the telecommunication equipment (especially switching equipment) manufacturers are multi-billion dollar, multi-national organizations with

strong symbiotic links to telecommunication service providers and large research arms of their own. Such organizations are likely to be much less receptive towards research carried out outside their 'proprietary' reach than smaller size companies. This observation is supported by the experience gained during the prototype optoelectronic switch research project and its demonstration at the Telecom '95 exhibition.

In comparison, companies which develop communication and switching equipment for computer networks are generally smaller in size, and as pointed out earlier, engaged in developing a variety of standards at data rates of 1 Gbps and above. Research and development in the area of high performance computer networks is also free of 'legacy' signal support problems that requires all telecommunication equipment to be compatible with the equipment currently in place.

It is pertinent to point out that the data rates proposed in the standards under consideration for high bit rate computer networks are similar to those used in telecommunication networks. The most widely used SONET transmission equipment in continent wide data transport networks operates at the OC-48 (2.5 Gbps) data rate. Equipment at OC-192 (9.95 Gbps) rate is available though not expected to be in commercial use till end of 1996. In comparison, proposals such as HIPPI 6400 also call for data rates up to 6.4 Gbps in computer communication networks by end of 1996.

Therefore, the current and the next generation of computer networks will require broadband switching capabilities similar to those required in

telecommunication networks and computer communication networks potentially constitute a fast growing, high volume application area for broadband switching.

Optoelectronic switch properties, as demonstrated by the prototype implementation, are uniquely suited to providing a comprehensive solution for broadband computer networks. The complete signal format and bit rate transparency available in an optoelectronic switches implies that the same switch fabric may be used to implement broadband switching solutions for various data networks and standards, each of which may have unique signal formats or data rates.

The fact that signal transparency in optoelectronic switches is available with electrical signals at the input or output of the switch is relevant to this application as well. Broadband computer networks with data rates of the order of 1 Gbps may use low cost electrical interfaces and media for short distance transmission of data, which can be easily supported in the optoelectronic approach without compromising the transparency of the switching medium.

### **8.2.2 Optical switching and transparency issues**

Broadband switching techniques for optical signals that allow optical input and output signals without conversion to the electronic domain are generally called optical switches. Some of the technologies currently available commercially or under development were noted in Table 2.1 (section 2.3).

Optical switches provide signal transparency features as well though no single technology has yet found widespread commercial acceptance. As seen in Table 2.1, and as often mentioned in relevant literature [17, 39], optical switches

have no outstanding advantage over optoelectronic means of switching except for an all optical path through the switch. However, this 'advantage' needs to be examined closely.

Signal conversion, such as the one utilized in optoelectronic switching, does not violate the signal transparency often mentioned as the primary advantage of an optical switching element. In fact, sacrificing an optical path through the switch permits valuable other functions to be implemented [39]. These include electronic amplification if needed, access to signals for network monitoring purposes, and wavelength-conversion in WDM networks (see Figure 7.11).

Use of WDM technologies in conjunction with optoelectronic wavelength-conversion strategies has been shown to increase the capacity as well as the flexibility of a network as compared to an all optical network with optical switches [37, 39]. Optical means of wavelength conversion which use complex integrated devices employing cross-gain compression in semiconductor optical amplifiers have been reported [144]. However, these devices suffer from a variety of limitations such as low conversion efficiency, modulation bandwidth, and low extinction ratio [145].

Complete signal format transparency coupled with the excellent contrast and crosstalk immunity realized with the optoelectronic switching technology make it an attractive candidate for a variety of broadband switching applications.

Following the signal transparency demonstrated in this work, a *virtual-transparent-path* based network layer may be envisioned. A manuscript proposing



the use of optoelectronic switches with transparency in photonic connectivity layer of a multi-wavelength network is given in Appendix H.

### **8.2.3 Conclusion**

Photonic communication techniques have increased the information transmission bandwidths to unprecedented levels, exceeding a terabit on single fibres [146]. However, electronic signals dominate the control, interface, and access sections of communication networks. Optoelectronics bridges the two domains, by necessity *and* by choice, to provide a unique class of phenomenon which are not realizable in either photonic or electronic domain. This work implemented a broadband switching and signal processing structure which utilizes optoelectronic mechanisms for routing and filtering signals of diverse formats. A new approach to design of broadband photodetector arrays was also formulated. Application of optoelectronic switches to network restoration was introduced, and shown to be competitive with other options. Format transparency of optoelectronic switching was confirmed and its potential benefit to broadband switching networks was highlighted. Spectrally efficient modulation for short distance photonic interconnects was proposed and demonstrated to increase the data throughput in the prototype switch.

## Bibliography

- [1] R.I. MacDonald, E.H. Hara, "Optoelectronic broadband switching array", *Electronics Letters*, vol. 16, pp. 502-503, 1978.
- [2] R.I. MacDonald, "Optoelectronic switching", *IEEE Communications Magazine*, vol. 25, pp. 33-36, May 1987.
- [3] M.C. Veilleux, "Construction of a broadband 10x10 optoelectronic switching matrix", *M.Sc. Thesis*, University of Alberta, Fall 1990.
- [4] D. Lam, "Reflex optoelectronic signal processor", *M.Sc. Thesis*, University of Alberta, Spring 1994.
- [5] S.R. Forrest, G.L. Tangonan, V. Jones, "A simple 8x8 optoelectronic crossbar switch", *IEEE Journal of Lightwave Technology*, vol. 7, no. 4, pp. 607-614, April 1989.
- [6] M.Veilleux, R.I. MacDonald, "An optoelectronic switching matrix with high isolation", *IEEE Journal of Lightwave Technology*, vol. 10, no. 7, pp. 988-991, July 1992.
- [7] R. Sharma, R.I. MacDonald, D. Lam, D. Clegg, R. Tholl, L. Zmeko, "Broadband optoelectronic switch for digital and analog signals", *Proceedings of SPIE Conference on Optical Interconnects in Broadband Architectures, Photonics West '96*, vol. 2692, San Jose, California, pp. 190-193, January 31 - February 1, 1996.
- [8] E. Munter, J. Parker, "High capacity ATM switch: architecture and technologies", *Proceedings of SPIE Conference on Optical Interconnects in Broadband Switching Architectures - Photonics '96*, vol. 2692, San Jose, California, pp. 178-189, January 31 - February 1, 1996.

- [9] N. Vethanayagam, "Demonstration of a novel code division multiple access system at 800 Mchips/s", *M.Sc. Thesis*, University of Alberta, Spring 1991.
- [10] B. Swekla, "An optoelectronic transversal filter", *M.Sc. Thesis*, University of Alberta, Fall 1992.
- [11] S.B. Kumar, "Polymer waveguides with taps in silicon v-grooves", *M.Sc. Thesis*, University of Alberta, Summer 1992.
- [12] R. Narendra, "Phosphorus doped glass waveguides on silicon substrates", *M.Sc. Thesis*, University of Alberta, Fall 1992.
- [13] M.Y. Fei, "Micromachined centre taps for silicon v-groove waveguides", *M.Sc. Thesis*, University of Alberta, Spring 1993.
- [14] K.J. MacLeod, "Micromachined serial taps in silicon v-groove waveguides", *M.Sc. Thesis*, University of Alberta, Fall 1995.
- [15] B.P. Keyworth, J.N. McMullin, R. Narendra, R.I. MacDonald, "Computer-controlled pressure-dispensed multimode polymer waveguides", *IEEE Transactions on Components, Packaging, and Manufacturing Technology*, Part B, vol. 18, no. 3, pp. 572-577, August 1995.
- [16] E. Munter, J. Parker, P. Kirby, "A high capacity ATM switch based on advanced electronic and optical technologies", *IEEE Communications Magazine*, pp. 64-71, November 1995.
- [17] F. Derr, M. N. Huber, G. Kettler, N. Thorweihe, "An optical infrastructure for future telecommunications networks", *IEEE Communications Magazine*, pp. 84-88, November 1995.
- [18] H. Matsunga, H. Uematsu, "A 1.5 Gb/s 8x8 cross-connect switch using a time reservation algorithm," *IEEE Journal on Selected Areas in*

*Communications*, vol. 9, no. 8, pp. 1308-1317, October 1991.

- [19] W.D. Grover, "The selfhealing network: a fast distributed restoration technique for networks using digital cross-connect machines", *Proceedings of IEEE Globecom '87*, pp. 1090-1095, 1987.
- [20] B.D. Venables, "Algorithms for spare capacity design of mesh restorable networks", *M.Sc. Thesis*, University of Alberta, Fall 1992.
- [21] R.R. Iraschko, "Optimized path restoration algorithms", *Ph.D. Thesis*, University of Alberta.
- [22] F.E. Ross, "An overview of FDDI: the fibre distributed data interface", *IEEE Journal on Selected Areas in Communications*, vol. 7, no. 7, pp. 1043-1051, September 1989.
- [23] "GigaRing Channel", Product Literature, <http://www.cray.com/PUBLIC/product-info/T3E/gigaring.html>, 1-800-BUY-CRAY, 1996.
- [24] "High performance parallel interface: X3T9.3 Specifications", *HIPPI Networking Forum*, 305 East Drive, Suite A, Melbourne, FL 32904, 1-800-97-HIPPI.
- [25] "High performance parallel interface - 6400 Mbit/s physical layer", *X3T11 Technical Committee of Accredited Standards Committee X3*, Los Alamos National Laboratory, CIC-5, MS-B255, Los Alamos, NM 87545, USA.
- [26] <http://www.cic-5.lanl.gov/land/project/hippi64.html>
- [27] <http://www.nas.nasa.gov/NAS/Groups/netops/FutureTech/hsnet/>
- [28] "Fibre Channel Standard", ANSI X3.230-1994, American National Standards Institute.

- [29] "Scalable Coherent Interface: SCI", *IEEE standard 1596-1992*.
- [30] N.J. Boden, D. Cohen, R.E. Felderman, A.E. Kulawik, C.L. Seitz, J.N. Seizovic, W. Su, "Myrinet - a gigabit-per-second local-area network", *IEEE Micro Magazine*, vol. 15, no. 1, pp. 29-36, February 1995.
- [31] GigaNet Inc., Product Literature, <http://www.tiac.net/users/giganet/index.html>, Suite 220b, 118 Great Rd., Stow, MA 01775, USA.
- [32] "ATM White Papers", *The ATM Forum*, <http://www.atmforum.com/>, World Headquarters, 2570 West El Camino Real, suite 304, Mountain View, CA 94040-1313.
- [33] Gigabit Logic Data Book, 1995.
- [34] J. Parker, "Optical interconnects and packaging: current trends and future perspectives", *Proceedings of SPIE Conference on Optoelectronic Interconnects and Packaging, Photonics West '96*, vol. CR62, San Jose, California, January 30 - 31, 1996.
- [35] R. Sharma, R.I. MacDonald "A signal-transparent, distributed optical interconnect based optoelectronic switch", *Proceedings of International Conference on Applications of Photonics Technology - ICAPT '96*, July 29 - August 2, 1996, Montreal, Quebec.
- [36] R.I. MacDonald, "Terminology of photonic switch matrices", *IEEE Journal on Selected Areas in Communications*, vol. 6, no. 7, pp. 1141-1151, August 1988.
- [37] D. Blumenthal, L. Thylen, "Coherent crosstalk induced BER floors in NxN space photonic switches", *Proceedings of IEEE/LEOS Topical Meeting on Optical Networks and Their Enabling Technologies*, Lake Tahoe, Nevada, 1994.

- [38] G. Hill, "A transport layer based on optical network elements", *IEEE Journal of Lightwave Technology*, vol. 11, no. 5, pp. 667-669, 1993.
- [39] L. Thylen, G. Karlsson, O. Nilsson, "Switching technologies for future guided wave optical networks: potentials and limitations of photonics and electronics", *IEEE Communications Magazine*, pp. 106-113, February 1996.
- [40] Lithium Niobate Products, AT&T Lightwave Product Catalog, United Technologies Photonics (UTP) Product Catalog, 1995.
- [41] R.F. Kalman, L.G. Kazovsky, J.W. Goodman, "Space division switches based on semiconductor optical amplifiers", *IEEE Photonics Technology Letters*, vol. 4, pp. 1048-1051, September 1992.
- [42] E. Almstrom, C.P. Larsen, L. Gillner, W.H. van Berlo, M. Gustavsson, E. Berglind, "Experimental and analytical evaluation of packaged 4x4 InGaAs/InP semiconductor optical amplifier gate switch matrices for optical networks", *IEEE Journal of Lightwave Technology*, vol. 14, no. 6, pp. 996-1004, June 1996.
- [43] Programmable 1xN Optical Fibre Switches - SV, SB, SC Series, JDS Fitel Inc., Nepean, Ontario.
- [44] R.S. Lytel, F. Lipscomb, "Packaging and applications of active polymer optical switching arrays", *Proceedings of SPIE Conference on Optoelectronic Interconnects and Packaging - Photonics '96*, vol. CR62, San Jose, California, January 30-31, 1996.
- [45] C.F. Janz, B.P. Keyworth, W. Allegretto, R.I. MacDonald, M. Fallahi, G. Hillier, C. Rolland, "Mach-Zehnder switch using an ultra-compact directional coupler in a strongly confining rib-structure", *IEEE Photonics Technology Letters*, vol. 6, no. 8, pp. 981-983, August 1994.

- [46] J.C. Chon, A.K. Jen, E. Binkley, "High thermal stability EO polymer waveguide devices", *Proceedings of SPIE Conference on Optoelectronic Interconnects and Packaging - Photonics '96*, vol. CR62, San Jose, California, January 30-31, 1996.
- [47] A. Himeno, "Recent progress on silica based optical switches and free space optical switches", Invited paper, *Proceedings of SPIE Conference on Optical Interconnects in Broadband Switching Architectures - Photonics '96*, vol. 2692, San Jose, California, pp. 72-83, January 31-February 1, 1996.
- [48] J.E. Midwinter, Ed., "Photonic Switching, Volume 1: Background and Components", Academic Press, pp. 169-193, 1993.
- [49] C. Tai, W.I. Way, "Dynamic range and switching speed limitations of an N x N optical packet switch based on low-gain semiconductor optical amplifiers", *IEEE Journal of Lightwave Technology*, vol. 14, no. 4, pp. 525-533, April 1996.
- [50] B.P. Keyworth, "Optical and optoelectronic switching: approaches and limitations", Invited Presentation, EdTel and Telecommunications Research Laboratories, Edmonton, April 1996.
- [51] A.L. Lentine, D.J. Reiley, R.A. Novotny, R.L. Morrison, J.M. Sasian, M.G. Beckman, D.B. Buchholz, S.J. Hinterlong, T.J. Cloonan, G.W. Richards, F.B. McCormick, "Optoelectronic ATM switch employing hybrid silicon CMOS/GaAs FET-SEEDs", *Proceedings of SPIE Conference on Optical Interconnects in Broadband Switching Architectures - Photonics '96*, vol. 2692, San Jose, California, pp. 100-108, January 31 - February 1, 1996.
- [52] T.J. Cloonan, G.W. Richards, A.L. Lentine, "Optical implementation of a parallel out-of-band controller for large broadband ATM switch

- applications”, *Proceedings of SPIE Conference on Optical Interconnects in Broadband Switching Architectures - Photonics '96*, vol. 2692, San Jose, California, pp. 73-85, January 31 - February 1, 1996.
- [53] R.I. MacDonald “Switched optical delay line signal processors”, *IEEE Journal of Lightwave Technology*, vol. LT-5, pp. 856-861, 1987.
- [54] R.R. Bitmead, C.R. Johnson, C.R. Pollock, “Optical adaptive signal processing: an appraisal”, *International Journal of Adaptive Control and Signal Processing*, vol. 5, no. 2, pp. 87-92, March-April 1991.
- [55] Y. Koshiha, J. Ohta, S. Tai, T. Toyoda, K. Kyuma, “Active matrix addressing operation of a dynamic optical neurochip with monolithically integrated InGaAs/GaAs MSM-FETs”, *IEEE Photonics Technology Letters*, vol. 4, no. 6, pp. 617-620, June 1992.
- [56] N.H. Farhat, “Architectures for optoelectronic analogs of self-organizing neural networks”, *Optics Letters*, vol. 12, no. 6, pp. 448-450, June 1987.
- [57] J. Ohta, Y. Nitta, K. Kyuma, “Dynamic optical neurochip using variable sensitivity photodiodes”, *Optics Letters*, vol. 16, no. 10, pp. 744-746, May 15, 1991.
- [58] A. Von Lehmen, E.G. Paek, L.C. Carrion, J.S. Patel, A. Marrakchi, “Optoelectronic chip implementation of a quadratic associative memory”, *Optics Letters*, vol. 15, no. 5, pp. 279-281, March 1, 1990.
- [59] J. Jang, S. Jung, S. Lee, S. Shin, “Optical implementation of the Hopfield model for two-dimensional associative memory”, *Optics Letters*, vol. 13, no. 3, pp. 248-250, March 1988.
- [60] N.M. Barnes, P. Healey, P. McKee, A.W. O'Neill, M.A.Z. Rejman-Greene, E.G. Scott, R.P. Webb, D. Wood, “High-speed optoelectronic neural



- network", *Electronic Letters*, vol. 26, no. 15, pp. 1110-1112, July 19, 1990.
- [61] J.J. Hopfield, "Neural networks and physical systems with emergent collective computational abilities", *Proceedings of National Academy of Science*, USA, vol. 79, pp. 2554-2558, April 1982.
- [62] D.W. Tank, J.J. Hopfield, "Simple "neural" optimization networks: an A/D converter, signal decision circuit, and a linear programming circuit", *IEEE Transactions on Circuits and Systems*, vol. 33, no. 5, pp. 533-541, May 1986.
- [63] TRILabs Optoelectronic Matrix Processor, *User Manual and Design Documents*, contact: Director, Photonics Division, TRILabs, Edmonton.
- [64] Rogers Corporation, "Selector Guide for Microwave Laminates", 1993.
- [65] Mitsubishi Optical Semiconductors Data Book, 1989.
- [66] Microwave Laser QLM3S900, *Lasertron*, 37 North Avenue, Burlington, MA 01803.
- [67] Low Noise Amplifiers, *Miteq*, 100 Davids Drive, Hauppauge, NY 11788.
- [68] TGA 8549-SCC, dc-14 GHz amplifier, *Texas Instruments*.
- [69] W.B. Jones, Jr., "Introduction to Optical Fiber Communications", Holt, Rinehart, and Winston Inc., 1988.
- [70] Y. Chen, S. Williamson, T. Brock, F.W. Smith, A.R. Calawa, "375 GHz bandwidth photoconductive detector", *Applied Physics Letters*, vol. 59, no. 16, pp. 1984-1986, October 1991.
- [71] S.M. Sze, D.J. Coleman, A. Loya, "Current transport in metal-semiconductor-metal (MSM) structures", *Solid State Electronics*, vol. 14,

pp.1209-1218, Pergamon Press, 1971.

- [72] J.B.D. Soole, H. Schumacher, "InGaAs metal-semiconductor-metal photodetectors for long wavelength optical communications", *IEEE Journal of Quantum Electronics*, vol. 27, no. 3, pp. 737-752, March 1991.
- [73] W.C. Koscielniak, J.L. Pelouard, M.A. Littlejohn, "Intrinsic and extrinsic response of GaAs metal-semiconductor-metal photodetectors", *IEEE Photonics Technology Letters*, vol. 2, no. 2, pp.125-127, February 1990.
- [74] J. Rosenzweig, C. Moglestue, A. Axmann, J. Schneider, A. Hulsmann, "Characterization of picosecond GaAs metal-semiconductor-metal photodetectors", *SPIE: Physical Concepts of Materials for Novel Optoelectronic Device Applications II: Device Physics and Applications*, vol. 1362, pp. 168-178, 1990.
- [75] R. G. DeCorby, "Frequency response characterization of GaAs MSM photodetector arrays: test facility and experimental results", *M.Sc. Thesis*, University of Saskatchewan, Saskatoon, Saskatchewan, August 1994.
- [76] F.W. Grover, "Inductance Calculations", Originally published by D. Van Nostrand Company Inc., 1946, *reprinted for Instrument Society of America by permission of Dover Publications*, New York. 1973.
- [77] N. Ohkawa, "Fibre optic multi-gigabit GaAs MIC front end circuit with inductor peaking", *IEEE Journal of Lightwave Technology*, vol. 6, no. 11, pp. 1665-1671, November 1988.
- [78] R. Sharma, R.B. Tholl, R. DeCorby, D.D. Clegg, "Frequency response characteristics of GaAs MSM photodetector arrays", *TRLabs Technical Report*, No. TR-94-03, April 1994.
- [79] Hewlett Packard Microwave and RF Design System, HP 85150B.

- [80] E. Sano, "A device model for MSM detectors and its application to OEIC simulations", *IEEE Transactions on Electron Devices*, vol. 37, no. 9, pp. 1964, September 1990.
- [81] E.H. Bottcher, D. Kuhl, F. Hieronymi, E. Droge, T. Wolf, D. Bimberg, "Ultrafast semi-insulating InP:Fe-InGaAs:Fe-Inp:Fe MSM photodetectors: modelling and performance", *IEEE Journal of Quantum Electronics*, vol. 28, no. 10, pp. 2343-2357, October 1992.
- [82] J. Burm, K.I. Litvin, W.J. Schaff, L.F. Eastman, "Optimization of high-speed metal-semiconductor-metal photodetectors", *IEEE Photonics Technology Letters*, vol. 6, no. 6, pp. 722-724, June 1994.
- [83] D. Kuhl, F. Hieronymi, E.H. Bottcher, T. Wolf, D. Bimberg, J. Kuhl, M. Klingenstein, "Influence of space charges on the impulse response of InGaAs metal-semiconductor-metal photodetectors", *IEEE Journal of Lightwave Technology*, vol. 10, no. 6, pp. 753-759, June 1992.
- [84] D.L. Rogers, "Integrated optical receivers using MSM detectors", *IEEE Journal of Lightwave Technology*, vol. 9, no. 12, pp. 1635-1638, December 1991.
- [85] E.J. Wilkinson, "An n-way hybrid power divider", *IRE Transactions on Microwave Theory and Techniques*, vol. 8, pp. 116-118, January 1960.
- [86] Z. Galani, S.J. Temple, "A broadband n-way combiner/divider", *IEEE Microwave Theory and Techniques Symposium Digest*, (IEEE Catalog no. 77CH1219-5MTT), pp. 499-502, June 1977.
- [87] D.M. Pozar, "Microwave Engineering", Addison-Wesley Company, N.Y., 1990.
- [88] A.A.M. Saleh, "Planar electrically symmetric n-way hybrid power dividers/

combiners", *IEEE Transactions on Microwave Theory and Techniques*, vol. 28, no. 6, pp. 555-563, June 1980.

- [89] B.P. Keyworth, R. Narendra, J.N. McMullin, R.I. MacDonald, "Direct dispensing of polymer waveguides on silicon substrates", *Proceedings of LEOS 1993 Summer Topical Meeting Digest on Optical Microwave Interactions*, T1.3, Santa Barbara, California, pp. 41-42, July 1993.
- [90] R. Nagarajan, J.N. McMullin, B.P. Keyworth, R.I. MacDonald, "3x3 Optoelectronic switch using diffractive optics", *Technical Digest: Optical Society of America Annual Meeting*, MJJ-5, pp. 61, September 1995.
- [91] B.P. Keyworth, D.J. Corazza, R.I. MacDonald, "Beam extractor card for free-space optical backplanes", *Proceedings of SPIE Conference on Optical Interconnects in Broadband Switching Architectures - Photonics '96*, vol. 2692, San Jose, California, pp.109-113, January 31-February 1, 1996.
- [92] N. Rajkumar, J.N. McMullin, B.P. Keyworth, R.I. MacDonald, "3x3 Optoelectronic cross-bar switch using vertical cavity surface emitting laser arrays", *Optical Society of America Technical Digest Series*, vol. 5, pp. 75-78, April-May 1996.
- [93] "Integrated Tunable Receiver (TOR-1)", *Preliminary Specification Sheet*, Advanced Optical Networking Group, IBM T.J. Watson Research Center, 30 Saw Mill River Road, Hawthorne, NY 10532.
- [94] Private communication from Chung-Sheng Li, Advanced Optical Networking Group, IBM T.J. Watson Research Center, 30 Saw Mill River Road, Hawthorne, NY 10532.
- [95] B.S. Kawasaki, K.O. Hill, Y. Tremblay, "Modal noise generation in biconical-taper couplers", *Optics Letters*, vol. 6, no. 10, pp. 499-501, October 1981.

- [96] National Cable Television Association, "NCTA recommended practices for measurements on cable television systems", November 1989.
- [97] T.E. Darcie, G.E. Bodeep, "Lightwave subcarrier CATV transmission systems", *IEEE Transactions on Microwave Theory and Techniques*, vol. 38, no. 5, pp. 524-533, May 1990.
- [98] C.J. Chung, I. Jacobs, "Practical TV channel capacity of lightwave multichannel AM SCM systems limited by the threshold nonlinearity of laser diodes", *IEEE Journal of Lightwave Technology*, vol. 4, no. 3, pp. 289-292, March 1992.
- [99] R. Citta, R. Lee, "Practical implementation of a 43 Mbit/sec (8 bits/Hz) digital modem for cable television", *1993 NCTA Technical Papers*, pp. 271-279, 1993.
- [100] P. Crespo, A.F. Elrefaie, T.R. Hsing, "Transmission of four level signals using LED and single mode fibers for local loop applications", *Proceedings of International Conference on Communications (ICC '88)*, pp. 593-598, 1988.
- [101] J.H. Winters, R.D. Gitlin, "Electrical signal processing techniques in long-haul fibre-optics systems", *IEEE Transactions on Communications*, vol 38, no. 9, pp. 1439-1453, September 1990.
- [102] S. Walklin, J. Conradi, "Multilevel signalling for extending the dispersion limited transmission distance in high speed fiber optic communication systems", *Proceedings of the 1996 Canadian Conference on Electrical and Computer Engineering (CCECE)*, vol. I, session 11.5, pp. 233-236, Calgary, Alberta, May 26-29, 1996.
- [103] B. Wedding, W. Pohlmann, B. Franz, H. Geupe, "Multi-level dispersion supported transmission at 20 Gbit/s over 46 km installed standard single

mode fibre”, paper no. MoB.4.4, to be presented at *22nd European Conference on Optical Communication*, Oslo, Norway, September 15-19, 1996.

- [104] J.G. Proakis, “Digital Communications”, 2nd edition, McGraw-Hill Inc., 1989.
- [105] D.M. Gookin, M.H. Berry, “Finite impulse response filter with large dynamic range and high sampling rate”, *Applied Optics*, vol. 29, pp. 1061-1062, March 1990.
- [106] B. Swekla, R.I. MacDonald, “Optoelectronic transversal filter”, *Electronic Letters*, vol. 27, no. 19, pp. 1769-1770, September 12, 1991.
- [107] R.I. MacDonald, “Optoelectronic filter with variable gain bi-polar taps”, *US Patent No. 5,376,786*, December 1994.
- [108] R.I. MacDonald, S. Lee, “Photodetector sensitivity control for weight setting in optoelectronic neural networks”, *Applied Optics*, vol. 30, pp. 176-178, 1991.
- [109] Y. Nitta, J. Ohta, S. Tai, K. Kyuma, “Variable-sensitivity photodetector that uses a metal-semiconductor-metal structure for optical neural networks”, *Optics Letters*, vol. 16, pp. 611-613, 1991.
- [110] D.K.W. Lam, B.A. Syrett, “Gigahertz signal processing using reflex optoelectronic switching matrices”, *IEEE Journal of Lightwave Technology*, vol. LT-5, no. 3, pp. 398-402, March 1987.
- [111] B. Moslehi, J.W. Goodman, M. Tur, H. J. Shaw, “Fiber-optic lattice signal processing”, Invited Paper, *Proceedings of the IEEE*, vol. 72, no. 7, pp. 909-930, July 1984.

- [112] C.R. Johnson, "Adaptive IIR filtering: current results and open issues", *IEEE Transactions on Information Theory*, vol. IT-30, no. 2, pp. 237-250, March 1984.
- [113] S. Haykin, "Adaptive Filter Theory", Prentice Hall Inc. 1986, 1991.
- [114] C.F.N. Cowan, P.M. Grant, Editors, "Adaptive Filters", Prentice Hall Inc., 1985.
- [115] B. Widrow, S.D. Stearns, "Adaptive Signal Processing", Prentice Hall Inc., 1985.
- [116] E. Perrenoud, "Broadband optoelectronic signal processing", Project report, TRILabs, May-August 1995.
- [117] R.J.S. Bates, "Equalization and mode partition noise in all-plastic optical fiber data links", *IEEE Photonics Technology Letters*, vol. 4, no. 10, pp. 1154-1157, October 1992.
- [118] M.J. Hackert, S.M. Sibley, P. Sendelbach, "Performance of telecommunications grade multimode fiber at 780 nm", *IEEE Journal of Lightwave Technology*, vol. 10, no. 6, pp. 712-719, June 1992 .
- [119] S.U.H. Qureshi, "Adaptive equalization", *Proceedings of the IEEE*, vol. 73, no. 9, pp. 1349-1387, September 1985.
- [120] R.I. MacDonald, "Optoelectronic equalization", *IEEE Phtotonics Technology Letters*, vol. 6, no. 4, pp. 565-567, April 1994.
- [121] "Hinsdale Center Office Fire Final Report: Executive Summary", prepared by Forensic Technologies International Corporation, Annapolis, Maryland, March 1989.
- [122] W.D. Grover, "Selfhealing networks: a distributed algorithm for k-shortest

link-disjoint paths in a multi-graph with applications in real time network restoration", *Ph.D. Thesis*, University of Alberta, Fall 1989.

- [123] T.H. Wu, D.J. Kolar, R.H. Cardwell, "Survivable network architectures for broadband fibre optic networks: model and performance comparisons", *IEEE Journal of Lightwave Technology*, vol. 6, no. 11, pp. 1698-1709, November 1988.
- [124] T.H. Wu, D.J. Kolar, R.H. Cardwell, "High speed self-healing ring architectures for future interoffice networks", *Proceedings of IEEE Globecom '89*, pp. 23.1.1-23.1.7, November 1989.
- [125] T.H.Wu, R.C. Lau, "A class of self-healing ring architectures for SONET network applications", *Proceedings of IEEE Globecom '90*, San Diego, California, pp. 403.2.1-403.2.8, December 1990.
- [126] T.H. Wu, "A passive protected self-healing mesh network architecture and applications", *IEEE/ACM Transactions on Networking*, vol. 2, no. 1, pp. 40-52, February 1994.
- [127] Bellcore Document "Digital Cross-Connect Systems", Technical Report TR-NWT-000233.
- [128] Bellcore Document "Digital Cross-Connect Systems in Transport Network Survivability", Special report SR-NWT-002514, Issue 1, January 1993.
- [129] H. Obara, M. Sasagawa, I. Tokizawa, "An ATM cross-connect system for broadband transport networks based on virtual path concept", *Proceedings of Globecom '90* (IEEE Catalog no. CH2829-0/90/0000-0839), pp. 839-843, 1990.
- [130] K.I. Sato, S. Ohta, I. Tokizawa, "Broadband ATM network architecture based on virtual paths", *IEEE Transactions on Communications*, vol. 38,



no. 8, pp. 1212-1222, August 1990.

- [131] T.H. Wu, "Fiber Network Service Survivability", Artech House, 1992.
- [132] W.D. Grover, B.D. Venables, M.H. MacGregor, J.H. Sandham, "Development and performance assessment of a distributed asynchronous protocol for real-time network restoration", *IEEE Journal on Selected Areas in Communications*, vol. 9, no. 1, pp.112-125, January 1991.
- [133] R.R. Iraschko, M.H. MacGregor, W.D. Grover, "Optimal capacity placement for path restoration in mesh survivable networks", *IEEE International Conference on Communications (ICC) '96*, Dallas, Texas, vol. 3, pp. 1513-1517, June 23-27 1996.
- [134] W.D. Grover, "Distributed restoration of the transport network", Book Chapter in "Telecommunications Network Management into the 21st Century: Techniques, Standards, Technologies, and Applications", Edited by S. Aidarous and T. Plevyak, IEEE Press, 1994.
- [135] R.D. Doverspike, "Algorithms for multiplex bundling in a telecommunications network", *Operations Research*, vol. 39, no. 6, November-December 1991.
- [136] M. Bonatti, S.S. Katz, C.F. Newman, G.C. Varvaloucas (Guest Editors), "Special Issue on Telecommunications Networks Design and Planning", *IEEE Journal on Selected Areas in Communications*, vol. SAC-7, no. 8, October 1989.
- [137] Siliconix Analog Crosspoint Switch - DG884.
- [138] C.H. Yang, S. Hasegawa, "FITNESS: A failure immunization technology for network service survivability", *Proceedings of IEEE Globecom '88*, pp. 1549-1554, Ft Lauderdale, FL, 1988.

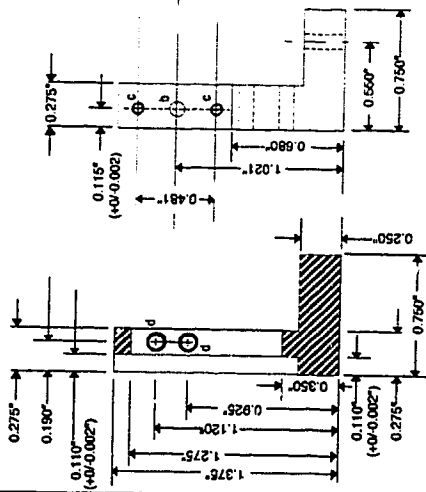
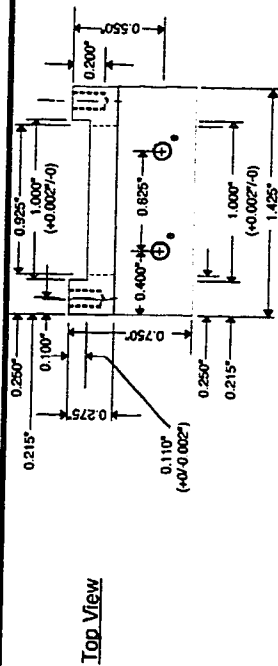
- [139] R.S. Vodhanel, F. Shehadeh, J-C. Chiao, G-K. Chang, C. Gibbons, T. Suzuki, "Performance of an 8-wavelength 8-node WDM ring network experiment with 80 Gb/s capacity", Post-deadline paper PD28, *Proceedings of Optical Fibre Communication Conference (OFC '96)*, San Jose, California, February 25-February 29 1996.
- [140] 4-Channel Narrow Band WDM Mux/Demux Filters, WD5555A M/D, JDS Fitel Inc., Nepean, Ontario.
- [141] J. Gamelin, M. Goodman, J. Jackel, B. Pathak, G-K. Chang, W.J. Tomlinson, R. Cordell, C.E. Zah, T.P. Lee, C. Brackett, C. Dreze, D. Pollex, J. Sitch, H. Willemsen, K. Pedrotti, K.C. Wang, R. Walden, W. Stanchina, D. Fritz, R. Ade, R. Hobbs, R. Haigh, K. McCammon, W. Lennon, " 8-Channel reconfigurable WDM networking demonstration with wavelength translation and electronic multicasting at 2.5 Gbit/s", Post-deadline paper PD29, *Proceedings of Optical Fibre Communication Conference (OFC '96)*, San Jose, California, February 25-February 29 1996.
- [142] Fitel Ribbon Forming Fixture S-612, Distributed by JDS-Fitel Inc., Nepean, Ontario.
- [143] M.R. Paiam, R.I. MacDonald, "Design of phased-array wavelength division multiplexers using multimode interference couplers", submitted to *Applied Optics*, August 1996.
- [144] T. Durhuus, B. Mikkelsen, C. Joergensen, S.L. Danielsen, K.E. Stubkjaer, "All optical wavelength conversion by semiconductor optical amplifiers", *IEEE Journal of Lightwave Technology*, vol. 14, no. 6, pp. 942-954, June 1996.
- [145] R.C. Alferness, "Semiconductor components for WDM systems and networks", Invited Paper, *Proceedings of Optical Fibre Communication*

*Conference (OFC '96), San Jose, California, February 25-February 29 1996.*

- [146] A.H. Gnauck, A.R. Charplyvy, R.W. Tach, J.L. Zyskind, J.W. Sulhoff, A.J. Lucero, Y. Sun, R.M. Jopson, F. Forghieri, R.M. Derosier, C. Wolf, A.R. McCormick, "One Terabit/s transmission experiment", Post-deadline paper PD20, *Proceedings of Optical Fibre Communication Conference (OFC '96), San Jose, California, February 25-February 29 1996.*

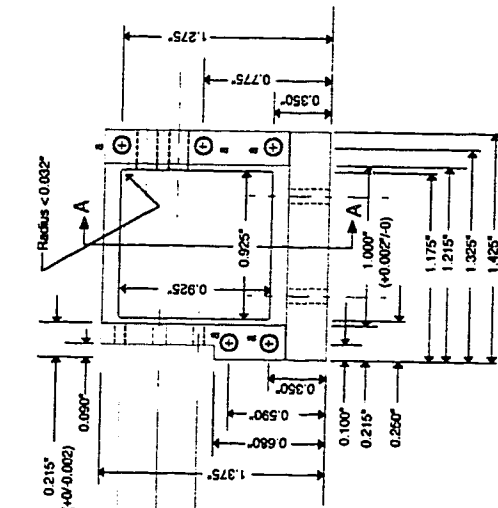
## **Appendix A**

The mechanical design drawings for optoelectronic receiver module (Chapter 3), are included here. Design drawings for the substrate used in the module follow the mechanical drawings .



**Section A-A**      **Side View 1**

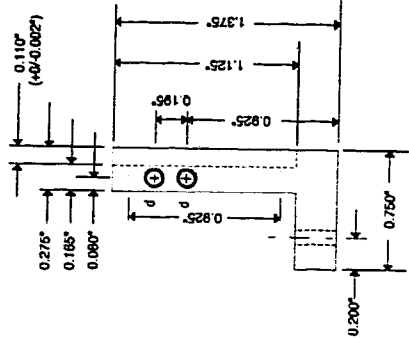
- Holes:**
- a) Drill # 50 (0.070" dia.) 0.200" deep, Tap 2-56, 5 places
  - b) Drill Thru # 44 (0.086" dia.), 1 place
  - c) Drill # 50 (0.070" dia.), 0.125" deep, Tap 2-56, 2 places
  - d) Drill Thru # 33 (0.113" dia.), Tap 6-40, 2 places
  - e) Drill Thru # 43 (0.089" dia.), Tap 4-40, 2 places



**Front View**

**Material:**  
Aluminium

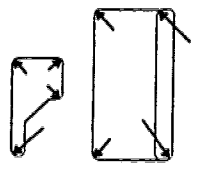
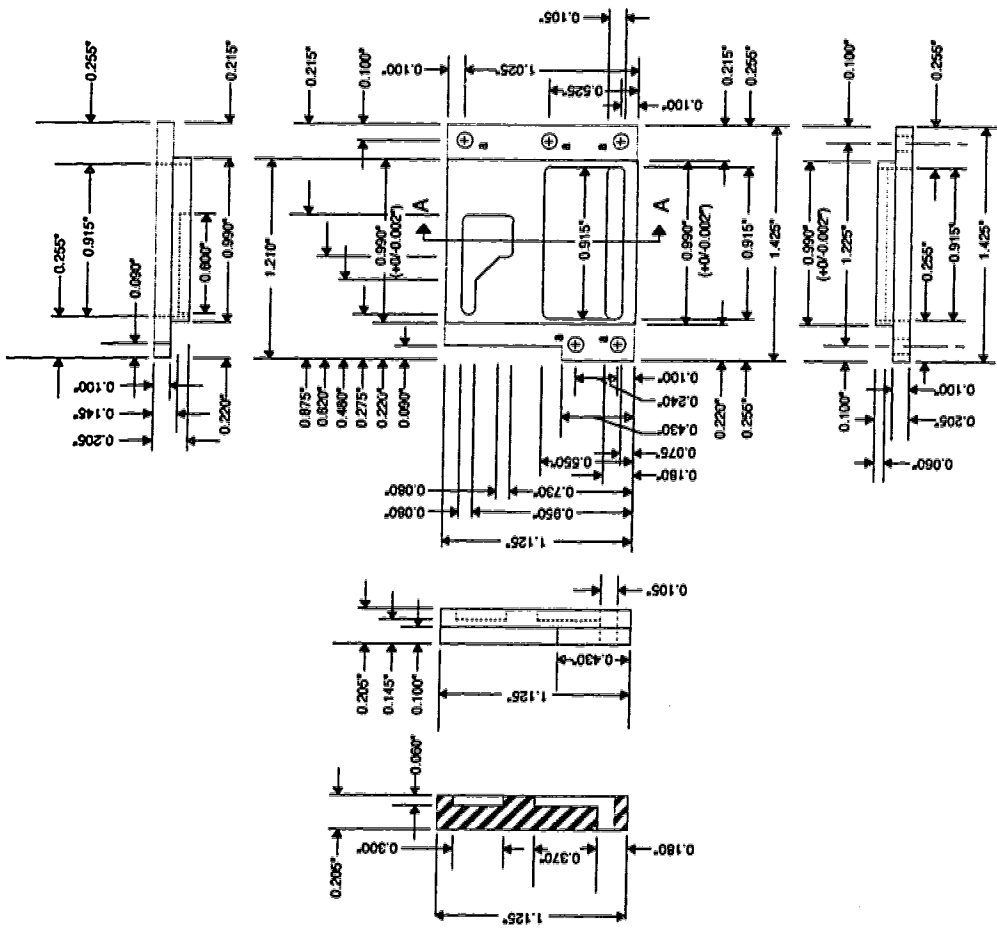
**Tolerances:**  
X.XXX = +/- 0.004" unless indicated otherwise



**Side View 2**

<b>Drawn By:-</b> Rohit Sharma	<b>Title:</b> OESM Detector Array Assembly	
	<b>Dwg. No:</b> RS_OESM_01_A	<b>Rev:</b> C <b>Date:</b> January 25, 1994

File: SHARMAPrecimax-BackPlate



All Radii 0.040"

Holes:  
a) Drill Thru # 43, (0.086" dia.), 5 places

Material:  
Aluminium

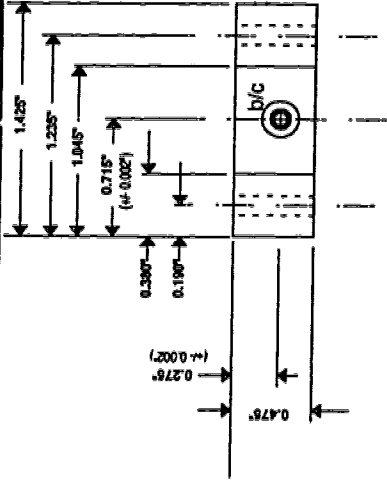
Tolerances:  
X.XXX= +/-0.004" unless otherwise indicated

<b>Drawn By:-</b> Rohit Sharma	<b>Title:</b> MSM Detector Array Assembly - Back Plate
	<b>Dwg. No:</b> imm_back_plate
<b>Rev:</b> D <b>Date:</b> April 25, 1994	

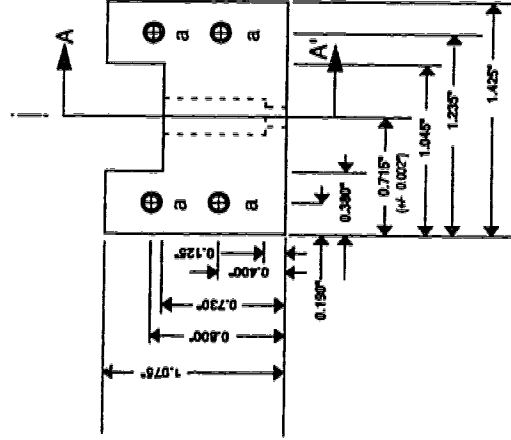
Material:  
ALUMINIUM

Holes:

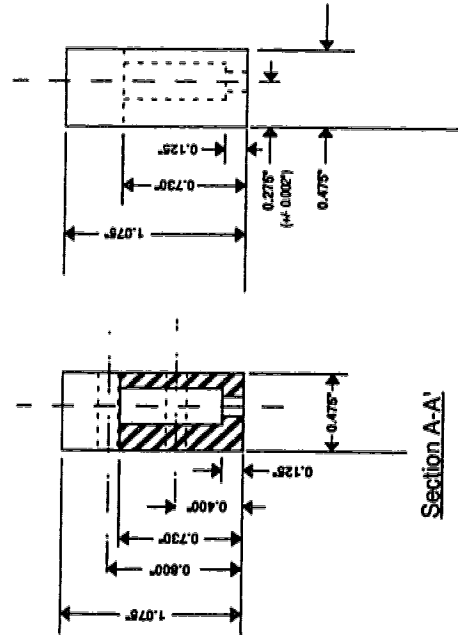
- a) Drill Thru # 43 (0.089" dia)  
and Tap 4-40, 4 places
- b) Bore # 2 (0.2210" dia) to 0.125" (from bottom reference line)  
1 place
- c) Drill Thru # 32 (0.1160" dia)  
1 place



center line



Section A-A'

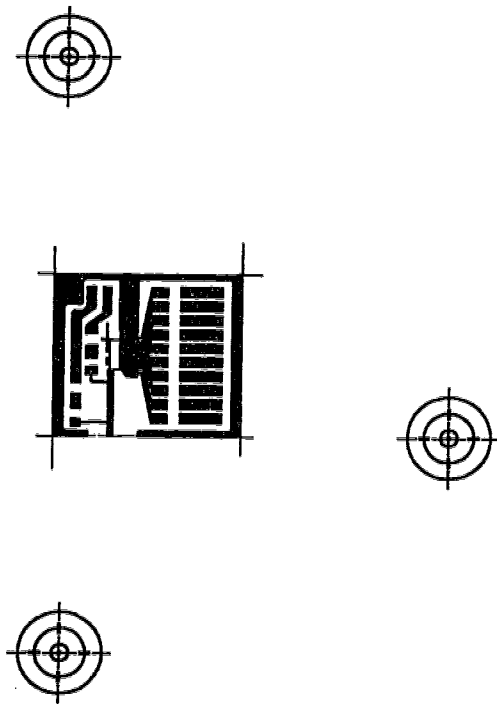


Tolerances:  
X.XXX = 0.004 unless indicated otherwise

Title: COVER PLATE ASSEMBLY - Main Plate	
Dwg. No: RS OESM CP-1	Rev: B Date: FEB 14, 1995

Drawn By:- Rohit Sharma

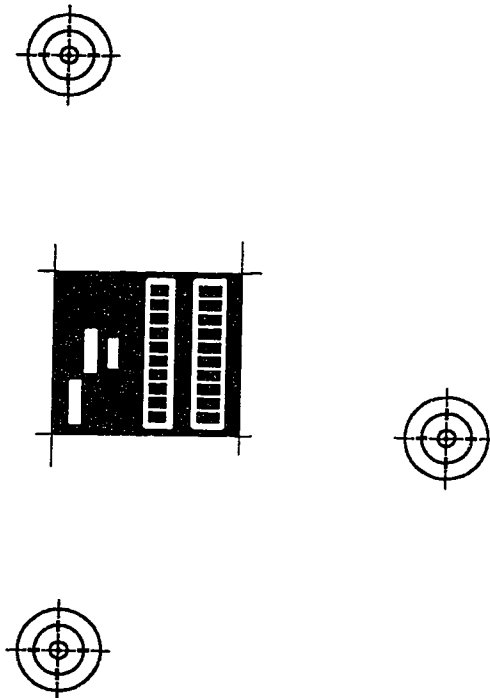
FILE: ~sharma/mac/1995 Drawings/Cover PlateRevB



Layers

1. Drawing Master	2. Drawing	3. layout_msm_side
-------------------	------------	--------------------

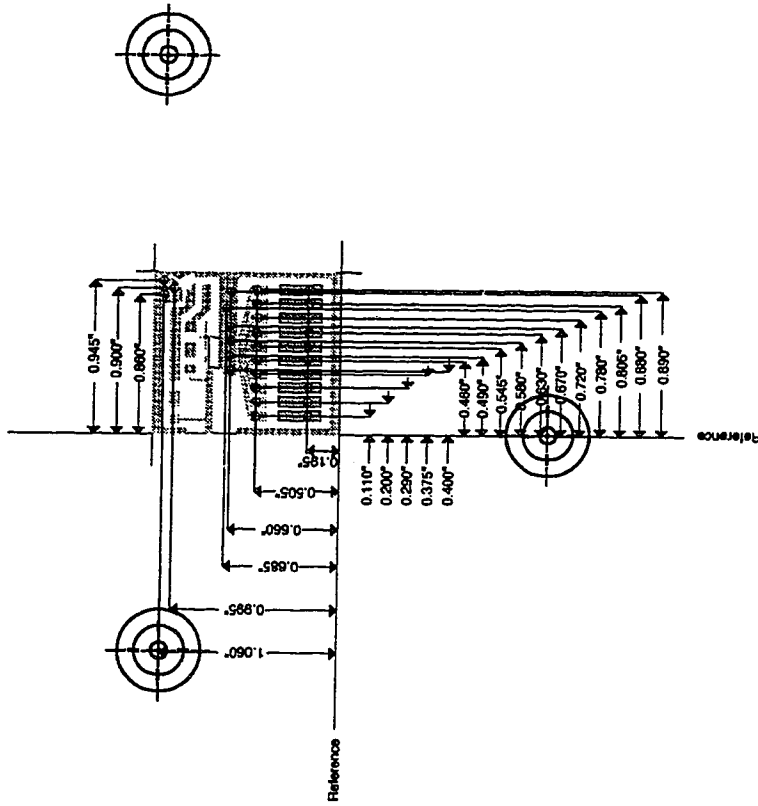




Layers

1. Drawing Master	2. Drawing
-------------------	------------

4. layout_ground_plane
------------------------



All Holes:

0.040" dia. after plating  
(29 places)

Tolerances:

Hole Location:  $\pm 0.001"$   
Hole diameter:  $\pm 0.002"$

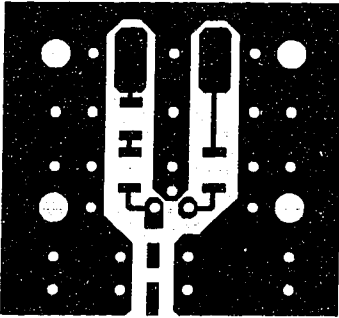
Layers

1. Drawing Master	2. Drawing
5. via_holes	

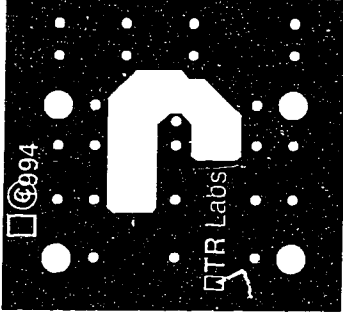
## **Appendix B**

### **Laser bias-tee**

The layout for the laser bias-tee substrate design is given here. Details about the laser transmitter section are available in [63].



**View on Component Side of Substrate.**



**View on Ground Plane Side of Substrate.**

**SPECIFICATION:**

**MATERIAL:** RT/Duroid® 5880 Glass/PTFE  
**DIELECTRIC THICKNESS:** 0.010"  
**COPPER THICKNESS:** 1/2 Oz/ Sq Ft. (0.0007" each side).  
**PLATING:** 50µ inches Gold over 100 µ inches Nickel.

**DIMENSIONS:** See Attached Sheet.

**NOTE:** The addition of date codes, company logos, etc., is **EXPRESSLY PROHIBITED.**

**Drawn By:** David D. Clegg.  
**Rev:** A  
**Date:** 1st May, 1994.

**File:** Bias Tee-02 PCB Spec-01

## **Appendix C**

### **Prototype Switch Drawing**

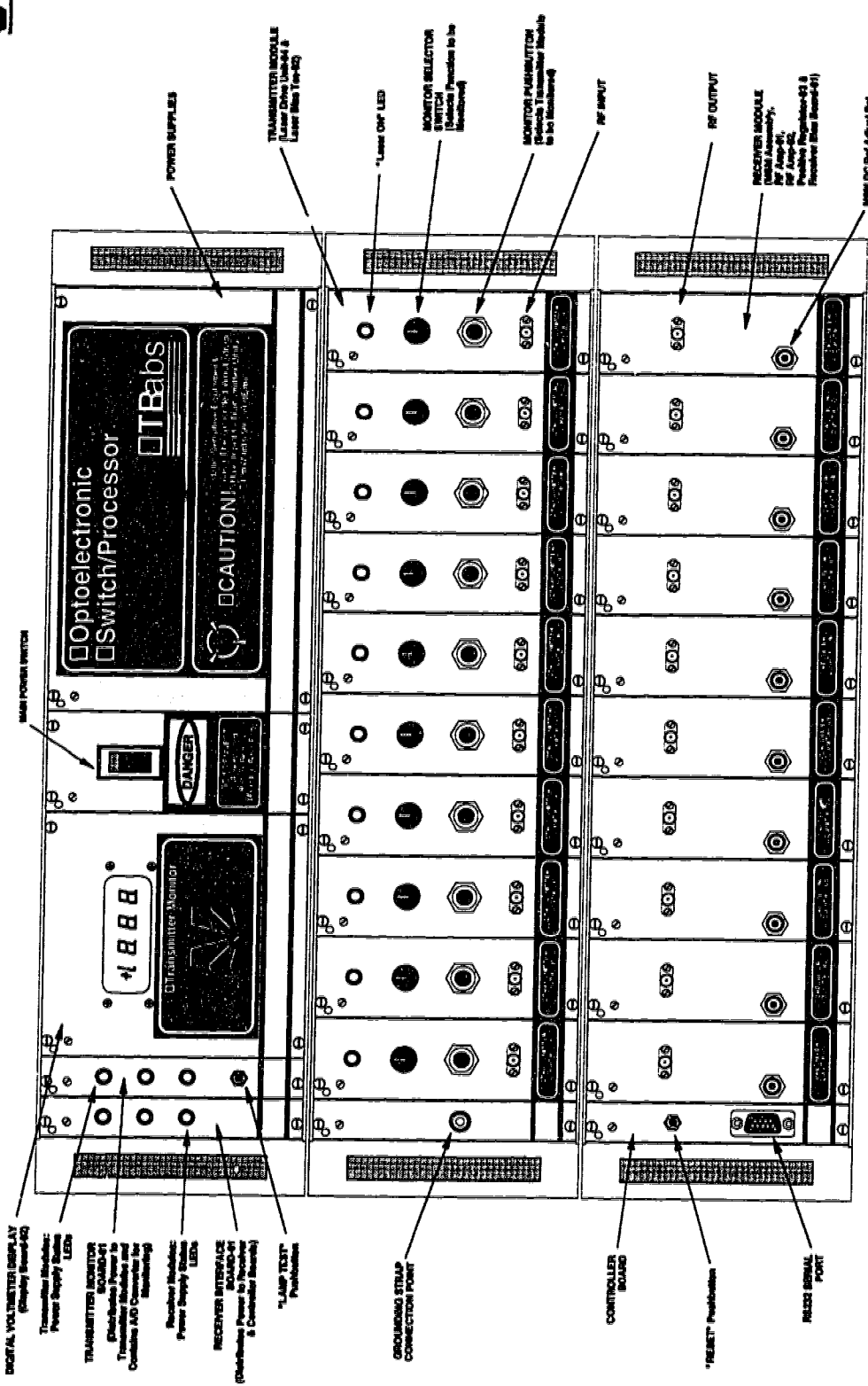
The front view of the prototype optoelectronic switch is shown here. The diagram shows the three main component shelves in the switch:

Power supply

Transmitters (input ports)

Receivers (output ports)

Details for all sub-systems in the switch can be found in [63].



**TR Labs 10 X 10 OPTOELECTRONIC SWITCH/SIGNAL PROCESSOR.**

Drawn By: David D. Chigg & Loren R. Zwick

## Appendix D

### CATV Channel and Frequency Designations [96]

Historic Channel Designation	NCTA Channel Designation	Video Carrier Frequency (MHz)
2	2	55.25
3	3	61.25
4	4	67.25
5	5	77.25
6	6	83.25
A	14	121.25
B	15	127.25
C	16	133.25
D	17	139.25
E	18	145.25
F	19	151.25
G	20	157.25
H	21	163.25
I	22	169.25
7	7	175.25
8	8	181.25
9	9	187.25
10	10	193.25
11	11	199.25
12	12	205.25
13	13	211.25
J	23	217.25
K	24	223.25
L	25	229.25
M	26	235.25
N	27	241.25
O	28	247.25

<b>Historic Channel Designation</b>	<b>NCTA Channel Designation</b>	<b>Video Carrier Frequency (MHz)</b>
P	29	253.25
Q	30	259.25
R	31	265.25
S	32	271.25
T	33	277.25
U	34	283.25
V	35	289.25
W	36	295.25
AA	37	301.25
BB	38	307.25
CC	39	313.25
DD	40	319.25
EE	41	325.25
FF	42	331.25
GG	43	337.25
HH	44	343.25
II	45	349.25



## Appendix E

### E.1 Loop delay for optoelectronic matrix processor

A simple feedback loop can be set up to measure the total delay through the switch, and obtain the delay of all components other than the fibre delay lines as shown in Figure E.1. The resulting frequency separation of the resonant peaks corresponds to the propagation delay.

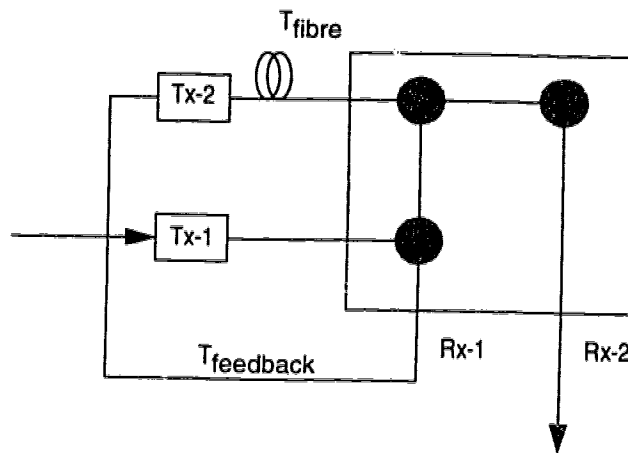


Figure E.1 Feedback loop for measurement of propagation delay

The loop delay is

$$T_{\text{loop}} = T_{\text{fibre}} + T_{\text{feedback}} + T_{\text{internal}}$$

A sample frequency response obtained in this configuration is shown in Figure E.2. From the frequency separation shown in the plot:

$$T_{\text{loop}} = 23.8 \text{ ns} \quad (f_{\text{loop}} = 42.0 \text{ MHz})$$

For the transmitters and receivers used in the switch,  $T_{\text{fibre}} = 6 \text{ ns}$ , and

$$T_{\text{feedback}} = 1.4 \text{ ns}$$

$$T_{\text{internal}} \text{ (minimum propagation delay)} = 16 \text{ ns (averaged for all Tx)}$$

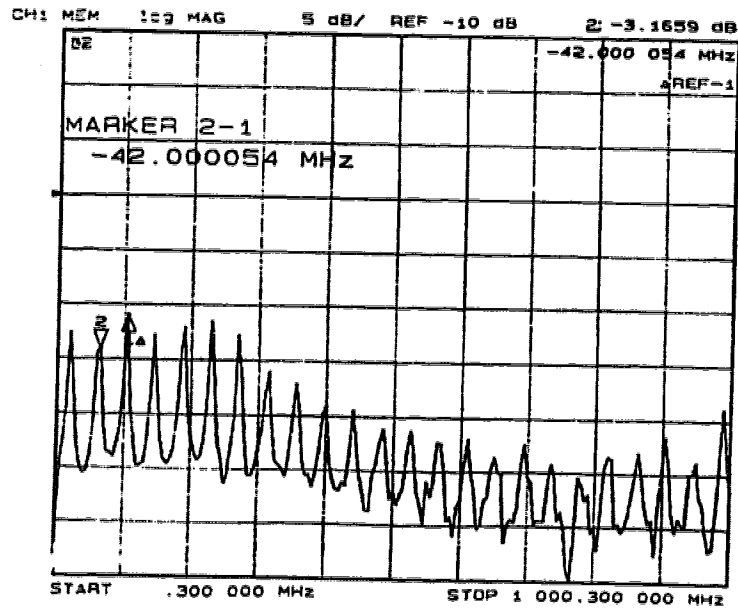


Figure E.2 Resonant loop frequency response

### E.2 Multimode fibre channel impulse response

For a parabolic refractive index profile optical fibre with radius 'a', the refractive index 'n' as a function of fibre radius is given by [following 116, 118]:

$$n(r) = \begin{cases} n_0 \cdot \sqrt{\left[1 - 2\Delta \left(\frac{r}{a}\right)^\alpha\right]} & r \leq a \\ n_0 \cdot \sqrt{1 - 2\Delta} & r \geq a \end{cases} \quad \text{Eqn. E.1}$$

where ' $\alpha$ ' is the profile parameter (2.02) and  $\Delta=0.018$  is the index difference with ' $n_0$ ' = 1.50.

Group delay in a fibre of length 'L' is given by:

$$\tau = \frac{Ln_0}{c} \left[ 1 + \frac{\alpha-2}{\alpha+2} \delta + \frac{3\alpha-2}{\alpha+2} \frac{\delta^2}{2} \right] \quad \text{Eqn. E.2}$$

where  $Ln_0/c$  is the total propagation time and  $\delta$  is the propagation constant.

For  $t = \tau c/Ln_0 - 1$ ,

$$\delta = \frac{\left( \frac{\alpha-2}{\alpha+2} \right) \delta + \sqrt{\left[ \frac{\alpha-2}{\alpha+2} \right]^2 + 2 \left( \frac{3\alpha-2}{\alpha+2} \right) t}}{\left( \frac{3\alpha-2}{\alpha+2} \right)} \quad \text{Eqn. E.3}$$

and the impulse response results from a count of modes which arrive between 't' and 'dt':  $\frac{1}{M} \frac{dm}{dt}$ , where M is the total number of mode groups and 'm' is the mode group number related to  $\delta$  as:

$$\frac{m}{M} = \left[ \frac{\delta}{\Delta} \right]^{\frac{2}{\alpha} + 1} \quad \text{Eqn. E.4}$$

By introducing Eqn. E.3 into E.4, the impulse response is given as:

$$h(t) = \frac{1}{M} \frac{dm}{dt} = \frac{\left[ \left( \frac{\alpha-2}{\alpha+2} \right) \delta + \sqrt{\left[ \frac{\alpha-2}{\alpha+2} \right]^2 + 2 \left( \frac{3\alpha-2}{\alpha+2} \right) t} \right]^{\frac{2}{\alpha}}}{\sqrt{\left[ \frac{\alpha-2}{\alpha+2} \right]^2 + 2 \left( \frac{3\alpha-2}{\alpha+2} \right) t}} \quad \text{Eqn. E.5}$$

where  $\delta$  varies from 0 to  $\Delta$ ,

and, 't' changes from 0 to  $t_{\max}$  given as:

$$t_{\max} = \frac{\alpha - 2}{\alpha + 2} \Delta + \frac{3\alpha - 2\Delta^2}{\alpha + 2} \frac{1}{2} \quad \text{Eqn. E.6}$$

and delay  $\tau$  changes from  $Ln_0/c$  to  $\frac{Ln_0}{c} \cdot (1 + t_{\max})$ . Outside of this interval, the impulse response is zero.

## Appendix F

### Bellcore Metropolitan Network-I [138] cross-connect requirements

For the sample network shown in Figure 7.9, the following table provides traffic demand between various nodes in the network. The units are STS-1 data rate = 51.84 Mbps. Each row of the following table provides a demand and its routing path. The first column in each row is the source node, while the last column with an entry is the destination node. All other nodes in between are the transit nodes. The last column in each row provides the traffic demand in STS-1 units.

**Table F.1 Point-to-point demand map for network**

Source Node	Transit or Destination Node	Transit or Destination Node	Transit or Destination Node	Transit or Destination Node	Destination Node	Traffic demand (STS-1 units)
1	0					12
2	0					8
4	7	5	13	1	0	4
5	13	1	0			4
10	9	14	0			4
13	1	0				4
14	0					8
2	1					16
3	1					12
4	7	5	13	1		4
5	13	1				4
6	13	1				8

Source Node	Transit or Destination Node	Transit or Destination Node	Transit or Destination Node	Transit or Destination Node	Destination Node	Traffic demand (STS-1 units)
8	7	5	13	1		4
9	14	3	1			4
10	9	14	3	1		4
13	1					8
14	3	1				12
3	1	2				8
6	13	1	2			4
10	9	14	2			4
13	1	2				4
14	2					12
5	13	3				4
6	13	3				4
7	5	13	3			4
8	7	5	13	3		4
9	14	3				4
10	9	14	3			8
13	3					8
14	3					16
9	10	7	4			
10	7	4				8
6	5					8
7	5					8
10	7	5				52
11	7	5				4
12	10	7	5			4
13	5					8
14	13	5				16

Source Node	Transit or Destination Node	Transit or Destination Node	Transit or Destination Node	Transit or Destination Node	Destination Node	Traffic demand (STS-1 units)
8	6					8
9	6					8
10	9	6				32
11	7	6				4
12	10	9	6			4
13	6					8
14	13	6				16
10	7					24
12	10	7				16
9	10	7	8			12
10	7	8				40
11	7	8				8
12	10	7	8			16
13	5	7	8			12
14	9	10	7	8		28
10	9					40
11	7	10	9			4
12	10	9				4
13	6	9				4
14	9					16
11	7	10				20
12	10					36
13	5	7	10			10
13	6	9	10			10
14	9	10				88
12	11		8			8
14	9	10	7	11		4

Source Node	Transit or Destination Node	Transit or Destination Node	Transit or Destination Node	Transit or Destination Node	Destination Node	Traffic demand (STS-1 units)
14	9	10	12			4
14	13					16

Using the point-to-point demands tabulated above, the total traffic terminating or originating at each node, as well as the traffic to be cross-connected at each node can be calculated. Table F.2 provides a list of traffic that terminates/originates at the respective nodes.

**Table F.2 Terminating/Originating Traffic**

Node	Terminating Traffic (STS-1)	Originating Traffic (STS-1)	Total originating or terminating (STS-1)
0	44	0	44
1	76	12	88
2	32	24	56
3	52	20	72
4	20	8	28
5	100	8	108
6	80	20	108
7	40	12	52
8	116	16	132
9	72	40	108
10	164	140	380
11	12	40	52
12	4	88	92
13	16	76	92



Node	Terminating Traffic (STS-1)	Originating Traffic (STS-1)	Total originating or terminating (STS-1)
14	0	236	236

And the traffic to be cross-connected for each node is given in Table F.3 below:

**Table F.3 Cross-Connected Traffic**

Node	Cross-Connect Traffic
0	no cross connects, 44 STS-1 units terminate/originate at node.
1	4, 4, 4 (13 - 0), 4,4 (13 - 2), 8 (3 - 2)
2	no cross connects, 56 STS-1 terminate/originate at node.
3	4, 4, 12 (14 - 1)
4	no cross connects, 28 STS-1 terminate/originate at node.
5	4, 4, 4, 4, 4 (7 - 13), 12, 10 (13 - 7)
6	4, 10 (13 - 9)
7	12 (5 - 8), 10 (5 - 10), 4, 4 (8 - 5), 28, 12, 40, 16 (10 - 8), 12, 8 (10-4), 52, 4 (10-5), 4 (10 - 11), 4 (11 - 6), 8 (11 - 8), 4, 20 (11 - 10), 4, 4 (4 - 5), 4 (11 - 5)
8	no cross connects, 132 STS-1 terminate/originate at node.
9	10 (6 - 10), 4, 4, 4, 8 (10 - 14), 32, 4 (10 - 6), 28, 88, 4, 4 (14 - 10)
10	4 (7 - 9), 12, 12, 28, 4 (9 - 7), 4 (9 - 12), 4, 16, 16 (12 - 7), 4, 4 (12 - 9)
11	no cross connects, 52 STS-1 terminate/originate at node.
12	no cross connects, 92 STS-1 terminate/originate at node.
13	4, 4, 4, 4 (5 - 1), 4, 4, 4 (5 - 3), 4, 8, 4 (6 - 1), 4 (6 - 3), 16 (14 - 5), 16 (14 - 6)
14	4 (9 - 0), 4, 4, 4, 8 (9 - 3), 4 (9 - 2)

Note: The cross-connected demand shown in the table F.3 represents bi-directional demand between pairs of nodes.

After the various demands to be cross-connected at each node are known, the traffic on each port required for a cross-connect as well as the size of the cross-connect (given 2.488 Gbps per port maximum capacity of the prototype switch), can be calculated as shown below:

*Note: All demands considered below are bi-directional, e.g. a 4 STS-1 cross-connect requirement between node x and y implies 4 STS-1 from x-to-y and 4 STS-1 from y-to-x. However, some demands shown as in Node-7 mean a total demand of m Mbps and n Mbps summed together. These demands are noted down as separate x-to-y, and y-to-x demands for the purpose of allowing a quick comparison to the working capacity allocation.*

#### **Node 1**

cross-connect (to nodes 0, 2, 3, 13)

13 - 0: 4, 4, 4 = 12 STS-1 = **622.08 Mbps**

13 - 2: 4, 4 = 8 STS-1 = **414.72 Mbps**

3 - 2: 8 = 8 STS-1 = **414.72 Mbps**

#### **Node 3**

cross-connect (to nodes 1, 14)

14 - 1: 4, 4, 12 = 20 STS-1 = **1036.8 Mbps**

#### **Node 5**

cross-connect (to nodes 7, 13)

7 - 13: 4, 4, 4, 4, 4 = 20 STS-1 = **1036.8 Mbps and**

13 - 7: 12, 10 = 22 STS-1 = **1140.48 Mbps**

#### **Node 6**

cross-connect (to nodes 13, 9)

**13 - 9: 4, 10 = 14 STS-1 = 725.76 Mbps**

**Node 7**

cross-connect (to nodes 4, 5, 6, 8, 10, 11)

**5 - 8: 12 = 12 STS-1 = 622.08 Mbps and**

**8 - 5: 4, 4 = 8 STS-1 = 414.72 Mbps**

**5 - 10: 10 = 10 STS-1 = 518.4 Mbps and**

**10 - 5: 52, 4 = 56 STS-1 = 2903.04 Mbps**

**10 - 8: 28, 12, 40, 16 = 96 STS-1 = 4976.64 Mbps**

**10 - 4: 12, 8 = 20 STS-1 = 1036.8 Mbps**

**10 - 11: 4 = 4 STS-1 = 207.36 Mbps and**

**11 - 10: 20 = 20 STS-1 = 1036.8 Mbps**

**11 - 6: 4 = 4 STS-1 = 207.36 Mbps**

**11 - 8 = 8 = 8 STS-1 = 414.72 Mbps**

**4 - 5: 4, 4 = 8 STS-1 = 414.72 Mbps**

**11 - 5: 4 = 4 STS-1 = 207.36 Mbps**

**Node 9**

cross-connect (to nodes 6, 10, 14)

**6 - 10: 10 = 10 STS-1 = 518.4 Mbps and**

**10 - 6: 32, 4 = 36 STS-1 = 1866.24 Mbps**

**10 - 14: 4, 4, 4, 8 = 20 STS-1 = 1036.8 Mbps and**

**14 - 10: 28, 88, 4, 4 = 124 STS-1 = 6428.16 Mbps**

### **Node 10**

cross-connect (to nodes 7, 9, 12)

**7 - 9: 4 = 4 STS-1 = 207.36 Mbps and**

**9 - 7: 12, 12, 28, 4 = 56 STS-1 = 2903.04 Mbps**

**9 - 12: 4 = 4 STS-1 = 207.36 Mbps and**

**12 - 9: 4, 4 = 8 STS-1 = 414.72 Mbps**

**12 - 7: 4, 16, 16 = 36 STS-1 = 1866.24 Mbps**

### **Node 13**

cross-connect (to nodes 1, 3, 5, 6, 14)

**5 - 1: 4, 4, 4, 4 = 16 STS-1 = 829.44 Mbps**

**5 - 3: 4, 4, 4 = 12 STS-1 = 622.08 Mbps**

**6 - 1: 4, 8, 4 = 16 STS-1 = 829.44 Mbps**

**6 - 3: 4 = 4 STS-1 = 207.36 Mbps**

**14 - 5: 16 STS-1 = 829.44 Mbps**

**14 - 6: 16 STS-1 = 829.44 Mbps**

**Node 14**

cross-connect (to nodes 0, 3, 9)

9 - 0: 4 = 4 STS-1 = **207.36 Mbps**

9 - 3: 4, 4, 4, 8 = 20 STS-1 = **1036.8 Mbps**

9 - 2: 4 = 4 STS-1 = **207.36 Mbps**

Once the cross-connect traffic is known between each set of two nodes, the traffic is grouped into sets of 2.488 Gbps each and one switch port is allocated to the set. Thus, the cross-connect size at each node can be calculated. A sample calculation is shown below for node 1.

**Node 1**

cross-connect (to nodes 0, 2, 3, 13)

13 - 0: 4, 4, 4 = 12 STS-1 = **622.08 Mbps**

13 - 2: 4, 4 = 8 STS-1 = **414.72 Mbps**

3 - 2: 8 = 8 STS-1 = **414.72 Mbps**

Thus, at node 1, a cross-connection would be required from node 13 to node 0 (and vice versa), node 13 to node 2 (and vice versa), and from node 3 to node 2 (and vice versa). The result is a 6x6 cross-connect size since two ports would be required for each of the bi-directional demand to be cross-connected.

Figure F.1 illustrates the cross-connect required at node 1.3.

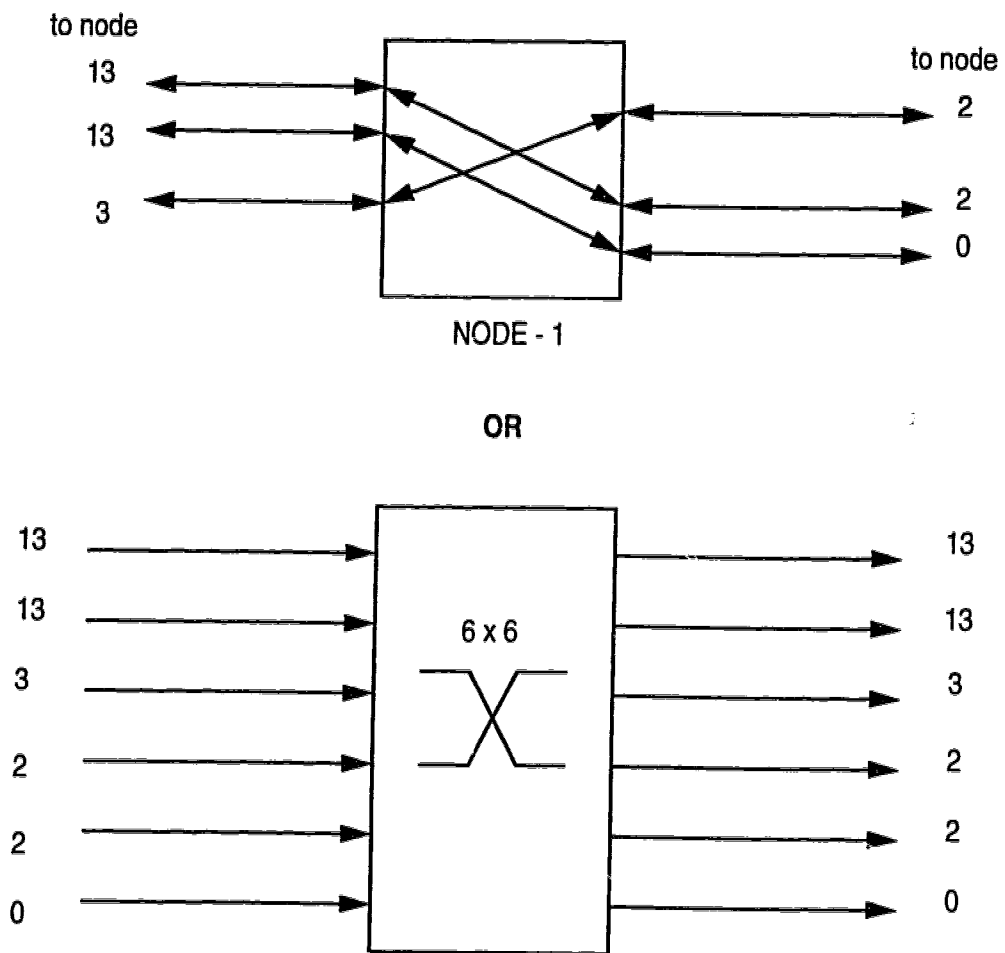


**Figure F.1 Cross-connect requirement at node 1 (6x6)**

The optical switch cross-connect size simply follows the total number of ports required at each node with no bandwidth limitation. Table F. 4 shows the cross-connect sizes required in each case. Cross-connect switch sizes for 5 Gbps per port capacity are also shown for comparison.

**Table F.4 Cross-Connect Sizes at each node**

<b>NODE</b>	<b>Total Demand (to be cross- connected) STS-1 units</b>	<b>Cross- Connect Size (assuming 2.488 Gbps max)</b>	<b>Cross- Connect Size (assuming 5 Gbps max)</b>	<b>Optical Switch cross-connect size</b>
0	None	None	None	None
1	56	6 x 6	6 x 6	6 x 6
2	None	None	None	None
3	40	2 x 2	2 x 2	2 x 2
4	None	None	None	None
5	84	2 x 2	2 x 2	2 x 2
6	28	2 x 2	2 x 2	2 x 2
7	508	20 x 20	18 x 18	18 x 18
8	None	None	None	None
9	380	10 x 10	6 x 6	4 x 4
10	216	8 x 8	6 x 6	6 x 6
11	None	None	None	None
12	None	None	None	None
13	160	12 x 12	12 x 12	12 x 12
14	56	6 x 6	6 x 6	6 x 6

# Appendix G

## Switching Time Measurements

The switching time for the crosspoints in the switch is limited by the controller speed and the bandwidth of the dc bias circuit (see Figure 4.7). Since the dc bias circuit has a 3 dB bandwidth of ~200 MHz, the switching time is expected to be dominated by the controller reconfiguration time. Figures G.1 and G.2 show a typical switching time measurement from the optoelectronic switch. In these experiments, a single tone is fed to the input and the output is switched from OFF to ON (Figure G.1) and ON to OFF (Figure G.2) state. The output trace is captured with a high speed oscilloscope with 100 MHz bandwidth for single trace capture (HP 16500 A system, 16510A option).

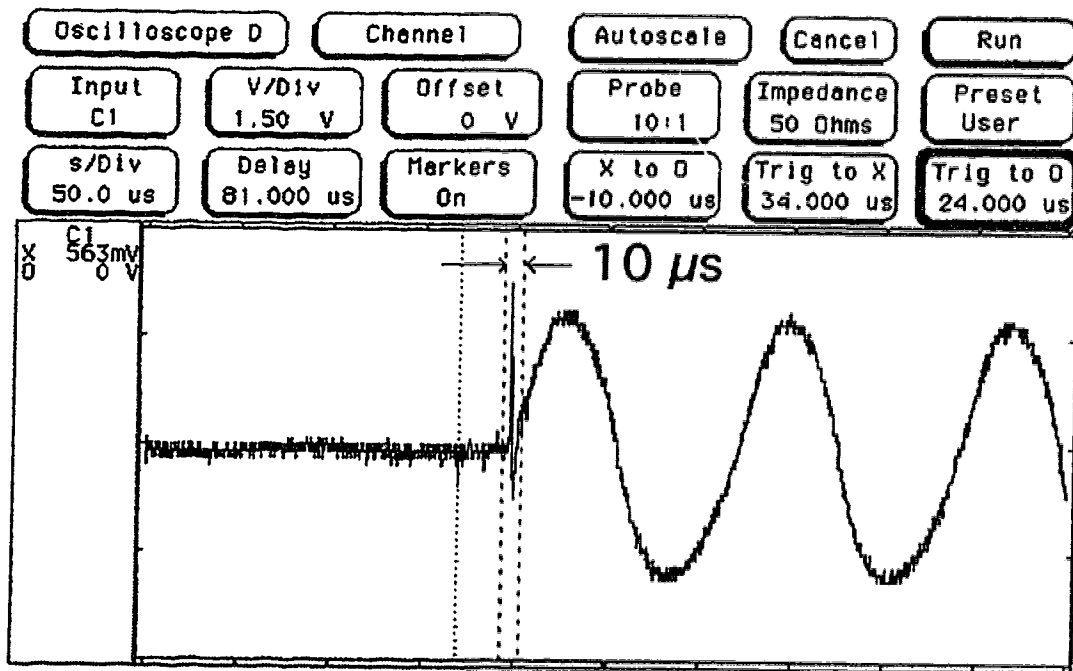


Figure G.1 Switching Time Measurement (OFF to ON)



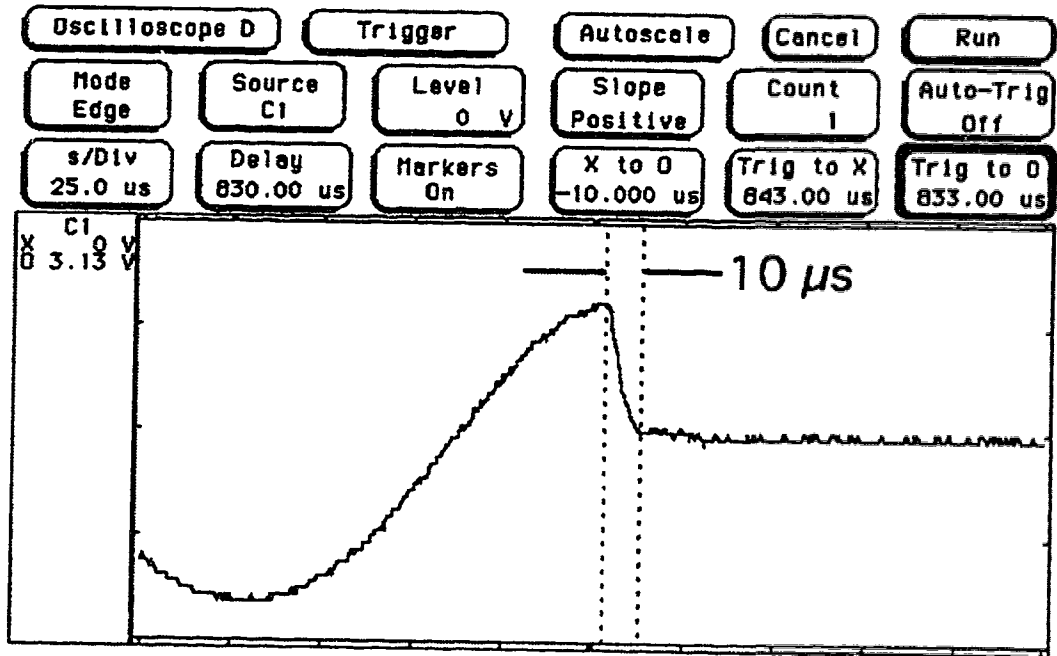


Figure G.2 Switching Time Measurement (ON to OFF)

## Appendix H

### **A Signal Transparent 10x10 Space-Division Optoelectronic Switch Core for Virtual-Transparent-Path based Multi-Wavelength Networks**

Rohit Sharma, *Student member, IEEE*

R. Ian MacDonald, *Senior member, IEEE*

*sharma@edm.trlabs.ca & ianmac@edm.trlabs.ca*

Telecommunications Research Laboratories (TRLabs)

#800 Park Plaza, 10611-98 Ave. Edmonton, Alberta, Canada. T5K 2P7

#### Abstract

Broadband optoelectronic space division switch matrices used in conjunction with optical (de) multiplexers and optical-electronic-optical wavelength regenerators can provide capabilities for wavelength conversion and translation in wavelength routed multi-wavelength networks. Such switches are required to be transparent to bit-rate, format, and modulation of the signals carried on various wavelengths to enable high capacity, scalable multi-wavelength networks. A 10x10 implementation of a transparent optoelectronic switch matrix capable of routing any bit rate up to 2.5 Gbps per port as well as high quality analog video signals with >60 dB contrast and >60 dB crosstalk suppression is presented. Transparency is demonstrated with digital signals ranging from 622 Mbps to 2.5 Gbps per port along with analog video signals routed through the switch core.

## I. Introduction

Wavelength division multiplexing (WDM) techniques offer potential to provide an increasingly needed expansion in information transmission system capacity. Multihop wavelength routed networks are configurable on a link- by- link basis to allow optimization of capacity allocation, management, and scalability of network size [1]. Wavelength reuse on different links of the network is likely to be required to realize the full benefit of WDM technologies because the number of wavelength channels available is limited for practical reasons to a few tens [2, 3]. A wavelength-interchanging cross-connect function is necessary in the nodes of such a network, and much effort has been expended in identifying methods by which the wavelength of an optical signal can be altered at will [4].

Transparency, the ability to pass signals without regard to rate or format, is often cited as one of the primary requirements for a WDM network [5] and is recognized to have important implications on evolution of current facilities to multi-wavelength optical networks [1, 2, 5, 6]. It is acknowledged that fundamental physical limitations make strict optical transparency very difficult to achieve [7], and of limited value [2]. Two degrees of transparency to signals have been identified in [6]: (a) transparency to digital signals of arbitrary bit rates, protocols and formats, and (b) transparency to signals of any type (both analog and digital). It should be noted that neither type of transparency actually requires the uninterrupted transmission of light. We refer here to transparency in the sense of (a) and (b) as "*signal transparency*".

A very simple and practical method of wavelength conversion and interchange is available for WDM networks if the nodes may contain optical/electronic/optical (O/E-E/O) repeater stages. After wavelength demultiplexing and detection, the signals of the incoming WDM channels can be switched to transmitters on the output side of the node according to the desired wavelength assignments as shown in Figure 1. It is often stated that this approach is not practical because of the cost and noise associated with the optoelectronic repeater stages, given the difficulty of constructing a suitable electronic switch. Such a switch must be an analog cross-connect with both sufficient bandwidth and sufficient dynamic range to pass any signal carried by the network

through as many stages as required. However, if sufficient performance were available in a switched repeater stage, this wavelength conversion technique would offer the benefit of polarization insensitivity, high conversion efficiency, access to the signals at the nodes, and possibly low cost by comparison with other methods.

We aver that with appropriate use of photonics to achieve an electronic switching function, a cross-connect of adequate performance can in fact be constructed. We provide comprehensive experimental results with a 10x10 prototype to demonstrate that an “optoelectronic” space division switch can preserve bit rate, format, and modulation transparency for digital and analog signals. Results are shown for digital signals at 622 Mbps (OC-12), 1.0 Gbps, 1.5 Gbps, 2.0 Gbps and 2.488 Gbps (OC-48), in addition to the ability to switch NTSC analog television signals on their carriers as required in CATV networks. Any or all of these signals can be simultaneously routed with crosstalk below -60 dB (section V). Results from characterization of the switch for bit error rate, carrier to noise ratio and harmonic distortion tests for CATV payloads are provided to demonstrate the complete signal transparency of this type of switch. Extension of signal transparency to higher data rates or bandwidth is shown to be relatively straightforward.

Although end-to-end optical paths are not possible with this form of wavelength routing, the end to end paths are signal transparent. No distinction between signal and optical transparency can be made at the normal points of access to the network, the electronic terminals.

## **II. Photonic Connectivity Layer and Virtual-Transparent-Path Concept**

Brackett [2] has very instructively pointed out that the introduction of WDM technologies in the network essentially adds a “photonic” layer between the physical layer and the transport layer. We extend this idea to propose that it is this layer that is required to be “transparent” in the transport of signals through the network. Since the connectivity of the network is determined in the photonic layer of a WDM network with wavelength routing, it may properly be termed the “photonic connectivity layer”. This layer provides paths that are “signal” transparent, but not

necessarily optically transparent.

The photonic connectivity layer is supported by the underlying physical layer which is optically transparent because the WDM fibre link between any two nodes is transparent to light. The photonic connectivity layer is an extension of the concept of the virtual wavelength path [8], with the added feature of transparency. The network path between source and destination requires only signal transparency, and is therefore designated a virtually transparent path (VTP). The VTP plays a role analogous to the virtual path (VP) concept of ATM networks in that each VTP can be routed over a variety of wavelength channels. Figure 2 shows the new proposed layer in a multi-wavelength network.

Optoelectronic space division matrices used to implement wavelength- interchanging cross-connects (WXC) can provide the basis for VTP based network configurations in the photonic connectivity layer. This layer can also serve as the execution layer for network restoration strategies based on wavelength overlay protection networks [9, 10] where spare capacity for restoration purposes is allocated and managed as virtually transparent paths. This restoration strategy is analogous to VP-based network restoration methods [11], as well as path restoration methods [12].

We describe the optoelectronic switching principle by which such switches can be made in section II and the 10x10 prototype fabricated to implement this approach in section III. Section IV provides the results of routing digital and analog signals through the switch.

### **III. Optoelectronic Switching**

Optoelectronic routing of signals is a photonic technique that utilizes optical distribution and controlled optical-to-electronic conversion of signals to achieve a broadband switching function [13]. As shown in Figure 3, each input signal is accepted as, or converted to an optical signal and distributed to every output port following an 'N'-way power split. There are 'N' different signals (one from every input port) present at every output port after a 'shuffle' of optical paths to rearrange the signals. At each output port, each group of 'N' signals is made incident on a

photodetector array ( $1 \times N$ ) containing independently biased photodetectors with a common output terminal (Figure 4). To achieve routing of an input signal to the desired output port, the appropriate photodetector is switched 'ON' (biased) while all others are left unbiased ('OFF'). Thus, the 'selected' signal is switched to the desired output port following a 'broadcast' of the input signals to all output ports.

Optical 'broadcast' and optoelectronic 'select' for routing of broadband signals has been shown to achieve high isolation and contrast [14, 15, 16]. Optical distribution of signals gives high crosstalk immunity and bias controlled 'selection' of the signals provides high ON/OFF contrast ratio (with suitable photodetectors) while preserving the crosstalk immunity since only 1 out of  $N$  signals is present at each output port in electronic form. It is pertinent to note here that optical or electronic signals are never present on a common substrate in any stage of this type of switch, and the output ports may be physically isolated to suppress electromagnetic coupling to desired levels.

The electronic signal at the output of the switch matrix may be amplified to a suitable level with broadband amplifiers. In the prototype switch reported in this paper, the receiver gain is adjusted to provide zero overall insertion loss. Scalable non-blocking matrices may be constructed by cascading multiple stages of such switching matrices [17].

#### **IV. Prototype 10x10 Switch**

A prototype of the 10x10 optoelectronic switch is shown in Figure 5. Each of the input ports accepts digital or analog signals with  $50 \Omega$  impedance. The ten input signals can be routed (or broadcast) to any (all) of the ten output ports. The nominal input and output levels are 0 dBm.

The laser transmitters at the input ports use that use GaAs lasers with external bias-tee circuits that couple 5 mW power into  $50 \mu\text{m}$  core graded index multi-mode fibre pigtails. A  $1 \times 10$  multimode optical splitter is included in each transmitter to divide the powers, providing ten optical outputs. The required 'shuffle' of signals (see Figure 4) is carried out by routing the fibre bundles between the transmitters and the output ports (receivers) via a connectorised optical backplane.

A monolithic GaAs Metal-Semiconductor-Metal (MSM) photodetector array is used at each output port to convert the optical signals to electronic domain. The optoelectronic assembly has ten fibres aligned to the MSM photodetector array which is mounted on a custom designed substrate with the required dc-bias circuits. The fibres are aligned to the photodetector array with the help of a Silicon v-groove assembly containing micro-machined v-grooves at 250  $\mu\text{m}$  spacing matching the photodetector pitch. The output of the photodetector array is coupled to electronic amplifiers through a micro-strip transmission line. A 3-stage amplifier with a bandwidth of 2.25 GHz provides a total gain of 56 dB to amplify the received signal to the nominal output level of 0 dBm. The bias on each photodetector is set independently through a digital-to-analog converters capable of controlling the bias to within 2 mV between -5 to +5 volts. Continuous control of the MSM photodetector bias voltage can provide bipolar weight setting elements for broadband matrix-vector processors. This technique has been used to demonstrate broadband tunable filter structures [18].

## V. Results

Performance and properties of the prototype switch are evaluated in this section with a view to assessing the application of optoelectronic switching technology to signal transparent routing. The high ON/OFF contrast and crosstalk immunity that can be achieved with this technique are demonstrated in section A. Transparency to digital signals of arbitrary bit rates is shown in section B. Performance of the prototype switch for analog video signals is characterized in section C, and a signal transparency experiment describing simultaneous switching of a 2.5 Gbps digital signal and analog video signal is presented in section D.

### A. ON/OFF Contrast and Crosstalk

The contrast between ON and OFF states of the switching elements is one of the primary performance parameters of broadcast and select matrix switch since crosstalk from OFF state crosspoints accumulates into the output ports. MSM photodetectors provide very high ON/OFF contrasts when the photodetector is appropriately turned off [13]. Figure 6 shows a signal at 1

GHz routed through the switch with the routing crosspoint turned ON and OFF. The contrast between ON and OFF states is more than the 60 dB.

Since only one photodetector in the array is turned ON at any given time, there is only one signal present at each output in electronic form and electromagnetic coupling is not a problem. Extremely low crosstalk interference levels are obtained. Figure 7 shows the result of a crosstalk measurement experiment where two signal tones (995 MHz and 1 GHz) are incident on neighbouring channels in the switch. The upper trace (with two equal magnitude peaks) shows the signals at the output port when the neighbouring crosspoints are turned ON. The second trace shows the output with one channel turned OFF. The difference between the magnitudes of the signal tone is a direct measurement of the total crosstalk in the switch. Crosstalk suppression greater than 60 dB is demonstrated.

The primary cause of crosstalk is the residual signal contribution by the inactive photodetectors in the array due to very small amounts of bias that may be present as a result of non-zero ground potential in the array biasing circuit. Note that this experiment provides a measure of the total crosstalk contribution. This consists of the OFF state photocurrents from all the photodetectors except the one that is switched ON, as well as the optical crosscoupling between the neighbouring channels.

Network transparency requires that signals can pass through multiple stages of optoelectronic switches on their way through the network. The current prototype has been measured to have a noise figure of ~15 dB per stage and does not permit multiple stages at rates beyond 622 Mbps. However, by improving the laser relative-intensity-noise (RIN), transmitter power, and by designing low-noise amplifiers, we estimate that signal to noise ratios can be improved by up to 20 dB. In that case, it will be possible to go through at least six consecutive stages at bit rates up to 10 Gbps at an SNR of >22 dB. Another practical option is the use of '2R remodulator' stages (regeneration/reshaping) at the output of the switches. 2R remodulation is a bit rate transparent operation without any reclocking of data and limited signal transparency is maintained [19].



### *B. Bit-Rate Independent Switching*

Broadband binary digital formats constitute the most common signals in modern communications networks. Since optoelectronic switches have no digital circuitry, data rates at any input port can be continuously changed without any changes required in switch hardware or software. Eye diagrams for signals of various data rates ranging from 622.08 Mbps (OC-12) to 2.488 Gbps (OC-48) are shown in Figures 8 and Figure 9. Bit error ratios for these signals are measured to be  $< 10^{-10}$  for signals up to 2.0 Gbps and  $< 10^{-9}$  for 2.488 Gbps. The prototype switch is capable of routing any arbitrary data rate up to 2.5 Gbps at each port, resulting in a maximum aggregate capacity of 25 Gbps. The capacity of this prototype is limited by the bandwidth of the photodetector array and the inexpensive laser transmitters used. We are now developing next generation prototypes capable of routing more than 10 Gbps per port.

### *C. Analog Signal Switching*

Transmission of analog video signals in a lightwave system (such as the optoelectronic switch which consists of a laser transmitter and receiver in each path) is affected by noise performance of the system as well as the distortion effects due to nonlinearities present in the system. The signal path through an optoelectronic switch provides a high quality channel capable of routing analog video signals in addition to the digital signals described above in section B. Performance of the prototype switch has been characterized for composite 42 channel CATV payload with video carrier frequencies ranging from 55.25 MHz (Channel 2) to 349.25 MHz (Channel 45).

All results reported in this section follow the standard procedures recommended by the National Cable TV Association (NCTA) for measurement of noise and distortion in CATV systems given in [20].

The noise performance of an analog system is measured in terms of carrier power to noise power ratio - Carrier-to-Noise Ratio (CNR). Figure 16 shows the result of the CNR measurement for NTSC video signal. The measured CNR of 71.46 dB in the 30 kHz resolution bandwidth shown

in Figure 10 corresponds to 49.95 dB in the 4.25 MHz video bandwidth of the signal. The modulation depth is 21.2% for this measurement.

Multichannel systems such as a CATV system also suffer from “beat stacking” resulting from several nonlinear distortion products falling at the same frequency. For these systems, nonlinear distortion is characterized in terms of Composite Second Order (CSO) distortion and Composite Triple Beat (CTB) distortion products which are the strongest second and third order beat stacks within the 6 MHz channel bandwidth [21]. Following [20], CSO is measured (in dBc) as the power present at a frequency  $\pm 1.25$  MHz from the video carrier frequency of channel under test, relative to the power of the video carrier signal. The third order beat products are located at the video carrier frequency in the channel under test and thus CTB is measured at the carrier frequency as the difference between the power at that frequency, and the signal power present at that frequency when the carrier signal is switched off at the source.

CSO and CTB measurements with the prototype switch were carried out using NCTA specified procedures [20]. RF power per channel ranging from -20 dBm to -5.0 dBm was used for the distortion measurements. The effective modulation index ‘ $m_{eff}$ ’ is calculated as [22]:

$$m_{eff} = \sqrt{\frac{Nm^2}{2}} \quad \text{Eqn. 1}$$

where  $N$  is the total number of channels, and  $m$  is the modulation depth per channel.

CSO and CTB products were measured at two channels (Channel 2 and 43) situated at either end of the composite channel spectrum. Figure 11 shows the CTB distortion products measured with respect to the carrier power at 55.25 MHz (Channel 2) and 337.25 MHz (Channel 43) for different modulation depths. The CSO products measured at 54.0 MHz & 56.5 MHz for Channel-2, and at 336.0 MHz & 338.5 MHz for Channel-43 are shown in Figure 12.

These levels are insufficient for switching CATV payloads [20]. The semiconductor lasers used in the prototype switch were directly driven Fabry-Perot types intended for use in compact disc players, and are not optimized for linear modulation at high speed. It is anticipated that the

use of linearized lasers or external modulators in the input port transmitters for optoelectronic switches will provide improved distortion performance.

#### *D. Format-Transparent Digital and Analog Signal Switching*

Simultaneous routing of digital and analog signals can be achieved with the optoelectronic switch. Complete transparency to modulation is demonstrated in Figure 13 by simultaneous switching of a 2.488 Gbps digital signal and an analog NTSC video signal on its carrier. The figure shows the experimental set up with results shown in the inset. The photograph corresponding to the video signal is a video-print of the analog signal at the output of the switch as displayed on a television monitor. Actual signal quality is indistinguishable from the original. Applications in signal transparent routing introduced in section-I as well as in multimedia networks where broadband digital and analog signal switching capabilities may be required are anticipated.

### **VI. Conclusion**

Optoelectronic switching techniques have been successfully employed to demonstrate signal transparent routing of broadband digital and analog signals. A 10x10 prototype with 25 Gbps aggregate digital throughput has been described. High ON/OFF contrast and crosstalk immunity is experimentally demonstrated. Data rates of up to 2.5 Gbps per port are supported in the prototype switch, and development of prototypes for 10 Gbps per port operation is in progress. The optoelectronic switch matrix is shown to be transparent to data rate, format, and modulation. Simultaneous routing of broadband digital signals up to 2.5 Gbps per port and analog signals has been achieved in a prototype which confirms the signal transparency. Such switch matrices can be used to implement signal-transparent wavelength interchanging cross-connect (WXC) structures for multi-wavelength networks.

The concept of virtual-transparent-paths (VTP) has been introduced to describe signal transparent routing through the photonic connectivity layer in the network. Optoelectronic switch matrices, such as the one described in this work, can be used as the basis for VTP based network configurations, capacity allocation and management through WXC nodes in the photonic

connectivity layer.

## VII. References

1. C.A. Brackett, A.S. Acampora, J. Sweitzer, G. Tangonan, M.T. Smith, W. Lennon, K.C. Wang, R.H. Hobbs, "A scalable multiwavelength multihop optical network: a proposal for research on all-optical networks", *IEEE Journal of Lightwave Technology*, vol. 11, May/June 1993, pp. 736-753 .
2. C.A. Brackett, "Is there an emerging consensus on WDM networking?", Foreword to Special Issue on Multiwavelength Optical Technology and Networks, *IEEE Journal of Lightwave Technology*, vol. 14, no. 6, June 1996, pp. 936-941.
3. M. Kovacevic, A. Acampora, "Benefits of wavelength translation in all-optical clear-channel networks", *IEEE Journal on Selected Areas in Communications*, vol. 14, no. 5, June 1996, pp. 868-880.
4. S.J.B. Yoo, "Wavelength conversion technologies for WDM network applications", Invited Paper, *IEEE Journal of Lightwave Technology*, vol. 14, no. 6, June 1996, pp. 955-966.
5. A.A.M. Saleh, "Transparent optical networks for the next generation infrastructure", *Proc. OFC '95*, paper ThEI, 1995.
6. R.E. Wagner, R.C. Alferness, A.A.M. Saleh, M.S. Goodman, "MONET: Multiwavelength optical networking", *IEEE Journal of Lightwave Technology*, vol. 14, no. 6, June 1996, pp. 1349-1355.
7. L. Thylen, G. Karlsson, O. Nilsson, "Switching technologies for future guided wave optical networks: potentials and limitations of photonics and electronics", *IEEE Communications Magazine*, February 1996, pp. 106-113.
8. S. Okamoto, A. Watanabe, K. Sato, "Optical cross-connect node architectures for photonic transport networks", *IEEE Journal of Lightwave Technology*, vol. 14, no. 6, June 1996, pp.1410-1422.
9. S. Okamoto, K. Sato, "Optical path cross-connect systems for photonic transport

- networks", *Proc. IEEE Globecom '93*, Houston, TX, November 1993, pp. 474-480.
10. Y. Hamazumi, N. Nagatsu, K. Sato, "Number of wavelengths required for constructing optical networks considering failure restoration", *Proc. OFC '94*, San Jose, CA, February 1994, TuE2.
  11. R. Kawamura, K. Sato, I. Tokizawa, "Self-healing ATM networks based on virtual path concept", *IEEE Journal on Selected Areas in Communications*, vol. 12, no. 1, January 1994, pp. 120-127.
  12. R.R. Iraschko, M.H. MacGregor, W.D. Grover "Optimal capacity placement for path restoration in mesh survivable networks", *Proc. ICC'96*, Dallas, TX, pp. 1568-1574.
  13. R.I. MacDonald, "Optoelectronic Hybrid Switching" in "*Photonics in Switching*" Ed. J.E. Midwinter, vol. 1, Academic Press, 1994.
  14. R.I. MacDonald, E.H. Hara, "Optoelectronic broadband switching array", *Electronics Letters*, vol. 16, 1978, pp. 502-503.
  15. S.R. Forrest, G.L. Tangonan, V. Jones, "A simple 8x8 optoelectronic crossbar switch", *IEEE Journal of Lightwave Technology*, vol. 7, no. 4, April 1989, pp. 607-614.
  16. M. Veilleux, R.I. MacDonald, "An optoelectronic switching matrix with high isolation", *IEEE Journal of Lightwave Technology*, vol. 10, no. 7, July 1992, pp. 988-991.
  17. R.I. MacDonald, D. Lam, J. Noad, "Multistage optoelectronic switch networks", *IEE Proc. - Optoelectronics*, vol. 141, no. 3, June 1994, pp. 173-177.
  18. E. Perrenoud, R. Sharma, R.I. MacDonald, "Broadband adaptive optoelectronic discrete time signal processor", *Proc. International Conf. on Applications of Photonics Technology, ICAPT '96*, Montreal, Quebec, July 29-August 2, 1996.
  19. P.E. Green Jr., F.E. Janniello, R. Ramaswami, "WDM protocol-transparent distance extension using R2 remodulation", *IEEE Journal of Selected Areas in Communications*, vol. 14, no. 5, June 1996, pp. 962-967.
  20. National Cable Television Association, "NCTA recommended practices for measurements on cable television systems", November 1989.

21. T.E. Darcie, G.E. Bodeep, "Lightwave subcarrier CATV transmission systems", *IEEE Transactions on Microwave Theory and Techniques*, vol. 38, no. 5, May 1990, pp. 524-533.
22. C.J. Chung, I. Jacobs, "Practical TV channel capacity of lightwave multichannel AM SCM systems limited by the threshold nonlinearity of laser diodes", *IEEE Journal of Lightwave Technology*, vol. 4, no. 3, March 1992, pp. 289-292.

**FIGURES**

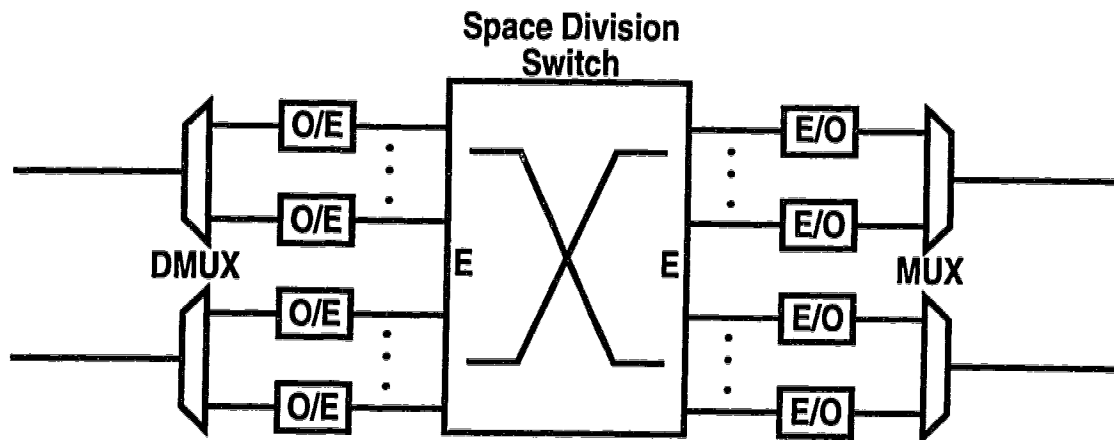


**Figure 1 O/E/O Wavelength Routing Using Space-Division Switches**

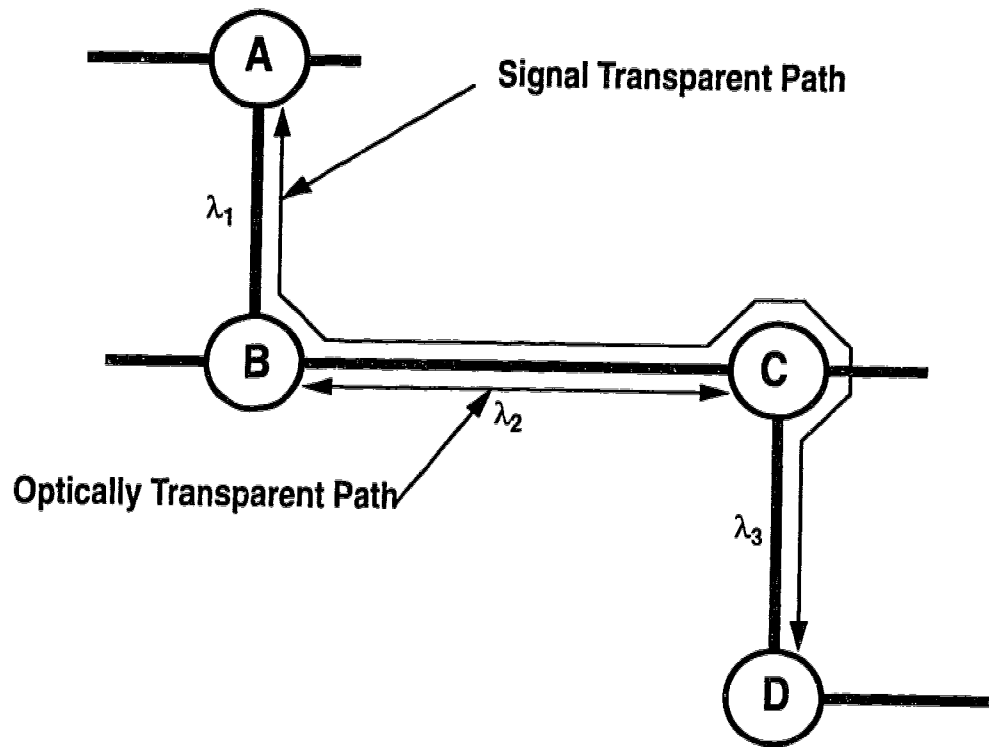


**Figure 2** Photonic Connectivity Layer with Transparent Signal Paths: Path A-D is transparent to the format/bit-rate/modulation of the signal. Path A-B, B-C, C-D may be optically transparent spans. Each node in this diagram contains the wavelength routing mechanism shown in Figure 1. The signal in the photonic connectivity layer can traverse the path on distinct wavelengths on each span.

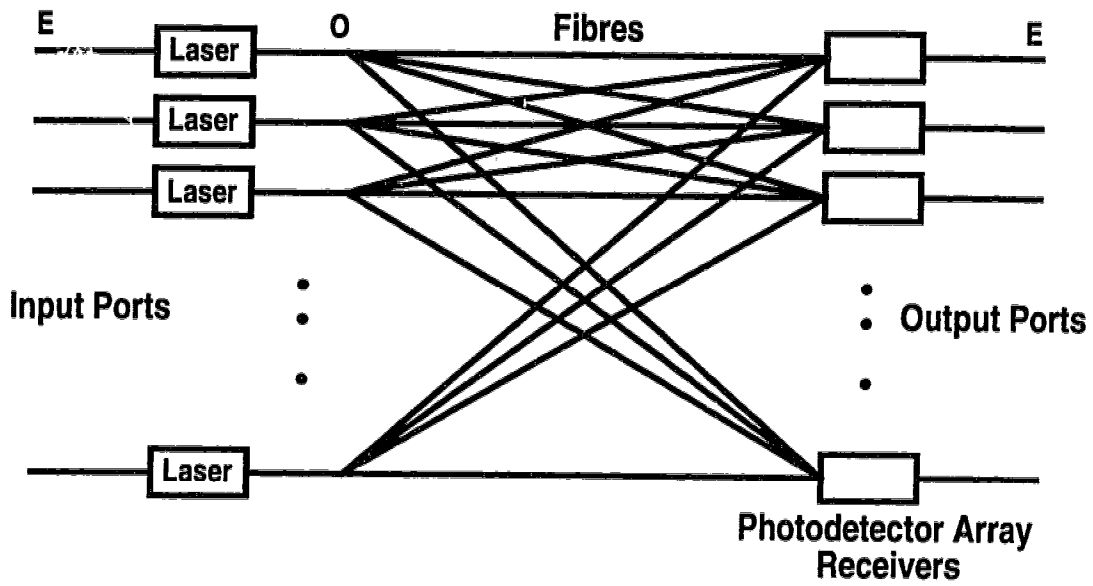


**Figure 3 Optoelectronic 'Broadcast' and 'Select' Space-Division Switching**

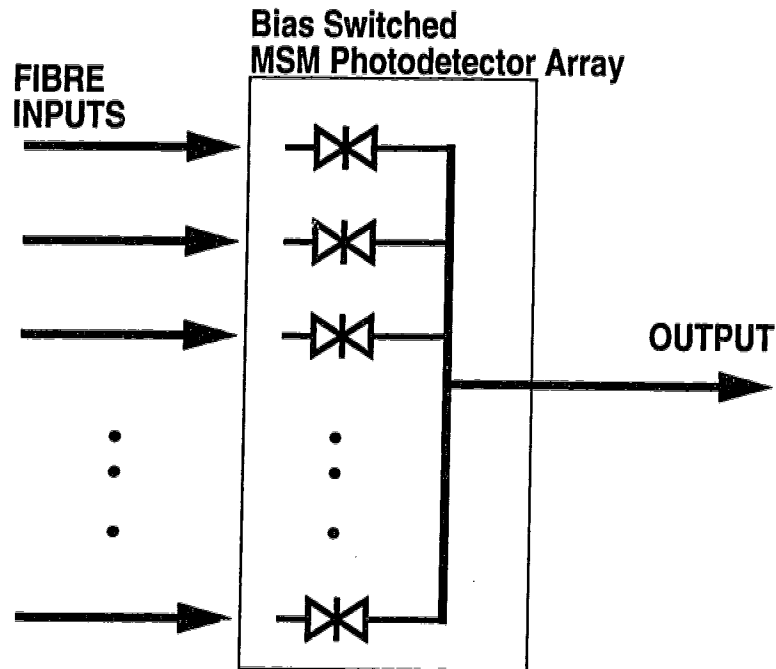


**Figure 4 Optoelectronic '1 of N' selection with Bias-Switched MSM Photodetector Arrays. One of N detectors is biased ON and thus only 1 of N input signals is present in electronic form at output of the array.**



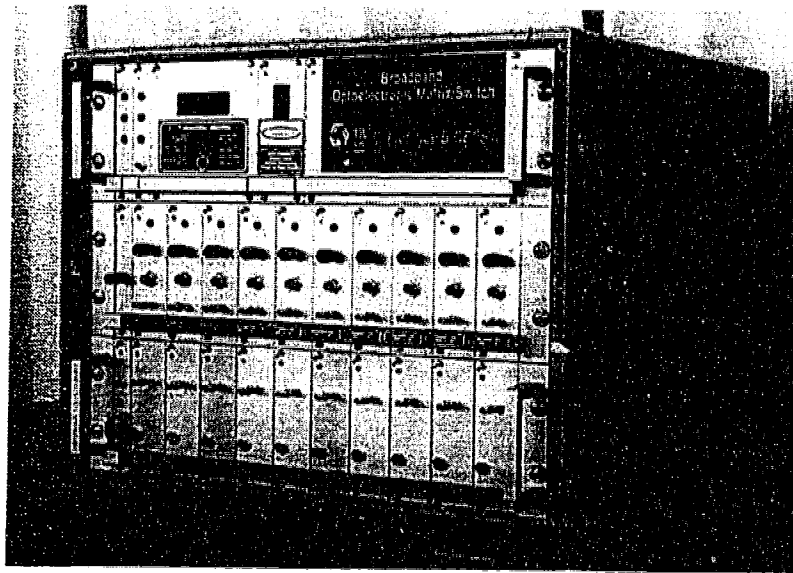


**Figure 5 Prototype 10x10 Optoelectronic Matrix Switch**

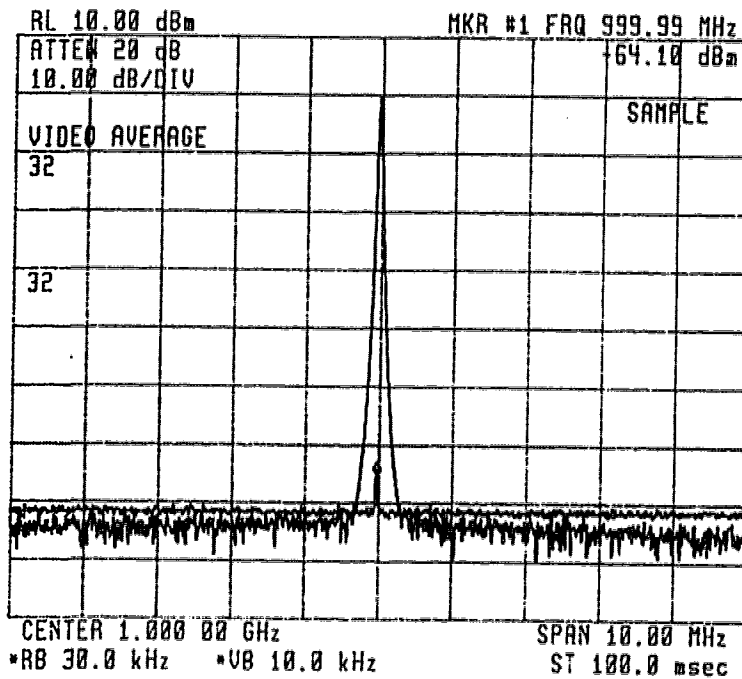


**Figure 6 Measured ON/OFF Contrast for optoelectronic switch**

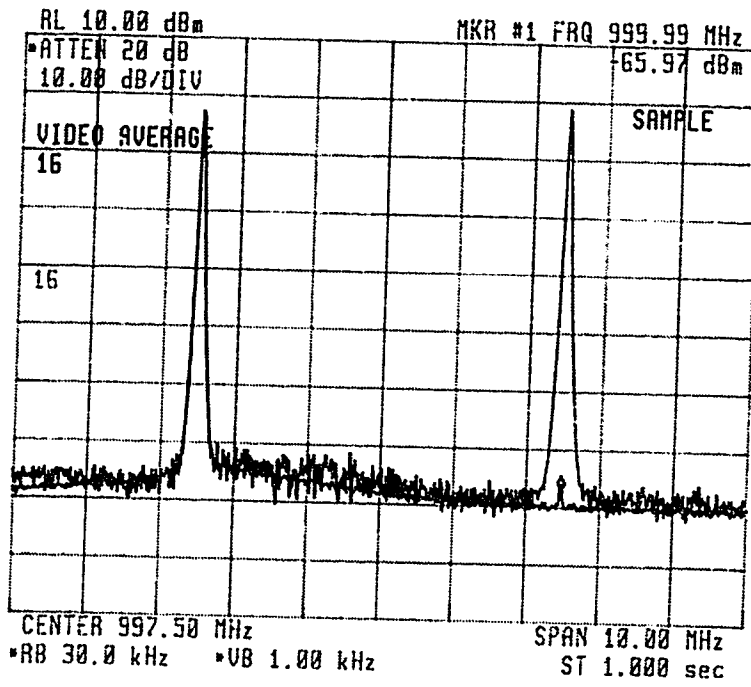
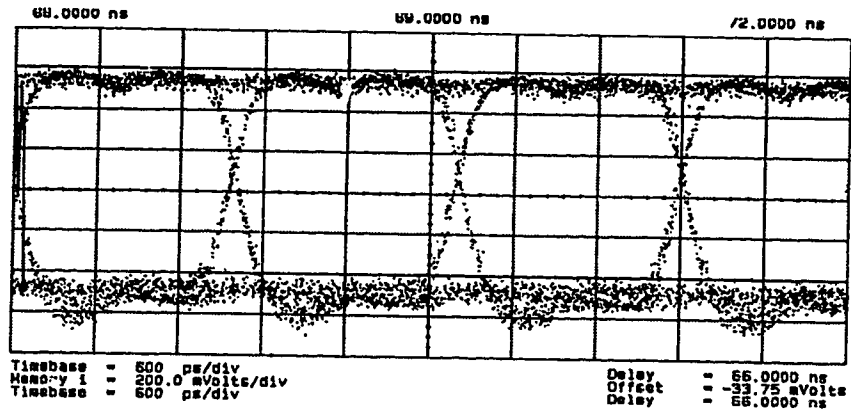
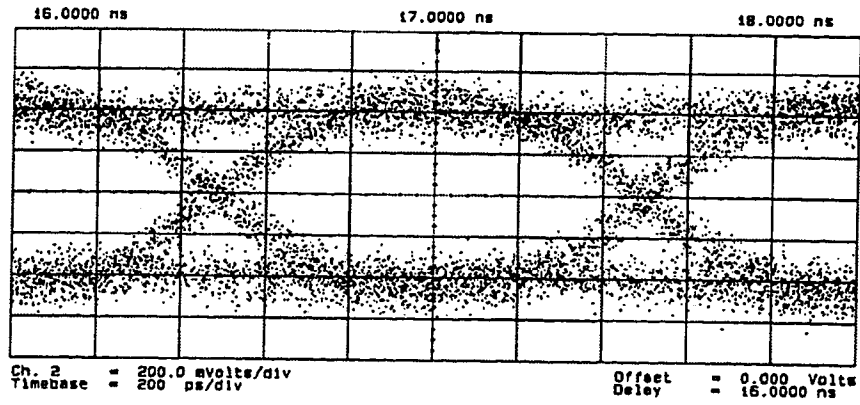


**Figure 7 Measured Crosstalk Level for Adjacent Channels**



(a)



(b)

Figure 8 Eye-Diagram for (a) 622 Mbps and (b) 1.0 Gbps data ( $2^{23}-1$  PRBS sequence)

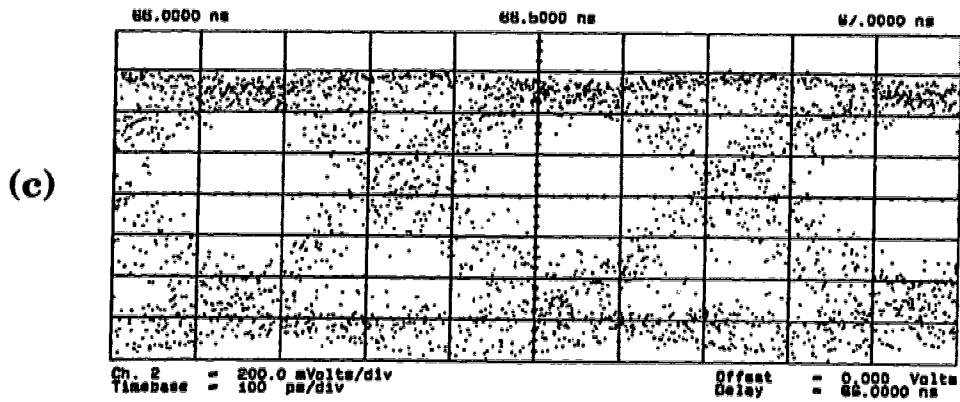
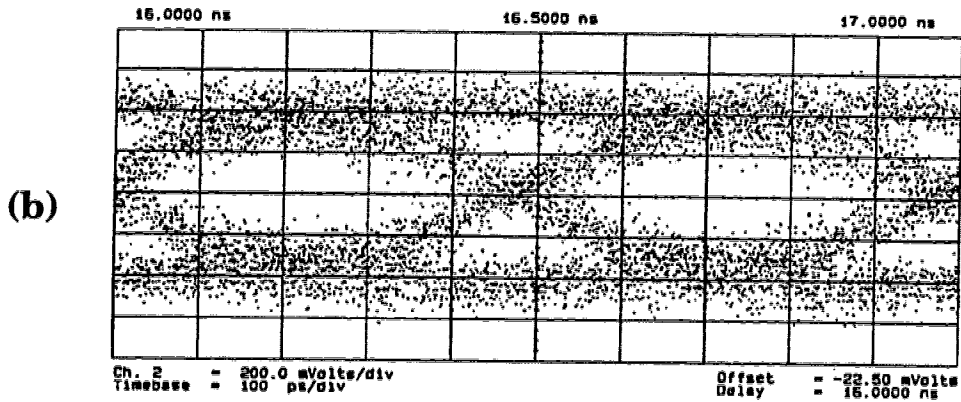
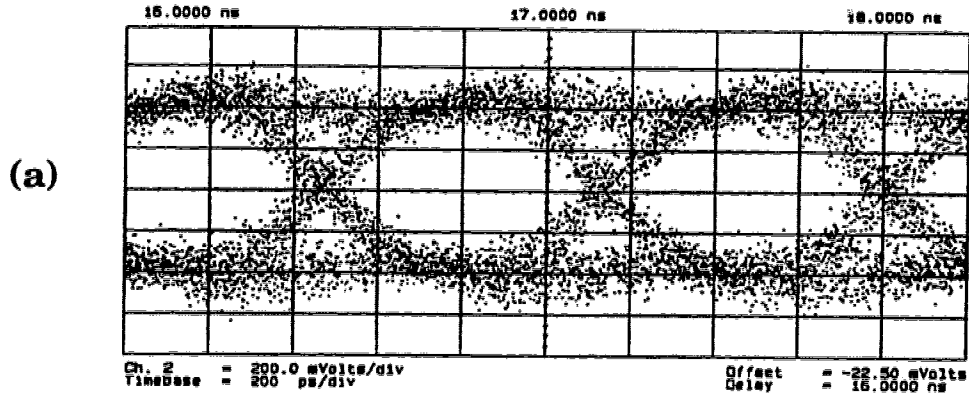


Figure 9 Eye-Diagram for (a) 1.5 Gbps, (b) 2.0 Gbps and (c) 2.488 Gbps data

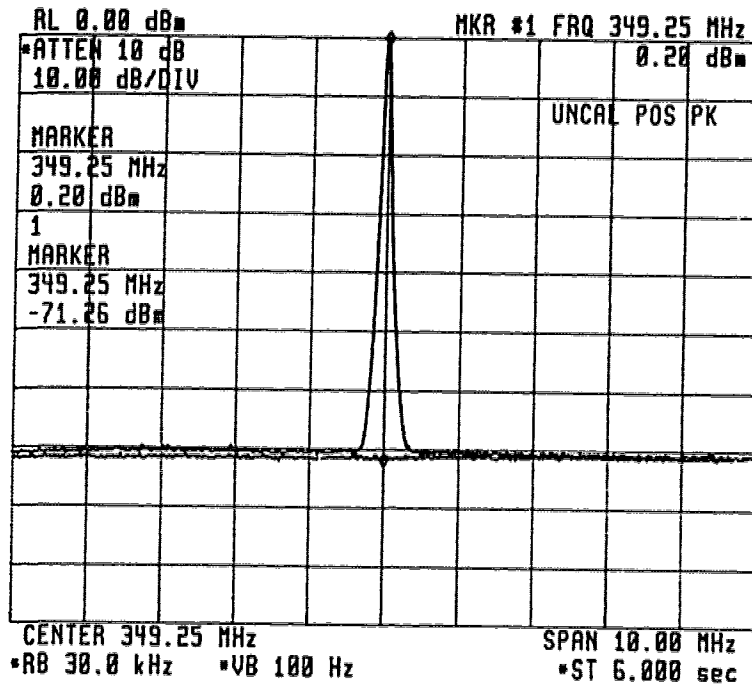


Figure 10 Carrier-to-Noise Ratio (CNR) Measurement: NTSC Analog Video Signal

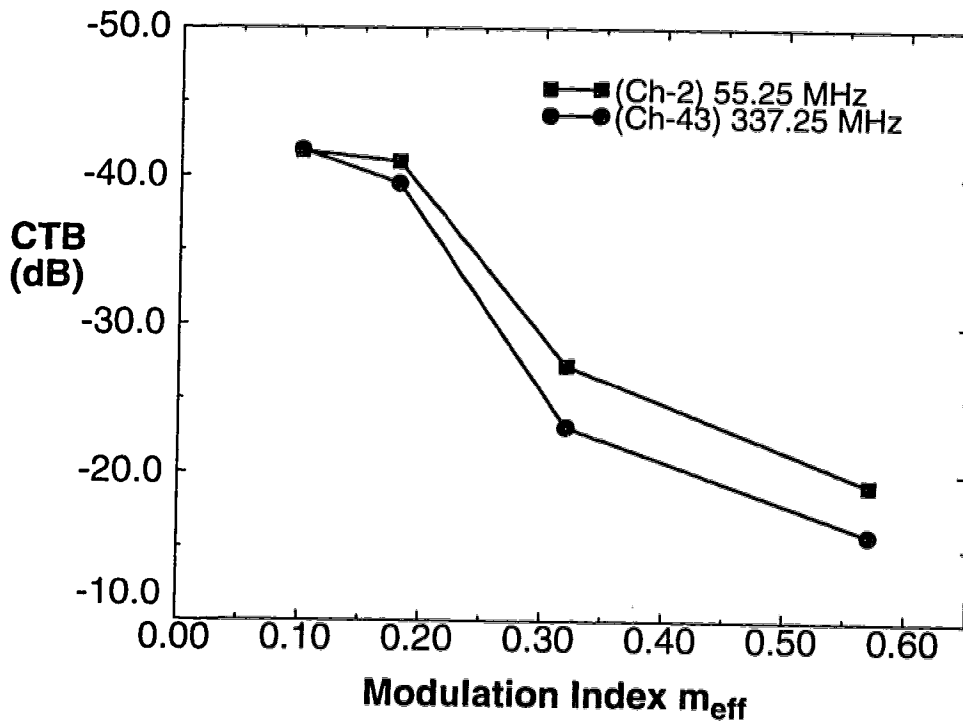


Figure 11 Composite Triple Beat (CTB) Measurement at Channel-2 and Channel-43

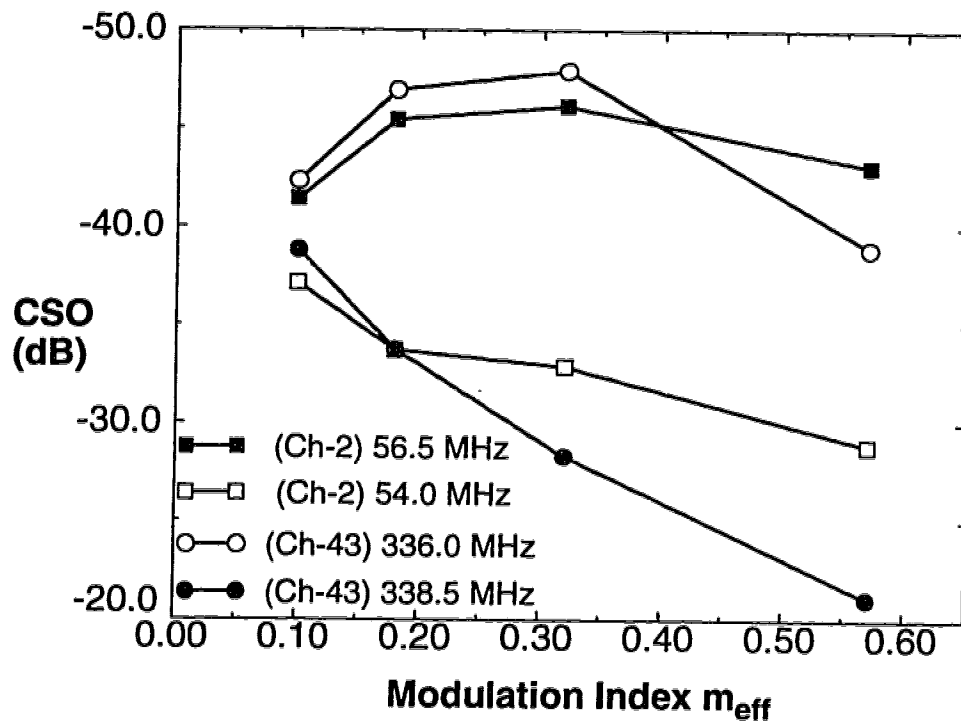
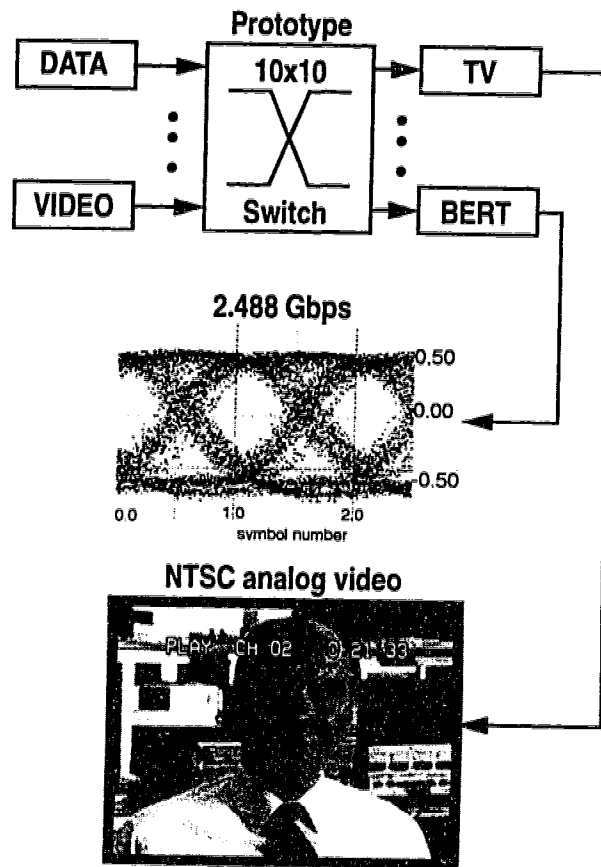


Figure 12 Composite Second Order (CSO) Measurement for Channel-2 and Channel 43



**Figure 13** Format Transparency Switching Experiment: NTSC Analog Video and 2.48 Gbps Data Switching